Kelvin waves in a shoaling shallow sea

by

VASTHIAMPILLAI JOSEPH JESUTHASAN

June 15, 2009

A thesis presented for the Degree of Doctor of Philosophy in the London Metropolitan University

CCTM DEPARTMENT

LONDON METROPOLITAN UNIVERSITY

LONDON

ABSTRACT

We revisit Taylor's problem and discuss some model test problems both through Taylor's approach and other numerical methods such as a 'Finite approximation method' and 'Green's function technique'. The solutions generated by each method are compared for consistency. The objective lies in the fact that the more difficult generalization of Taylor's problem where the sea floor is in the form of a slope may be reduced to a sequence of problems, each of which may be approached by the techniques described above.

The Taylor's problem is effected with three mutually independent techniques in order to get insight of the problem and to obtain consistent solutions by these methods.

The problem of a propagation of a Kelvin wave over a step-bottom in a semi-infinite canal closed at one end is considered.

The solution obtained is compared with that generated by the long-time limit of a numerical solution for the time dependent initial value problem. A mean square error analysis indicate good agreement.

Diagrams for co-range and co-tidal lines are displayed and it is found that the amphidromic points align along the central axes of the channel. This accounts for non-dissipation of wave energy.

Two methods of solution are presented for the problem of a Kelvin wave propagation over a step in an infinite channel open at both ends.

One of the methods is the 'collocation method' which was first used by Defant (1960).

The second method is a Fourier series method where the Kelvin wave system is first expanded as a half-range Fourier series. This idea was first used by Taylor(1921) in the analytical representation of the reflection of a Kelvin wave in a semi-infinite

channel closed at one end.

Similar solutions are obtained and diagrams for 'co-range' and 'phase lines' are displayed. It is found that the amphidromic points are displaced from the central axis towards the east and this is attributed to a loss of reflected energy in that region.

Finally the problem of a Kelvin wave propagation over a step is generalized by assuming a sloping sea bed instead and treating the problem as two semi-infinite channels connected by a slope-like bottom topography. A technique is proposed to solve this system for the simplest configuration but in principle the technique should be extendable to deal with a more general situation.

ACKNOWLEDGEMENTS

I wish to owe my indebtedness and to express my deep gratitude to my Director of studies Prof Ulf Ehrenmark for his inspirational and tireless help, guidance and motivation in every walk of this work.

I wish to thank one of my supervisors Dr.Z.Hou for who was kind enough to help me in my difficulties and motivated me in my work.

It is a great pleasure and a privilege to acknowledge Dr.Bryan Johns for who accepted to act as one of my supervisors and also was kind enough to give me the numerical formulation and the associated Fortran programming in order to effect comparisons with corresponding analytical counterparts.

I wish to express my thanks to Dr.Pete Williams for his valuable advice on questions involved in computing and allied problems.

I want to thank Dr.Amir Khossousi, Mr.Lyn Rees (who was my previous second supervisor) and Dr. Bryan D'Olier for their general comments and encouragement and also to the department for providing funds to visit British Applied Mathematics Colloquium in April 2006.

Finally, I wish to express my sincere thanks to the London Metropolitan University in general and in particular to the administration and the staff namely Miss

Judith A.Gray and her successor Ms.Chiara Francesconi who helped me with the official matters during my study for this work.

CONTENTS

Chapter 4 127

Kelvin wave reflection in a semi-infinite canal closed at one end

In this chapter we review Taylor's problem in dimensional form in order to effect a comparison with a numerical model kindly provided by Dr. B.Johns, henceforth known as *Johns'model*.

Chapter 5 147

Computation of Kelvin wave propagation into a semi-infinite rectangular basin with uniform depth

In this chapter we consider a time dependent solution of Taylor's problem from a numerical method developed by Dr. Bryan Johns. The entire numerical formulation together with a Fortran Program was provided me in order to enable a good comparison with the analytical counterpart considered in Chapter 4.

Chapter 6 162

Propagation of a Kelvin wave over a step-bottom in a Semi-infinite Canal closed at one end

This chapter is devoted to the consideration of the problem of 'Propagation of a Kelvin wave over a step-bottom in a Semi- infinite Canal closed at one end'. Two methods of solution are considered. The first treatment is Analytical where we used the 'collocation method' to determine the unknown coefficients. The second method is entirely numerical where the methodology and programming were provided by Dr.B.Johns to make comparison between two solutions.

INDEX TO FIGURES

Introduction

This work is concerned with the analysis of tidal motion in models simulating the North Sea. The main objective is to develop an analytic or semi-analytic model of the chief (M_2) tidal constituent which takes account of the North-South shoaling nature of the sea bottom. This is an area poorly understood at present and any analytical progress can potentially be a great aid to the increasing number of computer models currently being developed.

The various frequencies of orbital forcing which contribute to tidal variations are called constituents. In most locations, the largest is the 'principal lunar semidiurnal' constituent, also known as the M_2 tidal constituent. Its period is about 12 hours and 25.2 minutes, exactly half a lunar day.

The gravitational forces of the earth, of the moon, and of the sun act upon a mass element dm of the ocean. The greatest part of the gravitational forces of the moon and of the sun are compensated by the centrifugal forces originating from the revolution of the earth-moon and earth-sun systems around their respective center of gravity [25]. The remaining forces are called tide generating forces.

The tidal potential of the moon or sun is

$$\Phi(\theta,\lambda,t) = \frac{m_i R}{2}\,[\frac{1}{3}(1-3\sin^2\theta)(1-3\sin^2\delta_i) + \sin 2\theta \sin 2\delta_i \cos(\omega_i t+\lambda+\alpha_i) + \cos^2\theta\cos^2\delta_i\cos(2\omega_i t+2\lambda+2\alpha_i)]$$

m_i=M or S for the moon or sun respectively, (0.1)

where, R is the radius of the earth (6371km), λ is the longitude of the observational point, θ is the latitude of the observational point, α is a phase angle, t represents

time and ω is the angular velocity of the earth, M is the mass of the moon, r_0 is the distance from center of the earth to the center of the moon, ν is the gravitational constant and δ the declination.

The first term of the tidal potential includes a time-independent as well as a long-period part, the period of which is approximately 14 days (constant moon tide or lunar fortnightly tide M_0). The corresponding solar tide is a semi-annual tide S_0. These cause a depression of the sea level at the pole of about 20 cm and an elevation at the equator by about 10 cm.

The second term in (0.1) describes diurnal tides whose period is 24 hours 50.47 minutes..

The third term in (0.1) describes semi-diurnal tides whose period is 12 hours and 25.2 minutes.

Tides are created as a result of gravitational attraction between the Earth and the Moon as well as the Earth and the Sun although this is to a lesser extent.

The surface of the Atlantic is pulled approximately half a meter from its mean level, once when the moon is immediately overhead and once when the moon is on the opposite side of the earth.

When the moon is immediately overhead it pulls the water causing a high water, however when the moon is on the opposite side it pulls the earth again causing a high water on the other side of the earth. An equivalent depression is created when the moon is on either horizon, thus creating a tidal wave.

Although this tidal wave generated in the deep ocean, this wave passes over the continental shelf and, once on the continental shelf itself, increases in amplitudes because of the conservation of mass. Similarly the tidal velocities also increase on the conti-

nental shelf. The tidal flow over the continental shelf region is much faster than the flow in the deep sea. Usually the tidal currents in the shelf regions are about ten times stronger than currents from other sources [10].

For the formulation of this equation (0.1) please see W.Krauss [25] (p.25).

Although we are concerned with the main tidal constituents, the ocean also responds to excitation over a much broader range at higher frequencies such as wind waves (sea, swell, capillaries) as described by Platzman [31]

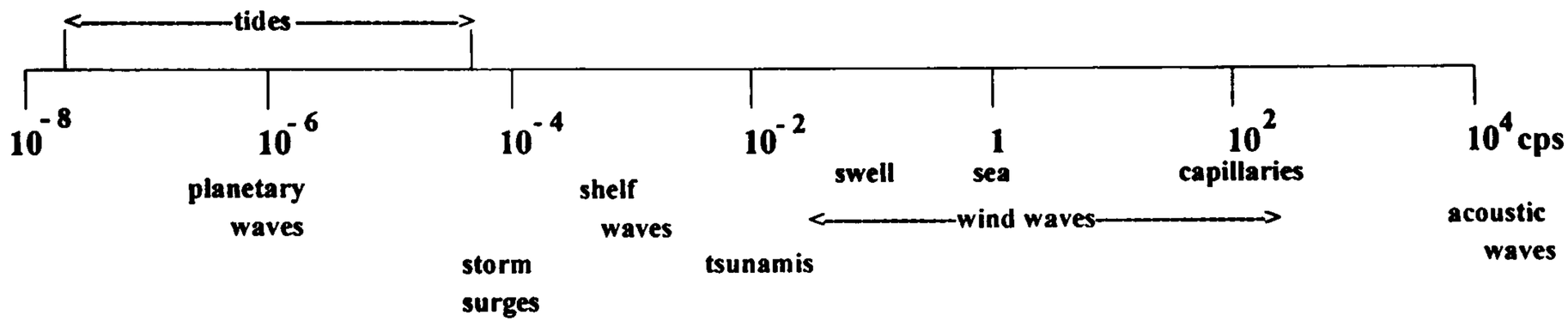

Figure 0.1: **Platzman;** Tides are at the low-frequency end of a broad range that spans much diverse activity in the oceans.

The simplified hydrodynamical equations obtained after low pass filtering approximations that suppress resonances at frequencies higher than 10^{-2} cycles per second (cps) are called 'long-wave' equations. That is, Platzman explains that by suppressing resonances at frequencies higher than 10^{-2} cps we can obtain long wave equations. Platzman adds that the word 'long' refers to wave length as well as period which we adopt for 'the pragmatic reason that they offer the only mathematically tractable basis for a theory of tides'. As Platzman points out, by suppressing resonances at frequencies higher than 10^{-2} cps, we are left with the dynamical effects of (a) gravity operating on the pressure field, (b) the earth rotation. We must therefore consider resonances modified or controlled by dynamical effects of the Earth's rotation as they naturally fall into this range of tidal frequencies.

The North Sea and Irish Sea are examples of shallow seas. By shallow sea we mean, $\frac{H}{L} << 1$, where L denotes the average width of the sea and H denotes the average depth of the sea. The M_2 tides in these shallow water regions originate from the Atlantic Ocean. It can be shown that the M_2 tide in these regions is induced by the M_2 tide in the Atlantic Ocean by solving the equations of hydrodynamics for a model of the region, assuming external motion at the open boundary. Such work was undertaken for other areas, see e.g., [14].

As early as in 1833 Whewell ([15]) recognized that maps of the amplitude and phase of the tide reveal an explicit pattern characteristic of tides. Kelvin (1879) [22] introduced the concept of a type of wave motion in which the Coriolis acceleration exerted on the current field is balanced by a transverse gradient in the surface displacement. This means that this type of wave is characterized by increased amplitude on the right-hand side and by small amplitude on the left-hand side looking in the direction of travel of waves in Northern Hemisphere. The practical reason for this assumption is that otherwise, the transverse component of the current must be retained, leading to much heavier mathematics (Poincaré,1910) [19].

The two possible types of solutions obtained from the same basic set of equations, came to be known as Kelvin and Poincaré waves.

These waves can be analyzed through the equations of hydrodynamics.

We refer to the depth averaged equations of motion and continuity equation from chapter 1.

$$\frac{\partial u}{\partial t} - fv = -g\frac{\partial \zeta}{\partial x}, \qquad \text{(i)}$$
$$\frac{\partial v}{\partial t} + fu = -g\frac{\partial \zeta}{\partial y}. \qquad \text{(ii)} \qquad (0.2)$$

$$\frac{\partial \zeta}{\partial t} + h\left(\frac{\partial u}{\partial x} + \frac{\partial u}{\partial x}\right) = 0. \tag{0.3}$$

We take $f = 2\omega \sin\phi$, ϕ is the latitude, and note that the horizontal axes (x, y) are arbitrary and not necessarily (east, north).

For a Kelvin wave propagated in the x-direction, the variation with y is exponential. Hence the Kelvin wave solution can be found by putting v=0 in the equations. We look for a solution of the above equations with v=0.

Thus,

$$\frac{\partial u}{\partial t} = -g\frac{\partial \zeta}{\partial x}, \tag{0.4}$$

$$fu = -g\frac{\partial \zeta}{\partial y}, \tag{0.5}$$

$$\frac{\partial \zeta}{\partial t} + h\frac{\partial u}{\partial x} = 0. \tag{0.6}$$

The equations (0.4)- (0.6) are shallow water equations, (with v=0), derived using the hydrostatic approximation.

The equations (0.4) and (0.6) govern ζ and u variations on any line y= constant, and contain no Coriolis force and thus the wave motion is identically the same as the non-rotating shallow water motion. Thus in the vertical plane of the bounding wall and in any parallel vertical plane, the motion is exactly the same as that in a non-rotating system and hence the wave is a shallow water gravity wave.

The depth-averaged linearized model that describes the tidal wave is obtained from (0.4) and (0.6),

$$\frac{\partial^2 \zeta}{\partial t^2} = gh\frac{\partial^2 \zeta}{\partial x^2} \tag{0.7}$$

Thus we have general solution of (0.7) consisting of the sum of two non-dispersive

waves travelling in the opposite directions, namely,

$$\zeta = A_1(y)F_1(x - \sqrt{ght}) + A_2(y)F_2(x + \sqrt{ght}),$$

$$u = \sqrt{\frac{g}{h}}A_1(y)F_1(x - \sqrt{ght}) - \sqrt{\frac{g}{h}}A_2(y)F_2(x + \sqrt{ght}).$$

where A_1 and A_2 are functions with properties to be determined. The way the functions A_1 and A_2 vary with y can be found from the one remaining equation, namely (0.5).

By using (0.5) we arrive at two Kelvin waves travelling in opposite directions given by,

$$\zeta = e^{-\frac{f}{\sqrt{gh}}y}F_1(x - \sqrt{ght}) + e^{\frac{f}{\sqrt{gh}}y}F_2(x + \sqrt{ght}), \tag{0.8}$$

the speed of propagation being $\sqrt{gh}$.

The wave, represented by F_1, if $f > 0$ decays exponentially in the positive y direction, whereas the other decay exponentially in the negative y direction. This exponential behavior is very similar to that of the Lamb wave (Gill(1982), page 378) and so the Kelvin wave is also among the class of waves called boundary waves, edge waves, trapped waves, or surface waves (see Gill(1982)) [11]

As Kelvin (Thomson,1879) [22] remarked, 'the velocity of propagation is the same' as for the non-rotating case, and 'the influence of rotation is confined to the factor' $\exp(-y/a)$, where 'a' is a length scale of fundamental importance, defined by $a = \sqrt{gh}/f$, and denoted the Rossby radius of deformation (or simply called 'Rossby radius'). 'Many interesting results follow from the interpretation of this factor'. The important property is, of course, the scale of a. Typical values of a for barotropic (constant density) Kelvin waves are 2000 km for the deep sea and about 200 km for coastal waters and shallow seas. But, in the case of baroclinic Kelvin waves (which

are important in the description of coastal upwelling) the values of a are only about 30 km

Since the wave amplitudes are exponential in the y direction, we must limit this direction by imposing a coastline or boundary, say at y=0. The boundary condition v=0 is then automatically satisfied, and the solution $\zeta = e^{-\frac{y}{a}} F_1(x - \sqrt{ght})$ represents a Kelvin wave in the region $y > 0$ moving in the positive x direction along the straight coast. We note that $\zeta \to 0$ as $y \to \infty$. In addition, in the Northern Hemisphere the wave travels with the boundary to the right of its direction of propagation, since $f > 0$ in this case. In the Southern Hemisphere the boundary lies to the left of the direction of propagation.

Thus, the Kelvin type of tidal wave is one that can be propagated in a rotating channel. As the wave progresses along the length of an infinite long uniform straight channel, a horizontal pressure gradient is created because the amplitude of wave is greater on one side of the channel than on the other. This gradient force is counterbalanced by the Coriolis force due to the earth's rotation. In the Northern Hemisphere the deflecting force is balanced by a pressure gradient provided by an increase in the amplitude of the wave on the right hand side of the channel (following the propagation).

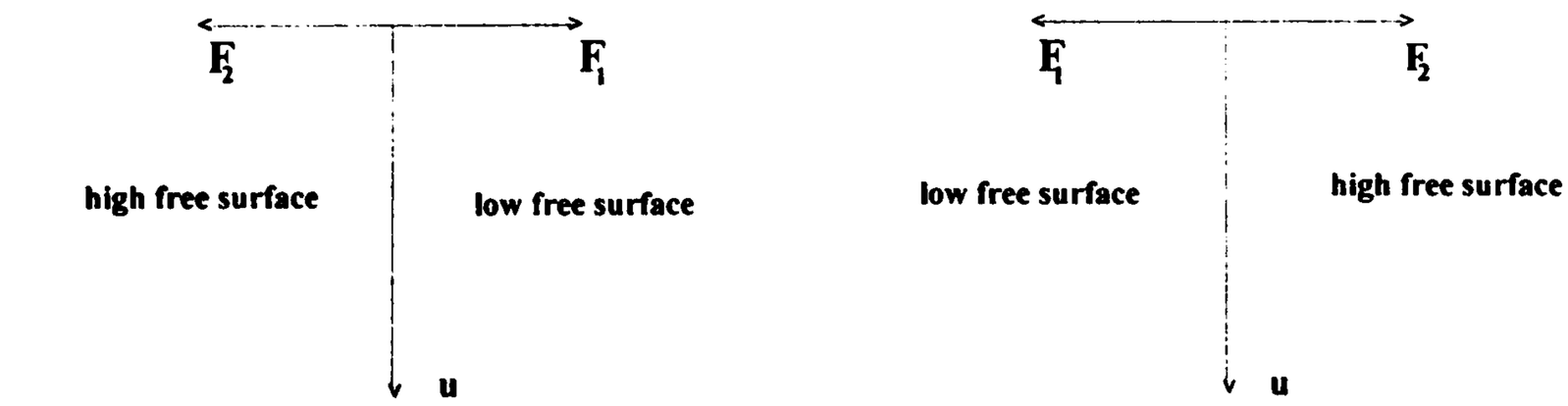

Figure 0.2: Balance of Coriolis force and pressure gradient

In particular, when F_1 is sinusoidal in character, then the complete Kelvin-wave solution takes the form

$$\zeta = \zeta_0 e^{-y/a}\cos(\frac{\sigma}{\sqrt{gh}}x - \sigma t), \quad u = (g/h)^{\frac{1}{2}}\zeta_0 e^{-y/a}\cos(\frac{\sigma}{\sqrt{gh}}x - \sigma t), \tag{0.9}$$

Now consider the energy of a Kelvin wave of the form (0.9).

If a coast is put at $y = 0$, then the amplitude of the wave at the coast is ζ_0. Since the solution for a fixed value y is as in the non-rotating case, the energy of a Kelvin wave is partitioned equally between the kinetic and potential forms.

The mean value (denoted by over line) per unit length of coast is given by,

$$\text{Kinetic energy (K.E)} = \int_0^\infty \frac{1}{2}\rho H\overline{u^2}dy,$$

and

$$\text{Potential energy (P.E)} = \int_0^\infty \frac{1}{2}\rho g\overline{\zeta^2}dy,$$

where, H denotes the depth.

Hence,

$$\int_0^\infty \frac{1}{2}\rho H\overline{u^2}dy = \int_0^\infty \frac{1}{2}\rho g\overline{\zeta^2}dy = \frac{1}{8}a\rho g\zeta_0^2. \tag{0.10}$$

The average value of the energy flux along the coast is

$$\int_0^\infty \rho H\overline{u\zeta}dy = \frac{1}{4}\frac{\rho g^2 H\zeta_0^2}{|f|}. \tag{0.11}$$

This formula (0.11) is of interest when a Kelvin wave moves through a region in which H varies.

For the energy flux to remain constant, the amplitude ζ_0 must vary in proportion with $(\frac{|f|}{H})^{\frac{1}{2}}$. For a local sea (f=constant) this amplitude varies inversely with $\sqrt{H}$ to maintain the energy flux constant.

It is of our interest to note that the Kelvin wave component of the tide entering the North Sea then moves down the west side into even shallower water in the Southern Bight, this providing a means of enhanced tidal amplitudes in this region.

Now consider retention of the transverse component of the current, and take a progressive shallow water wave, i.e., one for which ζ, u, and v are proportional to

$$\exp\ i(mx + ny - \sigma t). \tag{0.12}$$

The plane wave, given by (0.12), is sometimes given the special name of Sverdrup wave (see Platzman, 1971) [31]. The polarization relations, i.e., the relations between amplitudes and phases of ζ, u, and v, can be obtained by substituting this form of dependence on (x, y, t) in the governing equations (0.2) and (0.3).

However, we first assume a time factor $e^{-i\sigma t}$ in the field quantities (u, v, ζ), then we have the following set of equations obtained from (0.2) and (0.3).

$$\begin{aligned} -i\sigma u - fv &= -g\frac{\partial \zeta}{\partial x}, \\ -i\sigma v + fu &= -g\frac{\partial \zeta}{\partial y}, \\ -i\sigma\zeta + \frac{\partial}{\partial x}(hu) + \frac{\partial}{\partial y}(hv) &= 0, \end{aligned}$$

resulting in the wave equation

$$\nabla_H^2 \zeta + \frac{\sigma^2 - f^2}{gh}\zeta = 0, \tag{0.13}$$

where, $\sigma = 2\pi/(\text{period of tidal oscillation})$, and $\nabla_H^2 \equiv (\frac{\partial^2}{\partial x^2}, \frac{\partial^2}{\partial y^2})$.

In the wave equation (0.13) it has been assumed that the depth h is constant. Assuming a solution of the form $\zeta = e^{imx+iny-i\sigma t}$ in terms of constants n, m, then we must have the condition

$$m^2 + n^2 = \frac{(\sigma^2 - f^2)}{gh}.$$

Taking $k_H = (m^2 + n^2)^{\frac{1}{2}}$ as the magnitude of the horizontal wave number vector

$$\mathbf{k}_H = (m, n),$$

the dispersion relation is written as

$$\sigma^2 = f^2 + k_H^2 gH. \tag{0.14}$$

A. E. Gill [11], in his book, refers to all waves with dispersion relation (0.14) as Poincaré waves, although the name is sometimes reserved for the subset that satisfies the boundary conditions for a channel.

Thus plane Poincaré waves are only possible for $\sigma > f$. That is , such that their period $\frac{2\pi}{\sigma} < \frac{2\pi}{f} = T_p$ the half pendulum day. Thus locally (i.e,f a constant) energy can be transferred by plane waves independently of boundaries, without attenuation, only if it is in the form of short period waves (T_p=24hours at $\theta = 30^o$, T_p=17hours for the North Sea).

Equations (0.13) also yield the following relations for u and v in terms of ζ

$$u = \frac{1}{k_H^2 H}(m\sigma + inf)\zeta, \qquad v = \frac{1}{k_H^2 H}(n\sigma - imf)\zeta. \tag{0.15}$$

Thus we can infer that if a Kelvin wave is moving along an isolated boundary such as a semi-infinite coastline, on diffraction it can lose no energy if $\sigma < f$ and will eventually have the same amplitude. If $\sigma > f$, the amplitude is less after diffraction has taken place because energy will be lost in the form of Poincaré waves propagated to infinity (with an amplitude going to zero like $r^{\frac{-1}{2}}$ as distance r from the origin becomes large).

Poincaré waves are dispersive since a wave can be written in the form

$$\zeta = e^{i\left(k(\frac{m}{k}x + \frac{n}{k}y) - \sigma t\right)} = e^{i(k_H \underline{r}.\underline{n} - \sigma t)} \tag{0.16}$$

where $k_H = (m^2+n^2)^{1/2}$, $\underline{n}$ is a unit normal to the wave front, and thus lies along the direction of propagation. The distance between wave crests is $2\pi/k_H$, and the period

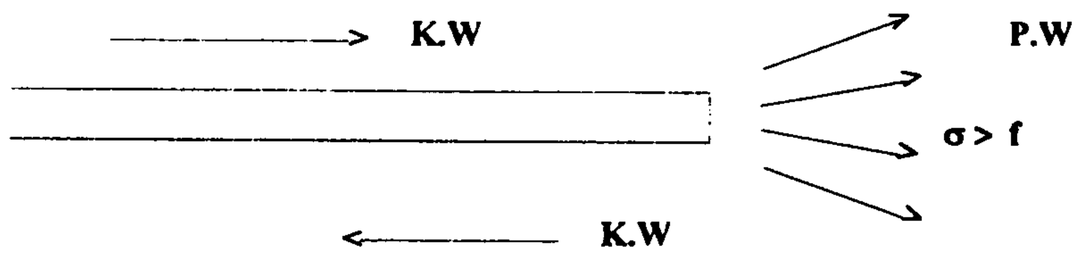

Figure 0.3: Kelvin wave along an isolated boundary.

is $2\pi/\sigma$, thus the speed of the wave is $U = \frac{2\pi}{k_H}/\frac{2\pi}{\sigma} = \sigma/k_H$.

i.e.,

$$U = \frac{\sqrt{f^2 + ghk_H^2}}{k_H} > \sqrt{gh}.$$

The speed of the wave is greater than the corresponding value for the non-rotating system.

Finally we note that if $m = \sigma/c$, $n^2 = k_H^2 - m^2 = -f^2/c^2$.

Thus, by taking $in = -f/c$, (0.16) yields the Kelvin wave,

$$\zeta = e^{i\left(\frac{\sigma}{c}x - \sigma t\right)} e^{(-f/c)y},$$

which travels with a speed $U = c = \sqrt{gh}$

During the process of this investigation of tides in the North Sea, the question arises as to what are the important factors which determine the basic tidal structure of the North Sea and outer Thames Estuary.

The interaction between the Southern Bight and Straits of Dover could be an important factor.

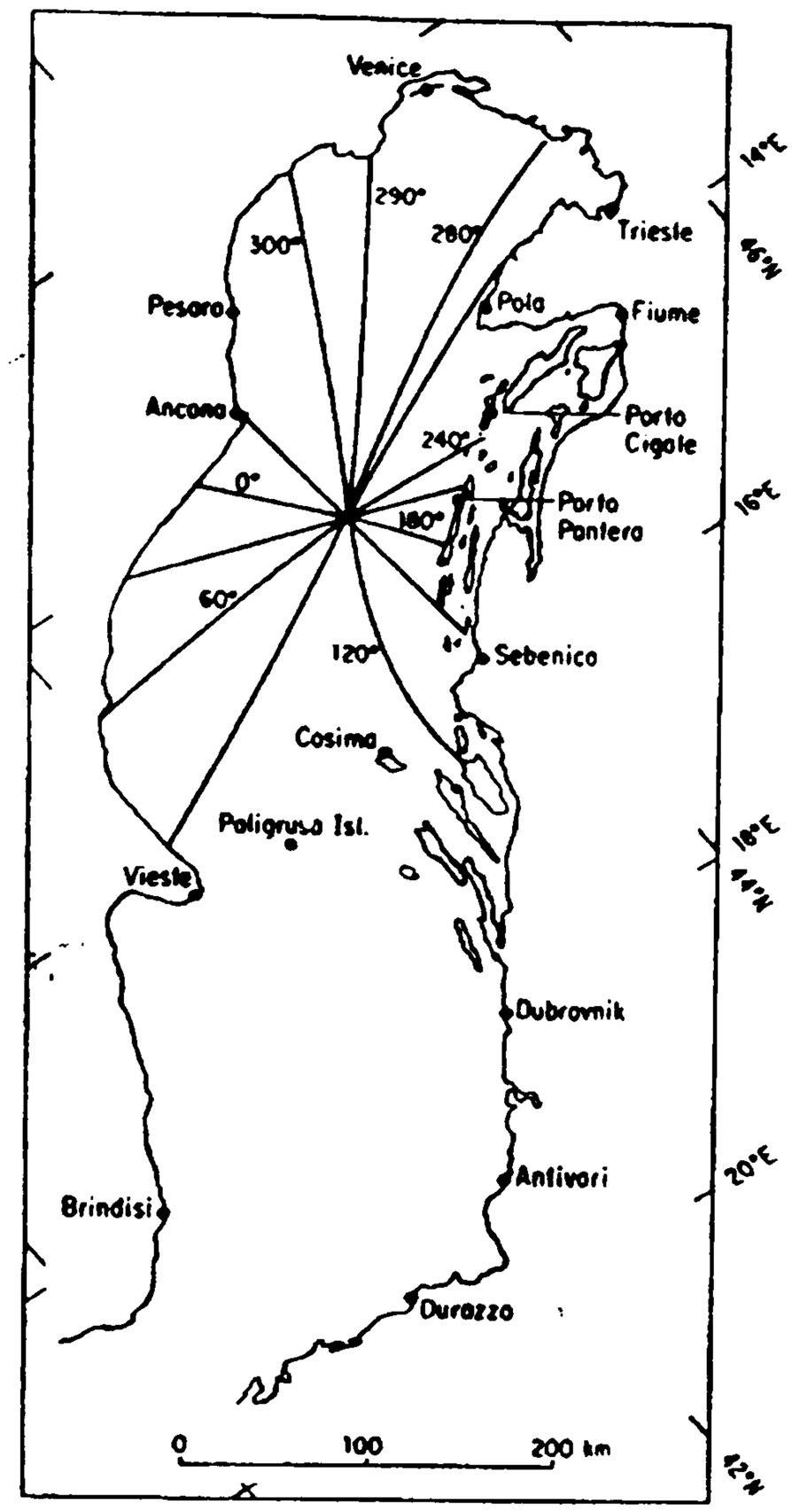

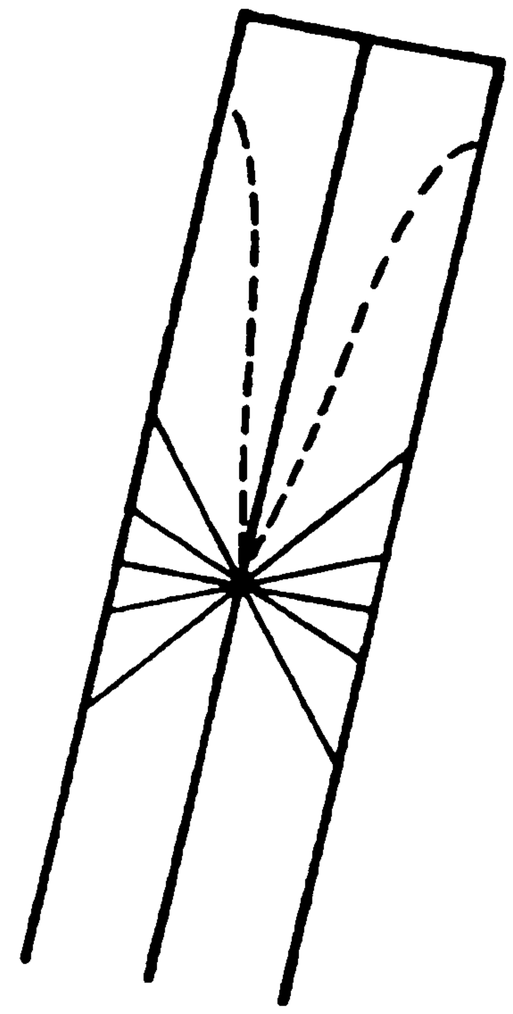

Figure 0.4: (**Gill, 1982**); (a) Co-tidal lines for the Northern Adriatic, [After Polli (1960); from Hendershot and Speranza (1971), Fig.7.] (b) Co-tidal lines for a simple model with depth increasing quadratically with distance from the end. The phase difference between the solid lines is 30^{o}. The phase on the broken lines differs by 10^{o} from that on the axis.

Frictional effects are also found to be significant according to the thoughts of many authors, i.e., [34].

The importance of the earth's rotation has been discussed to a reasonable extent in absence of boundaries at the side. An important feature of rotating fluid behavior is the geostrophic adjustment process in which the pressure and velocity fields adjust to each other to reach a geostrophic balance. When the balance is achieved, the flow at any level is along the isobars (see Gill, 1982, page 371)

Now, we suppose a boundary is placed so that it crosses the isobars. Then, further adjustment would take place because no flow is possible across the boundary. The presence of the boundary makes the long-shore component of the Coriolis acceleration to vanish so that the mutual adjustment of the long-shore velocity field and the pressure field along the boundary would occur. The situation is more like that in non-rotating field than like that in a rotating one.

In sufficiently narrow channels, gulfs or estuaries there are two boundaries close together, thus the effect of rotation may be ignored as a first approximation because the motion is mainly along the channel, gulf or estuary. This implies the component of Coriolis acceleration in this direction is negligible. The solutions for seiches and tides in many channels, gulfs, estuaries and lakes can be found on the assumption that the motion is everywhere parallel to the axis of the channel. Such solutions have been found to give good approximations to the behavior of seiches and tides in many channels, gulfs, estuaries etc, i.e. see (Gill, 1982, page 373)

At the next order of approximation, rotation modifies in two ways, one is to give a cross-channel pressure gradient in order geostrophically to balance the long-shore flow. The other is to produce a shear whenever surface elevation departs from its equilibrium level, this being required in order that potential vorticity be conserved. The potential vorticity is defined as $\chi = -(f/H)\zeta$, where H is the depth.

Suppose in a narrow channel the solution to a first approximation has the form

$$u = u_{nr}(x,t), \qquad \zeta = \zeta_{nr}(x,t) \tag{0.17}$$

where the subscript 'nr' denotes non-rotating.

Here the solution is a non-rotating one as the walls of the channel force the flow to be everywhere parallel to the walls.

Now our objective is to see what effects the rotation will have when these effects are small.

First of all, because of the adjustment, there will be a Coriolis acceleration fu_{nr} directed across the channel which must be balanced by small surface slope. The approximate form of the y component of the momentum equation is

$$fu = -g\frac{\partial \zeta}{\partial y}. \tag{0.18}$$

Choosing the origin of y, this integrates to give

$$\zeta = \zeta_{nr}(x,t) - g^{-1} f u_{nr}(x,t) y. \tag{0.19}$$

for the corrected surface elevation.

But for small correction

$$u = \mathrm{O}(\sqrt{(g/H)})\zeta.$$

Using this, the correction term in (0.19) can be written as

$$g^{-1} f (g/H)^{1/2} \zeta_{nr} W.$$

where H is the depth of the channel, W is the channel width. The condition for the correction term to be small relative to ζ_{nr} is obtained as

$$g^{-1} f (g/H)^{1/2} W \leq 1 \quad \text{i.e.,} \quad (W/a) \leq 1, \tag{0.20}$$

where a is the Rossby radius.

In other words, the condition for rotation effects to be small is that the width of the channel be small compared with the Rossby radius.

The corrected surface elevation in the form (0.19) can give a considerable improvement to the non-rotating solution.

The interesting new feature added by rotation is the crest of the tide, as given by (0.19), now moves cyclonically around the basin.

This is illustrated by an analytical solution which gives a good approximation to the northern end of the Adriatic taken as a channel of uniform width, W=135 km. The depth of the channel, which is assumed by a formula, $H = \gamma\, x^2$ ($\gamma = 6.5 \times 10^{-10} m^{-1}$), increases quadratically with distance, x, along the channel.

The Adriatic sea extends north west from $40^{\underline{o}}$ to $45^{\underline{o}}$ N with an extreme length of about 770 km. It has a mean breadth of about 135 km. The tidal movement is slight with an amphidromic point just off the north-western shore, near Ancona.

In the model Adriatic, the end of the channel (Venice) is situated at $x = x_0 = 150$ km. The Adriatic occupies the region $x > x_0$. A median value of the Rossby radius is 250 km, so that the condition (0.20), $W/a < 1$ is satisfied. For the solution and further discussion see (Gill, 1982) [11] and (Hendershott and Speranza, 1971) [34].

The usual way of displaying the tidal variations is in terms of the amplitude A and phase δ. That is, if the elevation of the free surface ζ is expressed in the form

$$\zeta = A \sin(\sigma t - \delta),$$

then (i) Contours of A are called co-range lines, on which the range $2A$ is given in meters, (ii) Contours of δ are called co-tidal lines and the phase is given either in degrees or as the time of high water in hours.

The Fig (0.4a) shows the observed co-tidal lines whereas Fig (0.4b) shows the corresponding diagram from the model for the Northern Adriatic Sea.

The seiches in the Adriatic are of importance because they are responsible for the flooding of Venice. The fundamental seiche has a period of 22 hours. The effect on Venice depends a great deal on whether or not the times of maximum seiche are close

to the times of high tide.

The narrow-channel approximation can be applied with success to studies of tides and seiches in gulfs, estuaries, and lakes, and even to the tides in the Atlantic Ocean. Now the questions arise as to what happens when the two sides of the channel are close together, and to how far from the shore the long-shore component of the Coriolis force can be neglected. For the narrow channel approximation to be valid the width of the channel must be small compared with the Rossby radius. For a wide channel there is a special form of adjustment near the boundary by means of a wave whose amplitude is only significant within a distance of the order of the Rossby radius from the boundary. This wave is called a Kelvin wave and some of its properties were discussed above.

The presence of boundaries also affects the Poincaré waves. As Kelvin remarked a plane progressive Poincaré wave cannot satisfy all the boundary conditions at a boundary. But obliquely directed two such waves of equal amplitude can satisfy the condition. We can expect such a situation from reflection of a plane wave at a straight boundary. As an example we consider the reflection of plane Poincaré waves at a boundary (see Fig(0.5)).

It is convenient to choose the x-axis in the direction of the bisector of the angle between the two wave number vector, and choose the origin of y on the line of symmetry for v, i.e., a line on which $\partial v/\partial y$ vanishes.

The combination of the two plane Poincaré waves can be constructed but with a shift

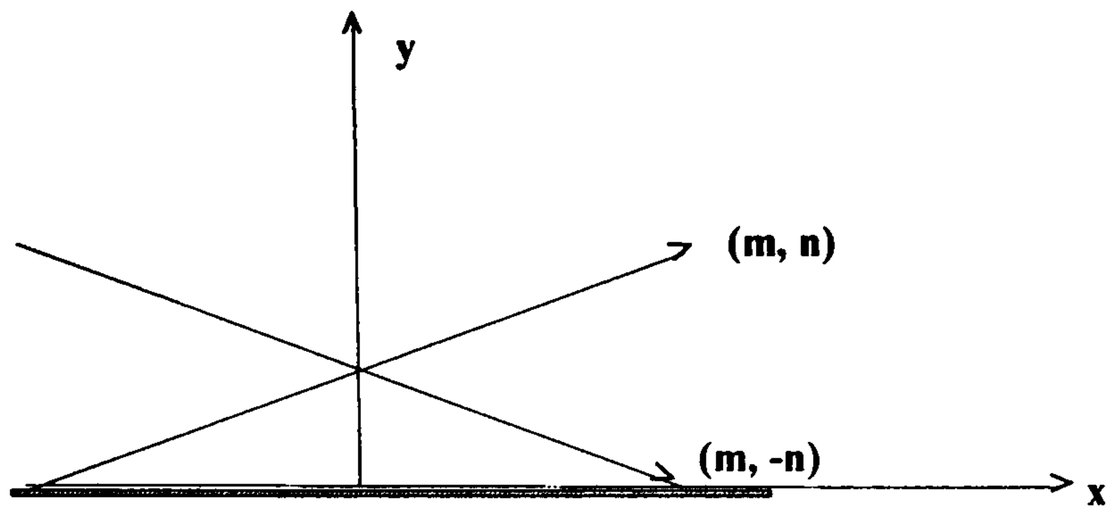

Figure 0.5: Wave-number vectors of incident and reflected waves.

in the origin of y so that $\partial v/\partial y$ will vanish at y=0. Then the solution is

$$\zeta = \left(\frac{2\zeta_0}{(m^2+n^2)^{1/2}\sigma_c}\right)(mf\cos ny + \sigma n \sin ny)\cos(mx-\sigma t),$$
$$u = \left(\frac{2g\zeta_0}{(m^2+n^2)^{1/2}\sigma_c}\right)(mn\sin ny + (\sigma f/gH)\cos ny)\cos(mx-\sigma t),$$
$$v = \left(\frac{2\sigma_c\zeta_0}{(m^2+n^2)^{1/2}H}\right)\cos ny \sin(mx-\sigma t), \tag{0.21}$$

where, σ_c, defined by

$$\sigma_c = f^2 + n^2 gH, \tag{0.22}$$

is the minimum frequency a wave with given n can have. Hence the dispersion relation is written in the form

$$\sigma^2 = \sigma_c^2 + m^2 gH. \tag{0.23}$$

A Poincaré wave can satisfy the boundary condition of no normal flow in a channel of uniform width W provided that

$$n = r(\frac{\pi}{W}), \qquad r = 1, 2, 3, 4, ... \tag{0.24}$$

For each r, there is a minimum frequency σ_{rc} that is necessary for propagation.

Using (0.24) the relation (0.22) can be written as

$$\sigma_{rc}^2 = f^2 + \frac{r^2\pi^2 gH}{W^2}, \quad r = 1, 2, 3..... \tag{0.25}$$

This minimum frequency increases with r, so the smallest value is σ_{1c}.

From (0.23) we can see that σ varies with m, thus

(1) if $m^{-1} \ll (gH)^{1/2}/\sigma_c$, then the waves are only weakly dispersive and propagate along the channel at speed close to $(gH)^{1/2}$ (phase velocity slightly more; group velocity slightly less),

(2) if $m^{-1} \gg (gH)^{1/2}/\sigma_c$, then the waves have relatively small group velocity and the frequency is close to σ_c,

(3) When $m = 0$, the wave does not propagate, but represents a standing wave spanning the channel.

In fig (0.6) we have shown propagation of a progressive wave of the form (0.21). In the northern hemisphere ($f > 0$), for an observer moving in the direction of the wave, the amplitude tends to be higher on the left side of the channel, and the particle trajectories are ellipses. The orbital motion is anticyclonic except for a region near the right bank that occupies a fraction of the channel width that is always less than a half.

The possible propagating modes in a channel of width W are Poincaré modes given by (0.21) and (0.24), and the two Kelvin waves associated with the two sides of channel. The dispersion curves form for these modes are shown in Fig (0.7)

(1) When the the channel is not too wide, $W \ll \pi a$, then in Fig (0.7a), the picture is not too different from that for the limit of no rotation.

(2) As the width of the channel increases, the critical frequencies σ_{rc} for propagation of Poincaré modes all approach f, and so the picture becomes more like that seen in

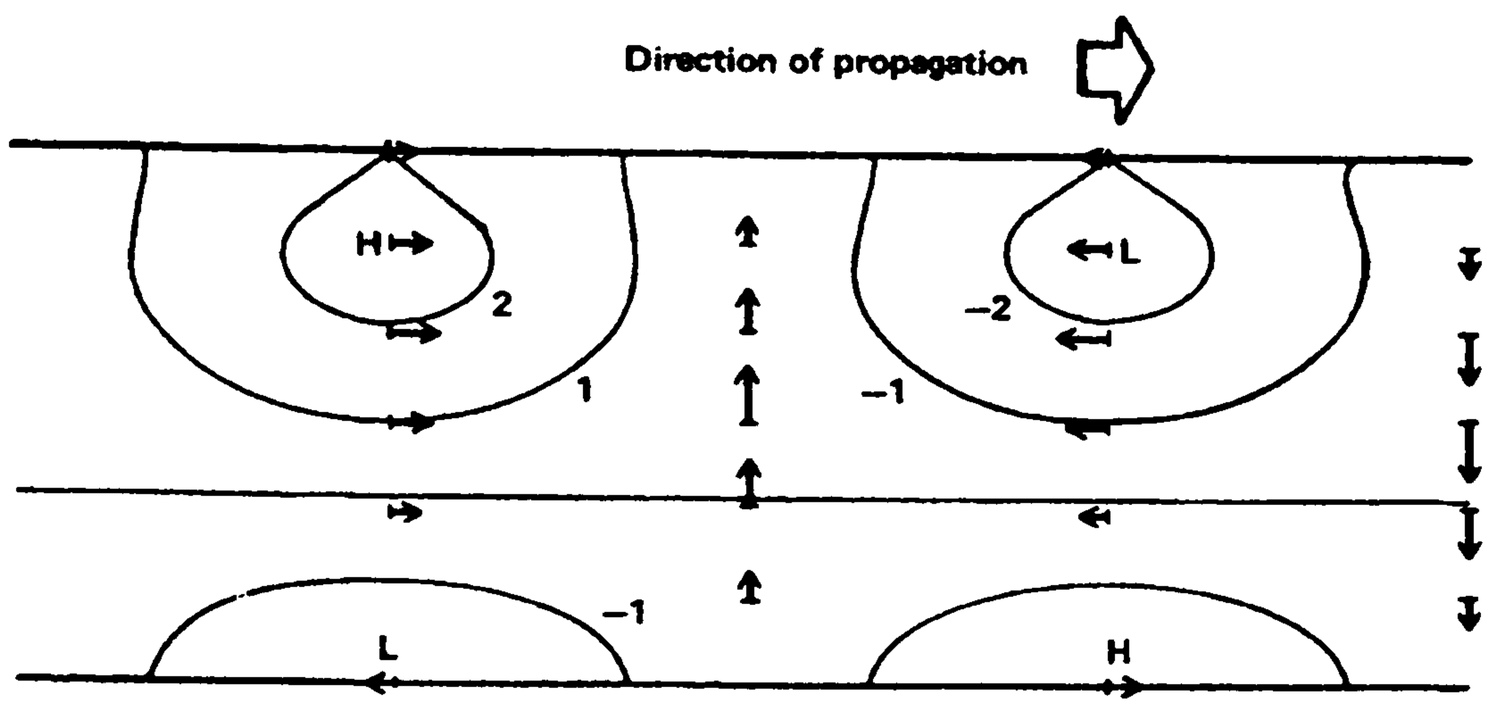

Figure 0.6: **(Gill, 1982)**; The progressive Poincaré wave in a channel of width $W = \pi a$. The cross-channel scale is $n = 1/a = c/f$, so the minimum frequency, $\sigma_c = \sqrt{2}f$ The scale m^{-1} in the direction of propagation is $\sqrt{\frac{3}{2}}\, c/f$, so $\sigma = \sqrt{\frac{8}{3}}f$ and $i\sigma = 2im$. The signs are those for the northern hemisphere, so the greatest elevations are found on the left side of the channel (facing in the direction of propagation), where particles move anticyclonically. The nodal line is about 65 percent of the way across the channel. Contours are of surface elevation, arrow indicates currents..

Fig (0.7b)

Kelvin's discussion of waves in a channel was confined to the modes that now bear his name. He noted that the more approximately nodal character of the tides on the north coast of the English channel than on the south or French coast is probably to be accounted for on the principle represented by this factor, $e^{-y/a}$, taken into account along with frictional resistance, by virtue of which the tides of the English channel may be roughly represented by more powerful waves traveling from west to east, combined with less powerful waves traveling from east to west.

The above description explains reasonably the tides in the English Channel which can be seen in Fig (0.8)

Kelvin also gave the solution for 'the problem of standing oscillations in an endless

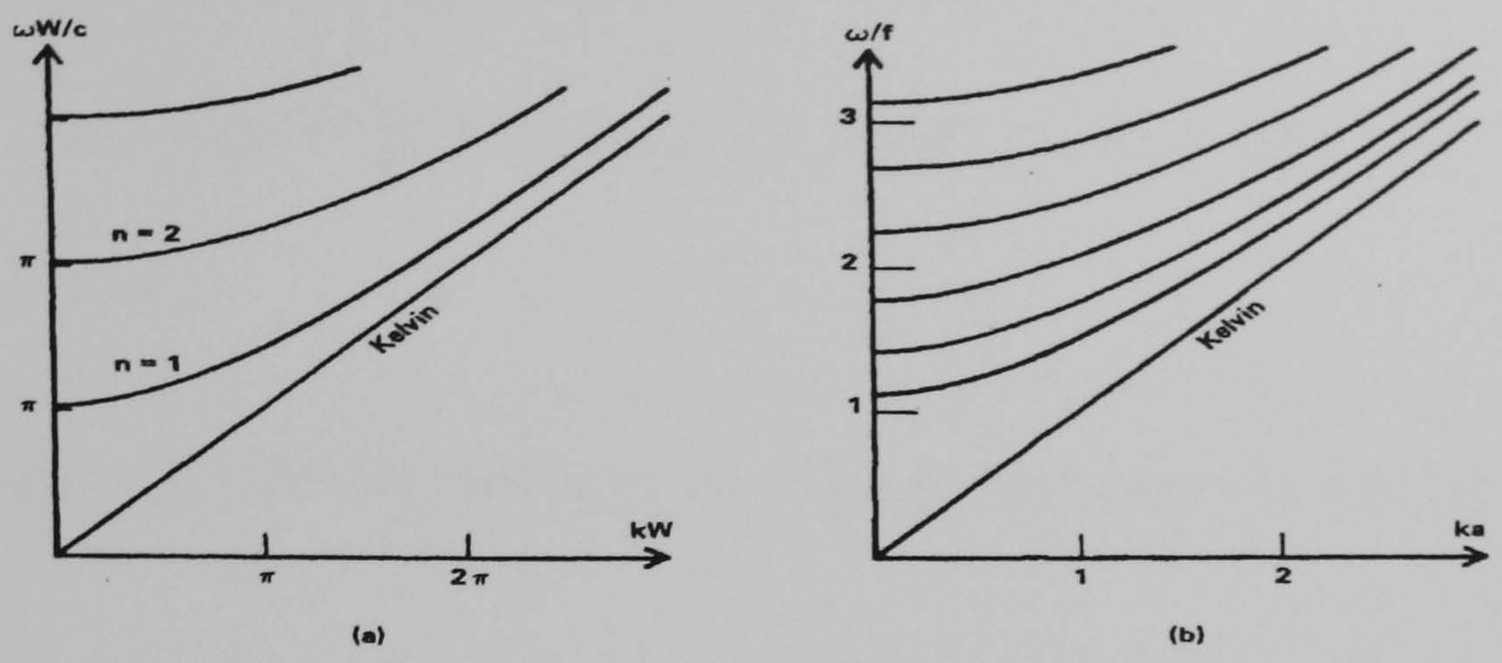

Figure 0.7: (**Gill, 1982**); Dispersion curves for a channel of uniform width W, m being the wave number component parallel to the sides of the channel. In case (a), the width is $0.3a$ and the dispersion relation, given by (0.22)–(0.24), becomes $(\frac{\sigma W}{c})^2 = (\frac{fW}{c})^2 + (r\pi)^2 + (mW)^2$. Rotation effects which are represented by the constant term, $(\frac{fW}{c})^2$=0.09, are barely discernible. In case (b),the width of the channel W=$2\pi a$ and the dispersion relation is $(\sigma/f)^2 = 1 + (r/2)^2 + (ma)^2$, if the width increased further, the coefficient of r^2 becomes smaller, so the curve move downward on the diagram and become more densely packed.

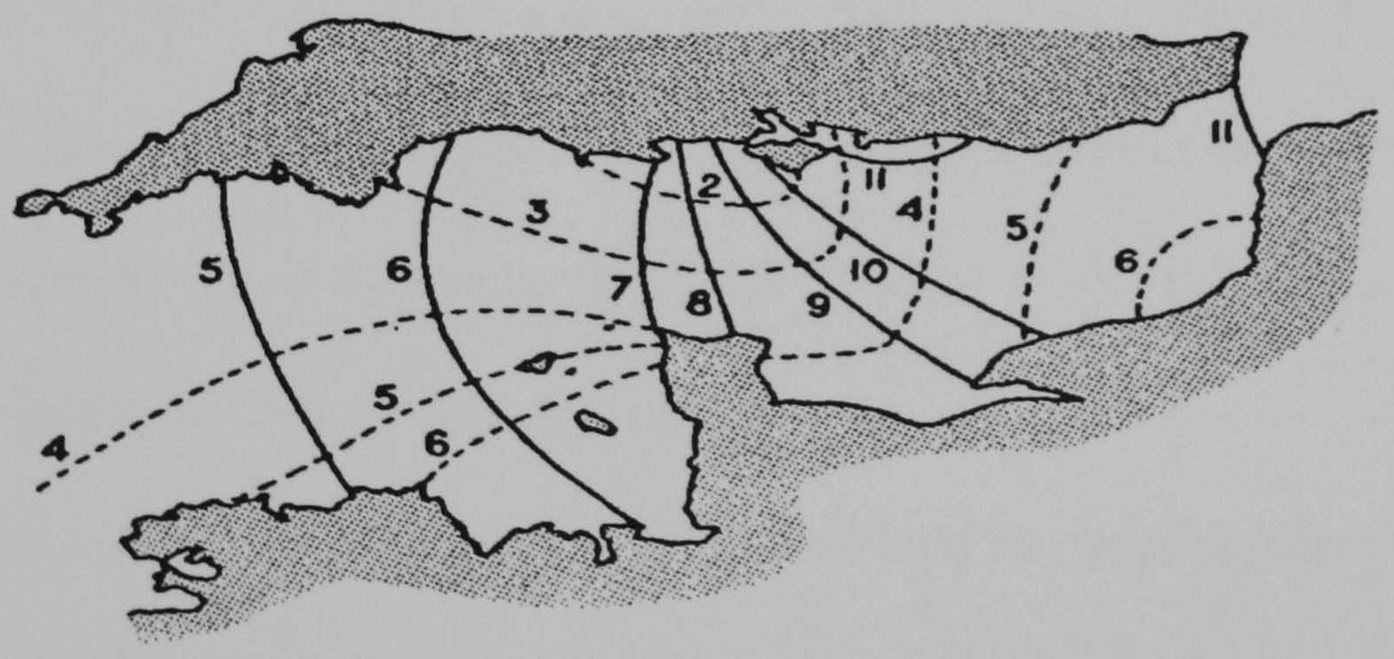

Figure 0.8: (**Gill, 1982**); Co-tidal lines (solid) with time in lunar hours, and co-range lines (dotted with values in meters) for the English Channel. [From Proudman (1953, p. 262); after Doodson and Corkan (1931).]

rotating canal.'

The solution for two Kelvin waves of equal amplitude travelling in opposite directions

is given as

$$\zeta = H\left\{e^{-y/a}\cos(mx-\sigma t) - e^{y/a}\cos(mx+\sigma t)\right\},$$

$$u = (gH)^{1/2}\left\{e^{-y/a}\cos(mx-\sigma t) - e^{y/a}\cos(mx+\sigma t)\right\},$$

$$v = 0.$$

He also noted the difficulty that arises in solving the problem by adding ends to the canal.

In discussing waves in an infinite canal, Poincaré (1910) considered the solutions (0.21) in his discussion.

He noted that the addition of the Poincaré wave does not solve the problem of finding the solution in a channel with an end, because the wave form (0.21) cannot undergo regular reflection.

But, this problem of dealing with the end condition was eventually solved by Taylor (1921) [12]. The new feature is the introduction of solutions like (0.21) with imaginary m so that this solution would have exponential fall-off away from the end of the channel. Then these terms influence the details of the solution near the end but do not affect the Kelvin waves except in the determination of the phase of the reflected Kelvin wave relative to that of the incident one.

The reflection is subject to a delay that increases with the width of the channel. As Taylor put it, the Kelvin wave progresses down one side of the channel, taking some time to cross the end of the channel before returning the other side.

If $\sigma < \sigma_{1c}$ (this is true in most natural channels when σ is the tidal frequency), the above assumption is true and no propagating Poincaré waves are possible. If $\sigma < f$ then the condition $\sigma < \sigma_{1c}$ is automatically satisfied.

If $\sigma > f$ then from (0.25), it can also be written

$$W^2 < \frac{\pi^2 g H}{(\sigma^2 - f^2)}$$

This means that the width of the basin should not be too large relative to the square root of the depth. If $\sigma > f$, then at least one Poincaré mode should be included in the description of the solution [see Brown, (1973)] [3].

In Fig(0.9), the solution obtained by Taylor is shown for a channel of 460 km wide

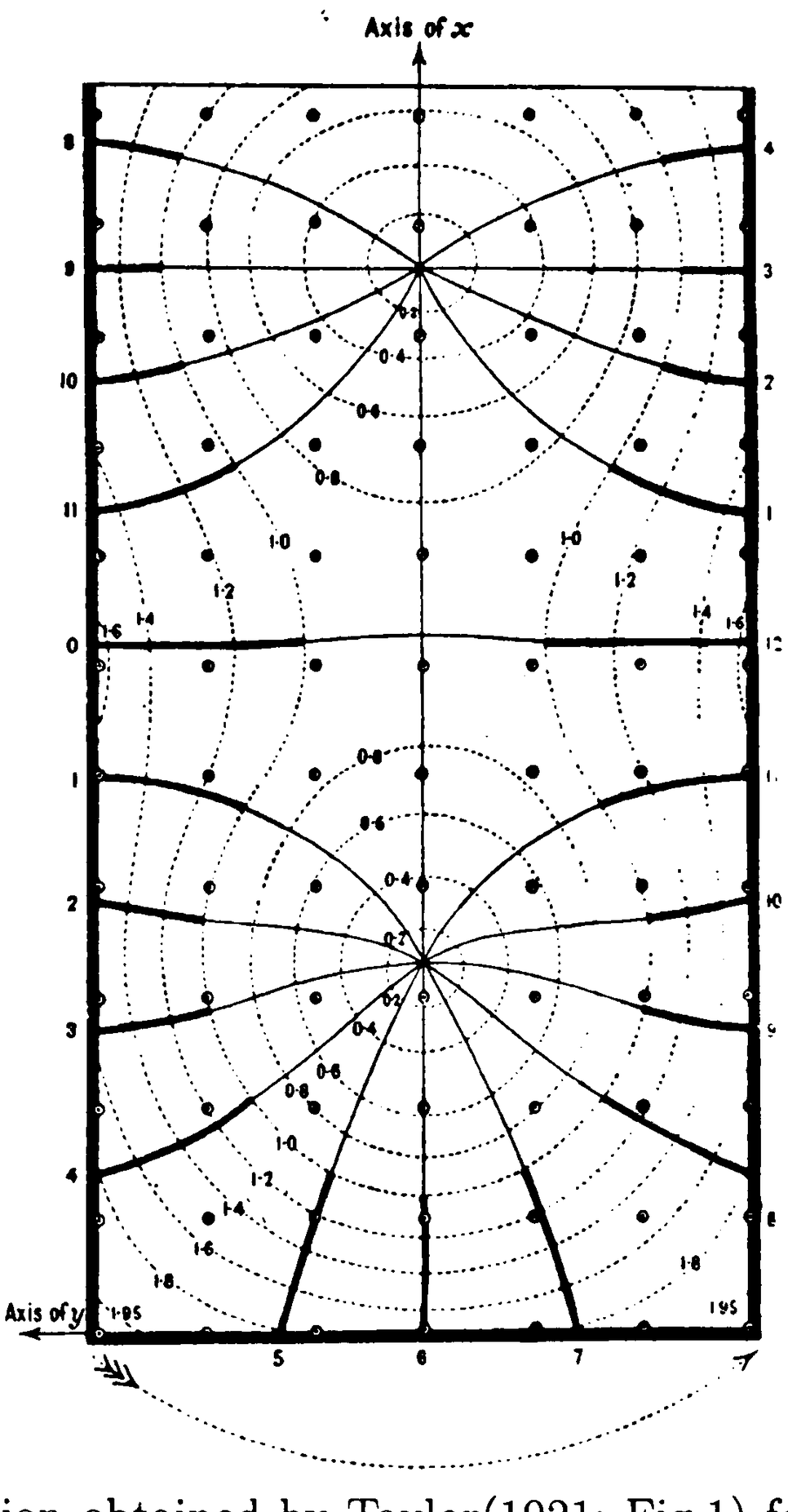

Figure 0.9: Solution obtained by Taylor(1921; Fig.1) for reflection of a Kelvin wave at the end of a channel with dimensions similar to those of the North Sea. Solid lines are co-tidal lines with time given in hours, and dotted lines show co-range lines.

and 73 m deep which resembles in dimensions and depth the North Sea. The value of c is 27 $m\ s^{-1}$. Since $\sigma = 1.4 \times 10^{-4}$, $f = 1.2 \times 10^{-4}$, the Rossby radius $a = 230$ km and therefore $W = 2\ a$. Therefore the above condition is well satisfied. In comparing

this solution with that for a narrow channel shown in Fig (0.4) we find that the configuration of co-tidal lines is similar. But the rate of progression of the phase around the head of the channel is very much slower than that in a narrow channel and also not very different from the rate progression along the sides.

Taylor(1921) states: In the lower part of the basin at a distance greater than about 250 miles from the closed end, the co-tidal lines and the motion of the particles correspond very nearly to two equal Kelvin waves moving up and down the channel. The tidal streams are very nearly parallel to the sides of the channel and the co-tidal lines move in along the right hand shore. The tidal wave then sweeps round the end wall of the basin at a rate rather greater than the velocity of the Kelvin wave, and moves back along the opposite shore to that along which it approached the end. In turning at right angles in order to cross the end of the channel, the wave produces a bigger rise and fall of the tide at the two corners than anywhere else in the field. On the scale chosen the range of the tide at the corners is represented by the number 1.95, whereas the greatest range in the distant parts of the channel, far from the influence of the end , is represented by 1.61.

To show more conspicuously the nature of the motion, the co-tidal lines have been drawn with heavy lines in the region where the rise and fall is greater than 1. The way in which the heavily marked parts of the co-tidal lines move down the left side of the diagram, cross the end and move up the right side, is conspicuous.

In the distant parts of the channel the tidal streams are parallel to the shores at all states of the tide. At distances less than the width of the channel, however the particles of water move in ellipses, except in regions close in shore they continue move parallel to the shore. The direction in which the particles move round the ellipses is

the same as that of the rotation of the earth.

The currents near the central part of the basin are considerably smaller than those close to the shore.

A particular interest is the behavior of a Kelvin wave at the channel end. A convenient way of describing the solution is in terms of a single Kelvin wave that propagates around the corners at the end of the channel without loss of energy, but with adjustments in phase produced by the process of turning the corner. This idea can be used in study of storm surges.

The wind can causes severe effects at the boundaries. The long-shore component of the wind stress causes an Ekman (wind exerts *frictional drag* on water surface, setting a thin layer of water at surface in motion) flow in the sea toward or away from the coast. In shallow seas, flow toward the coast produces piling up of water there and therefore abnormally high sea levels. This phenomenon is called a storm surge and it can play a major part in determining the shape of many coastal features.

Many early attempts to produce analytical solutions to tidal problems took the earth's rotation into account by incorporating the Coriolis parameter. In these investigations, basins of finite extent were employed as models and many approximations were invoked. By virtue of the closed nature of the basins the solutions of the tidal equations are solutions to eigenvalue problems. There are numerous examples of this, notably Lamb [18], who solved for circular basins in terms of Bessel functions and Taylor [12], who solved for rectangular basins in terms of exponential and circular functions.

The eigenfrequencies obtained in these cases are sufficient to show the possible frequencies of the tidal motion which would result if the systems were forced by an

external stimulus. Thus, without further information these solutions are not fully determinate [14].

Taylor [12] solved the co-oscillating tidal problem analytically in a rectangular basin open at one end so as to allow an incoming wave propagating from infinity to communicate with the basin. The resulting tide is then a forced oscillation and is said to 'co-oscillate' with the external tide. His solution represents the reflection of a Kelvin wave in a closed semi-infinite channel. Taylor's albeit simple model describes some of the essential features of the North Sea tides. He pointed out in his study 'Tidal Oscillations in Gulfs and Rectangular Basins' that streams in the south channel of the Irish Sea move backwards and forwards in a straight line. The rotation of the earth plays an important part in causing the rise and fall of the tide which is found to be four times greater on the Holyhead side of the channel than it is on the Irish side, but apparently without any elliptic motion of the water particles in the channel. He also pointed out that the tidal observations taken on both sides of the channel and the observations of tidal streams at various points across the channel indicate tidal waves of 'Kelvin' type moving in opposite directions up and down the channel.

Taylor further pointed out that in the southern entrance to the Irish Sea there exist two Kelvin waves moving inward and outward in the channel so that the Irish Sea acts as a reflector which reflects back the incoming Kelvin waves into waves of the same type. In this reflection the incoming Kelvin wave is greater on the shore that lies on the right hand side of the observer facing inwards while the outgoing wave is greater to his left.

Partial differential equations with elaborate boundary conditions can be solved numerically using finite element methods to yield very accurate solutions. There have been many computer simulations of tidal motion in the North Sea. The earliest was by Hansen (1956)[17]. Banks (1974) [20] investigated tide, surge and their interaction in the Thames-Southern North Sea region. The fig (0.10) illustrates the accuracy obtained and the amount of detail displayed using these computers.

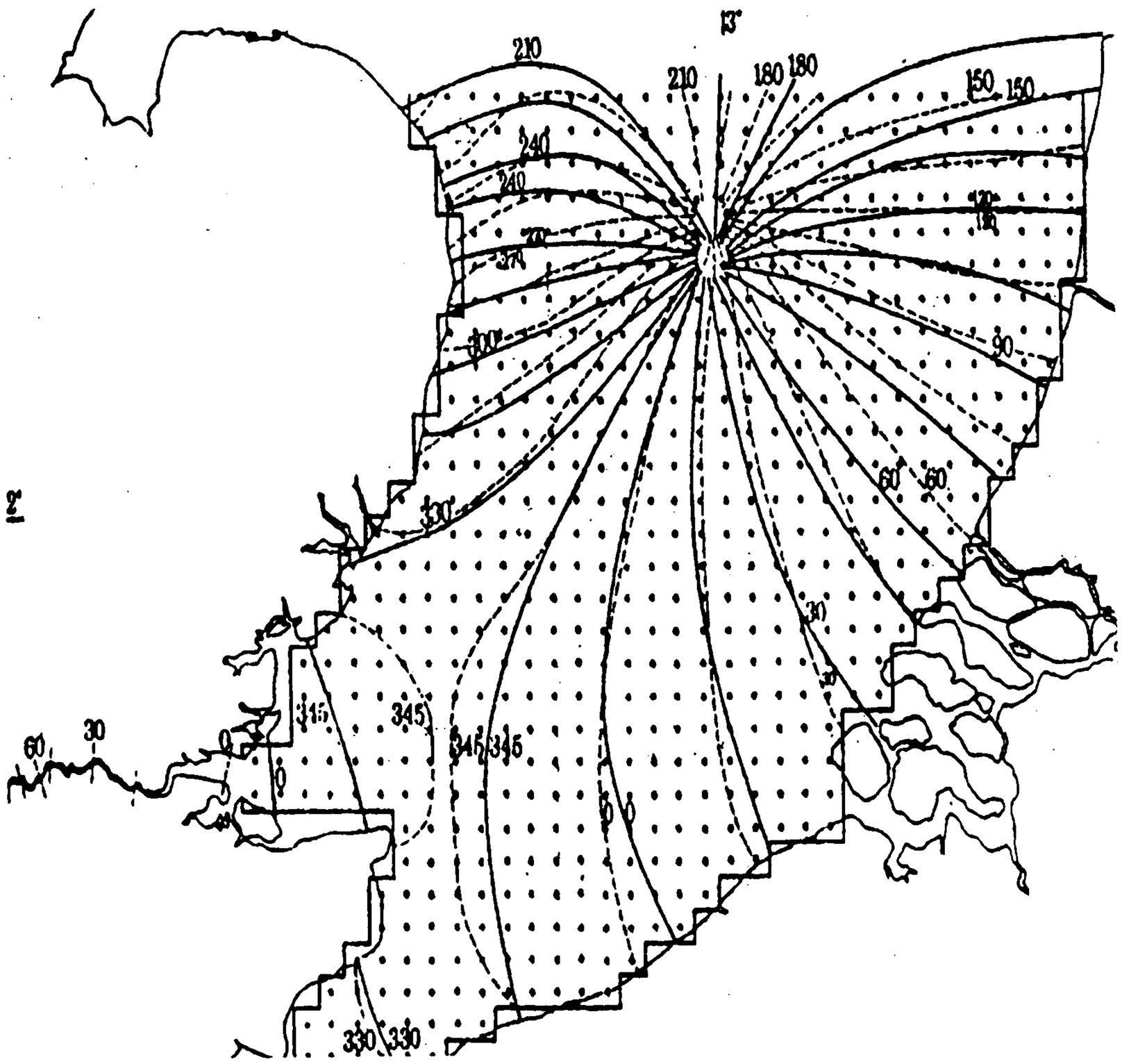

Figure 0.10: **(Banks,1974)** Co-tidal lines for the M_2 tide. -, Phase of tide in degrees, taken from Admiralty Chart 301; –, computed by means of Morass.

Davies(1994) [8] dealt with computation of large scale homogeneous tidal flow in the Irish Sea using two mutually exclusive methods. The models are three dimensional hydrodynamic numerical models. For an exhaustive list of contributions see

Davies (1994) [8].

Sand-Bank formation and the distribution and movement of sediment occur in the outer Thames Estuary. These processes are influenced by the tides and thus mathematical tidal models were considered by many authors initially in specific areas such as the outer Thames Estuary and the Southern Bight of the North Sea in conjunction with the Thames Estuary and the North Sea as a whole. Our present work is primarily concerned with tidal models in the North Sea taken as a whole.

Hunt and Johns (1963) [21] had extended the method used by Rayleigh and Schlichting in their investigation of non-linear effects in oscillatory boundary layers. It is suggested that the oscillatory tidal motion in shallow seas or oceans induces steady bottom currents, which contribute to the circulation within the North Sea and the movement of loose bed material by steady currents in conjunction with tidal oscillations lead to important changes in bottom topography. The movements of the Goodwin Sands and the Brake Bank provide well documented examples. The Norfolk Sandbanks (in the North Sea at $53^{o}N$, $2^{o}E$) are an example of tidal current ridges [29]. They are about 40km long and 2 km broad and rise to within 10 metres of the sea surface. Between the sandbanks (9km apart) the channels are fairly flat with a depth of about 40 metres. The tidal currents are approximately parallel to the sandbanks.

Hall and Davies (2004) [16] use a three-dimensional model to examine the influence of change in depth on the distribution of tidal bed stress. The geographical area they

covered is northwest European Shelf region and some parts of the Atlantic ocean. The direction of bed stress is an indicator of sediment movement as the bed load and various regions of convergence and divergence are in agreement with observations. Initially the model is forced by only the M_2 tides but subsequently they used other constituents such as S_2, N_2, K_1 and O_1 for tidal forcing. When water depths are reduced such that the North Sea and English Channel are separated then there is a significant change in the tidal distribution in the shallow Southern Bight which influences bed stress distribution and hence bed load sediment transport in the area.

By applying a two-dimensional, non-linear hydrodynamic numerical model incorporated with a semi-empirical equation for bed load sediment transport, Piney, Carbajal and Rivera (2005) [28] investigated the influence of geometry on the formation of sandbanks. The simplest configuration is a rectangular basin representing Taylor's problem as the solution of Taylor's problem explains fundamental properties associated with the propagation of tidal waves in semi-enclosed basin. Their aim is to extend the Taylor problem dynamics to the generation of sandbank patterns. They performed a numerical simulation for a rectangular basin 500 km long, 250 km wide and initial constant depth of 40 m. The geographical position of this basin corresponds to that of the North Sea. The basin was forced by a M_2 tidal wave with amplitudes and phases corresponding to the open northern boundary of the North Sea. After a simulation of 5 years the results reveal the formation of a group of sandbanks located in a small region at the closed boundary. These sandbanks occur where the incident Kelvin wave is reflected. Near the open boundary there is also a perturbation process which is related to the forced oscillation. As a result Poincaré waves are generated in this area.

Brown (1973) [3] generalized the Taylor's problem by carrying out a series of calcula-

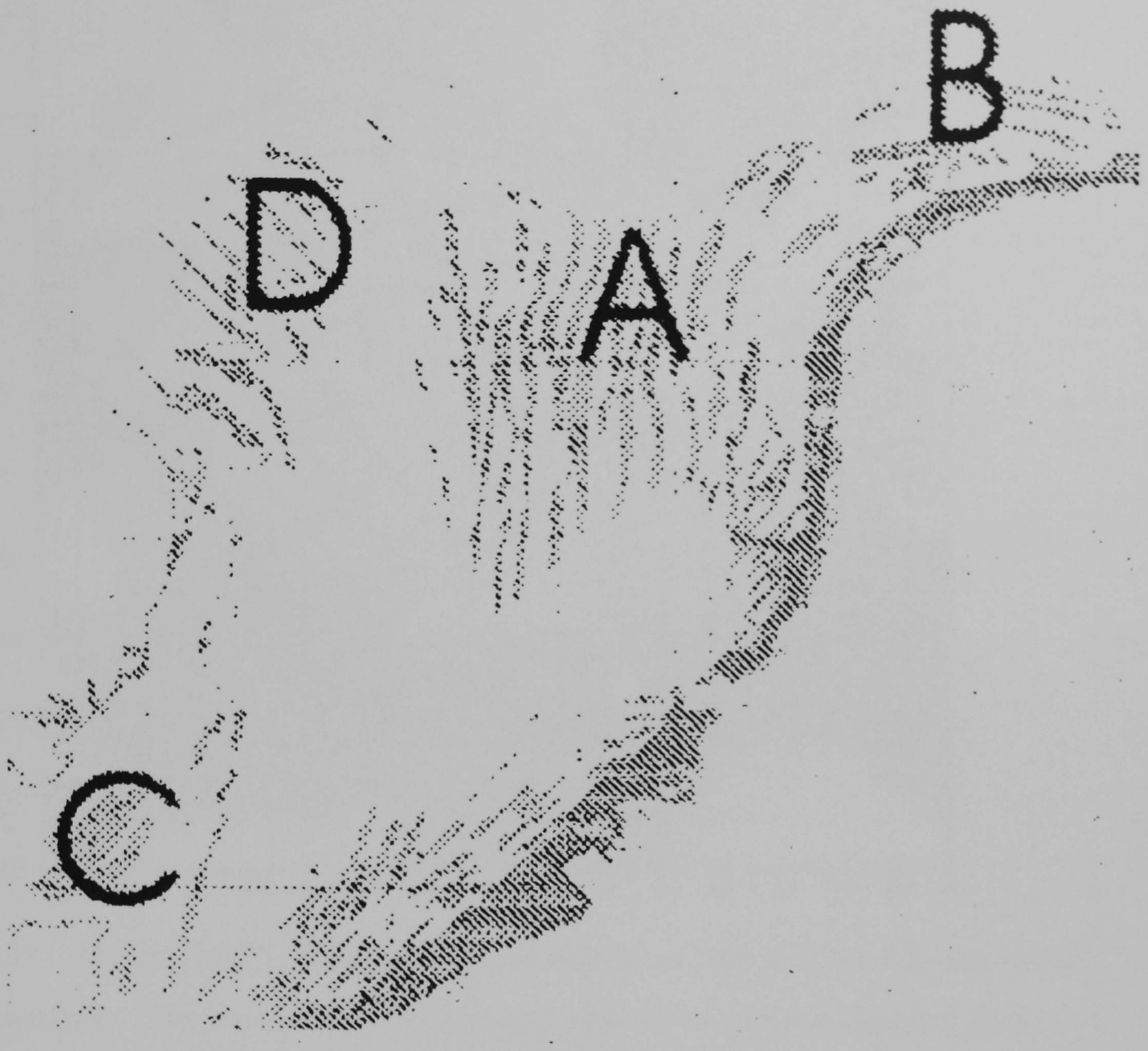

Figure 0.11: Sandbank patterns in the area of the Southern Bight of the North Sea. This plot was taken from Van de Meene and van Rijin (2000a,b).

tions for a fixed basin but with varying frequencies of the forced tides. For large wave lengths, the Poincaré modes are trapped at the closed boundary of a semi-enclosed basin. As the wave length of the incident wave decreases these modes can propagate towards the open boundary. The energy can then radiate in the form of Kelvin and Poincaré waves and the flow pattern in the basin varies as a function of the frequency of the forcing tide. One would expect that these flow structures influence the generation of sandbanks. In this investigation they found that with largest wave lengths,

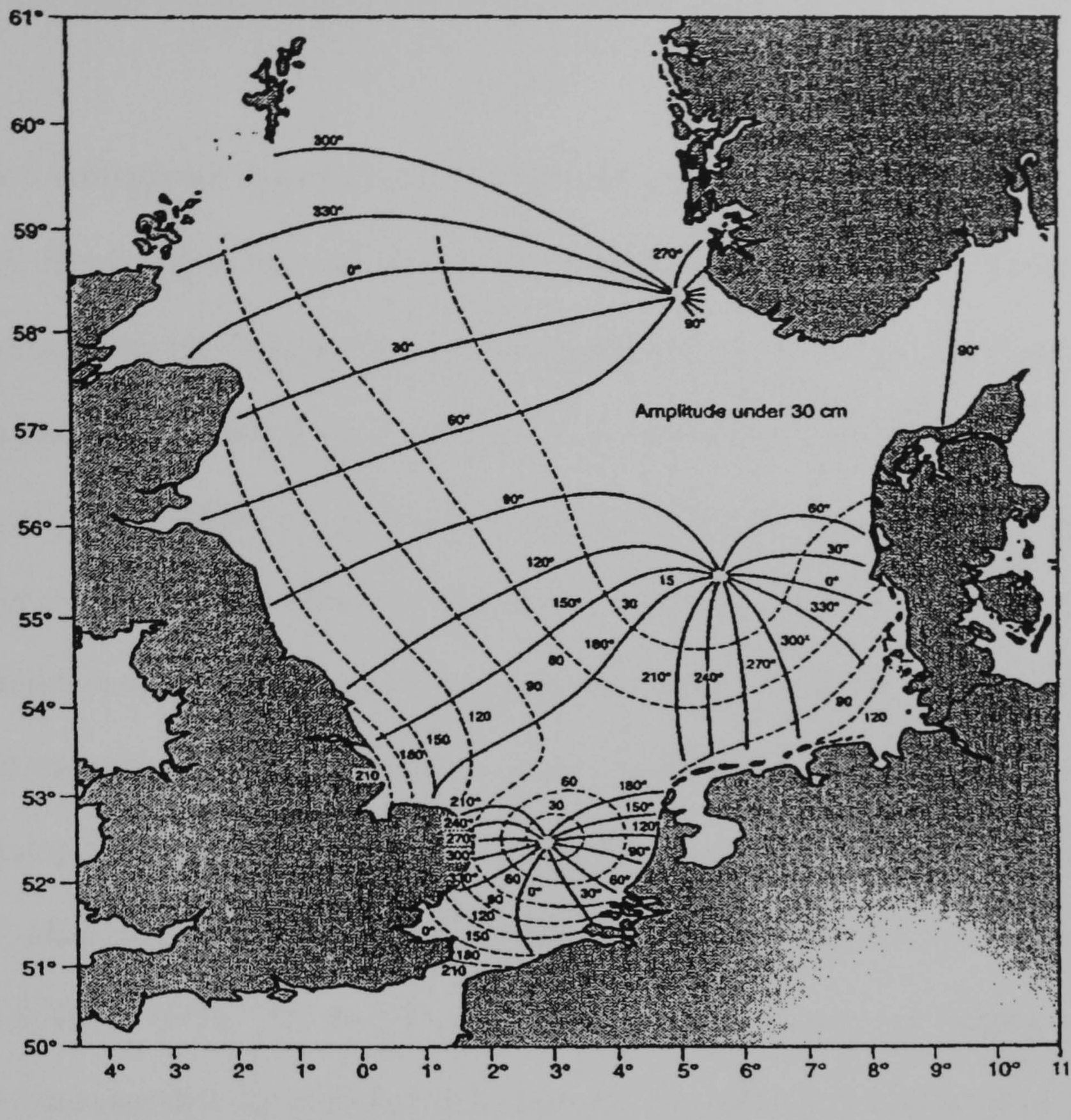

Figure 0.12: (**Dyke, 2007**); Cotidal and co-range lines, denoted by full and dotted lines respectively. The associated numbers give the values of θ (in degrees) and of A (in cm)

the sandbanks are generated more easily.

Near the southern boundary of the North Sea , particularly in the area where the Southern Bight and the North Sea are connected, there are a lot of sandbanks and shore-face-connected sand ridges. The plot in fig(0.11) was taken from Piney, Carbajal and Rivera (2005) [28]. A group of sandbanks extends across the sea between the land section and the peninsula is denoted by A. Similarly B and D can be related. The group of sandbanks located to the east of C are related to the Poincaré waves generated in the region where the English Channel and the Southern Bight of the

North Sea meet.

A closed rectangular channel can be considered as one formed by two right angled corners. Brown [4] in his work examined the works done by Buchwald (1968)[7] and in the same year by Packham & Williams (1968) [30] on the 'effect of a sharp corner on the passage of a Kelvin wave'. Buchwald considered the case of a Kelvin wave incident at a right-angled corner whereas Packham & Williams generalized Buchwald's work by considering the diffraction of a Kelvin wave at a corner of an arbitrary angle. It is shown that depending on the frequency, the Kelvin waves are either propagated around the corner without attenuation or alternatively they are propagated with reduced amplitude but with the addition of cylindrical waves called 'cylindrical Poincaré waves' which radiate from the corner at the expense of the diffracted Kelvin waves.

Webb & Pond (1986) [35] used Taylor's method to investigate the behavior of the Kelvin wave incident upon a bend in a channel. The solution is expressed as a truncated series of Kelvin waves and several evanescent cross-channel Pioncaré modes. Previous models of Kelvin waves propagating around bends have not included an opposite wall: they have bends in straight coastlines. In Buchwald's model a right-angled bend has been considered whereas Packham and Williams solved the problem of a bend at a general angle. Because there was no opposite wall, a reflected Kelvin wave was not possible and any energy not transmitted as a Kelvin wave had to be radiated as cylindrical Poincaré waves from the corner. A Kelvin wave with a certain frequency may be transmitted completely whereas Packham & Williams found there was only complete transmission for certain angles.

In the work of Webb & Pond (1986) they used linearized wave equations in a flat-

bottomed channel of rectangular cross-section. The incoming Kelvin wave incidents upon a bend.

In their method of solution they split the analysis domain into three regions- two straight channels (regions 1 and 3) and a sector of an annulus of a variable angle (region 2). The solutions in regions 1 and 3 are expressed as a sum of a Kelvin wave propagating away from the boundary with the region 2, and truncated infinite series of Poincaré modes, which decay away from the same boundary. The solution has a further component, namely an incident Kelvin wave of unit amplitude and zero phase. In region 2 (bend-region) the solution is expressed as a superposition of 'radial' Kelvin wave and Poincaré modes. Polar co-ordinates (r,θ) which are used to solve this problem.

There is a good account of discussion of 'Waves and Flows around Islands' using polar c-ordinates. This can be seen in (**Dyke, 2007**, page 351) [10].

Brown [4] considered some models incorporating the two effects of coastal curvature and friction.

His main aim was to extend the number of known analytical solutions to the first order equations by generalizing Taylors' model.

Taylor's model of Kelvin wave reflection in a closed semi-infinite is a simple basic mathematical model representing the tidal flow in the North Sea. However the method of solution is complicated as it requires the inversion of an infinite matrix. The difficulty arises from the mixed boundary conditions caused by the Coriolis effect. Despite its restrictive assumption the model proved successful in predicting the existence of amphidromic points and associated rotatory tides which are essential

features of the North Sea tides.

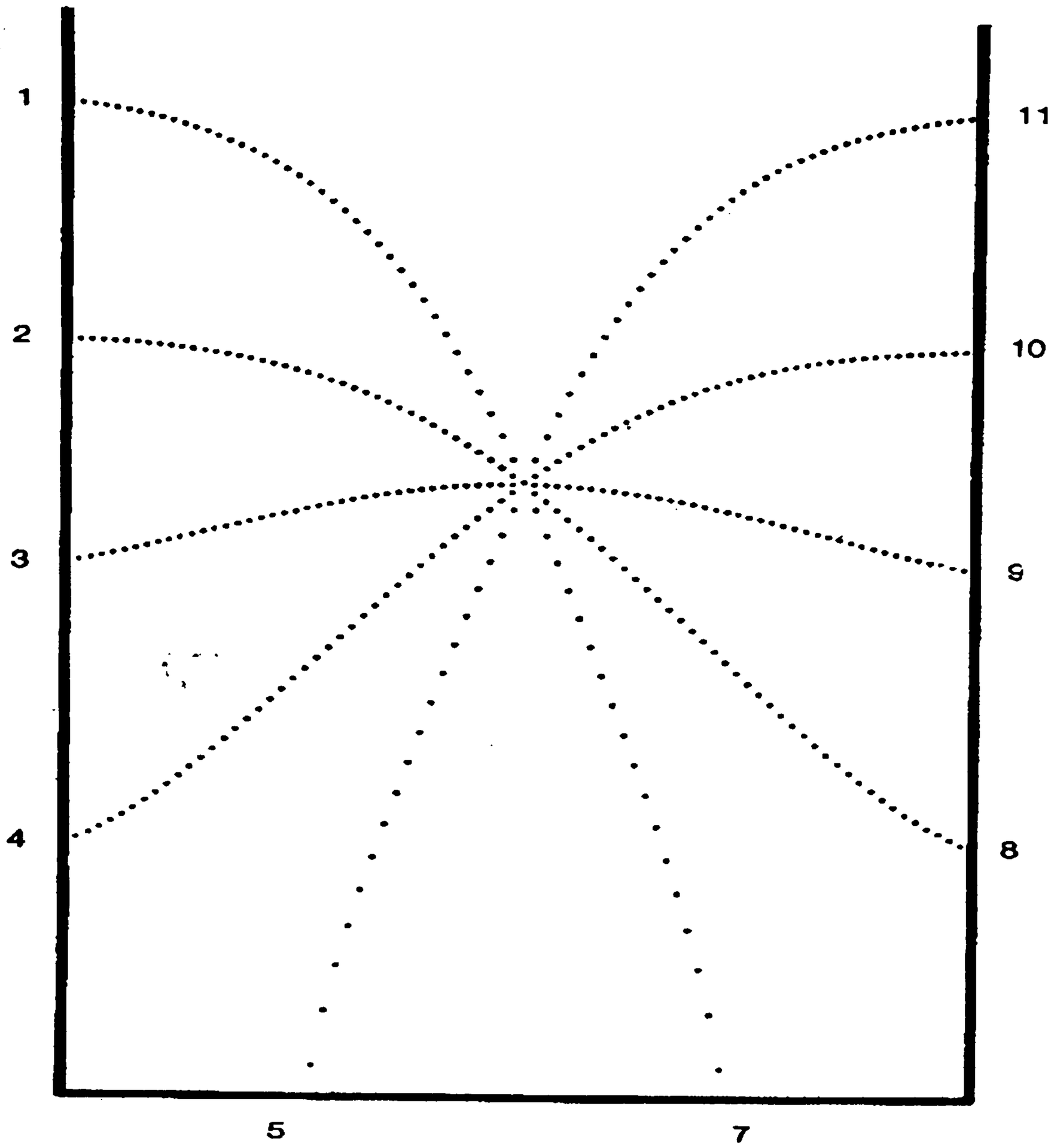

Figure 0.13:

However, Brown(1987) [5] pointed out that there are important features that Taylor's model fails to explain. For example, Taylor's model predicts that the tide would take nearly 3 hours to cross the channel at its closed end whereas from fig(0.12) we can see that the actual tide takes only one hour or so to cross the Southern Bight. Also we see that the tide in the Wash leads the Heligoland tide by approximately 5 h. Moreover, Taylor omits the effect of the strong tidal currents at the open southern

end of the North Sea. The strong influence of the oscillations in the Dover Strait or in Southern Bight on the reflection of the Kelvin wave in the North Sea is not considered. Brown extended Taylor's model to find the solution to the problem of perfect Kelvin wave reflection at an oscillating boundary which is representative of the Dover Strait or the Southern Bight. His solutions are found to be in much closer agreement than Taylor's with the actual tides in the North Sea.

Taylor considered a semi-infinite channel defined by $x > x_1$, $-\frac{1}{2}\pi \leq y \leq \frac{1}{2}\pi$, where (x, y) are horizontal co-ordinates. The value of x_1 has to be determined from the analysis. The depth of the channel is assumed uniform of depth h and rotate, about the vertical axis with an angular velocity of $\frac{1}{2}f$, where f is the Coriolis parameter. The long-channel and cross channel component velocity are given, respectively, by (u, v).

The system is 'Two equal Kelvin waves of angular frequency σ moving in opposite directions are combined with an infinite number of non-propagating Poincaré modes'. The superposition of these two systems of waves is such that the resultant long-channel velocity vanishes at the closed end $x = x_1$. The system is solved and the value of x_1 is found. The cotidal lines of Taylor's model are given in fig(0.13).

Thus, to incorporate the effects of the Dover Strait or the Southern Bight Brown (1978) generalized Taylor's problem by considering an oscillating boundary $F(y)e^{-i\sigma t}$ at the finite end of the semi-infinite channel $x_1 < x < \infty$.

The corresponding boundary condition for the long-channel velocity component then becomes

$$u(x, y, t) = F(y)exp\ (-i\sigma t) \qquad \text{on } x = x_1.$$

The function $F(y)$ is chosen to simulate the boundary flow. He found solutions for

any complex valued function $F(y)$ which has a Fourier expansion and showed that perfect reflection does not generally occur as some energy is lost or gained through the moving barrier at the end.

If the function $F(y)$ is real and even then

$$F(y) = F_1(y) + F_3(3y) + F_5(5y) + \ldots\ldots\ldots, \qquad (-\frac{1}{2}\pi \leq y \leq \frac{1}{2}\pi)$$

where,

$$F_m = \frac{2}{\pi}\int_{-\frac{2}{\pi}}^{\frac{2}{\pi}} F(y)\cos my dy. \qquad (m \text{ odd})$$

Taylor's analysis can then be carried out, resulting in the determinental equation for x_1. From this equation the value of x_1 can be found. The value of x_1 determines the relative phase of both the reflected Kelvin wave and the oscillating boundary with respect to the incoming Kelvin wave.

In the development of Taylor's model it is taken that $F(y)$ is real and even but this does not preclude $F(y)$ from taking on negative values. The inhomogeneity in the model produces a new feature. Thus a second solution can be obtained by replacing $F(y)$ by - $F(y)$. Now, there are two situations which represent perfect reflection and a corresponding zero energy flux across the boundary. The two solutions obtained with simulating functions $F(y)$ and $-F(y)$ respectively thus gives us two phases of the boundary oscillations which effect perfect reflection for a given flow profile.

Brown showed that all other phases of the boundary oscillation result in non-zero energy flux across the boundary. He further showed all such cases of imperfect reflection can be derived from the two perfect reflection solutions considered above.

He considered two simple profiles to simulate the boundary flow. Taking $F(y) = a\cos y$ where a is the maximum strength of the flow as a boundary layer oscillation

he applied Taylor's analysis and obtained the corresponding value of x_1; (x_1=0.9834, a=1). Similarly by considering the profile $F(y)$=-$a\cos y$, he obtained the value as (x_1 =-0.1280, a=-1). The corresponding co-tidal charts are given in fig(0.14) and fig(0.15). Clearly these two are independent solutions of perfect Kelvin wave reflection at an oscillating boundary of given profile.

In fig(0.14) it can be seen that the amphidromic point has been shifted southwards relative to Taylor's model fig(0.13) and the tide takes nearly 5h to cross from one side to the other side at the southern end. This amphidromic point corresponds closely to the Northern amphidromic point in the North Sea fig(0.12).

The amphidromic point in fig(0.15) on the other hand has been shifted northwards relative to Taylor's model and the tide takes less than 2h to cross the southern end. This corresponds closely with the North Sea southern amphidromic point in the southern Bight fig(0.12).

It is remarkable that the value of x_1=0.4278 in Taylor's solution is the arithmetic mean of the corresponding values (0.9834,-0.1280) in Brown's two solutions. Thus Taylor's model describes the 'mean' of the above two solutions. Brown tested with several representative profiles for the boundary function $F(y)$. For details of the investigation see (Brown, 1978,1987,1989) [4], [5] and [6].

In general, Taylor's formulation is not very practicable and thus Brown reformulated the model so that solutions can be directly obtained for any amplitude and phase of the boundary oscillation. He followed the formulation of Brown(1973) and adapted the collocation method to find a solution. For a given incoming wave and boundary flows, by varying the phase of the boundary oscillation he examined the effect on the reflected Kelvin wave and hence on the amphidromy. He added a set of Poincaré

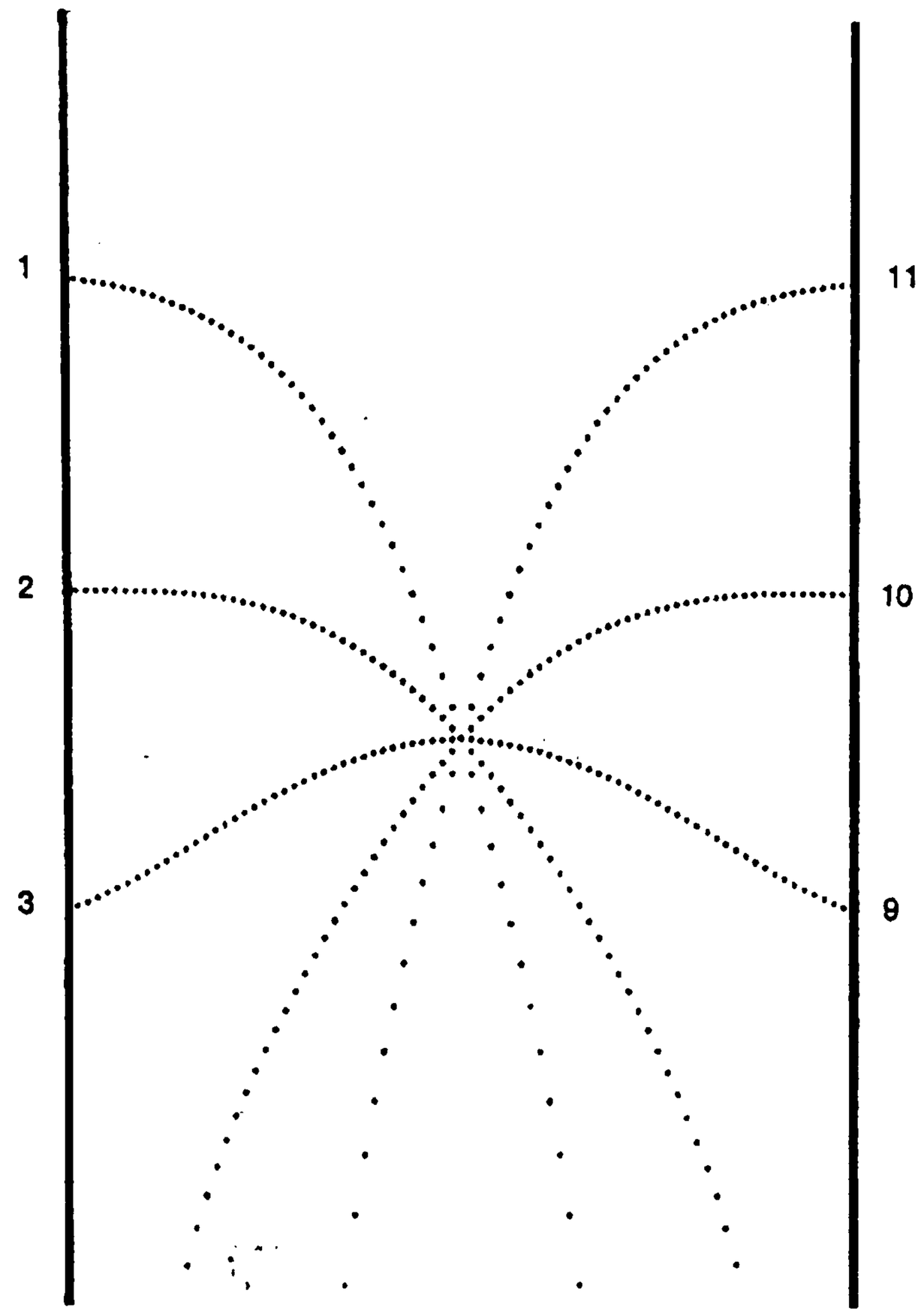

Figure 0.14:

modes to the Kelvin wave system and set the boundary condition as

$$u(0, y, t) = F(y)exp(i(\omega t + \varepsilon)).$$

where ε is the phase of the boundary flow. He used a simple boundary profile $F(y)$=$a\sin(\frac{\pi y}{l})$, a=parameter and l=width of the channel.

In fig (0.16) the plot of co-tidal lines at hourly intervals is given for the case $a = 0.3$. Only the amphidromic point nearest the boundary is drawn in the figures.

Brown's investigation successfully accounts for the strong influence of the Dover Strait

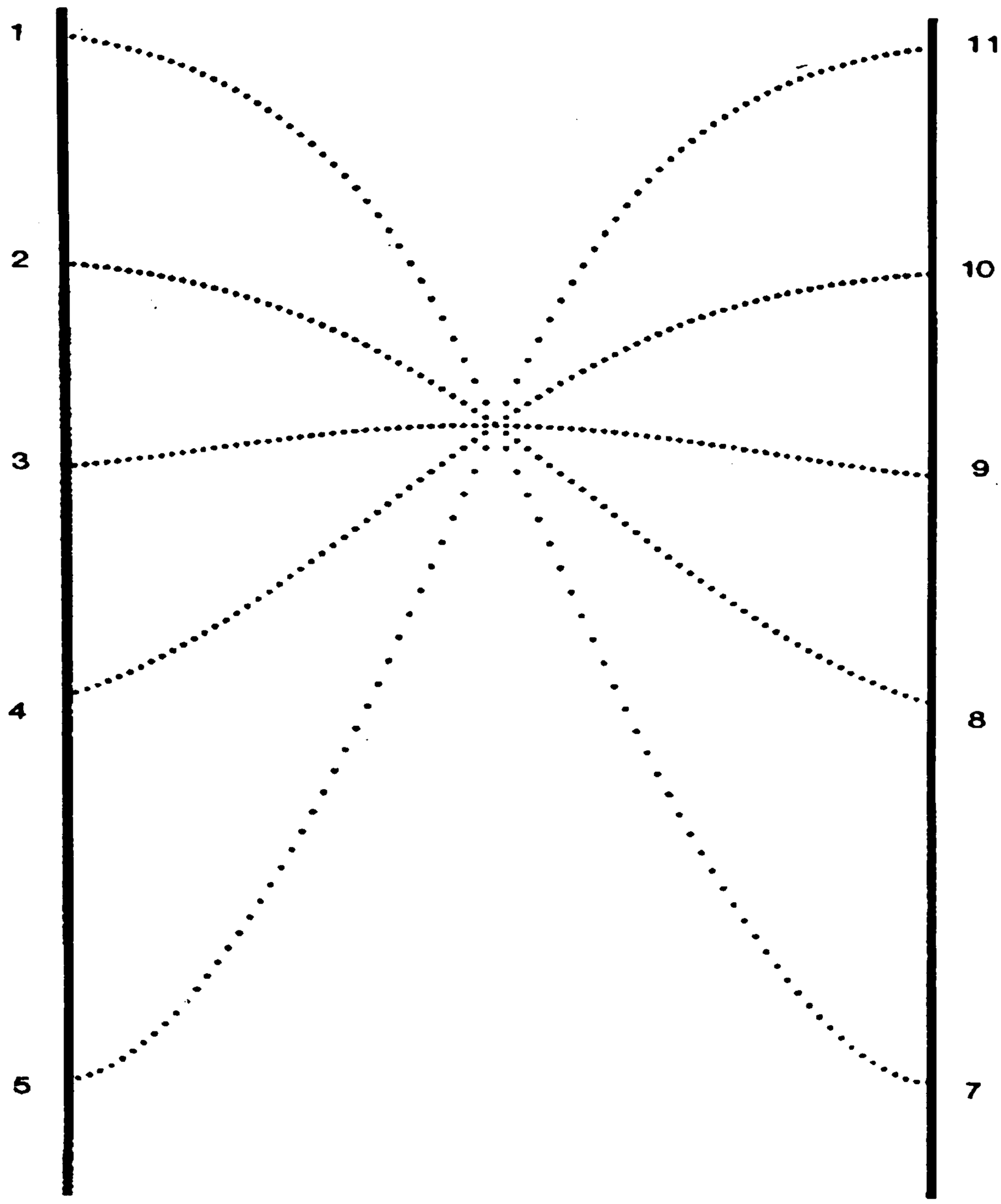

Figure 0.15:

or the Southern Bight. The method used may be called an indirect method because perfect reflection was first assumed and then the boundary located. In a cause and effect situation the reflected wave is treated as a cause rather than an effect.

In summary, Brown considered the effect of an oscillating boundary on the reflection of a wave and obtained analytical solutions.

The problem was well-posed because when the amplitudes and phases of the incoming wave and oscillating boundary are specified then the amplitude and phase of the

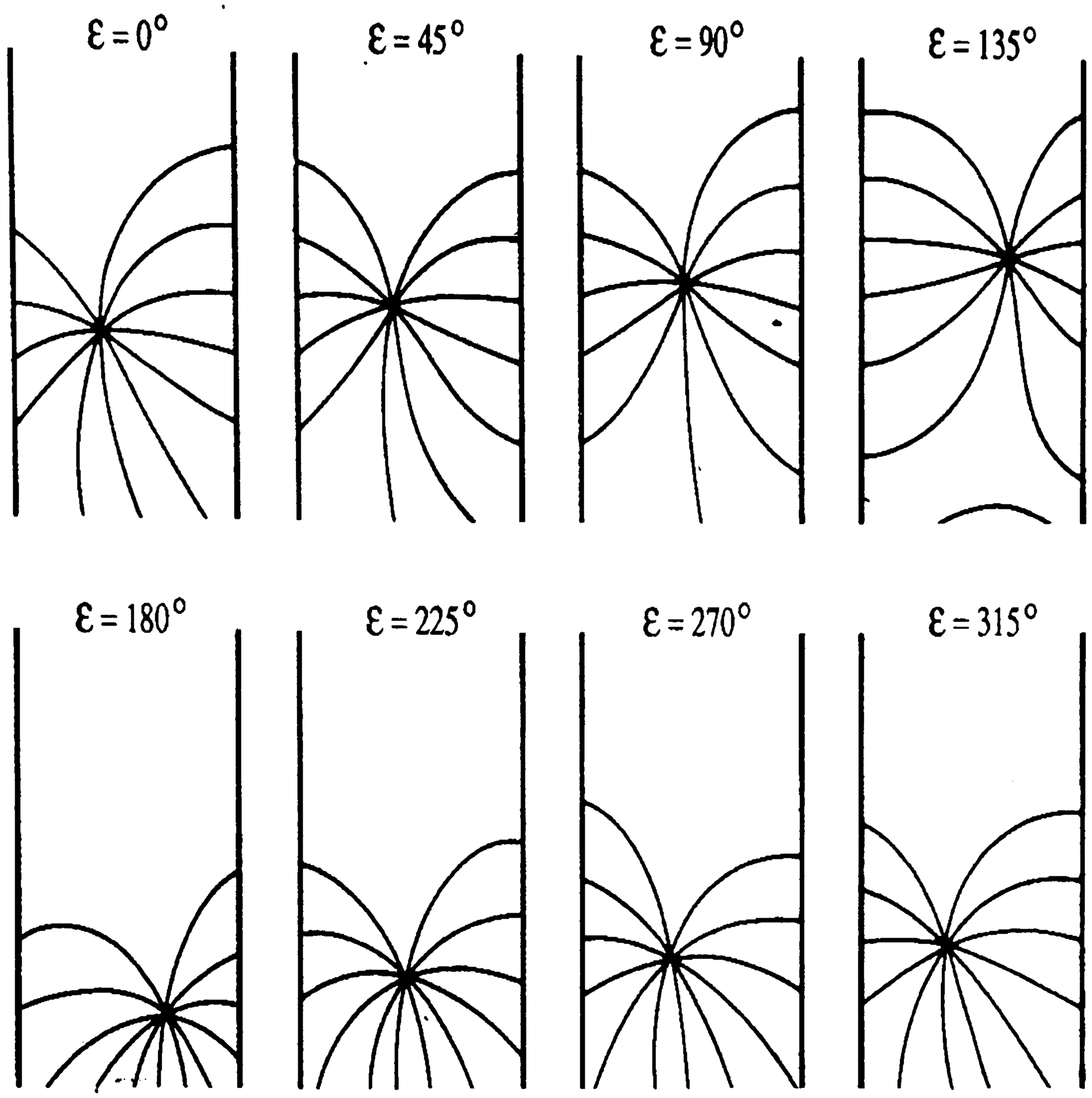

Figure 0.16:

outgoing wave is determined.

Furthermore he found there was a range of values which the reflection coefficient could take and thus perfect reflection does not generally occur.

If the reflection coefficient is less than unity the channel loses energy through the boundary and if the reflection coefficient is greater than unity the channel absorbs energy from the boundary. The direction of energy flow depends on the relative phase between the incoming wave and the oscillating boundary.

One of the important features of the ocean is the variety of bottom topography possessed by even a small basin such as the North Sea. It is notable that not enough is known about the interactions between ocean currents and waves and topography; and many analytic theories of ocean waves and currents generally ignore variations in depth. One of the reasons is that the interactions between oceanic flows(currents/waves) and topography are too complicated even in an idealized situation, to allow much analytic progress.

Energy can be propagated across the sea by a Kelvin wave system. In this propagation, waves are trapped or guided by a barrier or a coastline. The period of these waves is not restricted, Bondok(1980) [2].

Miles (1972, 1973) [26], [27] considered the diffraction of a Kelvin wave by variation in alongshore topography, such as the Earth's curvature and coastline geometry. Miles showed that alongshore varying topography can cause substantial changes in the amplitude and phase speed of Kelvin waves. The wave energy is approximately conserved for a Kelvin wave over a slowly varying topography along the coastline. The Kelvin wave evolves according to Green's law; that is the vertical displacement of the free surface is inversely proportional to the square root of the depth of the fluid and a phase that is given by the integral of the wave number. Miles showed that if the topography varies abruptly as a step, the Kelvin wave diffraction can be calculated by solving a singular integral equation whose solution is intractable without further approximation.

Killworth (1989a,b) [23] [24] generalized the problem by considering the Kelvin wave over a smooth ridge that is extending uniformly away from the coastline. The width

of the ridge is comparable to the Rossby radius.

Some work has been done e.g. Taylor(1921), Hendershott and Speranza (1971), T.Brown(1978), P.J.Brown(1973) on tides in small bays, gulfs etc such as the Adriatic Sea, Gulf of Califonia, Irish Sea and North Sea. These oceanic areas are too narrow and too deep for *Poincaré* modes to propagate energy, and *Poincaré* waves exist mainly as trapped waves in these regions. Thus the co-oscillating semidiurnal tidal energy in these areas primarily consists of superposition of Kelvin waves travelling in opposite directions.

In most of the works discussed, the depth of the sea is assumed uniform and the resulting co-tidal lines are drawn in the basin where a Kelvin wave is being reflected. In the case of the works of T.Brown,1978 [4] and Hendershott - Speranza(1971) [34] the displacement of amphidromic points away from the central axis of the bay become a unique measure of certain physical quantities (ie. energy loss) in contrast to Taylor's model in which he assumed perfect reflection of the Kelvin Wave.

More recently, S. Rizal (2002) [32] revisited the Taylor's problem and experiments were performed with channels at different geographical latitude with varying friction. Real and virtual (degenerate) amphidromic points were obtained and their displacement from the central axis of the channel accounted for the dissipation of tidal energy. The friction dependence of the amphidromic point on latitude strongly increases with decreasing latitude.

Our proposed work, focusing on the North Sea area, will be a development of the

work of previous authors, e.g. [12], Hendershot - Speranza (1971) but more particularly Brown,1978 [4], with a view ultimately to developing a semi-analytic model with a sloping bottom. For practical purposes the North Sea will be assumed about 550,000 km^2 in area, about 1000 km long and 640 km wide at its widest section. The bottom of the sea is not uniform but it generally slopes down from south to north and a broad section of the sea bed has irregular depths. Thus we propose to take possible 'depth changes' in the bottom of the sea into account in our model which we hope will result in closer agreement with observed values.

Taylor, in his paper determines the reflection of tidal waves from the closed end of a rectangular channel, which is infinite in one direction. This model represents an idealized North Sea where its depth is assumed to be uniform and coastline aligned North-South. But in a real situation the sea is not uniform. Towards the Danish coast the depth of the sea is about 37 m(120 ft). The water near the English coast is about 15 m (50 ft) deep. The greatest depth in the North Sea is found off the coast of Norway. Thus, by considering these variations in the depth of the sea, in a real situation, we cannot simply ignore effects of the bottom relief. Taking depth variation into account we look for a model of the sea, which is more realistic than that of Taylor.

As matter of simplicity we consider a simpler generalization to Taylor's problem wherein, two inter-communicating semi-infinite channels of different uniform depths meet at a boundary, say at $x = x_1$.

This may be regarded as the simplest model having some variation in bathymetry. The problem will be treated semi-analytically with a view to supporting other com-

putational models of the North Sea.

Chapter 1

Preliminaries

1.1 Equations of fluid motion on a rotating earth:

The equations of motion and continuity equation for a particle of water on a rotating earth of radius R rotating with angular velocity $\underline{\omega}$ may be written in the form [4]

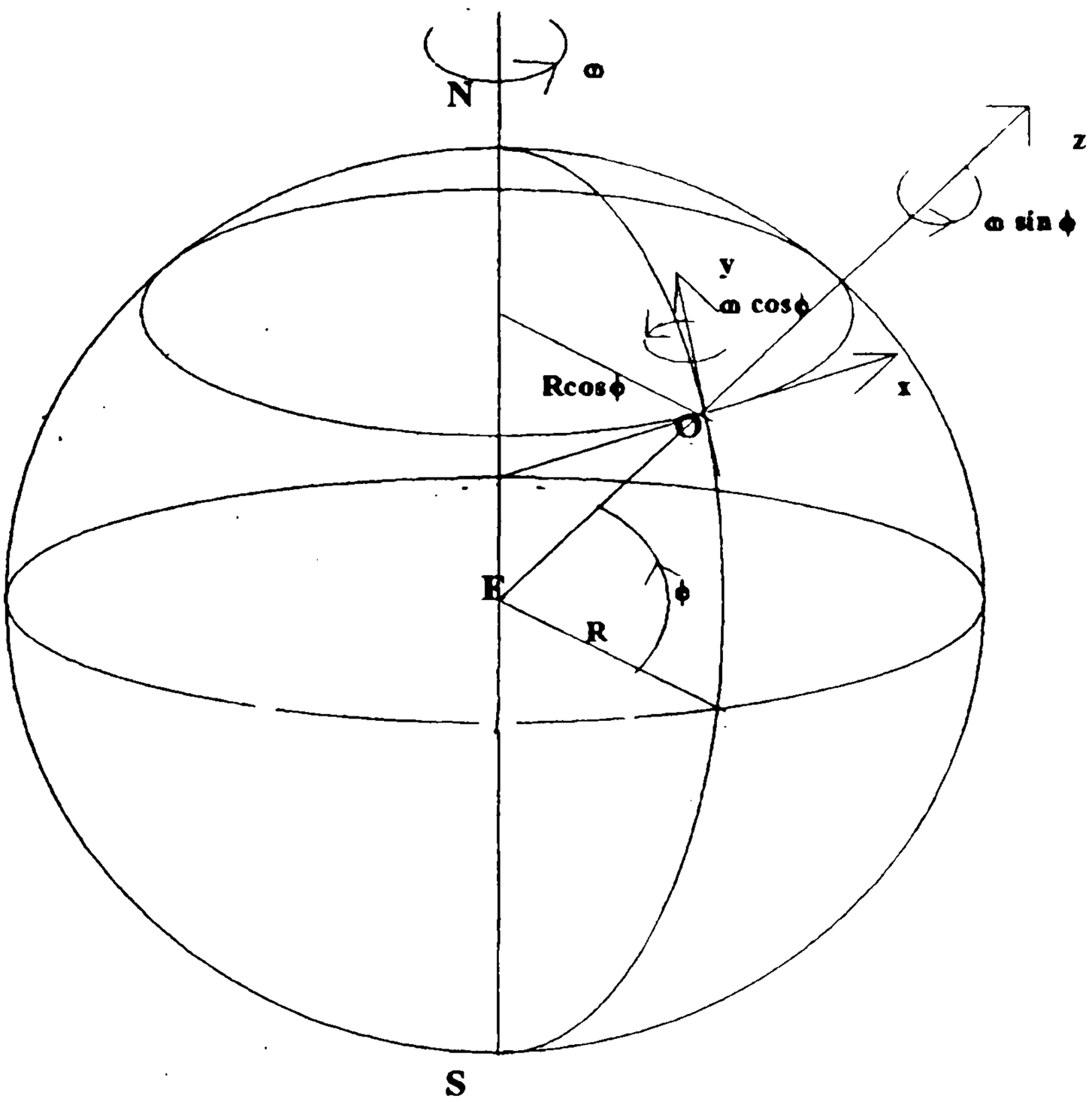

Figure 1.1: Rotating earth with angular velocity $\underline{\omega} \equiv (0, \omega\cos\phi, \omega\sin\phi)$, where ϕ is the latitude.

$$\begin{cases} \frac{du}{dt} - 2\omega\sin(\phi)v + 2\omega\cos(\phi)w = -\frac{1}{(R+z)\cos\phi}\left[\frac{1}{\rho}\frac{\partial p}{\partial x} + \frac{\partial G}{\partial x}\right] + X \\ \\ \frac{dv}{dt} + 2\omega\sin(\phi)u = -\frac{1}{(R+z)}\left[\frac{1}{\rho}\frac{\partial p}{\partial \phi} + \frac{\partial G}{\partial \phi}\right] + Y \\ \\ \frac{dw}{dt} - 2\omega\cos(\phi)u = -\frac{1}{\rho}\frac{\partial p}{\partial z} - \frac{\partial G}{\partial z} + Z \end{cases} \tag{1.1}$$

and

$$\frac{\partial \rho}{\partial t} + \mathrm{div}(\rho \underline{q}) = 0 \tag{1.2}$$

where

$$\underline{q} \equiv (u, v, w) \quad \text{and} \quad \underline{\omega} \equiv (0, \omega \cos\phi, \omega \sin\phi)$$

The symbols u, v and w represent the easterly, northerly and vertical components of the velocity $\underline{q}$ respectively and ψ, ϕ and z are longitude, latitude and height of the water particle with respect to an origin fixed on the surface of the earth and moving in a circle of radius $R\cos\phi$, where R is the earth radius along the line of latitude ϕ = constant.

The term G is defined by

$$G = -\frac{1}{2}(\underline{\omega} \wedge \underline{r})^2 + \Psi + \Omega. \tag{1.3}$$

where $\Psi = gz$ is the gravitational potential due to the earth's attraction and Ω is the potential due to the disturbing planetary forces. The blanket terms X, Y and Z include all other possible effects such as friction, turbulent stresses and wind.

The above equations (1.1) and (1.2) are non-linear owing to the term $\underline{q} \cdot \underline{\nabla}$ in Lagrangian accelerations $\frac{d\underline{q}}{dt}$.

1.2 Approximations

In order to find time-dependent solutions to the system defined by (1.1) and (1.2) above there are some useful approximations which can be used either separately or in some combination. In this section we shall deal with those which we shall have to resort to at one stage or another in this work.

As an immediate approximation we can ignore the small centrifugal term $\frac{1}{2}(\underline{\omega} \wedge \underline{r})^2$

in the equation (1.3) or alternatively it can be absorbed into the gravitational potential Ψ thereby obtaining an 'apparent gravity' [4].

The North sea area is relatively shallow and occupies a small volume in comparison with the world ocean. The height of the Lunar equilibrium tide in an open boundless ocean is about 0.5 meter (Wood, 1969)[37]. Thus the direct effect of the moon and the sun in the North Sea is negligibly small. We may thereby neglect Ω in equation (1.3).

The z-component of the equation of motion(1.1) can now be written as

$$\frac{dw}{dt} - 2\omega\cos(\phi)u = -\frac{1}{\rho}\frac{\partial p}{\partial z} - g \tag{1.4}$$

Clearly, the extraneous forces and the gravitational effects due to the moon and the sun in the vertical direction can be neglected in comparison with the earth's gravity [4].

Usually in equation (1.4) it is assumed that

$$|2\omega\cos(\phi)u| \;<<\; |g|$$

As an example at latitude $\phi = 53^o$ if the North Sea experiences a tidal velocity $u = 1m/sec$, we have for the l.h.s. approximately $\frac{2\pi}{24\times60\times60} \times \frac{1}{2} \times 1 = 0.00036361 <<$ 9.81.

Clearly, the vertical Coriolis force can be neglected from equation(1.4), since ap-

proximately

$$|\frac{2\omega u \cos\phi}{g}| < 4 \times 10^{-5}.$$

The vertical acceleration in equation (1.4) can also be neglected. This can be tentatively justified for a progressive tidal wave. If we integrate equation (1.4) with respect to z from an arbitrary point z to the free surface elevation ζ we obtain

$$\rho \int_z^\zeta \frac{dw}{dt} dz + \rho g(\zeta - z) = (p - p_a) \tag{1.5}$$

(where p_a is the atmospheric pressure at the free surface)

We assume for convenience $z = 0$ as the undisturbed free surface and we take the maximum vertical acceleration of the water particle as α. Then we have in equation (1.5)

$$\rho\alpha h + \rho g\zeta = (p - p_a) \tag{1.6}$$

where h is the undisturbed depth of water.

In equation (1.6), if we have

$$\alpha\ h << g\ \zeta \tag{1.7}$$

then the equation (1.4) can be further simplified to

$$0 = \frac{1}{\rho}\frac{\partial p}{\partial z} + g. \tag{1.8}$$

It follows that terms $\frac{\partial p}{\partial z}$ and ρg are always almost balanced. This is the near balance in the vertical between the gravity force and the vertical pressure gradient, called the hydrostatic approximation and expressed by

$$\frac{\partial p}{\partial z} = -\rho g. \tag{1.9}$$

The equation(1.9) states that the pressure deviation from atmospheric at a point is given by the weight of fluid above that point.

The balance of forces expressed by this equation is correct to a very high order of approximation for most large-scale oceanic phenomena including those considered here in the North Sea.

If the period of the wave is given by $\frac{\lambda}{c}$, where λ = wave length and c = wave speed (given by the formula $c^2 = gh$), then, provided the wave slope is small everywhere, the vertical velocity is of the order of $\frac{c}{\lambda}\zeta$ and the vertical acceleration is similarly of the order of $\frac{c^2}{\lambda^2}\zeta$. Here ζ denotes maximum elevation.

Thus the condition (1.7) is satisfied provided

$$\frac{h^2}{\lambda^2} << 1 \tag{1.10}$$

The inequality (1.10) is called the long wave condition and is certainly satisfied for tides in the North Sea. This condition may be satisfied also for open ocean tides where the depth of the ocean may be several miles. The hydrostatic approximation is a successful and useful assumption in the theory of tides.

1.3 North Sea:

Here, we consider the relevant features of the North Sea. The North Sea is the epicontinental sea containing water separating Great Britain from Belgium, the Netherlands, Germany, Denmark, Sweden and Norway. It is a shallow Sea described as a North-eastern arm of the Atlantic Ocean open to the North Atlantic in the North, extending from the edge of the continental shelf north of the Shetland Islands, southward to the Strait of Dover which leads into the English Channel and to the Skagerrak, a channel to the Baltic Sea in the east.

The area of the North Sea is about 570,000 km^2, 1000 km long and 600 km wide

Figure 1.2: map showing the locations of the places mentioned in this work

at its widest point with an average depth about 100 meters. The greatest average depths are found in the North (360 feet to 600 feet; 110 meters to 180 meters) and in a peculiar trench, the Norway Deep (or Gut) which runs parallel to the Norwegian coast depths generally decrease southward and between England and Denmark lies a plateau, Dogger Bank, over which depths of less than 60 feet (18 meters) occur in an area exceeding 250 square miles (650 sq km). That is, the bottom of the sea slopes steadily down to the north from south although south of the Dogger Bank, there is a broad area of irregular depths. In the south western portion of the North Sea specifically off the Norfolk coast in the outer Thames estuary and near the Dover straits we can see long straight sand banks which are linear and fairly stable and are

mainly orientated with the strong tidal currents. Some are exposed at low water.

We can divide the North Sea into four regions according to temperature and salinity stratification [4]. Along the Norwegian coast haline stratification is present the whole year.

Further out there is a region where haline stratification is still present but the annual salinity changes are irregular. The central region is homohaline throughout the year but thermally stratified seasonally. But throughout the whole year, the southern portion is both homohaline and essentially homothermal.

In the North Sea tides are primarily semi-diurnal. The ratio of diurnal to semi-diurnal waves along the coast varies from 0.1 to 0.2 (Defant, 1960)[9].

Tidal waves mainly enter the North Sea from the North Atlantic ocean through the opening between Scotland and Norway. Most of the wave energy propagates southwards and is reflected by the Heligoland coast or transmitted into the Southern Bight of the North Sea. A small portion of the wave energy passes through the Kattegat into the Baltic Sea. Tidal current also enters the North Sea into the Southern Bight through the Straits of Dover.

In fig (1.3) it can be seen clearly that there are two amphidromic points, one is situated in the Southern Bight ($52.7^{o}N$, $3^{o}E$) and the other one is situated in the east of Dogger Bank ($55.8^{o}N$, $5.3^{o}E$). Around these two amphidromic points, co-tidal

lines are rotating in the anti-clockwise direction. It is also found, off the southern coast of Norway, a crowding of co-tidal lines indicating a virtual amphidromic point inland. These are also important features for the North Sea.

Tidal range along the Scottish coast is about from 3 to 5 meters, along the east coast of England and at the Straits of Dover is about from 4 to 7 meters. Along the Heligoland coast the tidal range is about from 2 to 3 meters but in the open sea it is about from 0 to 2 meters.

Tidal currents near the Straits are higher ($1.5\ m\ sec^{-1}$ to $2.5\ m\ sec^{-1}$) than those in the open ocean ($1\ m\ sec^{-1}$ to $1.5\ m\ sec^{-1}$).

The North Sea area is relatively shallow and occupies only 2.5×10^{-5} percent of the world oceanic volume.

The principal constituent of the North Sea tides is the lunar semi-diurnal tide thereby the North Sea receives its tidal energy by co-oscillating with the external Atlantic tide at the M_2 frequency, see Brown [4].

On considering the size of the North Sea in comparison with the world ocean the sphericity of the earth can be neglected and the Coriolis parameter $f = 2\omega \sin\phi$ is taken as a constant. Then we can replace $\frac{1}{(R+z)\cos\phi}\frac{\partial}{\partial\psi}$ by $\frac{\partial}{\partial x}$ and $\frac{1}{(R+z)}\frac{\partial}{\partial\phi}$ by $\frac{\partial}{\partial y}$ in the first and second of the momentum equation (1.1) and the North Sea can be regarded as a plane rotating with angular velocity $\frac{1}{2}f$.

The density ρ in equation (1.2) may be taken as a constant as our present work is primarily concerned with the southern portion of the North Sea which is not strat-

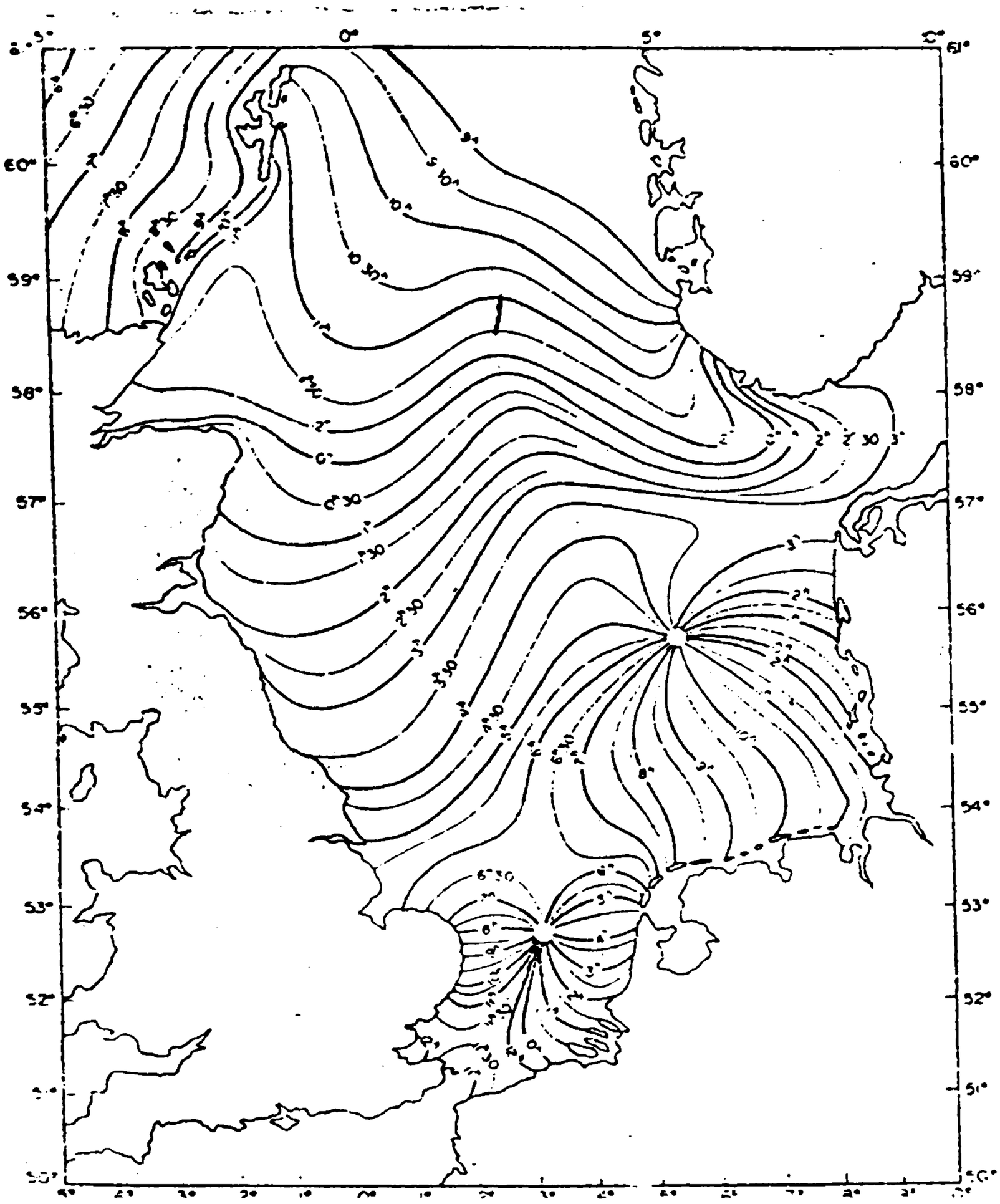

Figure 1.3: **Defant, 1960**, Lines of the same time interval between upper culmination of the moon in Greenwich (solar hours) and high water.

ified. Therefore, the equation (1.2) can be reduced to

$$div(\underline{q}) = 0,$$

which can be written in the rectangular co-ordinate system as

$$\frac{\partial u}{\partial x} + \frac{\partial v}{\partial y} + \frac{\partial w}{\partial z} = 0. \tag{1.11}$$

If we denote the average depth of the North Sea as 'H' and the average width of the North Sea as 'L' we have,

$$\frac{H}{L} << 1.$$

Similarly, if we denote the average velocities in the vertical and horizontal directions by W and V or U respectively then by the virtue of the condition (1.11) we infer that $\frac{U}{L}$, $\frac{V}{L}$ and $\frac{W}{H}$ are of the same order. Hence,

$$V >> W. \tag{1.12}$$

Thus, by (1.12), we can neglect the term $2\omega\cos(\phi)w$ in comparison with the term $2\omega\sin(\phi)v$ in the first momentum equation of (1.1).

Finally, the hydrostatic approximation (1.8) enables us to express the pressure in our first two momentum equations of (1.1) in terms of the free surface elevation, namely

$$p = p_a + \rho g(\zeta - z).$$

Having made all these approximations and simplifications, the field equations can be written as

$$\begin{cases} \frac{\partial u}{\partial t} - fv = -g\frac{\partial \zeta}{\partial x} + X, \\ \\ \frac{\partial v}{\partial t} + fu = -g\frac{\partial \zeta}{\partial y} + Y, \\ \\ \frac{\partial u}{\partial x} + \frac{\partial v}{\partial y} + \frac{\partial w}{\partial z} = 0. \end{cases} \tag{1.13}$$

The rotation of the earth is an important factor and it has an influence even on an area as small as the outer Thames Estuary. This effect manifests itself as an amphidromic point (a point in the sea which experiences no tide itself but around which the high water sweeps) in the Southern Bight. This amphidromic point can be seen in figs (1.3) and (0.10). This suggests that the Southern Bight and outer Thames Estuary in the North sea can be usually treated as a single entity.

The occurrence of amphidromes does not depend purely on earth's rotation because according to Krauss, 1973 (page 145)[36] the simplest amphidromic system can be formed by suitably combining waves at right angles. However, with regard to the Southern Bight, this possibility is ruled out because the Southern Bight receives tide only from the North and the South.

The importance of the earth's rotation reflects from another finding (Hydraulic Research Station, 1974) [4]. From the results of the numerical modeling of the outer Thames Estuary, the hypothetical effect of reversing the Coriolis force was examined. The results were shown in fig (1.4) and fig (1.5) for the low water interval. The differences observed in these two figures are striking evidence to show the importance of the earth's rotation. Thus, in most of our work, we do not neglect the effects of earth's rotation (i.e f).

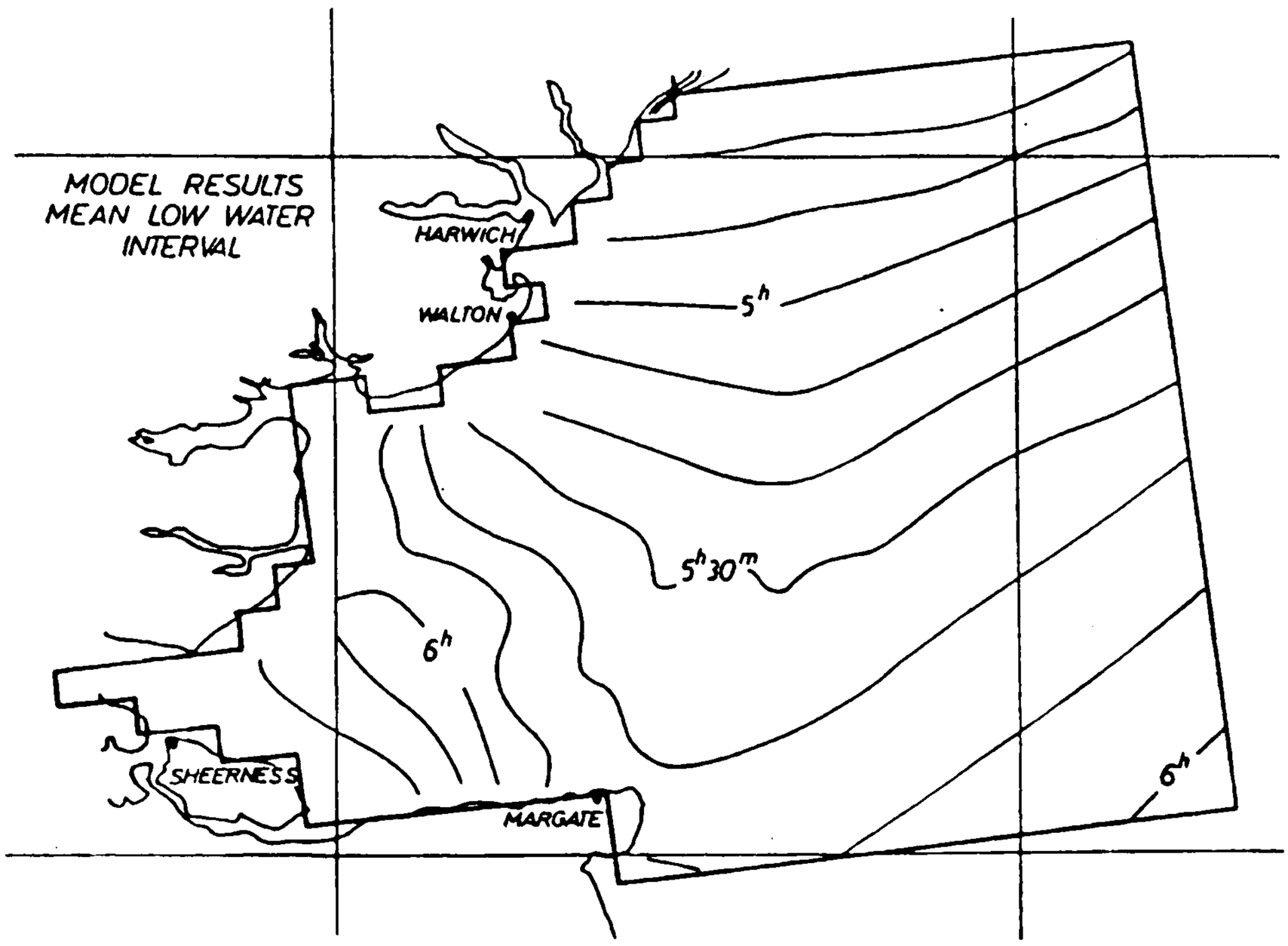

Figure 1.4: **(Hydraulics Research Station, 1974)**, (Brown, 1978)

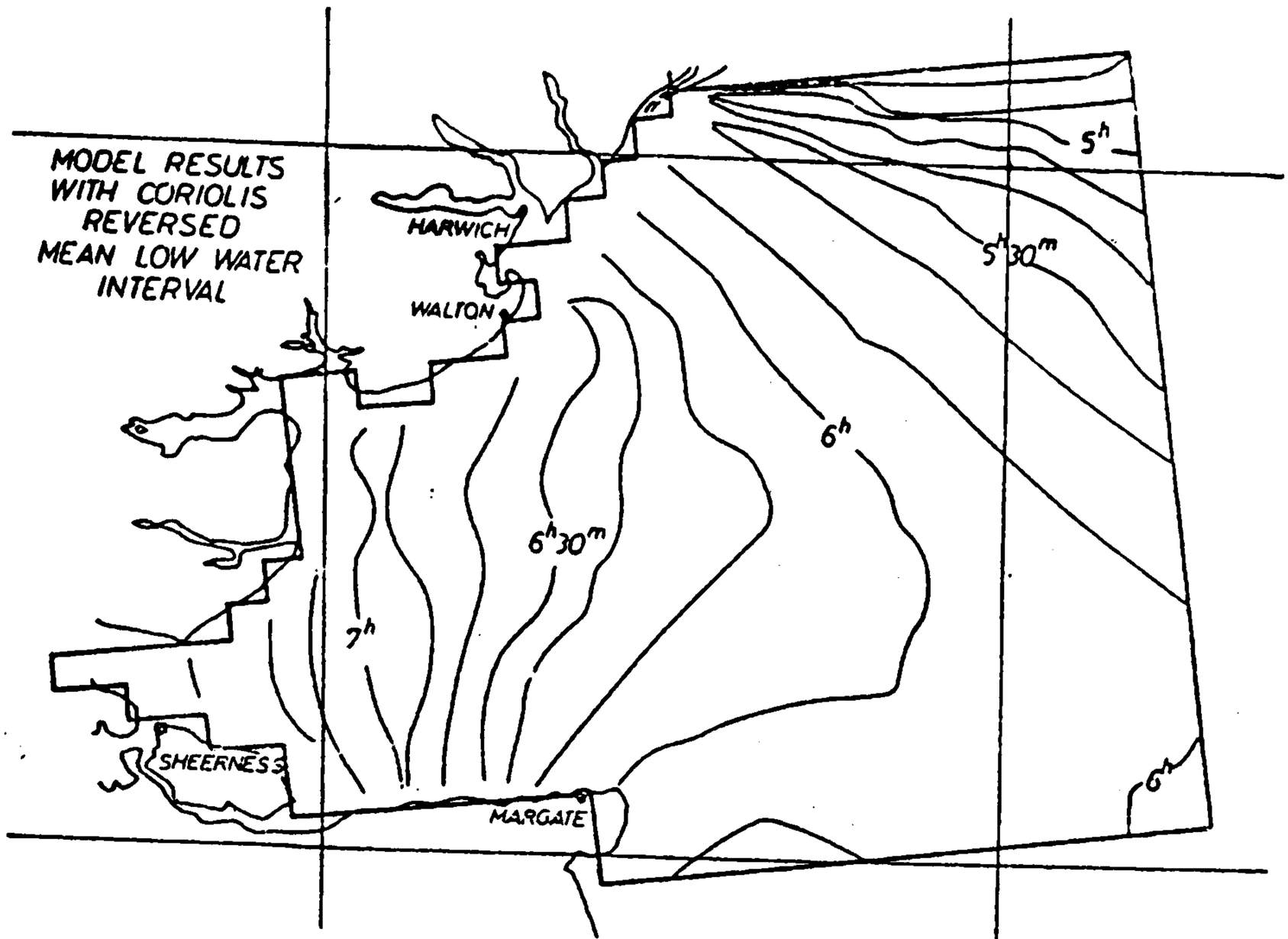

Figure 1.5: **(Hydraulics Research Station, 1974)**, (Brown, 1978)

1.4 The fundamental solutions:

In this section we consider oscillatory solutions to the basic tidal equations with (i) no earth's rotation (ii) earth's rotation.

1.4.1 Case of no rotation:

Here, we consider the nature of the tidal waves in the absence of the earth's rotation (i.e. the Coriolis force is neglected).

By ignoring the non-linear terms and extraneous forces (X,Y) in the system (1.13), the first two equations of the system can be written as

$$\frac{\partial u}{\partial t} = -g\frac{\partial \zeta}{\partial x} \qquad \text{(i)}$$

$$\frac{\partial v}{\partial t} = g\frac{\partial \zeta}{\partial y} \qquad \text{(ii)} \qquad (1.14)$$

We choose a sinusoidal plane wave solution of the form,

$$\zeta = A\sin(kx - \sigma t), \tag{1.15}$$

where,

A = Amplitude of the wave,

σ = angular frequency of the oscillation,

k = wave number.

Without loss of generality, the wave (1.15) has been chosen to propagate in the x-direction.

On inserting the solution (1.15) into the system (1.14) we obtain

$$u = \frac{gAk}{\sigma}\sin(kx - \sigma t)$$

$$v = 0. \tag{1.16}$$

We assume that the undisturbed depth of the ocean, h, as a constant. Then, in the absence of a steady current, on integrating the continuity equation in the system (1.13), we obtain

$$w = -\frac{Agk^2}{\sigma}(z + h)\cos(kx - \sigma t) \tag{1.17}$$

where

$w = 0$ at the sea floor $z = -h$.

The free surface condition requires that on $z = 0$,

$$w = \frac{\partial \zeta}{\partial t}. \tag{1.18}$$

Using (1.15) the condition (1.18) can be written as

$$w = \frac{\partial \zeta}{\partial t} = -A\sigma\cos(kx - \sigma t),$$

which, on introducing (1.17), yields a relation,

$$\frac{\sigma}{k} = \pm\sqrt{gh}. \tag{1.19}$$

For a given frequency the relation (1.19) gives us the value of the wave number k and hence also the wavelength $(\frac{2\pi}{k})$. This shows that the plane wave is possible for any given frequency but the waves are horizontally crested and the particle motion is rectilinear.

The relation (1.19) is called the dispersion relation although no dispersion occurs in this case because the phase speed $\sqrt{gh}$ is independent of the wave length.

Here, we see that the horizontal velocity is independent of depth whereas the vertical velocity depends on h and decreases linearly with depth.

Thus, the trajectory of a fluid particle is given by the ellipse

$$(x - x_0)^2 + \frac{(z - z_0)^2}{k^2 (z_0 + h)^2} = \left(\frac{Agk}{\sigma^2}\right)^2 \tag{1.20}$$

where, (x_0, y_0, z_0) denotes the equilibrium position of the fluid particle.

This elliptical orbit is highly oblate since $k\ h << 1$, which is the long wave requirement.

This elliptical path degenerates into a straight line on reaching the sea floor.

This type of non-rotating plane waves can propagate in the open ocean. Since the lateral particle velocity vanishes identically it can propagate along a straight coast line or in a rectangular channel provided the boundaries are parallel to the x-axis. According to (Arx, 1962) [1] combination of this type of wave in all directions crudely

accounts for the three dimensional behavior of the oceans.

Since our primary concern in this work is restricted to semi-diurnal frequency waves, it is interesting to investigate how the non-rotating and rotating systems independently account for the properties of tidal waves.

We consider two plane waves with same amplitude and frequency but travelling in opposite directions:

$$\zeta_1 = A_1 \sin(kx - \sigma t), \qquad \text{(i)}$$

$$\zeta_2 = A_2 \sin(-kx - \sigma t). \qquad \text{(ii)} \tag{1.21}$$

The resultant wave is given by

$$\zeta = \zeta_1 + \zeta_2 = -A\cos(kx)\sin(\sigma t). \tag{1.22}$$

As all points on this resultant wave (1.22) are either in phase or anti-phase we call this wave a standing wave.

Now the system is defined by

$$\begin{cases} \zeta = \zeta_1 + \zeta_2 = -A\cos(kx)\sin(\sigma t) \\ u = \frac{gAk}{\sigma}\sin(kx)\cos(\sigma t) \\ v = 0 \\ w = -\frac{AgK^2}{\sigma}(z+h)\cos(kx)\cos(\sigma t). \end{cases} \tag{1.23}$$

The longitudinal velocity vanishes for all time in the nodal plane,

$x = n\,(\frac{\pi}{k})$ where n is an integer,

Thus, if a barrier inserted at $x = 0$, say, the above motion would be undisturbed. We can then say that the constituent waves travelling towards the barrier is perfectly reflected.

We have seen that a sinusoidal plane wave solution to the system defined by (i) and

(ii) of (1.14) travelling in the x-direction impinge on a barrier at $x = 0$ perfectly reflected. The resultant wave is a standing wave.

Now a rectangular sea closed at one-end ($x = 0$) communicating with the open ocean at the other end $x = l$, at which it is subjected to a periodic oscillation given by

$$\zeta = A\cos\sigma t.$$

The sinusoidal wave solution of the above system in this rectangular sea subjected to the relevant boundary conditions can be written as

$$\zeta = A\frac{\cos(\sigma x/\sqrt{gh})}{\cos(\sigma l/\sqrt{gh})}\ \cos\sigma t,$$

$$u = A\sqrt{(\frac{g}{h})}\ \frac{\sin(\sigma x/\sqrt{gh})}{\cos(\sigma l/\sqrt{gh})}\ \sin\sigma t,\ \text{and}\ v = 0. \tag{1.24}$$

1.4.2 Rotating system:

Open Ocean:

When we account for the rotation of the earth, the relevant equations of motion are

$$\text{Momentum equations:} \begin{cases} \frac{\partial u}{\partial t} - fv = -g\frac{\partial \zeta}{\partial x} \\ \\ \frac{\partial v}{\partial t} + fu = -g\frac{\partial \zeta}{\partial y} \end{cases} \tag{1.25}$$

and the Equation of continuity

$$\frac{\partial u}{\partial x} + \frac{\partial v}{\partial y} + \frac{\partial w}{\partial z} = 0. \tag{1.26}$$

If equation(1.26) is integrated with respected to the z-co-ordinate; making use of the boundary conditions at $z{=}{-}h$ and $z{=}0$ we obtain

$$h\left(\frac{\partial u}{\partial x} + \frac{\partial v}{\partial y}\right) = -\frac{\partial \zeta}{\partial t}. \tag{1.27}$$

We try again a plane wave solution of the form

$$\zeta = A\sin(kx - \sigma t).$$

On inspection of the equations from (1.25) to (1.27) we gather that the field variables u and v also should be of the same form

$$u = B\sin(kx - \sigma t)$$

$$v = C\cos(kx - \sigma t) \text{ where } B \text{ and } C \text{ are constants.}$$

On substitution of these in these equations (1.25), (1.26)and(1.27) we obtain

$$B = \frac{\sigma}{kh}A,$$
$$C = -\frac{f}{kh}A \quad \text{and} \quad k^2 = \frac{(\sigma^2 - f^2)}{gh}.$$

Thus a plane wave solution is possible if and only if

$$\sigma > f \tag{1.28}$$

(i.e., wave frequency is greater than inertial frequency due to the rotation of the earth)

Sometimes this condition is expressed as $T_p < T_F$ where T_p is the period of oscillation and T_F is half a pendulum day.

(A pendulum day is the period of revolution of a Foucault pendulum which is equal to $\frac{2\pi}{\omega\sin\phi}$ where ϕ is the latitude)

This wave is known as Sverdrup wave [4] is in contrast with the non-rotating plane wave where the currents in a Sverdrup wave continuously change direction 'cum sole' (clockwise direction in the Northern Hemisphere and anti-clockwise direction in the Southern Hemisphere). The horizontal particle velocity of a Sverdrup wave never vanishes at any point or at any time. Thus a single Sverdrup wave can only propagate

in the open Ocean. Sverdrup waves are sometimes called horizontally crested waves or rotatory waves.

The phase velocity of a Sverdrup wave is given by

$$\frac{\sigma}{k} = \frac{(\sqrt{f^2 + k^2 gh})}{k}. \tag{1.29}$$

whereas the phase velocity for the corresponding non-rotating plane wave system is $\sqrt{gh}$. The equation (1.29) implies that the phase velocity for a Sverdrup wave system exceeds the phase velocity for the corresponding non-rotating plane wave system. Furthermore, the equation (1.29) indicates that the phase velocity of Sverdrup waves depends on the wave-length of the waves and thus Sverdrup waves are dispersive waves and their group velocity is given by

$$\frac{d\sigma}{dk} = \frac{kgh}{\sqrt{f^2 + k^2 gh}} \tag{1.30}$$

which is less than $\sqrt{gh}$.

It clear from above that in the case of no rotation of the earth (ie $f = 0$) Sverdrup waves reduce to non-rotating plane waves.

Kelvin waves:

We look for a solution of equations (1.25) and (1.27) with the transverse particle velocity v vanishes identically. This is equivalent of introducing a horizontal boundary so that it coincides with the x-axis and that a semi-infinite ocean is contained in the half-plane $y > 0$.

Thus equations (1.25) and (1.27) become

$$\frac{\partial u}{\partial t} = -g\frac{\partial \zeta}{\partial x}, \tag{1.31}$$

$$fu = -g\frac{\partial \zeta}{\partial y}, \tag{1.32}$$

$$h\frac{\partial u}{\partial x} = -\frac{\partial \zeta}{\partial t}. \tag{1.33}$$

On differentiating (1.33) with respect to t and (1.31) with respect to x we obtain the wave equation for ζ by eliminating u from the two resulting equations.

$$\frac{\partial^2 \zeta}{\partial t^2} = gh\frac{\partial^2 \zeta}{\partial x^2}. \tag{1.34}$$

Thus the solutions of(1.34) which satisfy (1.32) are given by

$$\zeta = e^{\frac{-f}{\sqrt{gh}}y} F_1(x - \sqrt{gh}\, t) + e^{\frac{f}{\sqrt{gh}}y} F_2(x + \sqrt{gh}\, t). \tag{1.35}$$

and

$$u = \sqrt{\frac{g}{h}}\, e^{\frac{-f}{\sqrt{gh}}y} F_1(x - \sqrt{gh}\, t) - \sqrt{\frac{g}{h}}\, e^{\frac{f}{\sqrt{gh}}y} F_2(x + \sqrt{gh}\, t). \tag{1.36}$$

where F_1 and F_2 are arbitrary functions.

In the Northern Hemisphere the Coriolis parameter, $f > 0$. Since exponentially large values are not physically acceptable we take $F_2 \equiv 0$. Thus we obtain the solution as

$$\zeta = e^{\frac{-f}{\sqrt{gh}}y} F_1(x - \sqrt{gh}\, t), \tag{1.37}$$

which represents a Kelvin wave in the region $y > 0$ moving in the positive x-direction along the straight coast. The speed of propagation is $\sqrt{gh}$. Since this speed is independent of the wave length, the waves are not dispersive, and thus it maintains

its shape in motion. The motion is rectilinear and the transverse wave profile is exponential. That is $\zeta \to 0$ as $y \to \infty$. In addition, in the Northern Hemisphere the wave travels with the boundary to right of its direction of propagation, since $f > 0$ in this case. In the Southern Hemisphere the boundary lies to the left of propagation. Thus we should expect such a wave moving northwards up the Californian coast, or northwards along the Atlantic Argentinian coast. The longitudinal wave profile in (1.37) is given by F_1 which can be regarded as a Fourier synthesis of many frequency components. As we are primarily concerned with the semi-diurnal frequency wave in this work, F_1 in (1.37) is replaced by a sinusoid of semi-diurnal frequency. Thus a harmonic Kelvin wave is obtained in the form

$$\zeta = e^{\frac{-f}{\sqrt{gh}}y} \sin(\frac{\sigma}{\sqrt{gh}}x - \sigma t),$$

$$u = \sqrt{\frac{g}{h}}\zeta \quad \text{and} \quad v = 0. \tag{1.38}$$

If we put $f = 0$ in the Kelvin wave system (1.38) it reduces to a non-rotating plane wave.

The current velocity here is positive. Thus we should expect the force due to earth's rotation to be to the right of the current motion. This is in fact so, for we can see that such a force is balanced by the slope of the sea surface in the y direction.

Infinite Channel: An infinite channel can be considered as a region bounded by two infinite straight coastlines. In such a region Kelvin wave motion is possible as the transverse velocity is identically zero. Though the length of the channel is infinite, the width of the channel is finite and thus Kelvin waves can propagate in either direction. The solutions implied by equation (1.35) are both admissible.

In particular we can add two harmonic Kelvin waves travelling in opposite directions

but with equal amplitudes,

$$\zeta = Ae^{(f/c)y}\cos[(\sigma/c)x + \sigma t] - Ae^{-(f/c)y}\cos[(\sigma/c)x - \sigma t], \tag{1.39}$$

where $c = \sqrt{gh}$.

We take the x axis to coincide with the central axis of the channel. This in fact has the effect of shifting the origin along the central axis to coincides with a point of zero amplitude-an amphidromic point about which the cotidal lines rotate.

On differentiating (1.39) partially with respect to time and setting $\frac{\partial \zeta}{\partial t} = 0$, we obtain

$$\frac{\tanh(f/c)y}{\tan(\sigma/c)x} = \tan(\sigma t + \pi/2), \tag{1.40}$$

which defines the lines of high (and low) water. This equation (1.40), in the neighborhood of the origin, can be written as

$$\frac{y}{x} = (\sigma/f)\tan(\sigma t + \pi/2), \tag{1.41}$$

The equation (1.41) shows that the line of high water rotates 'contra solem' about the origin.

Amphidromic points occur along the central axis of the channel at $x = \frac{n\pi c}{\sigma}$ where n is an integer.

In fig (1.6) we can see co-range and co-tidal lines as given by Defant(1960) [9]. The standing wave pattern of the non-rotating system implied by equations (1.23) is completely lost. Instead the wave is split up into cells consisting of star-shaped distribution of co-tidal lines called 'amphidromes'. Along the central axis the wave retains its standing character.

Poincaré waves:

Besides Kelvin waves another type of wave can propagate in an infinite channel.

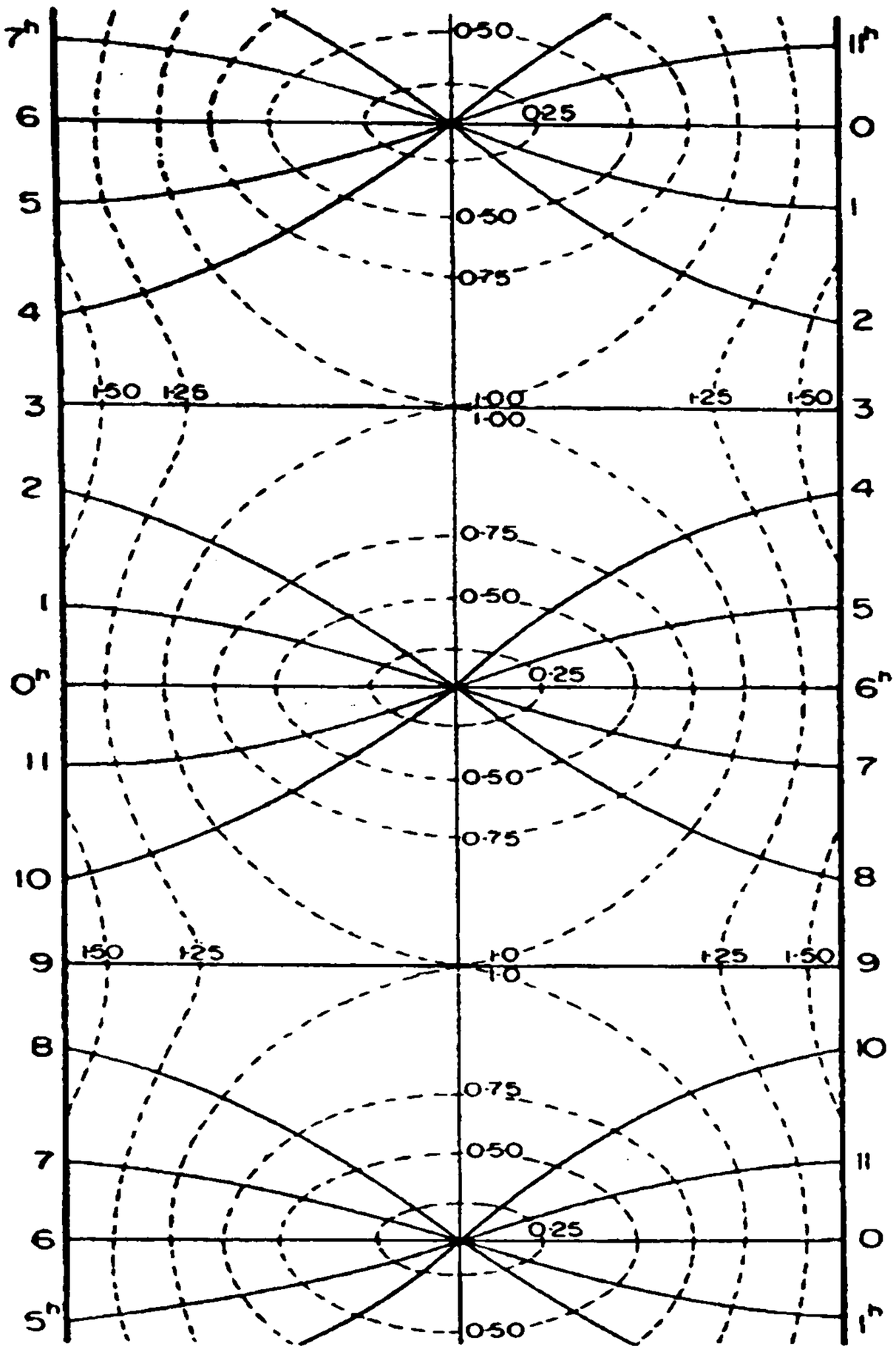

Figure 1.6: **Defant, 1960** Superposition of two Kelvin waves travelling in opposite directions in a canal with a uniform rectangular section. Period: 12 hrs (Southern Hemisphere)

We assume the following representation of wave in an infinite channel where the walls of the channel are taken as $y = 0$ and $y = b$.

$$\zeta = Z(y)\cos(\sigma t - kx),$$

$$u = U(y)\cos(\sigma t - kx),$$

$$v = V(y)\cos(\sigma t - kx). \tag{1.42}$$

On substitution of these expressions into the equations (1.25) and (1.27) we obtain

$$\frac{d^2V}{dy^2} + (\frac{\sigma^2 - f^2}{gh} - k^2)V = 0, \tag{1.43}$$

$$U(y) = \frac{1}{\sigma^2 - k^2 gh}\left(kgh\frac{dV}{dy} - \sigma f V\right), \tag{1.44}$$

and

$$Z(y) = \frac{h}{\sigma^2 - k^2 gh}\left(\sigma\frac{dV}{dy} - kfV\right). \tag{1.45}$$

The possible solutions of (1.43) which satisfy the condition of no flow through the boundaries are

$$V(y) = A_n \sin\frac{n\pi}{b}y, \tag{1.46}$$

where

$$\frac{\sigma^2 - f^2}{gh} - k_n^2 = (\frac{n\pi}{b})^2 \tag{1.47}$$

Since the value of k depends on n where n takes integer values, k has been subscripted as k_n.

These waves are called Poincaré waves and can propagate in either direction depending on the sign of k.

Since the quantities involved in (1.47) are all real, the equation (1.46) can be a valid solution for n = 1,2,3....p say where each value of n corresponds with a Poincaré mode. But the equation (1.46) may not possess a real solution for any integer value of n. Defant(1960) [9] states that plane Poincaré waves are only possible for

$$\sigma > f \tag{1.48}$$

and from (1.47)

$$\sigma > \frac{n\pi}{b}\sqrt{gh} \tag{1.49}$$

Thus the Poincaré wave can exists only if the period of the wave is shorter than half pendulum day and also shorter than the natural period of n-nodal transverse wave of the channel. These conditions are necessary but not sufficient for a Poincaré mode to exist.

The necessary and sufficient condition for the existence of an n-Poincaré mode can be obtained from (1.47) as

$$\frac{\sigma^2 - f^2}{gh} > (\frac{n\pi}{b})^2 \tag{1.50}$$

The condition (1.50) implies that the channel must be sufficiently wide or shallow for the propagation of Poincaré waves.

The word 'sufficiently' is a relative term and it takes into account of the depth of the channel and the frequency of the wave. Brown ([4]) in his thesis describes Poincaré waves as a Sverdrup wave undergoing multiple reflection between two parallel boundaries.

Semi-infinite channel:

When a Kelvin wave is moving into a rectangular channel closed at one end it cannot be reflected at the barrier in the usual sense but it is undergoing interesting tidal behavior. For the superposition of two Kelvin waves of any amplitudes moving in opposite directions does not result in zero horizontal velocity at any cross- section of the channel. Thus it is impossible to erect a barrier in the transverse direction which would not otherwise affect the motion. We shall follow this problem in details in Chapter-2 when we revisit Taylor's problem. Brown ([4]) in the analysis in his thesis about the propagation of Poincaré waves in an infinite channel discusses about the existence of another type of oscillation. For the imaginary solutions of the equation (1.47) there exists a type of oscillation in a 'sufficiently narrow' channel which is a standing wave in nature and exhibits exponential behavior in the longitudinal direction. He names this wave as 'Taylor wave' after Taylor (1921) who first used

these waves by applying them to closed channel. He states that when a Kelvin wave approaches a solid barrier in a semi-infinite channel it induces Taylor waves in the vicinity of the barrier which enable the Kelvin wave to be reflected. When we suppose two Kelvin waves of equal amplitudes moving in the opposite direction the resultant longitudinal velocity is given by $u_K(x, y)$. Brown explains that by combining an infinite number of Taylor modes he obtains a second solution $u_T(x, y)$ and by setting this solution equal to the Kelvin wave at a certain location obtains

$$u_T(x_1, y) = u_K(x_1, y),$$

where $x = x_1$ is some cross-section of the channel. The difference of these two solutions is also a solution.

That is, the solution

$$u_K(x, y) - u_T(x, y)$$

satisfies the condition that the longitudinal flow is zero at $x = x_1$ and therefore describes the flow in the region $x > x_1$.

In the analytical representation of the reflection of the Kelvin wave in a semi-infinite channel, Taylor expanded the Kelvin wave system $u_K(x, y)$ in terms of an undetermined half- range Fourier series. It is necessary to invert an infinite matrix which Taylor achieved by approximating numerically with considerable accuracy without the use of computers. The Taylor's idea of expanding Kelvin wave system in terms of Fourier series is used in the present work.

Defant (1960) [9] greatly simplified the method of Kelvin wave reflection by synthesising $u_T(x, y)$ with reasonable accuracy using only the first four Taylor modes of

$u_T(x, y)$ and required the equation equivalent to the condition $u_T(x_1, y) = u_K(x_1, y)$ to be satisfied for only five values of y across the channel. He determined values for unknowns and these values agreed approximately with those found by Taylor. This method is called collocation method or 'point matching', this method is used by P.J. Brown (1973).

If in contrast the condition for 'sufficiently narrow' channel is not met then Poincaé wave modes will exist at the expense of Taylor wave modes. Thus a Kelvin wave approaching a transverse barrier in a wide channel will induce Poincaré wave at the barrier and this wave is a progressive wave with un-diminishing amplitude, will carry away energy from the barrier. Hence the amplitude of the reflected Kelvin wave correspondingly reduced.

In 1973 Brown investigated the phenomenon of imperfect Kelvin wave reflection in wide channels by keeping the geometry of the channel fixed and allowing the frequency of the incoming Kelvin wave to vary until the critical frequency has been exceeded. Here, increasing the wave frequency is equivalent to widening the channel. The critical frequency σ_c is defined as

$$\frac{\sigma_c^2 - f^2}{gh} = (\frac{\pi}{b})^2.$$

where h is depth of the channel and b width of the channel.

Surely imperfect Kelvin wave reflection should occur for $\sigma > \sigma_c$. Brown's results are reproduced in figure (1.7). Clearly the diagram A represents perfect reflection and is similar to Taylor's (1921). The diagrams B-D still represent perfect reflection but the frequency approaching the critical frequency. The phase of the reflected wave undergoing changes which results in displacing the amphidromic points towards the closed end. The influence of the Taylor waves in the channel distorted several amphidromies.

In diagrams *E*-*H* the frequency of the wave exceeded the critical frequency and thus the amplitude of the reflected wave is severely reduced. Poincaré waves manifest themselves as the dominant reflecting mechanism and highly asymmetrical oscillations result.

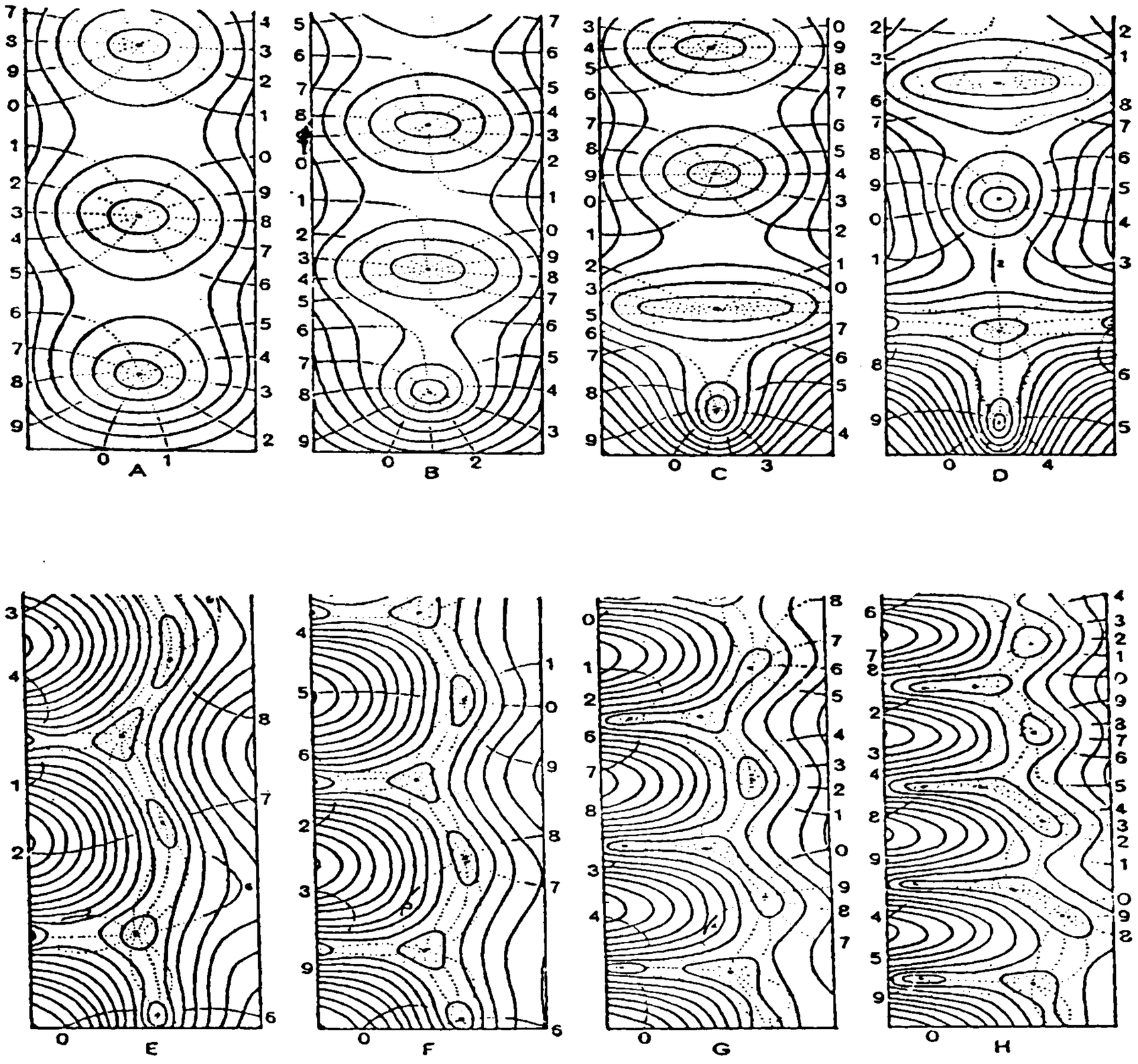

Figure 1.7: Brown, 1973

Interconnecting channels:

Channels of different cross-sections can be joined together or a single channel associated with an abrupt change in depth or width represent interconnecting channels. If the channel is 'sufficiently' narrow Taylor waves are produced at the discontinuities of the channel or alternatively Poincaré waves emanate from the discontinuity if that condition is not met. Moreover the numerical computations are very much simplified if the channels are 'very' narrow. Brown [4] treats 'sufficiently' narrow and 'very'

narrow are two distinct physical terms. As our work is primarily concerned with the semi-diurnal tides of the North Sea we use the second condition. That is,

$$\frac{\sigma^2}{gh} << (\frac{\pi}{b})^2.$$

This is the equivalent of saying that the width of the channel is very much less than the representative wavelength of the waves.

Parameters σ and f in the North Sea:

The principal constituent of the tidal motion is M_2 tide. Here we have given the values for σ and f of M_2 tide at a location in the north sea where latitude $= 56^o$ and the period of the wave T=12 hrs 25 mins. Thus

$$f = \frac{2 \times 2\pi \sin(56)}{24} = 1.21 \times 10^{-4} s^{-1} \text{ and } \sigma = \frac{2\pi}{12.25} = 1.41 \times 10^{-4} s^{-1}$$

Clearly $\sigma > f$ which is a condition for Poincaré waves to exist.

Chapter2

Revisiting Taylor's Problem

2.1 Taylor's solution of co-oscillating tides in a rectangular basin.

In order to make this work more self-contained, we revisit the Taylor problem (1921) where he derived a semi-analytic representation of the reflection of a Kelvin wave in a closed semi-infinite rectangular channel. This model successfully predicted the existence of amphidromic points and associated rotatory tides in the North Sea which are indeed the principal features of the North Sea tides.

In conjunction with his study (1919) of tides in the Irish Sea Taylor explained how the tide in the North Sea consists fundamentally of an incoming Kelvin wave from the North which is reflected at a rigid boundary in the South. He solved the problem using the usual shallow water equations with rotation for a long channel with uniform depth. The system was linearized and the f-plane approximation was invoked.

Assuming the flow quantities u, v and ζ have an $e^{i\sigma t}$ dependence, using the depth averaged (2HH) model, the momentum equations and continuity equation of tides in a rotating channel of uniform depth h are given by

$$i\sigma u - fv = -g\zeta_x \tag{2.1}$$

$$i\sigma v + fu = -g\zeta_y \tag{2.2}$$

$$i\sigma\zeta + h(u_x + v_y) = 0 \tag{2.3}$$

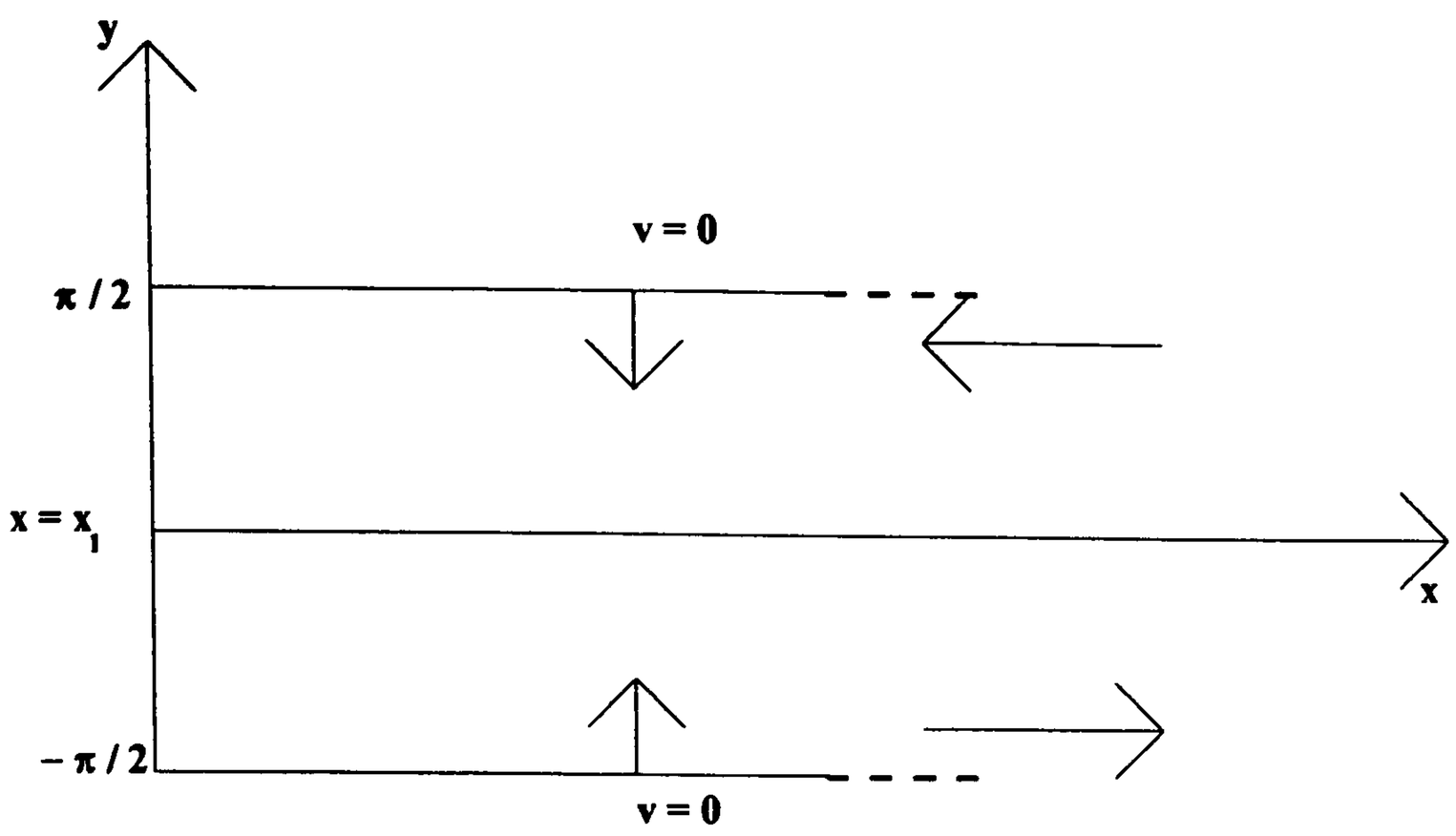

Figure 2.1: Schematic representation of the cross-section of the sea

where x and y are the long and cross channel directions, u and v are components of velocity parallel to x and y respectively, ζ is the elevation of the free surface, h is the depth of water assumed uniform, $\sigma = 2\pi/\text{period of tidal oscillation}$, t is time, g is acceleration due to gravity and f is the Coriolis parameter.

We indicated in equations (2.1) and (2.2) that momentum is conserved in the horizontal. The breadth of the channel is taken as π and the sides of the channel are the lines $y = \pm\frac{1}{2}\pi$.

On solving for u, v respectively from the two momentum equations we have

$$hk^2u = i\sigma\zeta_x + f\zeta_y \tag{2.4}$$

$$hk^2v = i\sigma\zeta_x - f\zeta_y \tag{2.5}$$

where $k^2 = \frac{f^2-\sigma^2}{c^2}$ and $c^2 = gh$ is the velocity of the long waves in the absence of earth's rotation.

Using (2.4) and (2.5) Taylor obtained from (2.3)

$$(\nabla^2 + k^2)\zeta = 0 \tag{2.6}$$

for the free surface elevation in a homogeneous channel of constant depth h. Since the expressions for u and v are linear it is evident that u and v also satisfy the same equation (2.6). That is,

$$(\nabla^2 + k^2)\begin{pmatrix} u \\ v \end{pmatrix} = 0.$$

The boundary conditions which have to be satisfied are that v shall vanish at $y = \pm\frac{1}{2}\pi$ and that u shall vanish at the closed end of the channel, which is to be taken arbitrarily as the line $x = x_1$. For a non-rotating channel, superposing of two equal 'plane wave trains' moving up and down the channel respectively there are points along the channel at which we can find planes perpendicular to its length across which there is no motion. At any one of these planes a barrier could be erected without affecting the motion on either side of it. The motion can then be confined to one side of the barrier, and it consists of a wave train which moves up the channel and is reflected at the end.

For a channel with rotation however, the superposition of two Kelvin waves, whatever their amplitudes, moving in opposite direction cannot result in zero horizontal velocity at any cross-section of the channel. It is therefore impossible to erect a solid transverse barrier which would not interfere with the motion. That is, we cannot find perfect reflection of the Kelvin waves in the channel without additional modes.

The principle on which the solutions could be found for a rotating channel is to construct an appropriate combination of a number of special solutions obtained from equation (2.6) which all satisfy the boundary conditions, $v = 0$ at $y = \pm\frac{1}{2}\pi$ but which

do not satisfy the second boundary condition, $u = 0$ at $x = x_1$. This combination of such special solutions can, however, make it possible to satisfy both boundary conditions.

We now review how Taylor achieved the analytical representation of the reflection of a Kelvin wave in the case of a rotating channel.

Let the incoming wave be given by

$$u_I = \exp\left\{\frac{fy - i\sigma x}{c} + i\sigma t\right\}$$

and

$$v_I = 0.$$

The reflected wave is taken as

$$u_R = \exp\left\{\frac{-fy + i\sigma x}{c} + i\sigma t\right\}$$

$$v_R = 0.$$

The incident wave is a Kelvin wave having the boundary wall at $y = \frac{1}{2}\pi$ to the right of its direction of propagation, the outgoing wave is another Kelvin wave having the wall at $y = -\frac{1}{2}\pi$ to the right of its direction of propagation. On superposing these two wave systems it can be found that, even though there are a number of points in the channel at which $u_I + u_R = 0$, there exists no value of x for which $u_I + u_R = 0$ for all values of y and t. Thus it is impossible to have a fixed barrier across the channel without altering the motion.

Taylor overcomes this difficulty by superposing a tidal motion u_p satisfying the bound-

ary condition $v = 0$ at $y = \pm\frac{1}{2}\pi$ on the two Kelvin waves so that $u_p = -(u_I + u_R)$ for all y and t at a certain value x_1 of x.

A barrier is then erected across the channel at $x = x_1$ without affecting the motion on either side of the barrier. The resultant motion represents an incident and reflected wave train.

The superposed motion u_p will be found to diminish rapidly away from the barrier and so the reflection of a Kelvin wave is achieved in the generalized sense that for large x the motion is essentially a combination of incoming and outgoing Kelvin waves.

The resultant longitudinal velocity due to the superposition of two Kelvin waves, incident and reflected waves can be written, after being multiplied by a constant quantity $\frac{1}{2}Si$, as

$$u = \frac{1}{2}Si(u_I + u_R) = S(\cosh(\alpha y)\sin(\frac{\sigma x}{c}) - i\sinh(\alpha y)\cos(\frac{\sigma x}{c})),$$

where $\alpha = \frac{f}{c}$.

The transverse velocity associated with this u vanishes identically.

The problem now is to find the velocity components v and u for the superposed tidal motion such that $v = 0$ at the walls $y = \pm\frac{1}{2}\pi$ and $u = -\frac{1}{2}Si(u_I + u_R)$ at the barrier $x = x_1$.

To find the velocity component v for the superposed motion we consider the equation

$$(\nabla^2 + k^2)v = 0$$

A particular solution of this equation is

$$v = \exp(-s_m x + imy) \tag{2.7}$$

where $s_m^2 = m^2 - k^2$ is real and m is taken as an integer.

The possible forms of the solution (2.7) are as follows

$$\begin{aligned}
&m^2 < k^2, \quad s_m^2 = k^2 - m^2, \quad \begin{cases} m \text{ is even}, & v = D_m \cos(s_m x)\sin(my), \\ m \text{ is odd}, & v = iC_m \sin(s_m x)\cos(my), \end{cases} \\
&m^2 > k^2, \quad s_m^2 = m^2 - k^2, \quad \begin{cases} m \text{ is even}, & v = D_m e^{-s_m x}\sin(my), \\ m \text{ is odd}, & v = iC_m e^{-s_m x}\cos(my), \end{cases}
\end{aligned} \tag{2.8}$$

where now s_m is real in all cases.

For the longitudinal velocity u we assume the following forms

$$\begin{aligned}
&m^2 < k^2, \quad u = A_m \sin s_m x \cos(my) + iB_m \cos s_m x \sin(my), \\
&m^2 > k^2, \quad u = A_m e^{-s_m x}\cos(my) + iB_m e^{-s_m x}\sin(my).
\end{aligned} \tag{2.9}$$

The coefficients A_m and B_m must be chosen such that the equations (2.1) and (2.2) are satisfied.

Eliminating ζ between (2.1) and (2.2) gives

$$i\sigma\frac{\partial u}{\partial y} - f\frac{\partial u}{\partial x} = i\sigma\frac{\partial v}{\partial x} + f\frac{\partial v}{\partial y}. \tag{2.10}$$

Substituting for u and v from (2.8) and (2.9) in equation (2.10), the coefficients of $\cos(my)$ and $i\sin(my)$ on the two sides of the equation are equated. The two resulting equations determine C_m and D_m in terms of A_m and B_m. A relationship between A_m and B_m can also be established so that v is of the above form

Now we write the relationships as:

$$m^2 < k^2, \quad \left\{ \begin{array}{ll} m & \text{is even}, \ \frac{A_m}{B_m} = \frac{-1}{r_m}, \\ m & \text{is odd}, \ \frac{A_m}{B_m} = r_m, \end{array} \right\}$$

$$m^2 > k^2, \quad \left\{ \begin{array}{ll} m & \text{is even}, \ \frac{A_m}{B_m} = \frac{-1}{r_m}, \\ m & \text{is odd}, \ \frac{A_m}{B_m} = -r_m, \end{array} \right\}$$

$$\text{where} \ \ r_m = \frac{f\sigma}{ms_m c^2}. \tag{2.11}$$

The constants C_m and D_m are then given as

$$D_m = \frac{m}{s_m} A_m - \frac{f}{\sigma} B_m; \qquad m \ \text{is even}$$

$m^2 < k^2$

$$C_m = \frac{f}{\sigma} A_m + \frac{m}{s_m} B_m; \qquad m \ \text{is odd}$$

$$D_m = \frac{m}{s_m} A_m - \frac{f}{\sigma} B_m; \qquad m \ \text{is even}$$

$m^2 > k^2$

$$C_m = \frac{f}{\sigma} A_m - \frac{m}{s_m} B_m; \qquad m \ \text{is odd}. \tag{2.12}$$

The following tasks remain:

(1) To choose a series of values for A_m and B_m so that the value of u is formed by the sum of all the terms is equal to $\frac{1}{2} Si(u_I + u_R)$ for all values of y at some value x_1 of x.

(2) Since the value of u for any value of x is expressed as a Fourier series in $\cos my$ and $\sin my$ it is necessary to express $\frac{1}{2} Si(u_I + u_R)$ by means of a similar Fourier series. To achieve this, first write down the trigonometrical series expressing $\cosh(\alpha y)$ and $\sinh(\alpha y)$ in terms of cosines of even and sines of odd multiples of y respectively between the limits $y = \pm \frac{1}{2}\pi$.

These are

$$\left\{ \begin{array}{l} \cosh(\alpha y) = \frac{4\alpha}{\pi} \sinh \frac{\alpha\pi}{2} \left(\frac{1}{2\alpha^2} - \frac{\cos 2y}{\alpha^2+2^2} + \frac{\cos 4y}{\alpha^2+4^2} - \ldots + (-1)^{\frac{1}{2}m} \frac{\cos my}{\alpha^2+m^2} \ldots \right) \\ \\ \sinh(\alpha y) = \frac{4\alpha}{\pi} \cosh \frac{\alpha\pi}{2} \left(\frac{\sin y}{\alpha^2+1^2} - \frac{\sin 3y}{\alpha^2+3^2} + \ldots + (-1)^{\frac{1}{2}(m-1)} \frac{\sin my}{\alpha^2+m^2} \ldots \right). \end{array} \right. \tag{2.13}$$

Using (2.13) the value of u for the original pair of Kelvin waves is given as

$$\frac{1}{2}Si(u_I+u_R)=\frac{4S\alpha}{\pi}\sinh\frac{\alpha\pi}{2}\sin\frac{\sigma x}{c}\left\{\frac{1}{2\alpha^2}+\sum_{m\ \text{even}}(-1)^{\frac{m}{2}}\frac{\cos my}{\alpha^2+m^2}\right\}-$$
$$\frac{4Si\alpha}{\pi}\cosh\frac{\alpha\pi}{2}\cos\frac{\sigma x}{c}\left\{\sum_{m\ \text{odd}}(-1)^{\frac{m-1}{2}}\frac{\sin my}{\alpha^2+m^2}\right\}. \qquad (2.14)$$

In this expression (2.14) it can be noted that only cosines of even multiples of y and sines of odd multiples of y occur, but in (2.9) every term contains either sines of my or cosines of my. Thus it becomes impossible to equate the coefficients of $\cos my$ and $\sin my$ in these equations directly. Similarly in (2.13) the series for $\cosh \alpha y$ contains no cosines of odd multiples of my and the series for $\sinh \alpha y$ contains no sines of even multiples of my.

In order to overcome this difficulty Taylor writes the following trigonometrical series for a cosine of an odd multiple of y and a sine of an even multiple of y in terms of cosines of the even multiples of y and the sines of the odd multiples of y respectively;

$$\begin{cases}(-1)^{\frac{1}{2}(s-1)}\frac{\pi}{4s}\cos sy=\frac{1}{2s^2}+\frac{\cos 2y}{2^2-s^2}-\frac{\cos 4y}{4^2-s^2}+\frac{\cos 6y}{6^2-s^2}-\ldots\ldots, & s\ \text{is odd}\\ (-1)^{\frac{1}{2}s}\frac{\pi}{4s}\sin sy=\frac{\sin y}{1-s^2}-\frac{\sin 3y}{3^2-s^2}+\frac{\sin 5y}{5^2-s^2}-\ldots\ldots\ldots, & s\ \text{is even.}\end{cases} \qquad (2.15)$$

Now, by using (2.15), add the multiples β_1, β_3, β_5,....., β_s,..... of $\cos sy$ (s odd) and the multiples γ_2, γ_4, γ_6,.....γ_s,.....of $\sin sy$ (s is even) to the series for $\frac{1}{2}Si(u_I+u_R)$ of

(2.14) and subtract the corresponding trigonometrical series from it. It is found that

$$\frac{1}{2}Si(u_I+u_R)=\sinh\frac{\alpha\pi}{2}\sin\frac{\sigma x}{c}\left[\frac{1}{2\alpha^2}-\frac{\cos 2y}{\alpha^2+2^2}+\frac{\cos 4y}{\alpha^2+4^2}-\cdots\right.$$
$$\left.+\sum_{s\ \text{odd}}\beta_s\left\{(-1)^{\frac{s-1}{2}}\frac{\pi\cos sy}{4s}-\left(\frac{1}{2s^2}+\frac{\cos 2y}{2^2-s^2}-\frac{\cos 4y}{4^2-s^2}+\cdots..\right)\right\}\right]$$
$$-i\cosh\frac{\alpha\pi}{2}\cos\frac{\sigma x}{c}\left[\frac{\sin y}{\alpha^2+1^1}-\frac{\sin 3y}{\alpha^2+3^2}+\frac{\sin 5y}{\alpha^2+5^2}-\right.\qquad ..$$
$$\left.+\sum_{s\ \text{even}}\gamma_s\left\{(-1)^{\frac{1}{2}s}\frac{\pi\sin sy}{4s}-\left(\frac{\sin y}{1^2-s^2}-\frac{\sin 3y}{3^2-s^2}+\frac{\sin 5y}{5^2-s^2}-\cdots.\right)\right\}\right] \quad (2.16)$$

where $\beta_s$and γ_s are yet to be found.

At the section $x=x_1$, the motion given by a series of terms of the forms (2.9) represent the same value of u as (2.16). The ratio of the coefficients of $\cos(my)$ to the coefficients of $i\sin(my)$ are obtained from (2.9). By substituting for the ratios $\frac{A_m}{B_m}$ from (2.11) we obtain

$$\frac{\text{coefficient of }\cos my}{\text{coefficient of }i\sin my}=\begin{cases}-(\frac{1}{r_m})\tan s_m x_1 & \text{when } m^2<k^2 \text{ and } m \text{ is even}\\ r_m\tan s_m x_1 & \text{when } m^2<k^2 \text{ and } m \text{ is odd}\\ -(\frac{1}{r_m}) & \text{when } m^2>k^2 \text{ and } m \text{ is even}\\ -r_m & \text{when } m^2>k^2 \text{ and } m \text{ is odd}\end{cases} \quad (2.17)$$

The condition is that, at the section $x=x_1$, the ratio of the coefficient of $\cos(my)$ to the coefficient of $i\sin(my)$ in (2.16) are equal to the above ratios. From this condition we can obtain

$$\text{when } m \text{ is odd}\begin{cases}\frac{1}{\alpha^2+m^2}-\frac{\gamma_2}{m^2-2^2}-\frac{\gamma_4}{m^2-4^2}-\frac{\gamma_6}{m^2-6^2}-\cdots & \\ \qquad=\frac{-\beta_m\pi}{4mr_m}\tanh\frac{\alpha\pi}{2}\tan\frac{\sigma x_1}{c}\cot s_m x_1 & \text{when } (m^2<k^2)\\ \qquad=\frac{\beta_m\pi}{4mr_m}\tanh\frac{\alpha\pi}{2}\tan\frac{\sigma x_1}{c} & \text{when } (m^2>k^2)\end{cases}$$

$$\text{when } m \text{ is even}\begin{cases}\frac{1}{\alpha^2+m^2}+\frac{\beta_1}{m^2-1^2}+\frac{\beta_3}{m^2-3^2}+\frac{\beta_5}{m^2-5^2}+\cdots & \\ \qquad=\frac{\gamma_m\pi}{4mr_m}\coth\frac{\alpha\pi}{2}\cot\frac{\sigma x_1}{c}\tan s_m x_1 & (m^2<k^2)\\ \qquad=\frac{\gamma_m\pi}{4mr_m}\coth\frac{\alpha\pi}{2}\cot\frac{\sigma x_1}{c} & (m^2>k^2)\end{cases} \quad (2.18)$$

For any given value of x_1 the above equations (2.18) enable us to obtain the β_s and

γ_s. The terms which are independent of y in (2.16) must vanish. This provides an extra equation.

$$\frac{1}{\alpha^2} - \frac{\beta_1}{1^2} - \frac{\beta_3}{3^2} - \frac{\beta_5}{5^2} - \quad \ldots\ldots = 0 \tag{2.19}$$

On elimination of $\beta's$ and $\gamma's$ between equations (2.18) and (2.19) we get an equation for x_1 in the form of an infinite determinant;

$$\begin{vmatrix} \frac{1}{\alpha^2} & \frac{-1}{1^2} & 0 & \frac{-1}{3^2} & 0 & \frac{-1}{5^2}\ldots \\ \frac{-1}{\alpha^2+1^2} & L_1 z & \frac{1}{1^2-2^2} & 0 & \frac{1}{1^2-4^2} & 0\ldots \\ \frac{1}{\alpha^2+2^2} & \frac{1}{2^2-1^2} & \frac{-M_2}{z} & \frac{1}{2^2-3^2} & 0 & \frac{1}{2^2-5^2}\cdots \\ \frac{-1}{\alpha^2+3^2} & 0 & \frac{1}{3^2-2^2} & L_3 z & \frac{1}{3^2-4^2} & 0\ldots \\ \frac{1}{\alpha^2+4^2} & \frac{1}{4^2-1^2} & 0 & \frac{1}{4^2-3^2} & \frac{-M_4}{z} & \frac{1}{4^2-5^2}\cdots \\ \ldots & \ldots & \ldots & \ldots & \ldots & \ldots \end{vmatrix} = 0, \tag{2.20}$$

where $z = \tan(\frac{\sigma x_1}{c})$ and

$$\left.\begin{aligned} L_m &= -(\tfrac{\pi}{4mr_m})\tanh(\tfrac{1}{2}\alpha\pi)\cot(s_m x_1), && (m \text{ is odd and } m^2 < k^2) \\ &= (\tfrac{\pi}{4mr_m})\tanh(\tfrac{1}{2}\alpha\pi), && (m \text{ is odd and } m^2 > k^2) \\ M_m &= (\tfrac{\pi}{4mr_m})\coth(\tfrac{1}{2}\alpha\pi)\tan(s_m x_1), && (m \text{ is even and } m^2 < k^2) \\ &= (\tfrac{\pi}{4mr_m})\coth(\tfrac{1}{2}\alpha\pi), && (m \text{ is even and } m^2 > k^2). \end{aligned}\right\} \tag{2.21}$$

In the case when $k^2 < 1$ we can obtain from (2.20) an equation for z. That is,

$$z\begin{vmatrix} \frac{1}{\alpha^2} & \frac{-1}{1^2} & 0 & \frac{-1}{3^2} & 0 & \ldots \\ 0 & L_1 & \frac{1}{1^2-2^2} & 0 & \frac{1}{1^2-4^2} & \ldots \\ \frac{1}{\alpha^2+2^2} & \frac{1}{2^2-1^2} & -M_2 & \frac{1}{2^2-3^2} & 0 & \ldots \\ 0 & 0 & \frac{1}{3^2-2^2} & L_3 & \frac{1}{3^2-4^2} & \ldots \\ \frac{1}{\alpha^2+4^2} & \frac{1}{4^2-1^2} & 0 & \frac{1}{4^2-3^2} & -M_4 & \ldots \\ \ldots & \ldots & \ldots & \ldots & \ldots & \end{vmatrix} = -\begin{vmatrix} 0 & \frac{-1}{1^2} & 0 & \frac{-1}{3^2} & 0 & \ldots \\ \frac{-1}{\alpha^2+1^2} & L_1 & \frac{1}{1^2-2^2} & 0 & \frac{1}{1^2-4^2} & \ldots \\ 0 & \frac{1}{2^2-1^2} & -M_2 & \frac{1}{2^2-3^2} & 0 & \ldots \\ \frac{-1}{\alpha^2+3^2} & 0 & \frac{1}{3^2-2^2} & L_3 & \frac{1}{3^2-4^2} & \ldots \\ 0 & \frac{1}{4^2-1^2} & 0 & \frac{1}{4^2-3^2} & -M_4 & \ldots \\ \ldots & \ldots & \ldots & \ldots & \ldots & \ldots \end{vmatrix} \tag{2.22}$$

Using the equation (2.22) $\tan(\frac{\sigma x_1}{c})$ can be found. Having obtained x_1, its value may be substituted in equation (2.18) and the resulting equations for $\beta's$ and $\gamma's$ are solved

numerically.

In the case when $k^2 < 1$ the Poincaré modes are represented by

$$u = \sum_m \left(A_m e^{-s_m x} \cos(my) + iB_m e^{-s_m x} \sin(my) \right)$$

and

$$\left.\begin{aligned} v &= D_m e^{-s_m x} \sin(my) \qquad (m \text{ is even}), \\ v &= iC_m e^{-s_m x} \cos(my) \qquad (m \text{ is odd}) \end{aligned}\right\}$$

where $s_m^2 = m^2 - k^2$

These Poincaré modes (due to the interaction of Kelvin waves with the barrier) decrease indefinitely at great distances from the closed end. Kelvin waves are thus reflected perfectly.

In the case when $k^2 > 1$, some of the L's and M's in (2.21) contain $\tan(s_m x_1)$, or $\cot(s_m x_1)$. The equation (2.20) can't therefore, be reduced to a simple equation for z. The equation (2.20) may be solved numerically by assuming various values for x_1 and finding when the determinant (2.20) changes sign.

In this case, ie. when $k^2 > 1$, at least one of the terms in the expressions in (2.8) and (2.9) contains sines and cosines of a multiple of x. These terms are finite for infinite values of x. Thus, in this case, perfect reflection of Kelvin waves cannot take place. The channel appears to be too wide to force the reflected tidal wave back into the condition in which the particles of water move only parallel to the walls. These terms, which occur when $k^2 > 1$, and contain sines and cosines of multiples of x, represent a pair of waves which were independently discovered by Poincaré and Proudman [4].

2.2 Numerical solution

The solution obtained of the motion in a region where tidal waves are being reflected from the end of the channel is so complicated in its form that it would be difficult to discuss the tidal regime in a general way. Thus Taylor considered a particular case for which $k = 0.5$, $\alpha = 0.7$. This corresponds with the reflection of a tidal wave of period 12hr in North Sea with 250 miles width and 40 fathoms depth and centered in lat.53^0 N. Moreover this case where k belongs to a range, 0-1, in which perfect reflection occurs, assumed to give typical features of a North Sea M_2 tide.

Taylor calculated the values of A_m, B_m, C_m, D_m for 10 terms up to A_{10}, B_{10}, C_{10} and D_{10}.

Furthermore, the quantities such as $\frac{\sigma}{c}$, s_m, r_m, L_m, M_m which appear in the equations are first determined and were inserted in the equation (2.22).

These quantities are functions of α and k only. We now recall them.

$$\left.\begin{aligned} \tfrac{\sigma}{c} &= \sqrt{(\alpha^2 + k^2)} = 0.860, \\ s_m^2 &= m^2 - k^2, \\ r_m &= \tfrac{2f\sigma}{ms_m c^2}, \\ L_m &= (\tfrac{\pi}{4mr_m}) \tanh(\tfrac{1}{2}\alpha\pi), \quad (m \text{ is odd}) \\ M_m &= (\tfrac{\pi}{4mr_m}) \coth(\tfrac{1}{2}\alpha\pi), \quad (m \text{ is even}) \end{aligned}\right\}$$

These quantities are calculated and tabulated below.

1	2	3	4	5
m	s_m	r_m	L_m	M_m
1	0.866	0.695	0.905	-
2	1.937	0.155	-	3.15
3	2.96	0.0680	3.09	-
4	3.97	0.0380	-	6.14
5	4.98	0.0242	5.19	-
6	5.98	0.167	-	9.72
7	6.99	0.0123	7.30	-
8	7.99	0.0094	-	12.98
9	9.00	0.0074	9.40	-
10	10.00	0.0060	-	16.25

In order to evaluate the first approximate value of z we take only two rows and columns for each determinant in (2.22).

That is,

$$z\begin{vmatrix} \frac{1}{\alpha^2} & \frac{-1}{1^2} \\ 0 & L_1 \end{vmatrix} = \begin{vmatrix} 0 & \frac{-1}{1^2} \\ -\frac{1}{\alpha^2+1} & L_1 \end{vmatrix} \Longrightarrow z\left(\frac{0.905}{0.49}\right) = \left(\frac{1}{1.49}\right)$$

An approximate value of z=0.363 is obtained.

Similarly by taking successively, 3, 4 and 5 rows and columns in each determinant, the values 0.383, 0.385 and 0.385 are obtained. Therefore, this method of approximating to the value of z seems to converge.

Now we have

$$\tan(\frac{\sigma x_1}{c}) = 0.385 \Longrightarrow \frac{\sigma x_1}{c} = 21^{\underline{0}}\ 3' = 0.367 \ \text{(in circular measure)}$$

$$\frac{\sigma}{c} = 0.860$$

therefore, $x_1 = 0.427$

Inserting the value $z = \tan(\frac{\sigma x_1}{c}) = 0.385$ in the first equation of (2.18) we obtained

$$0.348\beta_1 - 0.333\gamma_2 - 0.0667\gamma_4 - 0.0286\gamma_6 - 0.0159\gamma_8 - 0.0101\gamma_{10} - 0.6711 = 0.$$

The first approximate value of β_1 is taken as

$$\beta_1 = \frac{0.6711}{0.348} = 1.93$$

The second equation of (2.18) is then written down

$$0.223 + 0.333\beta_1 - 8.19\gamma_2 - 0.2\beta_3 - 0.048\beta_5 - ..... = 0.$$

The first approximate value of γ_2 is found as

$$\gamma_2 = \frac{(0.333\beta_1 + 0.223)}{8.19} = 0.106$$

Thus we can obtain, in this way, the first approximations for all the $\beta's$ and $\gamma's$.

These values are then inserted in equations (2.18) and a new value is found for β_1.

That is ,

$$\beta_1 = 2.03$$

This is then used to obtain a better approximation for γ_2, and so on. This process is repeated several times until convergence is achieved. Thus by repeatedly updating

the estimates for β_s and γ_s we eventually arrive at their true values.

In order to obtain A_m, B_m, C_m and D_m we rewrite the boundary condition at $x = x_1$ in full.

$$\sinh\frac{\alpha\pi}{2}\sin\frac{\sigma x_1}{c}\left[\frac{1}{2\alpha^2}-\frac{\cos 2y}{\alpha^2+2^2}+\frac{\cos 4y}{\alpha^2+4^2}-\cdots\right.$$
$$\left.+\sum_{s\ \text{odd}}\beta_s\left\{(-1)^{\frac{s-1}{2}}\ \frac{\pi\cos sy}{4s}-\left(\frac{1}{2s^2}+\frac{\cos 2y}{2^2-s^2}-\frac{\cos 4y}{4^2-s^2}+\cdots..\right)\right\}\right]$$
$$-i\cosh\frac{\alpha\pi}{2}\cos\frac{\sigma x_1}{c}\left[\frac{\sin y}{\alpha^2+1^1}-\frac{\sin 3y}{\alpha^2+3^2}+\frac{\sin 5y}{\alpha^2+5^2}-\right.\qquad ..$$
$$\left.+\sum_{s\ \text{even}}\gamma_s\left\{(-1)^{\frac{1}{2}s}\frac{\pi\sin sy}{4s}-\left(\frac{\sin y}{1^2-s^2}-\frac{\sin 3y}{3^2-s^2}+\frac{\sin 5y}{5^2-s^2}-\cdots.\right)\right\}\right]$$
$$-\sum_{m}^{\infty}\left(A_m e^{-s_m x_1}\cos(my)+iB_m e^{-s_m x_1}\sin(my)\right)=0. \tag{2.23}$$

It is convenient to transfer the origin of the co-ordinate system to the mid-point of the end of the channel in which case it follows from equation (2.23) after a slight re-definition that

$$\left.\begin{aligned} A_m &= (-1)^{\frac{1}{2}(m-1)}\ \tfrac{\beta_m\pi}{4m}\ \sinh(\tfrac{\alpha\pi}{2})\ \sin(\tfrac{\sigma x_1}{c}) \quad (m\ \text{ is odd})\\ B_m &= (-1)^{\frac{1}{2}(m-2)}\ \tfrac{\gamma_m\pi}{4m}\ \cosh(\tfrac{\alpha\pi}{2})\ \cos(\tfrac{\sigma x_1}{c}) \quad (m\ \text{ is even}) \end{aligned}\right\} \tag{2.24}$$

The values of A_m for m even and B_m for m odd are then obtained from equation (2.11). The values of C_m and D_m are found from the formulae (2.12).

Finally, the values of β_m, γ_m, A_m, B_m, C_m and D_m are then easily calculated for m varies from 1 to 10 and tabulated in tables below.

m	β_m	γ_m
1	2.03	-
2	-	0.108
3	0.07140	-
4	-	0.0124
5	0.0165	-
6	-	0.0035
7	0.0064	-
8	-	0.0015
9	0.0030	-
10	-	0.0007

.

m	A_m	B_m	C_m	D_m
1	0.765	-1.100	1.892	-
2	-0.427	0.066	-	-0.495
3	-0.0090	0.132	-0.138	-
4	0.1000	-0.004	-	0.103
5	0.0012	-0.050	0.510	-
6	-0.0425	0.0007	-	-0.043
7	-0.0003	0.027	-0.027	-
8	0.0245	-0.0002	-	0.024
9	0.0001	-0.017	0.017	-
10	-0.0147	0.0001	-	-0.015

From the continuity equation Taylor obtained the tidal range, i.e.,

$$\frac{\sigma\zeta}{h} = i\left(\frac{\partial u}{\partial x} + \frac{\partial v}{\partial y}\right)$$

Finally, the whole motion in the semi-infinite channel is thus approximately represented by

$$\begin{aligned} u &= 1.122\left\{\cosh(0.7y)\sin(0.860(x+0.427)) - i\sinh(0.7y)\cos(0.860(x+0.427))\right\} \\ &\quad - \sum_{m=1}^{m=10} A_m e^{-s_m x}\cos(my) + iB_m e^{-s_m x}\sin(my) \\ v &= \sum_{m \text{ even}} D_m e^{-s_m x}\sin(my) - i\sum_{m \text{ odd}} C_m e^{-s_m x}\cos(my) \end{aligned} \tag{2.25}$$

$$\begin{aligned} \tfrac{\sigma\zeta}{h} &= 0.965\left\{-\sinh(0.7y)\sin(0.860(x+0.427)) + i\cosh(0.7y)\cos(0.860(x+0.427))\right\} \\ &\quad + \sum_{m \text{ odd}}\left\{(-B_m s_m - mC_m)e^{-s_m x}\sin(my) + is_m A_m e^{-s_m x}\cos(my)\right\} \\ &\quad + \sum_{m \text{ even}}\left\{-B_m e^{-s_m x}\sin(my) + i(s_m A_m - mD_m)e^{-s_m x}\cos(my)\right\} \end{aligned}$$

$$\left(-\tfrac{\pi}{2} \le y \le \tfrac{\pi}{2}\ ,\ \ x \ge x_1\right)$$

Verification of the solution

The value of u at $x = 0$ should be 0 for all values of y.

(a) $x = 0$ and $y = 0$

$$u = 0.403 - \sum_{1}^{10} A_m \Rightarrow u = 0.403 - 0.3953 = 0.0077$$

Thus u very nearly vanishes at the mid-point of the end of the channel.

(b) $x = 0$ and $y = \frac{\pi}{2}$, (i.e., at the corner)

the value of u due to the incident and reflected Kelvin waves is calculated as

$$u = 0.67 - 1.40i$$

but part due to Poincaré modes is

$$(A_2 - A_4 + A_6 - A_8) - i(B_1 - B_3 + B_5 - B_7 + B_9 = -0.61 + 1.33i$$

So percentage error approximately

$$\frac{|0.06|}{|0.67|} \times 100 = \frac{|0.07|}{|1.4|} \times 100 \approx 5\%$$

Thus u nearly vanishes at the corner, $(0, \frac{\pi}{2})$, of the channel.

Hence at $(0, 0)$, $(0, \frac{\pi}{2})$ the two motions very nearly neutralize one another.

Therefore, we can conclude that, (2.25) represents the tidal motion approximately.

2.3 Result:

Contour (2.2) depicts the wave form of the tides at a particular instant of time. Animations can be created for values of θ differing by $\frac{\pi}{5}$ which corresponds to 1 hour and 12 min's difference in the state of the tide. Then we see from the diagram the motion of the tidal wave down one side of the channel; and the way in which it sweeps round the end to return along the opposite side.

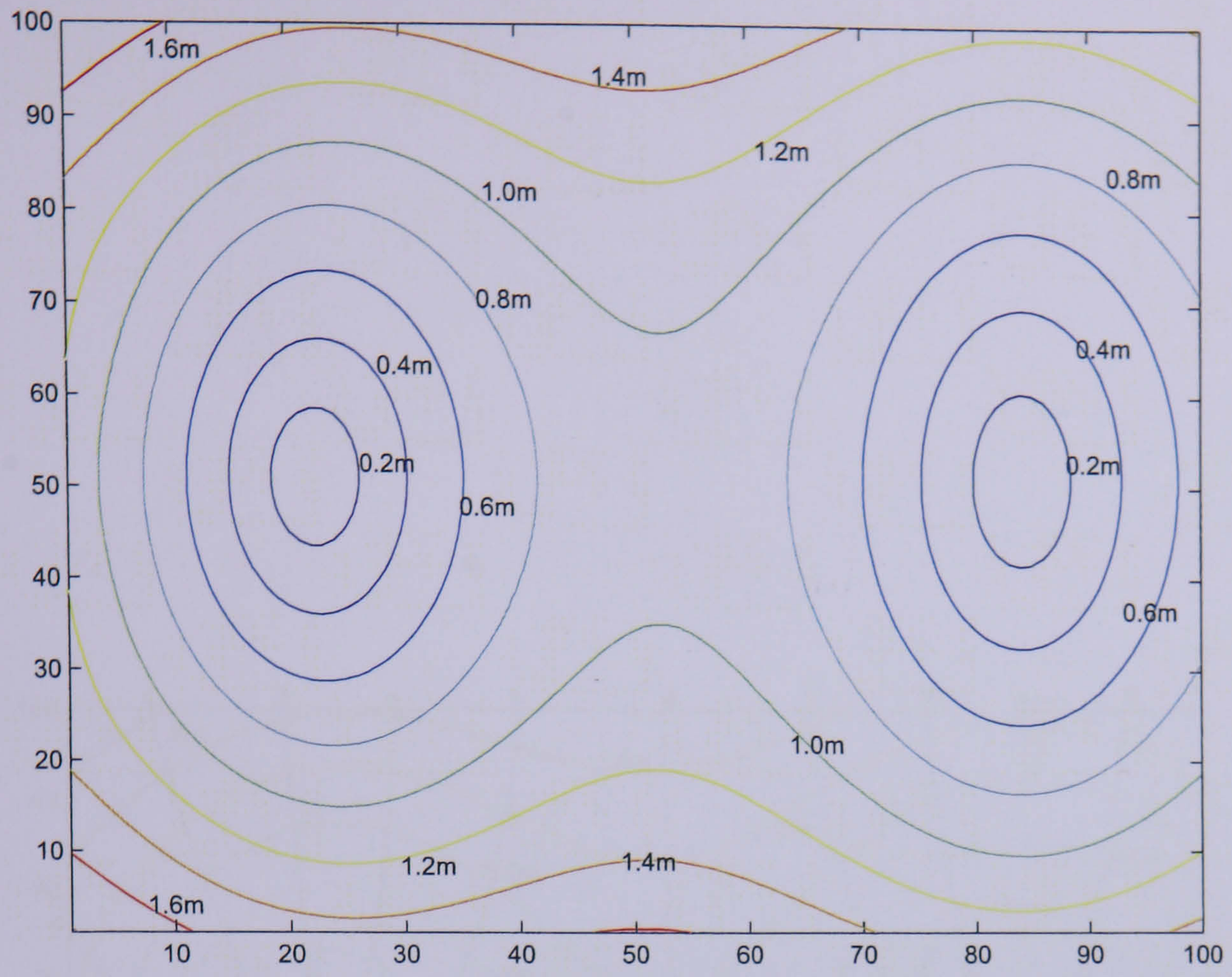

Figure 2.2: Co-range lines: Solution obtained by Taylor (1921; fig. 1) for reflection of a Kelvin wave at the end of a channel with dimension similar to those of the North sea.

We express the value of $\frac{\sigma\zeta}{h}$ at any point as

$$\frac{\sigma\zeta}{h} = P + iQ \qquad \text{where } P = \text{real part and } Q = \text{imaginary part.}$$

The phase, θ, of the tide is given by

$$\tan(\theta) = \frac{Q}{P} \, .$$

The co-tidal lines are lines of constant θ, i.e., lines at all points of which it is high water simultaneously. In fig (2.3) co-tidal lines have been drawn for values of θ differing by $\frac{\pi}{5}$ which correspond to 1hour and 12 mins' difference in the state of tide.

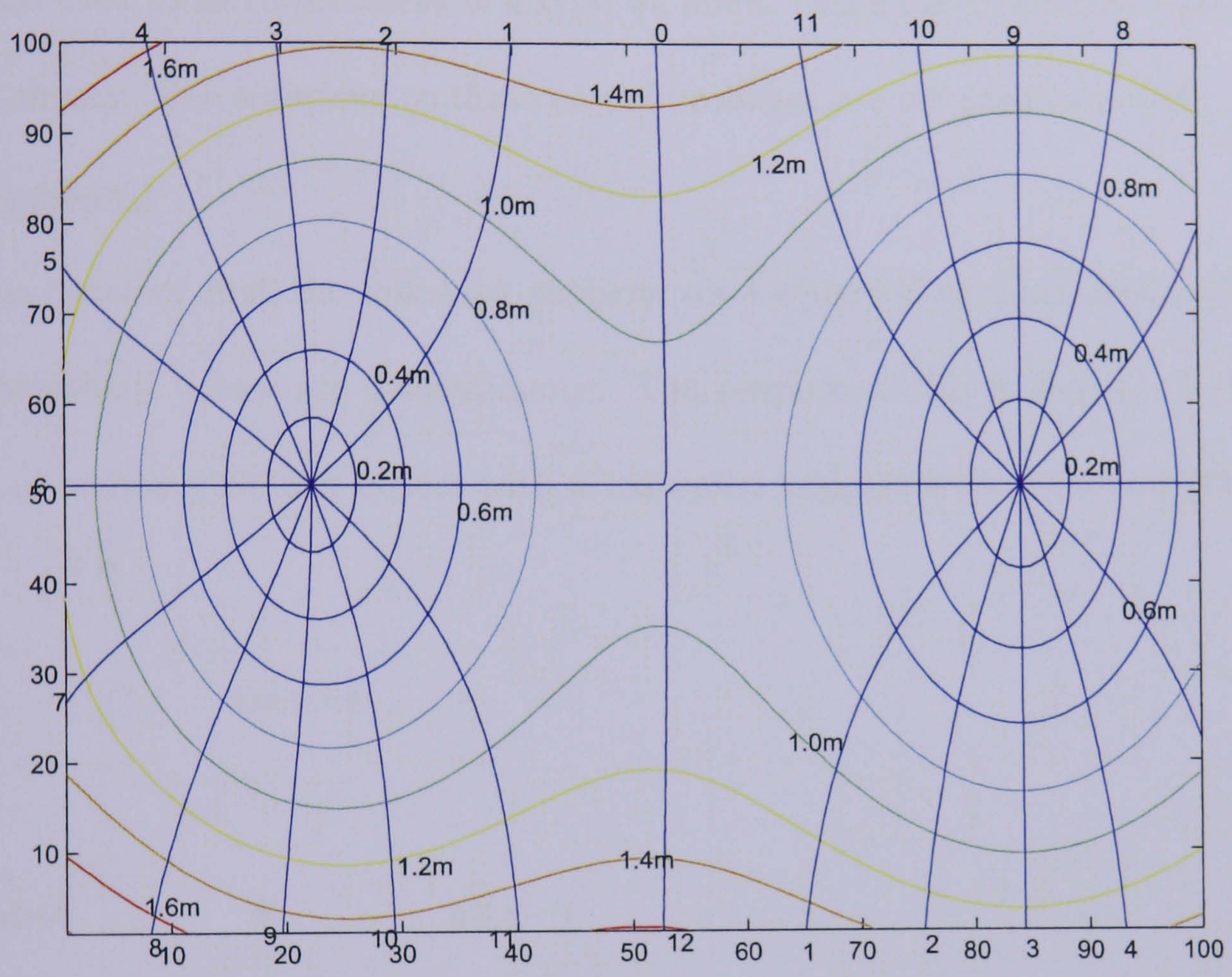

Figure 2.3: Co-tidal lines: Solution obtained by Taylor (1921; fig. 1) for reflection of a Kelvin wave at the end of a channel with dimension similar to those of the North sea.

Chapter3

Model Problems

3.1 Solutions to model problems

We consider the following boundary value problems to illustrate how Fourier series may be used to solve problems of a type we might encounter in shallow water Kelvin wave theory. The solutions to these model problems are adopted from [33].

Problem 1

Let us consider first the following problem on a square S as illustrated in fig (3.1); the boundary values are discontinuous. The purpose of this is to get a feel for the kind of accuracy we can expect with a truncated trigonometrical series solution.

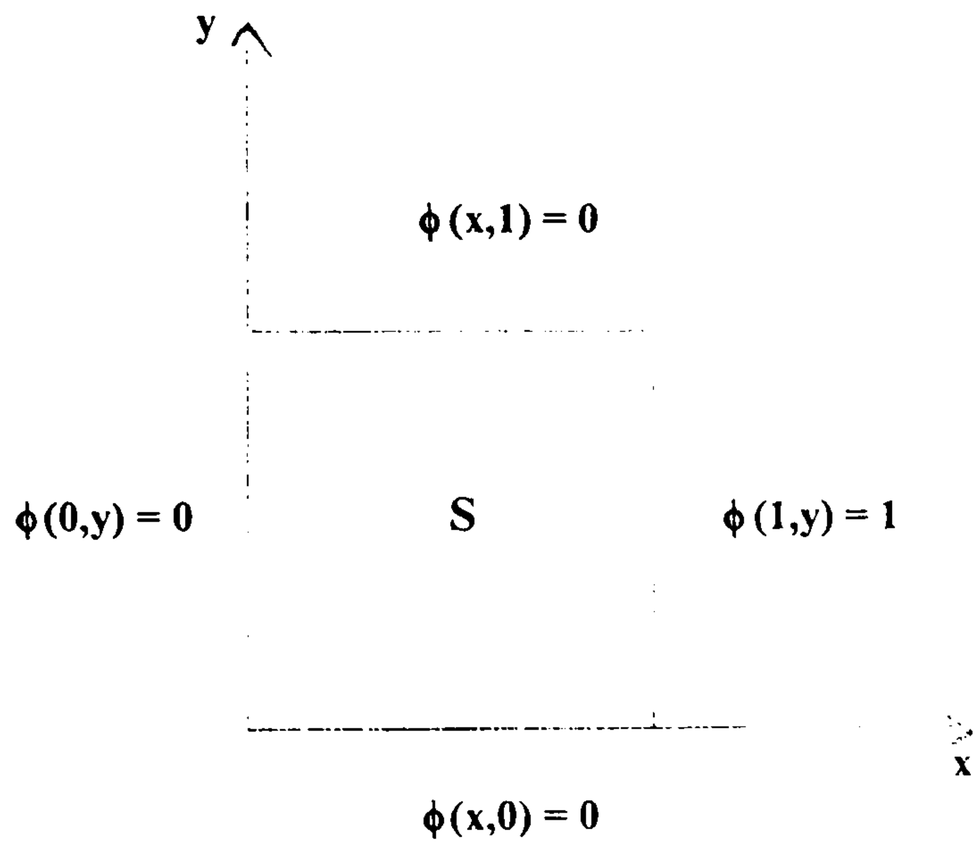

Figure 3.1:

The equation to solve is:

$$\frac{\partial^2 \phi}{\partial x^2} + \frac{\partial^2 \phi}{\partial y^2} = 0, \quad (x, y) \in \mathrm{S} \tag{3.1}$$

The solution must satisfy the following boundary conditions.

$$\begin{cases} \phi(0, y) = 0 \\ \phi(x, 0) = 0 \\ \phi(1, y) = 1 \\ \phi(x, 1) = 0 \end{cases} \tag{3.2}$$

This is a standard problem which can be easily solved by the method of separation of variables.

The general solution is obtained by using the principle of superposition following separation of variables and the homogeneous boundary conditions.

We obtain

$$\phi(x,y) = \sum_{n=1}^{\infty} A_n \sinh(n\pi x)\sin(n\pi y).$$

The inhomogeneous boundary condition $\phi(1,y) = 1$ leads us to

$$1 = \sum_{n=1}^{\infty} A_n \sinh(n\pi)\sin(n\pi y).$$

Using the theory of Fourier series, we then have

$$A_n = \frac{2\int_0^1 \sin(n\pi y)dy}{\sinh(n\pi)}.$$

Thus the exact solution is given by

$$\phi(x,y) = \sum_{n=1}^{\infty} A_n \sinh(n\pi x)\sin(n\pi y), \tag{3.3}$$

where the Fourier coefficients A_n of the half-range sine series for $f = 1$ are given by

$$A_n = \frac{2\int_0^1 \sin(n\pi y)dy}{\sinh(n\pi)} = \frac{2[1-(-1)^n]}{n\pi\sinh(n\pi)}.$$

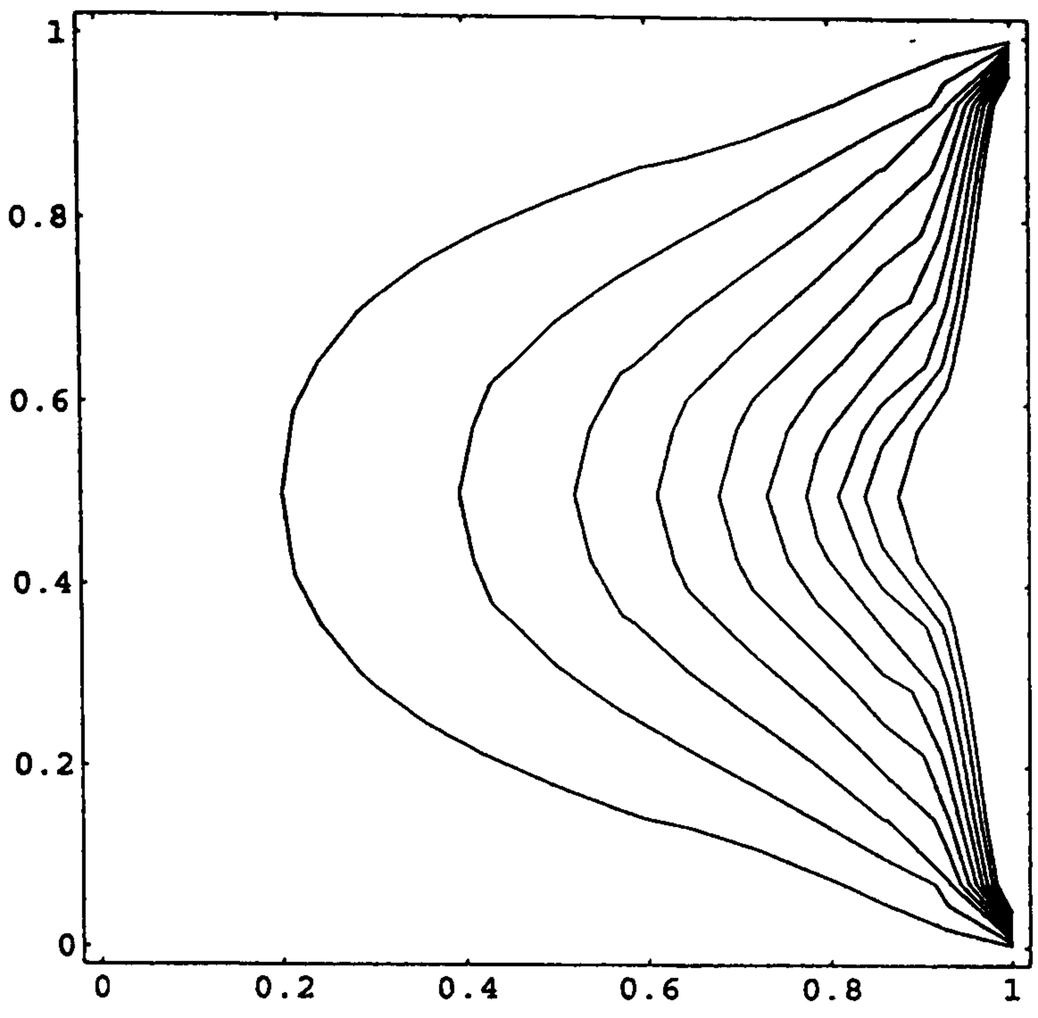

Figure 3.2: In this figure is given the graphical representation of the solution (3.3).

Problem 2

Because the hydrodynamic tidal problems will involve the Helmholtz operator, we now consider the Helmholtz equation $(\nabla^2 + \lambda^2)\phi = 0$ which can be solved in a similar way, with the same boundary conditions.

The general solution is obtained as before using the principle of superposition:

$$\phi(x,y) = \sum_{n=1}^{\infty} A'_n \sinh(\sqrt{(n^2\pi^2 - \lambda^2)}x)\sin(n\pi y)$$

The boundary condition $\phi(1,y) = 1$ implies that

$$\sum_{n=1}^{\infty} A'_n \sinh(\sqrt{(n^2\pi^2 - \lambda^2)})\sin(n\pi y) = 1$$

Using again the theory of Fourier series, we have

$$A'_n \sinh(\sqrt{(n^2\pi^2 - \lambda^2)}) = 2\int_0^1 \sin(n\pi y)dy = \{1 - (-1)^n\}\frac{2}{n\pi}$$

Thus the solution to Problem 2 is given by

$$\phi(x,y) = \sum_{n=1}^{\infty} A'_n \sinh(\sqrt{(n^2\pi^2 - \lambda^2)}x)\sin(n\pi y) \tag{3.4}$$

where

$$A'_n = \frac{\{1-(-1)^n\}\frac{2}{n\pi}}{\sinh(\sqrt{(n^2\pi^2-\lambda^2)})}$$

Problem 3

Let us now introduce a further difficulty into the model equation which is of a type to be encountered in the central oceanographic problems to be considered in this work.

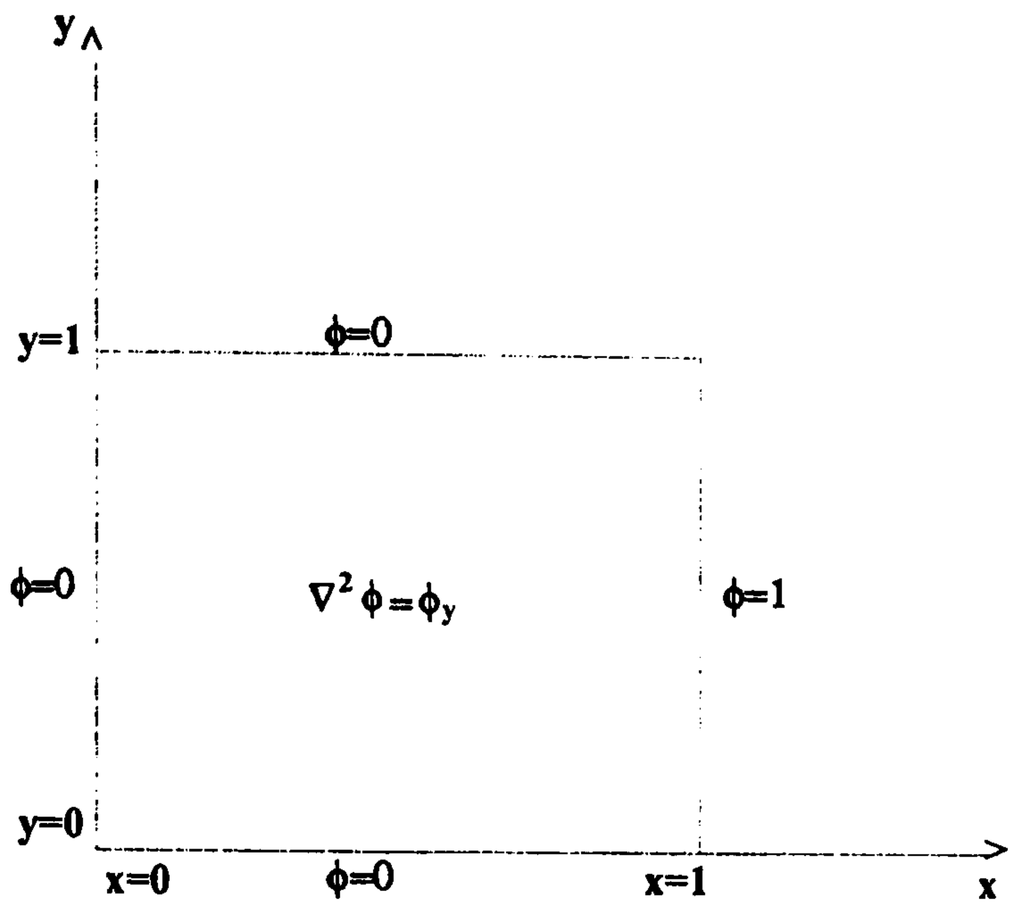

Figure 3.3: Schematic for Problem 3

The equation now considered is

$$\frac{\partial^2\phi}{\partial x^2}+\frac{\partial^2\phi}{\partial y^2}=\frac{\partial\phi}{\partial y},\ \ (x,y)\ \epsilon\ S\ . \tag{3.5}$$

This provides a more general problem, which highlights a difficulty symptomatic of the linearized rotating equations of motion.

In this problem we cannot represent the solution simply by means of a Fourier half-range series.

Suppose we attempt to solve (3.5) by means of a Fourier half-range sine series

$$\phi(x,y)=\sum_{n=1}^{\infty}A_n(x)\sin(n\pi y).$$

Then we are faced with a half-range sine series representation for $\nabla^2\phi$ and a half-range cosine series for ϕ_y. Thus, we cannot simply equate coefficients on both side.

To find exact solution of (3.5), we proceed with the usual separation of variables argument. Thus, writing $\phi = P(x)Q(y)$ we get the system

$$P''(x) - \omega^2 P(x) = 0 \quad \text{(i)}$$

$$Q''(x) - Q'(x) + \omega^2 Q = 0 \quad \text{(ii)} \tag{3.6}$$

where ω is a constant.

Consequently, if $|\omega| > \frac{1}{2}$,

$$\phi(x,y) = [a\cosh(\omega x) + b\sinh(\omega x)]\left(c\cos(\frac{\sqrt{4\omega^2-1}}{2}y) + d\sin(\frac{\sqrt{4\omega^2-1}}{2}y)\right)e^{\frac{1}{2}y}\ .$$

Using the boundary condition $\phi(0,y) = 0$ and $\phi(x,0) = 0$, we obtain $a = c = 0$ and from $\phi(x,1) = 0$ obtained

$$\omega = \sqrt{\left(n^2\pi^2 + \frac{1}{4}\right)}\ .$$

By applying the principle of superposition the general solution is,

$$\phi(x,y) = \sum_{n=1}^{\infty} A_n e^{\frac{1}{2}y}\sinh\left(\sqrt{(n^2\pi^2+\frac{1}{4})}x\right)\sin(n\pi y)\ .$$

The boundary condition $\phi(1,y) = 1$ implies

$$1 = \sum_{n=1}^{\infty} A_n e^{\frac{1}{2}y}\sinh\left(\sqrt{(n^2\pi^2+\frac{1}{4})}\right)\sin(n\pi y)\ .$$

By the theory of Fourier series we have,

$$A_n = \frac{2\int_0^1 e^{-\frac{1}{2}y}\sin(n\pi y)dy}{\sinh\left(\sqrt{(n^2\pi^2+\frac{1}{4})}\right)}\ .$$

Thus the more general solution is written as

$$\phi(x,y) = e^{\frac{1}{2}y}\sum_{n=1}^{\infty} A_n\sinh\left(\sqrt{(n^2\pi^2+\frac{1}{4})}x\right)\sin(n\pi y)\ . \tag{3.7}$$

where

$$A_n = \frac{-8\pi n}{4\pi^2n^2+1}\ \frac{\sqrt{e}(-1)^n - 1}{\sinh\left(\sqrt{(n^2\pi^2+\frac{1}{4})}\right)}\ .$$

So the $\phi(x, y)$, solution in (3.7) is no longer a Fourier series implying that a classical Fourier series ansatz would have been an inappropriate ansatz for this problem.

Here, it is worthwhile to note that it is the appearance of the odd-order y-derivative term which has caused the failure of the Fourier ansatz.

However the substitution

$$\phi(x, y) = \psi(x, y)e^{\frac{1}{2}y}$$

suggests itself and this would transform the problem for ψ into the Helmholtz equation (M2 above) but with $\psi(x, y) = e^{-\frac{1}{2}y}$ on $x = 1$ instead.

That is,

$$\left(\nabla^2 - \frac{1}{4}\right)\psi = 0$$

with boundary conditions

$$\psi(0, y) = 0 \quad \text{on} \quad x = 0$$

$$\psi(x, 0) = 0 \quad \text{on} \quad y = 0$$

$$\psi(x, 1) = 0 \quad \text{on} \quad y = 1$$

$$\psi(1, y) = e^{-\frac{1}{2}y} \quad \text{on} \quad x = 1$$

In fig(3.4) below, is given the graphical representation of the exact solution (3.7). It describes the equipotentials in this problem.

Problem 3 above is useful as a numerical bench mark. The well-known central difference approximation can be computed on the square at equally spaced and symmetrically placed internal nodes. If the solution (3.7) is computed 'exactly' then the numerical solution generates an 'error-standard' in the sense that this is an $O(h^2)$ method which can be used as a datum. Thus any other numerical innovations can

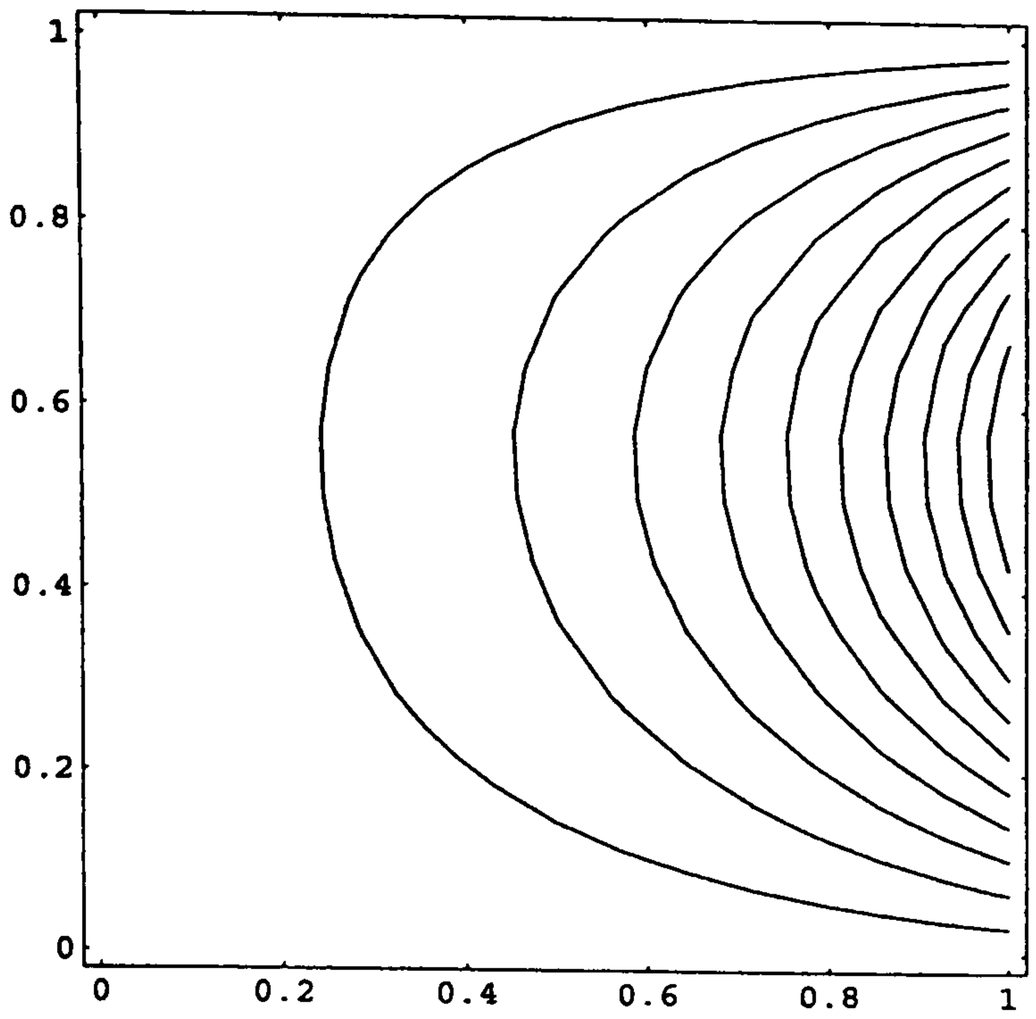

Figure 3.4: Equipotentials for solution to Problem 3

have their merits judged by reference to this 'standard'.

We suppose that it would not be possible, in the general equation we are ultimately facing, to eliminate odd order y-derivatives in this way. As such we need to look for an alternative scheme.

Alternative Scheme (a hybrid approach developed from Taylor's method)

In this approach we look for a way to eliminate, in the general equation, odd order y-derivatives .

To do this we invoke the procedure discussed earlier by Taylor in his problem [12] of replacing 'sines or cosines' in an expansion by further series of even multiples or odd multiples.

Suppose we attempt to solve the problem 3 by means of a Fourier half-range series.

$$\phi(x,y) = \sum_{n=1}^{\infty} A_n(x) \sin(n\pi y). \tag{3.8}$$

Then, assuming validity of differentiation inside the summation, we have

$$\nabla^2\phi = \sum_{n=1}^{\infty}\left\{A_n''(x) - n^2\pi^2 A_n(x)\right\}\sin(n\pi y); \qquad \phi_y = \sum_{n=1}^{\infty} n\pi A_n(x)\cos(n\pi y). \quad (3.9)$$

This then highlights the difficulty referred to earlier. We cannot simply equate coefficients because we are faced with a half-range sine series representation for $\nabla^2\phi$ and a half-range cosine series for ϕ_y.

However, we have seen that any suitable function $f \in C^0]0,\pi[$ can be expressed as both half-range sine and half-range cosine series.

We take Taylor's idea, so expand $\cos(n\pi y)$ as a Fourier half-range sine series.

Replace the result in (3.9) so there then follows

$$\phi_y = \sum_{n \text{ odd}} n\pi A_n(x) \sum_{m \text{ even}} \alpha_m^n \sin(m\pi y) + \sum_{n \text{ even}} n\pi A_n(x) \sum_{m \text{ odd}} \alpha_m^n \sin(m\pi y)$$

where

$$\alpha_m^n = \frac{(-)^m 4m}{\pi(n^2 - m^2)}.$$

Let us for the moment assume validity of exchanging the summation order.

Doing this, we find equation (3.5) in M2 is satisfied if

$$A_n''(x) - n^2\pi^2 A_n(x) = \sum_{\substack{k=1 \\ k \text{ odd}}}^{\infty} k\pi A_k(x)\alpha_n^k \qquad n=2,4,6,..... \quad \text{(i)}$$

$$A_n''(x) - n^2\pi^2 A_n(x) = \sum_{\substack{k=2 \\ k \text{ even}}}^{\infty} k\pi A_k(x)\alpha_n^k \qquad n=1,3,5,..... \quad \text{(ii)} \qquad (3.10)$$

Suppose initially, purely by way of illustration, we approximate ϕ with just a two-term expansion of (3.8).

$$\text{i.e} \qquad \phi(x,y) = A_1(x)\sin(\pi y) + A_2(x)\sin(2\pi y) \qquad (3.11)$$

The system (3.10) suitably truncated (i.e. take n=1,2) becomes

$$\begin{cases} A_2''(x) - 4\pi^2 A_2(x) = \alpha_2^1 \pi A_1(x) = \frac{8}{3} A_1(x) & \text{(i)} \\ A_1''(x) - \pi^2 A_1(x) = 2\alpha_1^2 \pi A_2(x) = -\frac{8}{3} A_2(x) & \text{(ii)} \end{cases} \tag{3.12}$$

This is easily solved. We have to fit $\phi(x, y) = 0$ on $x = 0$ and $\phi(x, y) = 1$ *on* $x = 1$.

We now impose the boundary condition $\phi(0, y) = 0$ on the solution (3.11).

This requires $A_1(0) = 0$ and $A_2(0) = 0$.

We assume, for $x > 0$, a solution of the form

$$A_1(x) = \alpha_1 \exp(\rho x),$$

$$A_2(x) = \alpha_2 \exp(\rho x). \tag{3.13}$$

In using (3.13) the system (3.12) yields

$$(\rho^2 - \pi^2)(\rho^2 - 4\pi^2) = -\frac{64}{9} \ . \tag{3.14}$$

The roots of the equation (3.14) are approximately

$$\rho_1 = 6.264 \qquad \text{and} \qquad \rho_2 = 3.180 \ .$$

Write the solution of the above system with $A_1(0) = A_2(0) = 0$ as

$$\begin{pmatrix} A_1(x) \\ A_2(x) \end{pmatrix} = \begin{pmatrix} \alpha_1 & \beta_1 \\ \beta_2 & \alpha_2 \end{pmatrix} \begin{pmatrix} \sinh(\rho_1 x) \\ \sinh(\rho_2 x) \end{pmatrix}. \tag{3.15}$$

Using the solution (3.15) in (3.12) yields

$$\alpha_2(\rho_2^2 - 4\pi^2) = \frac{8}{3}\beta_1,$$

$$\alpha_1(\rho_1^2 - \pi^2) = -\frac{8}{3}\beta_2. \tag{3.16}$$

On imposing boundary condition $\phi(x,y) = 1$ on $x = 1$ we have from (3.11)

$$\phi(1,y) = A_1(1)\sin(\pi y) + A_2(1)\sin(2\pi y) = 1. \tag{3.17}$$

Meanwhile for the two-term Fourier sine series expansion of 1 we have

$$1 = \sum_{n=1}^{2} C_n \sin(\frac{n\pi y}{1}) = C_1 \sin(\pi y) + C_2 \sin(2\pi y). \tag{3.18}$$

where

$$C_1 = \frac{2}{1}\int_0^1 \sin(\pi y)dy = \frac{4}{\pi}$$
$$C_2 = \frac{2}{1}\int_0^1 \sin(2\pi y)dy = 0$$

On equating the coefficients of $\sin(\pi y)$ and $\sin(2\pi y)$ in equations (3.17) and (3.18) we have

$$A_1(1) = \frac{4}{\pi} \qquad \text{and} \qquad A_2(1) = 0.$$

We then have

$$\frac{4}{\pi} = \alpha_1 \sinh(\rho_1) + \beta_1 \sinh(\rho_2) \quad \text{(i)}$$
$$0 = \alpha_2 \sinh(\rho_2) + \beta_2 \sinh(\rho_1) \quad \text{(ii)} \tag{3.19}$$

The system of conditions (3.16) and (3.19) yields the matrix equation as

$$\begin{pmatrix} 262.66 & 0 & 12.00 & 0 \\ 0 & 12.00 & 0 & 262.66 \\ 29.37 & 0 & 0 & 2.667 \\ 0 & 29.37 & 2.667 & 0 \end{pmatrix} \begin{pmatrix} \alpha_1 \\ \alpha_2 \\ \beta_1 \\ \beta_2 \end{pmatrix} = \begin{pmatrix} \frac{4}{\pi} \\ 0 \\ 0 \\ 0 \end{pmatrix} \tag{3.20}$$

The system (3.20) can be solved for β_2 , β_1 , α_2 , α_1 by Gaussian Elimination Technique.

That is,

$$\begin{pmatrix} 262.66 & 0 & 12.00 & 0 \\ 0 & 12.00 & 0 & 262.66 \\ 0 & 0 & -1.342 & 2.667 \\ 0 & 0 & 0 & -637.56 \end{pmatrix} \begin{pmatrix} \alpha_1 \\ \alpha_2 \\ \beta_1 \\ \beta_2 \end{pmatrix} = \begin{pmatrix} 1.2732 \\ 0 \\ -0.1424 \\ -0.283 \end{pmatrix}$$

By using backward substitution we obtain

$$\beta_2 = \frac{-0.283}{-637.56} = 4.438 * 10^{-4}$$

$$\beta_1 = \frac{-0.1424 - 2.667 * 4.438 * 10^{-4}}{-1.342} = 0.10698$$

$$\alpha_2 = \frac{-262.66 * 4.438 * 10^{-4}}{12} = -9.715 * 10^{-3}$$

$$\alpha_1 = \frac{1.2732 - 12 * 0.10698}{262.66} = -4.0304 * 10^{-5}$$

Now we are able to compute approximate values $\phi(x, y)$ at four internal nodes A,B,C,D as shown on the grid below.

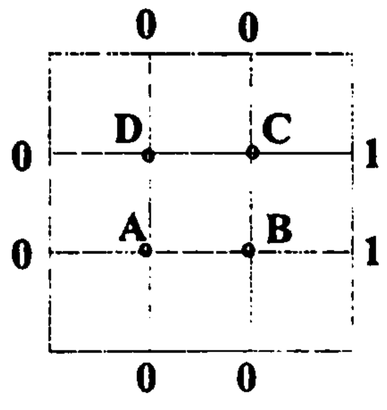

Figure 3.5:

A two-term expansion of (3.8) is

$$\phi(x, y) = (\alpha_1 \sinh \rho_1 x + \beta_1 \sinh \rho_2 x) \sin(\pi y) + (\alpha_2 \sinh \rho_2 x + \beta_2 \sinh \rho_1 x) \sin(2\pi y) \tag{3.21}$$

Now by taking $\rho_1 = 6.264$ and $\rho_2 = 3.180$ we evaluated from (3.21) the approximate value of $\phi(x, y)$ at the point $A \equiv (\frac{1}{3}, \frac{1}{3})$ as

$$\phi(\frac{1}{3}, \frac{1}{3}) = 0.1084$$

Similarly we evaluated the approximate values at point B,C,D and being tabulated below.

Points	Solutions
A	0.1084
B	0.3572
C	0.4013
D	0.1267

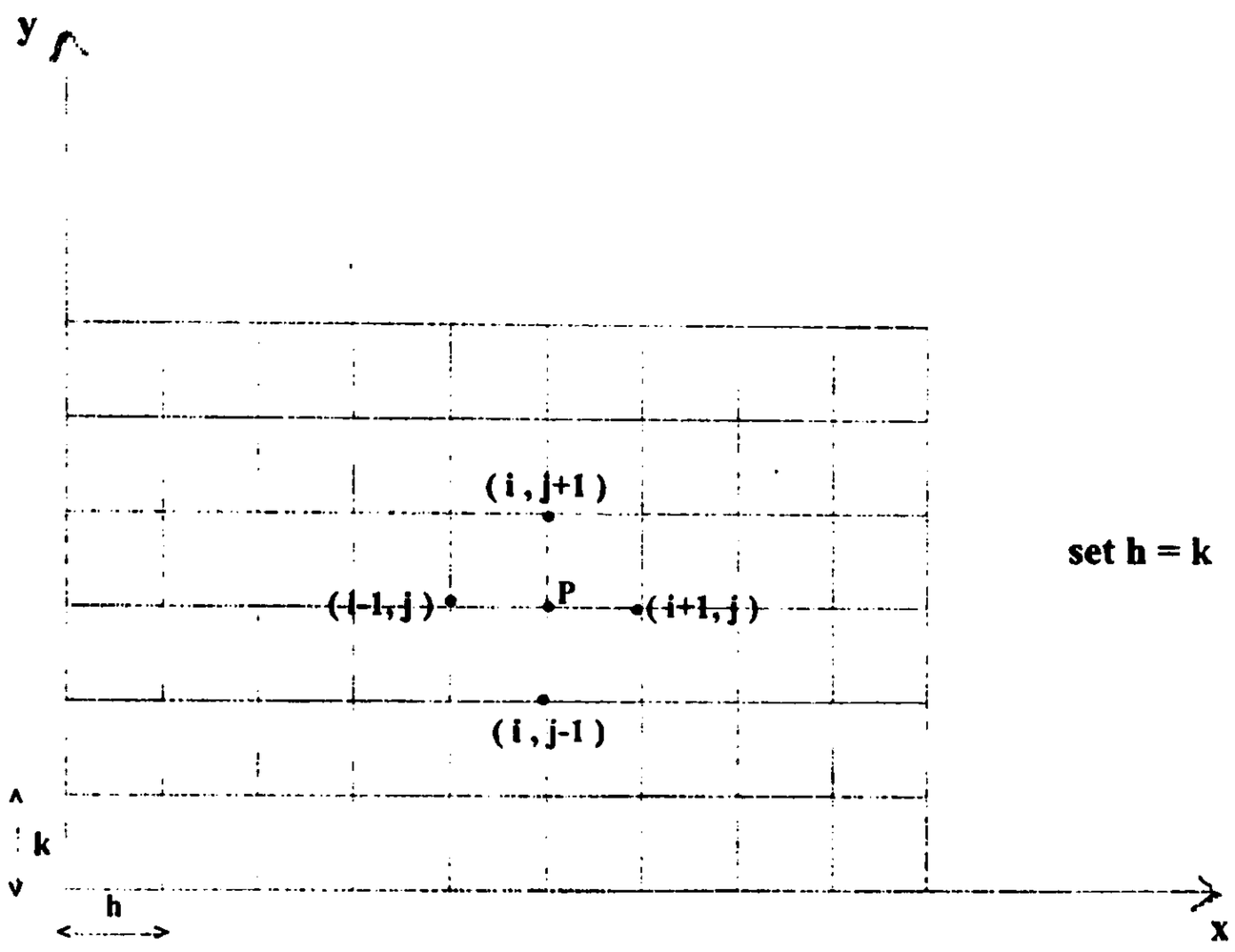

set h = k

Figure 3.6:

Finite Difference Method

As a further alternative we also obtain the results using a finite difference method. The corresponding difference equations for the differential equation (3.5) are developed as follows.

The left hand side of equation (3.5) is given as

$$\nabla^2\phi_{(i,j)} = \frac{1}{h^2}\left\{\phi_{(i+1,j)} + \phi_{(i-1,j)} + \phi_{(i,j+1)} + \phi_{(i,j-1)} - 4\phi_{(i,j)}\right\} + 0(h^2)$$

with leading error on the right-hand side of order $0(h^2)$.

The central difference rule allows us to write the right-hand side of equation (3.5) with the same order of accuracy.

$$\phi_y = (\frac{\partial \phi}{\partial y})_{(i,j)} = \frac{1}{2h}\left\{\phi_{(i,j+1)} - \phi_{(i,j-1)}\right\} + 0(h^2)$$

We adopt the same grid with 4 equally spaced and symmetrically placed internal nodes.

We get the following system with $h = \frac{1}{3}$.

$$\left\{\begin{array}{c} 9(-4\phi_A + \phi_B + 0 + \phi_D + 0) = \frac{3}{2}\phi_D \\ 9(-4\phi_B + 1 + \phi_A + 0 + \phi_C) = \frac{3}{2}\phi_C \\ 9(-4\phi_C + 1 + \phi_D + 0 + \phi_B) = -\frac{3}{2}\phi_B \\ 9(-4\phi_D + \phi_C + 0 + 0 + \phi_A) = -\frac{3}{2}\phi_A \end{array}\right\} \tag{3.22}$$

The system (3.22) can now be written as

$$\begin{pmatrix} -24 & 6 & 0 & 5 \\ 6 & -24 & 5 & 0 \\ 0 & 7 & -24 & 6 \\ 7 & 0 & 6 & -24 \end{pmatrix} \begin{pmatrix} \phi_A \\ \phi_B \\ \phi_C \\ \phi_D \end{pmatrix} = \begin{pmatrix} 0 \\ -6 \\ -6 \\ 0 \end{pmatrix}$$

The solution is,

$$\phi_D = 0.1313,$$

$$\phi_C = 0.3879,$$

$$\phi_B = 0.3601,$$

$$\phi_A = 0.1174.$$

By suitably defining a global error norm as

$$E = \frac{1}{4}\sum \left| \phi_{\text{exact}} - \phi_{\text{technique}} \right| .$$

we can compare the relative accuracies of different approximation methods.

Clearly, we can extend the definition of E to any number of points in the solution domain.

Points	exact solution	Taylor's procedure	Finite Difference Method
A	0.1098	0.1084	0.1174
B	0.3625	0.3572	0.3601
C	0.3938	0.4013	0.3879
D	0.1253	0.1267	0.1313
E		0.0039	0.00548

Where $E = Error$

Here, it appears that Taylor's technique gives a better approximation than the finite difference method.

Clearly, we have to adopt a numerical scheme for solving the system (3.10). This appears to be fairly straightforward where we can write down a Green's function solution integral for the even A_n in terms of an integral of the odd ones and vice versa. An iterative scheme based on initial guesses for $A_n(x)$ which might be those from Taylor's model over a bottom of uniform depth (taken as the mean) should, in principle, work.

Green's Function Technique:

Here, we use the Green's Function approach to solve the system (3.10) in an iterative manner.

When we use Green's function to solve boundary value problems, the Green's function is independent of the non-homogeneous term in the differential equation. Once the Green's function is determined, the solution of the non-homogeneous system for different non-homogeneous forcing terms is obtained by a single integration.

We call the system (3.12) here,

$$\begin{cases} A_1''(x) - \pi^2 A_1(x) = -\frac{8}{3} A_2(x) \\ A_2''(x) - 4\pi^2 A_2(x) = \frac{8}{3} A_1(x) \end{cases}$$

These two equations can here be written in a general form as

$$y_m''(x) - m^2\pi^2 y_m(x) = f(x) \tag{3.23}$$

where m is a positive integer.

Now we look for solutions of

$$G_m''(x|s) - m^2\pi^2 G_m(x|s) = 0 \tag{3.24}$$

where $x \in [0,1]_{x \neq s}$ and $x = s$ is a point of discontinuity in gradient.

$G_m(x|s)$ is the Green's function in general form corresponding to the two equations of the system (3.12).

The solution of (3.24) given as

$$G_-(x|s) = A\sinh(m\pi x) \qquad \forall \ 0 \leq x \leq s$$

$$G_+(x|s) = B\sinh(m\pi(x-1)) \qquad \forall \ s \leq x \leq 1$$

where A and B are arbitrary constants.

We require G to be continuous at $x = s$.

Thus $G_-(x|s) = G_+(x|s)$ at the point $x = s$, and we have

$$A\sinh(m\pi s) = B\sinh(m\pi(s-1)). \tag{3.25}$$

In equation(3.25) we set

$$A = \sinh(m\pi(s-1)) \qquad \text{and} \qquad B = \sinh(m\pi s).$$

The solution of (3.24) is written as

$$G_m(x|s) = \begin{cases} G_-(x|s) = \sinh(m\pi(s-1))\sinh(m\pi x) \\ G_+(x|s) = \sinh(m\pi s)\sinh(m\pi(x-1)). \end{cases}$$

To look for a general form of the solution of (3.12) we multiply the equation (3.23)

by the Green's function $G_m(x|s)$ and integrate with respect to x from 0 to 1.

$$\int_0^1 G_m(x|s)\left(\ \tfrac{d^2y_m}{dx^2} - m^2\pi^2 y_m\ \right)dx = \int_0^1 f(x)G_m(x|s)dx. \qquad \text{m=1,2} \qquad (3.26)$$

On integrating (3.26) by parts, we get

$$\left[\ G_m(x|s)\tfrac{dy_m}{dx}\ \right]_0^1 - \int_0^1 \left[\ \tfrac{dG_m(x|s)}{dx}\tfrac{dy_m}{dx} + m^2\pi^2 y_m G_m(x|s)\ \right]dx$$
$$= \int_0^1 f(x)G_m(x|s)dx. \qquad (3.27)$$

As $G(x|s) = 0$ at $x = 0$ and $x = 1$ (3.27) becomes

$$-\int_0^1 \left[\ \tfrac{dG_m(x|s)}{dx}\tfrac{dy_m(x)}{dx}\ \right]dx - \int_0^1 (m^2\pi^2 y_m(x)G_m(x|s))dx$$
$$= \int_0^1 f(x)G_m(x|s)dx. \qquad (3.28)$$

Since $G'_m(x|s)$ is discontinuous at $x = s$ we write (3.28) as

$$-\int_0^s \left[\ \tfrac{dG_m(x|s)}{dx}\tfrac{dy_m(x)}{dx}\ \right]dx - \int_s^1 \left[\ \tfrac{dG_m(x|s)}{dx}\tfrac{dy_m(x)}{dx}\ \right]dx - \int_0^1 (m^2\pi^2 y_m(x)G_m(x|s))dx$$
$$= \int_0^1 f(x)G_m(x|s)dx$$

Integrating by parts yields

$$-\left[\ \tfrac{dG_m(x|s)}{dx}y_m(x)\ \right]_0^s + \int_0^s \left[\ \tfrac{d^2G_m(x|s)}{dx^2}y_m(x)\ \right]dx - \left[\ \tfrac{dG_m(x|s)}{dx}y_m(x)\ \right]_s^1 +$$

$$\int_s^1 \left[\ \tfrac{d^2G_m(x|s)}{dx^2}y_m(x)\ \right]dx - \int_0^1 (m^2\pi^2 y_m(x)G_m(x|s))dx = \int_0^1 f(x)G_m(x|s)dx$$

Invoke the boundary conditions $y(0) = 0$ and $y(1) = 0$ to give

$$-y_m(s)\left\{ \frac{dG_m(x|s)}{dx}|_{x=s_-} \right\} + y_m(s)\left\{ \frac{dG_m(x|s)}{dx}|_{x=s_+} \right\} + \int_0^s \left[\frac{d^2G_m(x|s)}{dx^2} y_m(x) \right] dx$$
$$+ \int_s^1 \left[\frac{d^2G_m(x|s)}{dx^2} y_m(x) \right] dx - \int_0^1 (m^2\pi^2 y_m(x) G_m(x|s))dx = \int_0^1 f(x)G_m(x|s)dx \qquad (3.29)$$

From (3.24) we have

$$\frac{d^2G_m(x|s)}{dx^2} = m^2\pi^2 G_m(x|s)$$

The solution of (3.23) in terms of the Green's function can be written as

$$y_m(s) = \frac{\int_0^1 f(x)G_m(x|s)dx}{\left\{ \frac{dG_m(x|s)}{dx}|_{x=s_+} \right\} - \left\{ \frac{dG_m(x|s)}{dx}|_{x=s_-} \right\}}. \qquad (3.30)$$

It is seen that

$$\left\{ \frac{dG_m(x/s)}{dx}|_{x=s_+} \right\} - \left\{ \frac{dG_m(x/s)}{dx}|_{x=s_-} \right\} = m\pi \sinh(m\pi).$$

So the solution (3.30) becomes

$$y_m(s) = \frac{\int_0^1 f(x)G_m(x|s)dx}{m\pi \sinh(m\pi)}. \qquad (3.31)$$

Since $G'_m(x|s)$ is discontinuous at $x = s$, (3.31) can be rewritten as

$$y_m(s) = \frac{1}{m\pi \sinh(m\pi)} \left[\begin{array}{l} \int_0^s f(x) \sinh(m\pi(s-1)) \sinh(m\pi x)dx + \\ \\ \int_s^1 f(x) \sinh(m\pi s)) \sinh(m\pi(x-1))dx \end{array} \right]. \qquad (3.32)$$

Returning to our two-term expansion, $m = 1, 2$, the solution (3.32) can be written as

$$\begin{cases} y_1(s) = \frac{\sinh(\pi(s-1))}{\pi \sinh(\pi)} \int_0^s f(x) \sinh(\pi x)dx + \frac{\sinh(\pi s)}{\pi \sinh(\pi)} \int_s^1 f(x) \sinh(\pi(x-1))dx \\ \\ y_2(s) = \frac{\sinh(2\pi(s-1))}{2\pi \sinh(2\pi)} \int_0^s f(x) \sinh(2\pi x)dx + \frac{\sinh(2\pi s)}{2\pi \sinh(2\pi)} \int_s^1 f(x) \sinh(2\pi(x-1))dx. \end{cases}$$

In the system (3.12) we have the following boundary conditions

$$\begin{cases} A_1(x) = 0, \ A_2(x) = 0 \quad \text{at } x = 0, \\ A_2(x) = 0 \quad \text{at } x = 1, \ \text{and } A_1(x) = \frac{4}{\pi} \quad \text{at } x = 1. \end{cases}$$

Since $y_2(x)$=0 both at $x = 0$ and $x = 1$, we let $A_2(x)$=$y_2(x)$, but $y_1(x) = 0$ at both $x = 0$, $x = 1$ whereas $A_1(x) = 0$ at x=0, but $A_1(x) = \frac{4}{\pi}$ at $x = 1$ and thus we set $A_1(x) = y_1(x) + \frac{4}{\pi}x$.

Thus we can write

$$A_1''(x) - \pi^2 A_1(x) = y_1''(x) - \pi^2 y_1(x) - 4\pi x = -\frac{8}{3}A_2(x)$$

Thus

$$f(x) = -\frac{8}{3}A_2(x) + 4\pi x. \tag{3.33}$$

By taking $f(x)$ as described in (3.33) we can write down the solution $A_1(s)$ of the system (3.12) as

$$\begin{cases} A_1(s) = \frac{\sinh(\pi(s-1))}{\pi \sinh(\pi)} \int_0^s (-\frac{8}{3}A_2(x) + 4\pi x) \sinh(\pi x) dx \\ \qquad + \frac{\sinh(\pi s)}{\pi \sinh(\pi)} \int_s^1 (-\frac{8}{3}A_2(x) + 4\pi x) \sinh(\pi(x-1)) dx + \frac{4}{\pi}s. \end{cases}$$

Thus the solution of the system (3.12) is given implicitly by,

$$\begin{aligned} A_1(s) = & \frac{\sinh(\pi(s-1))}{\pi \sinh(\pi)} \int_0^s (-\frac{8}{3}A_2(x) + 4\pi x) \sinh(\pi x) dx \\ & + \frac{\sinh(\pi s)}{\pi \sinh(\pi)} \int_s^1 (-\frac{8}{3}A_2(x) + 4\pi x) \sinh(\pi(x-1)) dx + \frac{4}{\pi}s \\ A_2(s) = & \frac{\sinh(2\pi(s-1))}{2\pi \sinh(2\pi)} \int_0^s \frac{8}{3}A_1(x) \sinh(2\pi x) dx + \frac{\sinh(2\pi s)}{2\pi \sinh(2\pi)} \int_s^1 \frac{8}{3}A_1(x) \sinh(2\pi(x-1)) dx. \end{aligned} \tag{3.34}$$

We have written in (3.34) Green's function solution integral for the odd A_n in terms of an integral of the even ones and vice versa.

We use the trapezium rule to solve the two Green's function solution integrals based on as initial guess for $A_1(x)$. We thus initialize at internal points with $A_1 = 1$ (constant value) and integrate to achieve $A_2(x)$ at each point. Having A_2, we update

A_1 with the other equation. This process is repeated until we achieve the desired accuracy.

Once $A_1(x)$ and $A_2(x)$ have been determined, we compute the function (3.8) for $\phi(x, y)$ using the two-term expansion.

Approximate Solution of $\phi(x, y)$ with a 4-term expansion of (3.8)

Here, we extend our numerical scheme to find the approximate solution of the problem 3 by using a 4-term expansion of (3.8).

The 4-term expansion of (3.8) is

$$\phi(x, y) = A_1(x)\sin(\pi y) + A_2(x)\sin(2\pi y) + A_3(x)\sin(3\pi y) + A_4(x)\sin(4\pi y). \quad (3.35)$$

The boundary condition $\phi(0, y) = 0$ has to be satisfied.

$$0 = A_1(x)\sin(\pi y) + A_2(x)\sin(2\pi y) + A_3(x)\sin(3\pi y) + A_4(x)\sin(4\pi y) \quad (3.36)$$

The condition (3.36) is satisfied $\forall\ y$ only if $A_i(0) = 0, \quad \forall\ i = 1, 2, 3, 4.$

The system (3.10) becomes

$$\begin{cases} A_1''(x) - \pi^2 A_1(x) = -\frac{8}{3}A_2(x) - \frac{4}{15}A_2(x) & \text{(i)} \\ A_2''(x) - 4\pi^2 A_2(x) = \frac{8}{3}A_1(x) - \frac{8}{5}A_3(x) & \text{(ii)} \\ A_3''(x) - 9\pi^2 A_3(x) = -\frac{48}{7}A_4(x) + \frac{24}{5}A_2(x) & \text{(iii)} \\ A_4''(x) - 16\pi^2 A_4(x) = \frac{16}{15}A_1(x) + \frac{48}{7}A_3(x) & \text{(iv)} \end{cases} \quad (3.37)$$

Now we use the boundary condition $\phi(1, y) = 1$. Thus in (3.35) we have

$$1 = A_1(1)\sin(\pi y) + A_2(1)\sin(2\pi y) + A_3(1)\sin(3\pi y) + A_4(1)\sin(4\pi y) \quad (3.38)$$

The 4-term Fourier sine series expansion of '1' is

$$\begin{cases} 1 = \sum_1^4 b_n \sin(n\pi y) \\ \text{where} \quad b_n = 2\int_0^1 1 \sin(n\pi y) dy \end{cases} \qquad \text{n=1,2,3,4} \tag{3.39}$$

In (3.39), b_i(i=1,2,3,4) are evaluated as

$$b_1 = \frac{4}{\pi}, \quad b_2 = 0, \quad b_3 = \frac{4}{3\pi}, \quad b_4 = 0 \tag{3.40}$$

Thus from (3.40) we have

$$A_1(1) = \frac{4}{\pi}, \quad A_2(1) = A_4(1) = 0, \quad A_3(1) = \frac{4}{3\pi}.$$

Now we have to solve the system (3.37) with the following boundary conditions.

$$\begin{cases} A_1(1) = \frac{4}{\pi}, A_2(1) = A_4(1) = 0, A_3(1) = \frac{4}{3\pi}, \\ \\ A_1(0) = A_2(0) = A_4(0) = A_3(0) = 0. \end{cases} \tag{3.41}$$

The Green's function corresponding to each equation of the system (3.37) is, as before, given as

$$G_m(x,s) = \begin{cases} G_-(x,s) = \sinh(m\pi(s-1))\sinh(m\pi x) \\ G_+(x,s) = \sinh(m\pi s)\sinh(m\pi(x-1)) \end{cases}$$

where $m = 1, 2, 3, 4$

Thus the solution of the system (3.37) with boundary conditions (3.41) in terms of

the Green's function is given by

$$\begin{cases} A_1(s) = \frac{\sinh(\pi(s-1))}{\pi\sinh(\pi)}\int_0^s(-\frac{8}{3}A_2(x)-\frac{16}{15}A_4(x)+4\pi x)\sinh(\pi x)dx \\ \qquad\qquad +\frac{\sinh(\pi s)}{\pi\sinh(\pi)}\int_s^1(-\frac{8}{3}A_2(x)-\frac{16}{15}A_4(x)+4\pi x)\sinh(\pi(x-1))dx+\frac{4}{\pi}s \\ \\ A_2(s) = \frac{\sinh(2\pi(s-1))}{2\pi\sinh(2\pi)}\int_0^s(\frac{8}{3}A_1(x)-\frac{24}{5}A_3(x))\sinh(2\pi x)dx \\ \qquad\qquad +\frac{\sinh(2\pi s)}{2\pi\sinh(2\pi)}\int_s^1(\frac{8}{3}A_1(x)-\frac{24}{5}A_3(x))\sinh(2\pi(x-1))dx \\ A_3(s) = \frac{\sinh(3\pi(s-1))}{3\pi\sinh(3\pi)}\int_0^s(-\frac{48}{7}A_4(x)-\frac{24}{5}A_2(x)+12\pi x)\sinh(3\pi x)dx \\ \qquad\qquad +\frac{\sinh(3\pi s)}{3\pi\sinh(3\pi)}\int_s^1(-\frac{48}{7}A_4(x)-\frac{24}{5}A_2(x)+12\pi x)\sinh(3\pi(x-1))dx+\frac{4}{3\pi}s \\ \\ A_4(s) = \frac{\sinh(4\pi(s-1))}{4\pi\sinh(4\pi)}\int_0^s(\frac{48}{7}A_3(x)+\frac{16}{15}A_1(x))\sinh(4\pi x)dx \\ \qquad\qquad +\frac{\sinh(4\pi s)}{4\pi\sinh(4\pi)}\int_s^1(\frac{48}{7}A_3(x)+\frac{16}{15}A_1(x))\sinh(4\pi(x-1))dx \end{cases}$$

Generally, the solution of (3.10) subject to the boundary conditions, in terms of the Green's function is given by

$$A_n(s) = \int_0^1 G_n(x,s)\sum_{k\text{ odd}} k\pi\alpha_n^k A_k(x)dx \qquad n \text{ even}$$

$$A_n(s) = \frac{4s}{n\pi} + \int_0^1 G_n(x,s)\{\sum_{k\text{ even}}(k\pi\alpha_n^k A_k(x)+4n\pi x)\}dx \qquad n \text{ odd.}$$

where, $\alpha_n^k = \dfrac{-4n}{\pi(k^2-n^2)}$

We used Contour Plot in Mat-Lab(6.1) to get the graphical representation fig(3.7) below of the approximation of the 5-term expansion of ϕ with Green's function technique.

Concluding Remarks

Taylor's method of replacing sines/cosines in an expansion by further series of even or odd multiples appears to be a useful technique. We have seen that it gives slightly better result than the 'finite difference method', based on the order of matrix inverted being similar.

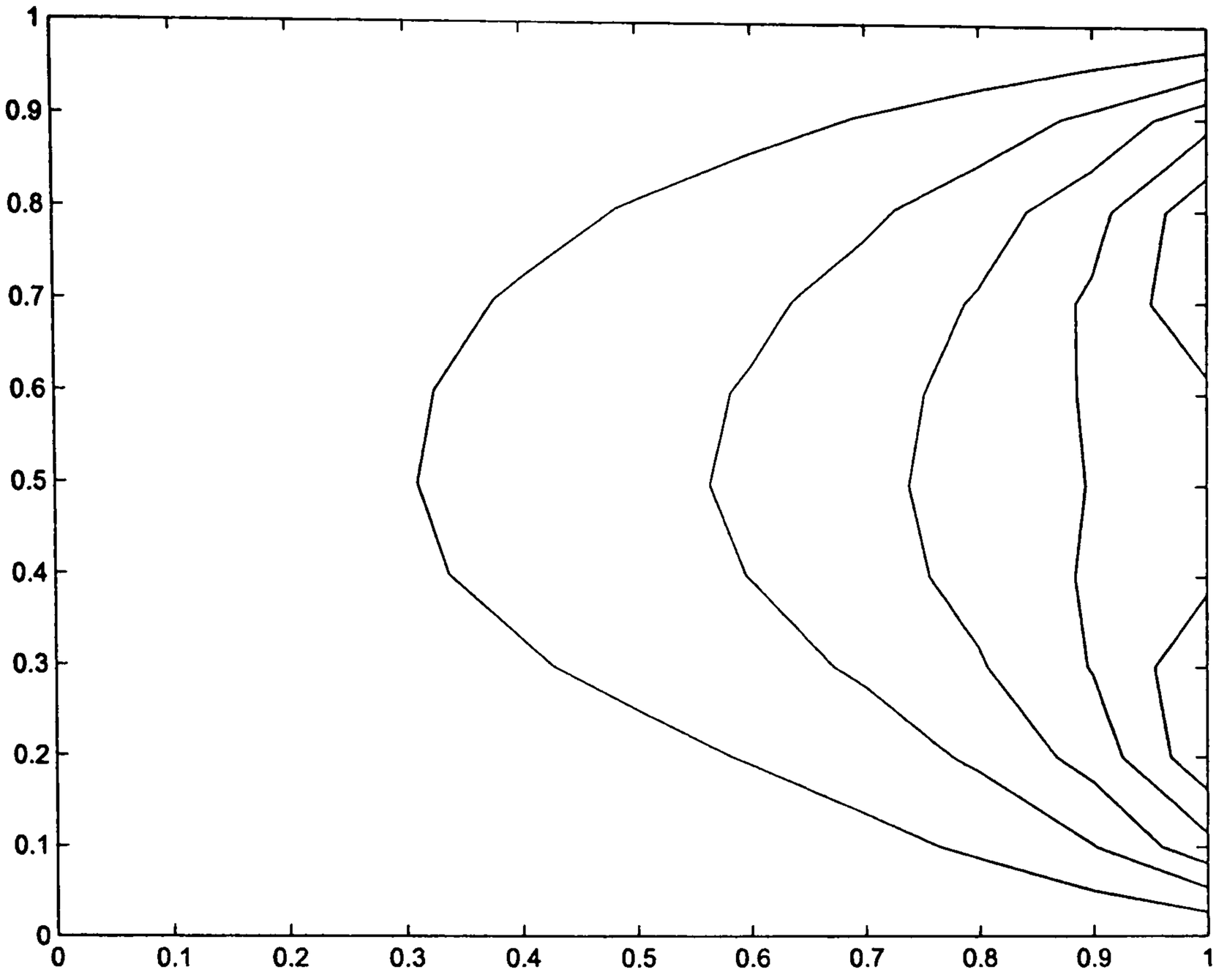

Figure 3.7: Equipotentials

The Green's function technique of writing down a Green's function solution integral for the even A_n in terms of an integral of the odd ones and vice versa allows us to write the approximate solution with an n-term expansion. It can be shown through the computation that in an n-term expansion, when n is large a better approximation is obtained.

Now the question is, would Green's function technique be suitable to solve the generalized Taylor's problem?

In solving the Model problem 3, we have seen that the Green's functions were solutions of the homogeneous system of the form

$$y'' + ay = 0, \qquad \text{with constant coefficient.}$$

In considering the generalized Taylor's problems, this could be a useful method for a simpler model (e.g. Step-Bottom) where the sea-beds are given by $h = h_0$ and $h = h_1$. But in the case of variable depth, given by, e.g., $h(x) = \alpha x + h_0$, the coefficient of

the homogeneous equation would not be constant but rather it would be of the form $ax + b$ which creates a further difficulty.

This will be a study area in the current work. The only solutions that currently exist for such geometries are numerical models.

Chapter 4

Kelvin wave reflection in a semi-infinite canal closed at one end

We expand the wave height in a Fourier Series across the channel and start with a look at Taylor's problem again but in dimensional form. This is done with a view to comparison with the limiting form a time dependent solution from a numerical method developed by Johns (personal communication).

4.1 Defining equation:

We have, as before, the system

$$\begin{cases} i\sigma u - fv = -g\zeta_x & \text{(i)} \\ i\sigma v + fu = -g\zeta_y & \text{(ii)} \\ \frac{\partial}{\partial x}(hu) + \frac{\partial}{\partial y}(hv) + i\sigma\zeta = 0 & \text{(iii)} \end{cases} \tag{4.1}$$

so that an equation for ζ in case where h varies with x can be written

$$h(x)\nabla^2\zeta - \lambda\zeta + \alpha(\frac{\partial\zeta}{\partial x} - \frac{if}{\sigma}\frac{\partial\zeta}{\partial y}) = 0$$

with the lateral boundary condition

$$L[\zeta] = 0, \quad y = 0 \text{ and } y = \pm b$$

where $L \equiv f\partial_x - i\sigma\partial_y$, $\lambda = \frac{(f^2-\sigma^2)}{g}$ and $\alpha = \frac{f}{c}$.

By elimination we obtain the consistency requirements.

$$i\sigma\frac{\partial u}{\partial y} - f\frac{\partial u}{\partial x} = i\sigma\frac{\partial v}{\partial x} + f\frac{\partial v}{\partial y}.$$

4.2 Brown's treatment of Taylor's tidal problem-Collocation Method:

Brown (1973) reformulated Taylor's tidal problem for a rotating semi-infinite canal so as to allow for the possibility of imperfect reflection of Kelvin waves. He obtained

solutions using the method of collocation at the closed end of the canal. He also discussed the behavior of the solution for the limiting cases of a narrow canal and of a short-period oscillation.

Taylor (1921) and subsequently Defant (1925) considered two Kelvin waves of equal amplitude traveling in opposite directions in the canal. The origin of the co-ordinate system was chosen such that the phases of both incident and reflected waves matched at the plane $x = 0$. They added an end-effect term so as to determine the position of closed end. Taylor used Fourier expansion methods whereas Defant used collocation and they obtained similar results.

Brown (1973) in his paper had chosen the origin of co-ordinates to be at one corner of the canal. He assigned unit amplitude of the incoming wave whereas the amplitude and phase of the outgoing wave were determined. The end-effect is chosen in such a way it excludes any incoming *Poincaré* modes. Brown used the collocation method to determine the relevant coefficients and found that results were in excellent agreement with those found by Taylor and Defant. Brown's method, which will be used widely in the present work, is therefore discussed briefly below as applied to Taylor's original problem.

4.3 Formulation:

A semi-infinite canal rotating about the vertical axis with constant angular velocity ω is considered. The horizontal coordinates are (x, y), defined such that the canal occupies the region $x \geq 0$, $0 \leq y \leq b$ as shown in fig (4.1).

We first rewrite Taylor's ansatz using the $[0, b]$ channel boundaries and the unknown

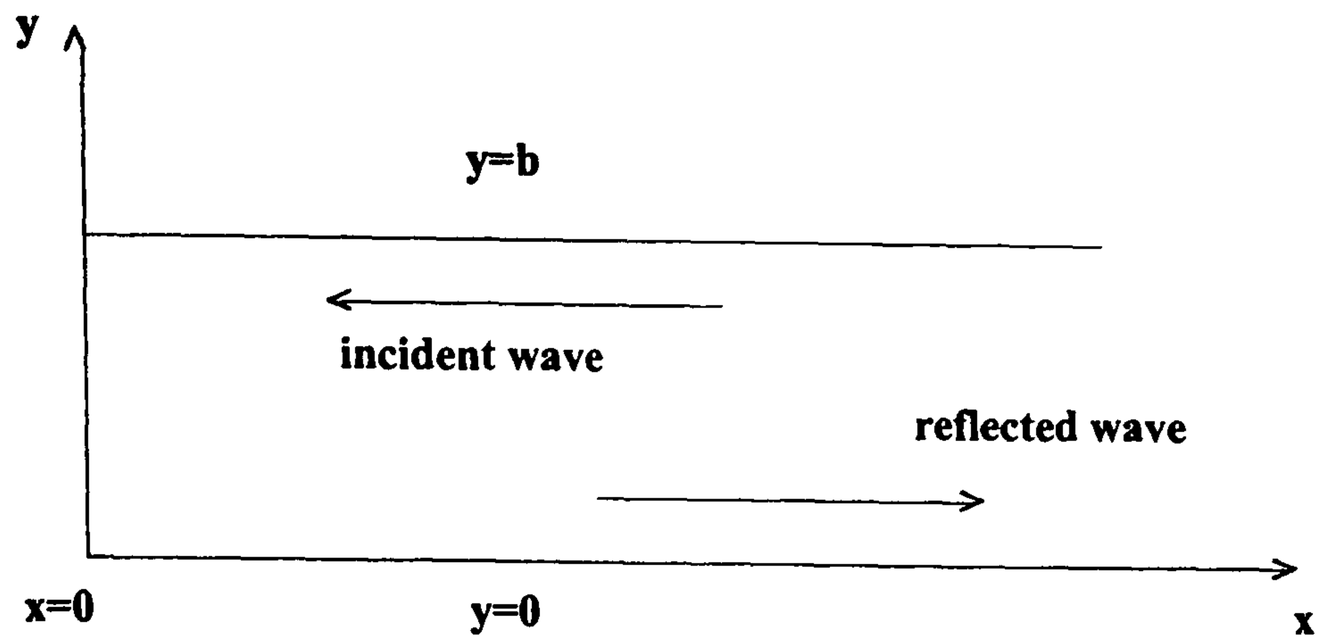

Figure 4.1:

reflection coefficient. Thus

$$\begin{cases} u_I = Ae^{\frac{fy}{c}}e^{i\sigma(\frac{x}{c}+t)} & \\ u_R = Re^{\frac{-fy}{c}}e^{-i\sigma(\frac{x}{c}-t)} & \text{Kelvin waves} \\ u_p = \sum_{m=1}^{\infty}(A_m \cos \nu_m y + iB_m \sin \nu_m y)e^{-s_m x+i\sigma t} & \\ v_p = \sum_{m=1}^{\infty} D_m \sin \nu_m y \; e^{-s_m x+i\sigma t} & \text{Poincaré modes} \end{cases}$$

where $\nu_m = \frac{m\pi}{b}$.

The velocity components are (u, v), and the canal depth is h, assumed constant.

The incident Kelvin wave is defined by

$$\zeta_I = e^{-(\frac{f}{c})(b-y)+i(\sigma t+\frac{\sigma x}{c})} \tag{4.2}$$

where ζ and t, are surface elevation and time respectively.

Also σ, and c are taken positive, with

$$c^2 = gh \;\text{ and }\; k^2c^2 = \sigma^2 - f^2.$$

Here c is the velocity of the long wave in the absence of earth's rotation.

From (i) and (ii) of (4.1) we obtain the linearized momentum equations

$$hk^2u = i\sigma\zeta_x + f\zeta_y$$

$$hk^2v = i\sigma\zeta_y - f\zeta_x \tag{4.3}$$

From this we obtain

$$u = \frac{g}{f^2 - \sigma^2}(i\sigma\zeta_x + f\zeta_y),$$
$$v = \frac{g}{f^2 - \sigma^2}(i\sigma\zeta_y - f\zeta_x). \tag{4.4}$$

Clearly ζ_I satisfies $(\nabla^2 - k^2)\zeta = 0$ and if u_I, v_I are the corresponding depth averaged velocities calculated from (4.4) then

$$u_I = (-\frac{g}{c})\zeta_I, \qquad v_I = 0.$$

The reflected Kelvin wave is defined as

$$\zeta_R = Re^{-(\frac{f}{c})y + i(\sigma t - \frac{\sigma}{c}x)}. \tag{4.5}$$

Clearly ζ_R satisfies $(\nabla^2 - k^2)\zeta = 0$ and if u_R, v_R are the corresponding depth averaged velocities calculated from(4.4) then

$$u_R = (\frac{g}{c})\zeta_R, \qquad v_R = 0.$$

By choosing the reflected coefficient R as a complex constant it is not possible to construct a nodal line across the canal so that the conditions on $x = 0$ and $y = 0$ are satisfied. Thus it is necessary to have an end-effect, u_E, v_E, ζ_E so that

$$u(0, y) = v(x, 0) = v(x, b) = 0.$$

and

$$u = u_E + u_I + u_R, \qquad v = v_E.$$

This end-effect may be written as a set of *Poincaré* modes:

$$v_E = (\frac{g}{c}) \sum_1^\infty \gamma_n \sin(l_n y) e^{-s_n x + i\sigma t},$$
$$u_E = (\frac{g}{c}) \sum_1^\infty \gamma_n \left\{A_n \cos(l_n y) + B_n \sin(l_n y)\right\} e^{-s_n x + i\sigma t},$$
$$\zeta_E = \sum_1^\infty \gamma_n \left\{C_n \cos(l_n y) + D_n \sin(l_n y)\right\} e^{-s_n x + i\sigma t}. \tag{4.6}$$

where

$$l_n = \frac{n\pi}{b}, \qquad s_n^2 = l_n^2 - k^2, \qquad k^2 = \frac{\sigma^2 - f^2}{c^2}.$$

Generally $s_n > 0$; if $s_n < 0$ then we take $s_n = i\alpha_n$ and $\alpha_n > 0$ so as to ensure outward propagation of these modes.

Clearly this set of *Poincaré* modes satisfy the linearized momentum equation. Thus by introducing these modes into the momentum equations (4.3) we obtain

$$hk^2(\frac{g}{c}) = fs_nD_n - i\sigma l_nC_n,$$

$$0 = fs_nC_n + i\sigma l_nD_n,$$

$$hk^2(\frac{g}{c})A_n = fl_nD_n - i\sigma s_nC_n,$$

$$hk^2(\frac{g}{c})B_n = -fl_nC_n - i\sigma s_nD_n.$$

From these there follows

$$\triangle_n \begin{pmatrix} A_n \\ B_n \\ C_n \\ D_n \end{pmatrix} = \begin{pmatrix} l_n s_n c^2 \\ -i\sigma f \\ i\sigma l_n c \\ -f s_n c \end{pmatrix} \tag{4.7}$$

where

$$\triangle_n = \sigma^2 + s_n^2 c^2.$$

Using the boundary condition $u(0, y) = 0$ we have

$$Re^{-\frac{f}{c}y} - e^{\frac{f}{c}(y-b)} + \sum_1^\infty \gamma_n[A_n \cos(l_n y) + B_n \sin(l_n y)] = 0, \quad \forall\ y \in [0, b]. \tag{4.8}$$

4.4 Method of Solution

The method of 'collocation' or 'point-matching' is introduced here. The equation (4.8) implies a requirement to invert an infinite matrix. However, we take instead that (4.8) holds at a finite set of points on $[0, b]$ with the series also truncated to a

finite number of terms. If only the first N terms of the series are included, then the points we used here are

$$y_k = \frac{(k-1)b}{N}, \qquad k = 1, 2, 3, ...N + 1.$$

Then when we define a matrix system based on the unknown vector $(\gamma_1, \gamma_2, \gamma_3, ..., \gamma_N, R)$, there remain $N + 1$ constants to be determined in (4.8); thus, setting $u(0, y) = 0$ at $N+1$ points on the interval $[0, b]$ should provide an approximate solution. This means the interval $[0, b]$ is divided into $N + 1$ points and one equation taken from each of the collocation points $y_k = \frac{(k-1)b}{N}, \quad k = 1, 2, 3, ...N + 1$, yielding $N + 1$ equations to be solved.

This gives a matrix system, $A\mathbf{x} = \mathbf{b}$

where,

$$\mathrm{A}= \begin{pmatrix} A_1\cos(l_1y_1) + B_1\sin(l_1y_1) & ..... & A_n\cos(l_ny_1) + B_n\sin(l_ny_1) & e^{-\alpha y_1} \\ A_1\cos(l_1y_2) + B_1\sin(l_1y_2) & ..... & A_n\cos(l_ny_2) + B_n\sin(l_ny_2) & e^{-\alpha y_2} \\ ..... & ..... & ..... & ..... \\ A_1\cos(l_1y_n) + B_1\sin(l_1y_n) & ..... & A_n\cos(l_ny_n) + B_n\sin(l_ny_n) & e^{-\alpha y_n} \\ A_1\cos(l_1y_{n+1}) + B_1\sin(l_1y_{n+1}) & ..... & A_n\cos(l_ny_{n+1}) + B_n\sin(l_ny_{n+1}) & e^{-\alpha y_{n+1}} \end{pmatrix},$$

with

$$\mathbf{x} = \begin{pmatrix} \gamma_1 \\ \gamma_2 \\ \gamma_3 \\ . \\ . \\ \gamma_n \\ R \end{pmatrix} \qquad \text{and} \qquad \mathrm{b}= \begin{pmatrix} e^{(y_1-b)} \\ e^{(y_2-b)} \\ e^{(y_3-b)} \\ . \\ . \\ e^{(y_n-b)} \\ e^{(y_{n+1}-b)} \end{pmatrix}.$$

The convergence of this method was tested by Brown by considering the accuracy of the equation (4.8) for the different collocation points and by the convergence of this value to a limiting solution for increasing N.

Taylor and subsequently Defant in their investigation used the case of $k = 0.5$ and $\alpha = 0.7$. Taylor in his study used a depth of 74 m, a period of 12 hrs, canal width of 500.5 m and a value of f corresponding to a point at $54.46^o N$. Using these parameters which are referred to as 'Taylor's example' the end of the canal was determined as $x_1 = 0.427$ and as a result the reflection coefficient was found as $R = 0.742 - 0.670i$.

N	R	abs(R)
4	0.7444-0.6677i	1.0000
6	0.7423-0.6701i	1.0000
8	0.7419-0.6705i	1.0000
10	0.7418-0.6707i	1.0000
12	0.7417-0.6707i	1

The table above lists the computed values of R for various values of N. The convergence is rapid and approximately inverse cubic in N as illustrated in fig (4.2) below. As $|R| \equiv 1$ there is no propagation of *Poincaré* modes as expected and perfect reflection thus occurs.

The tidal range ζ is found from the formula.

$$\frac{\sigma\zeta}{h} = i\left(\frac{\partial u}{\partial x} + \frac{\partial v}{\partial y}\right)$$

The case chosen in fig(4.4) is that of a channel situated in latitude 54.46º. The depth of the channel is, 74 m. This corresponds, roughly, to the case of the North Sea, though the water is shallower than 74 m at the Southern end. The results are exhibited by means of a diagram in the fig (4.4) where the height of the tidal wave is represented by means of co-tidal lines which are drawn through the points where it is high water at any specified time. These lines are drawn for every 36 $mins$ (or rather for every $\frac{1}{20}$ part of a period). The amount of rise and fall of tide in different parts of the basin is also shown in the diagram. The amplitudes in the diagram are in meters and in the right and left corners of the basin the amplitudes are equal to 1.28 m.

An inspection of the diagram at once reveals the nature and mechanism of the reflection. The tidal wave moves in along the right-hand shore and then sweeps round the end wall of the basin at a rate rather greater than the velocity of the Kelvin wave, and moves back along the opposite shore. In turning at right angles in order to cross the end of the channel, the wave produces a bigger rise and fall of the tide at the two corners of the basin than anywhere else in the field. On the scale chosen the range of tide at the two corners are given by 1.28 m whereas the range in the other parts of the channel is less than this value (1.28 m).

It is a known fact that *Poincaré* waves are only possible provided $\sigma > f$. That is, such that their period $\frac{2\pi}{\sigma} < \frac{2\pi}{f} = T_p$ the half pendulum day. Thus locally where f is a constant, energy can be transferred by Poincaré modes provided they are in the form of short period waves.

In fig (4.5) is exhibited the result for the case h=74 m, $\sigma = 1.4544 \times 10^{-4}$, latitude,

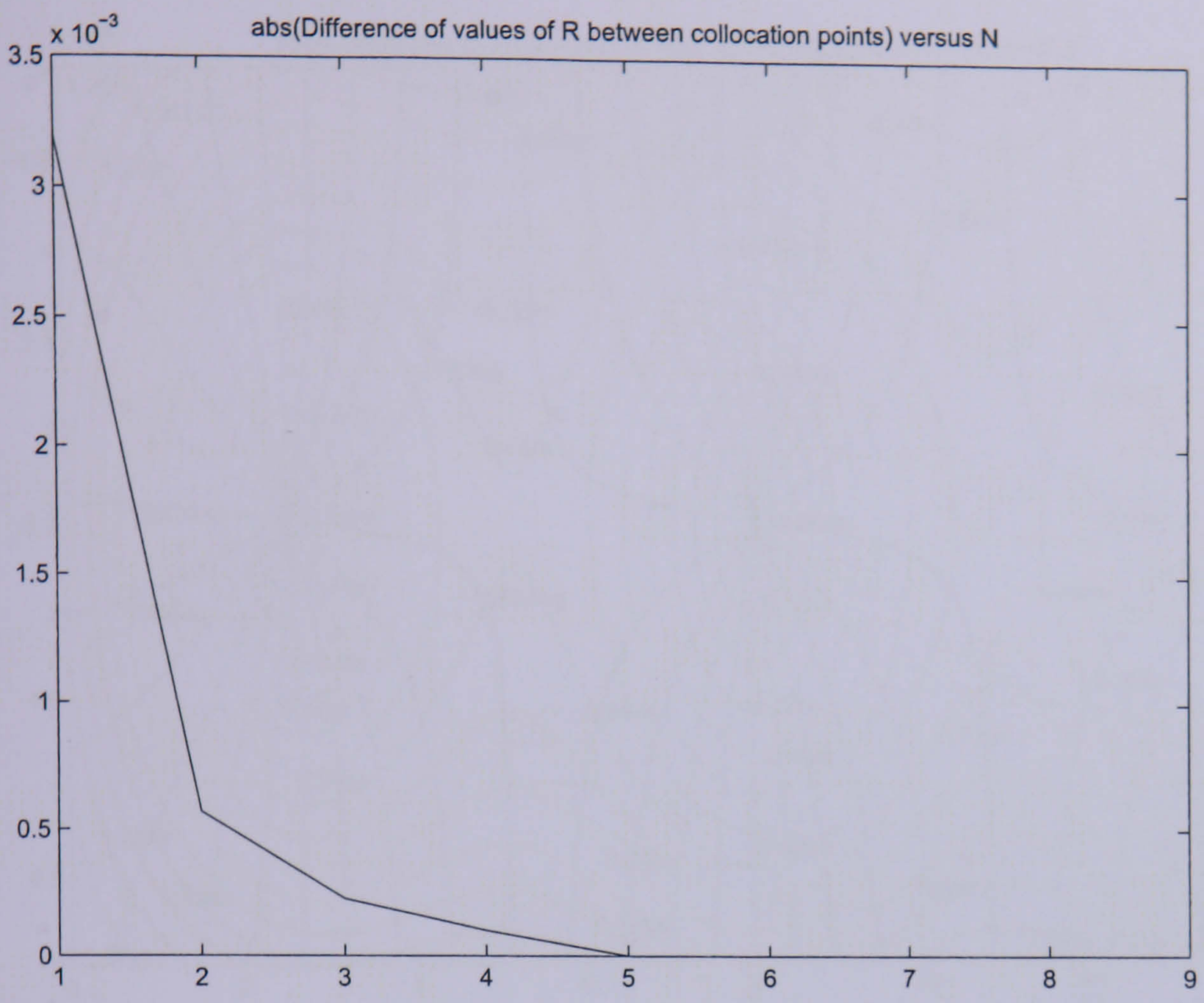

Figure 4.2: Figure to show that the convergence of the method is approximately inverse cubic in N - the number of collocation points. This curve is compared with figure(4.3)

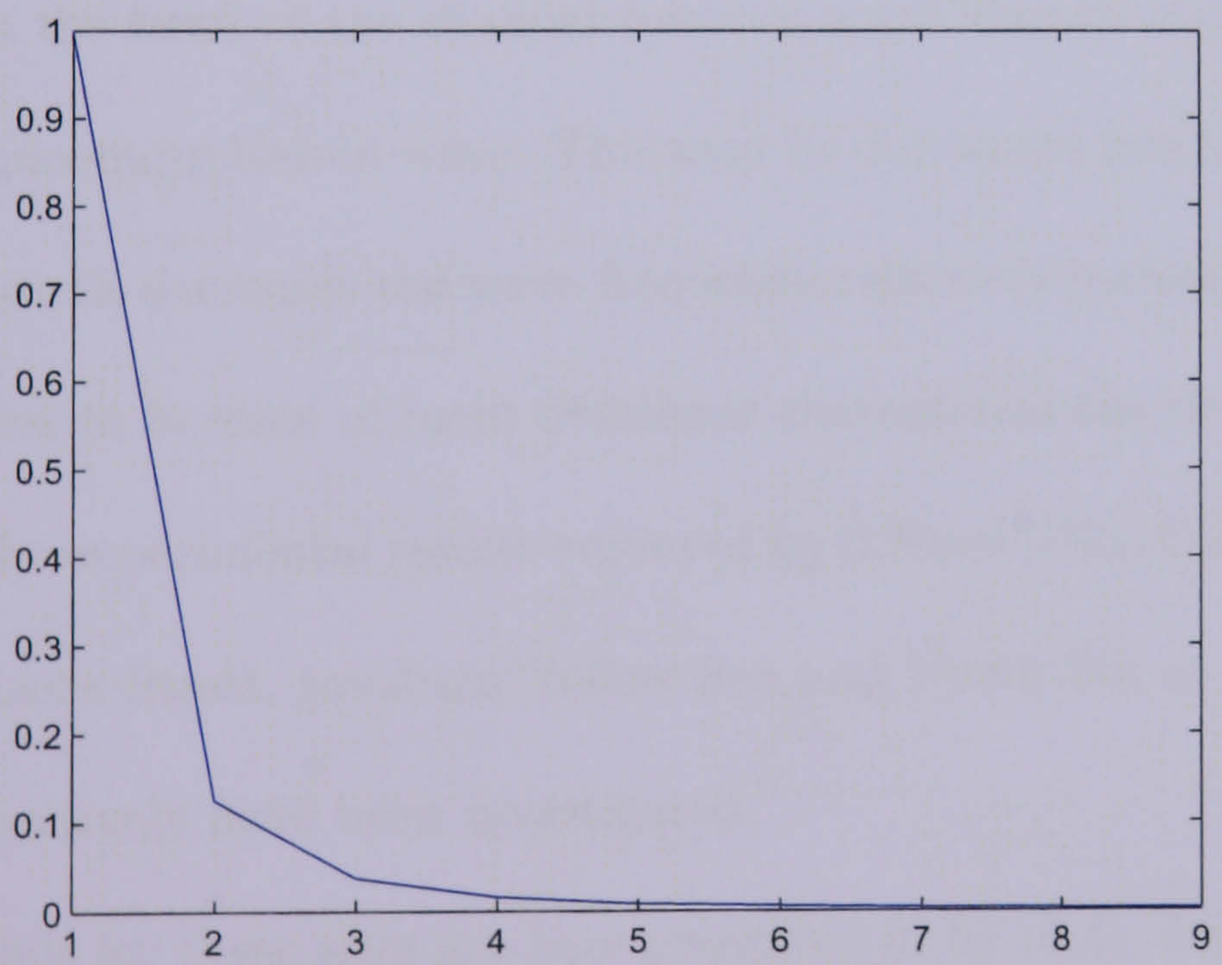

Figure 4.3: plot of $1/N^3$versus N

$\theta = 54.46^{o}$ and f $= 5.9175\times10^{-5}$. It can be seen that for the same wave frequency of the wave, a significant reduction in earth rotation moves the *amphidromic* points

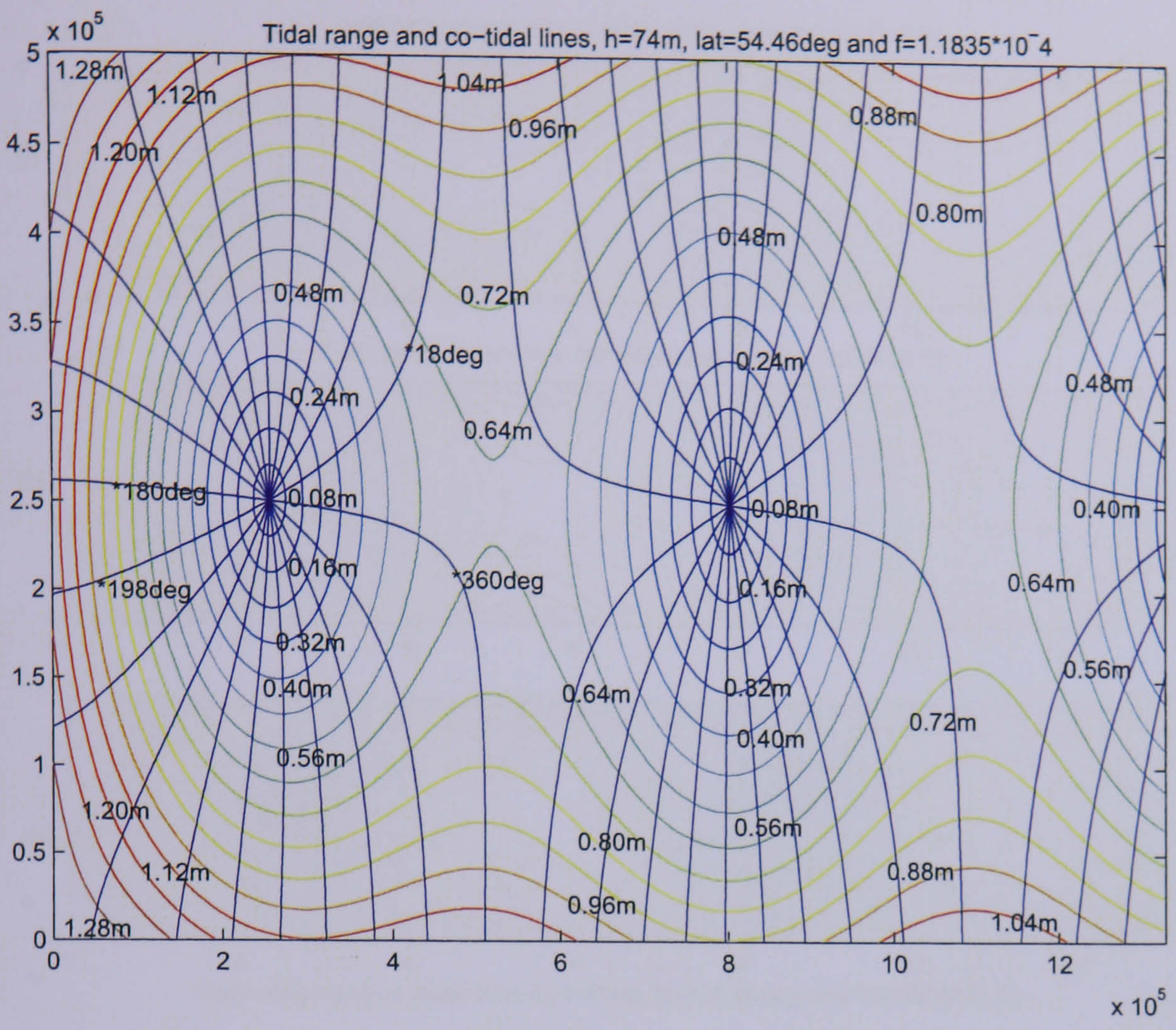

Figure 4.4: (i)Amplitudes and phases for the case of lat θ =54.46$^{\underline{0}}$. The phases are shown in degree and amplitudes in meters:

from the head of the channel towards north though there exists perfect reflection of the incoming Kelvin wave. This may be due to the fact that as the rotational effect of the earth decreases the wave frequency relatively increases which causes the Poincaré modes to become of more dominant character in the tidal motion.

In the experimental results surveyed by S.Rizal ([32]) three geographical areas namely Malacca Strait, southern Yellow Sea and North Sea at latitudes 3$^{\underline{o}}$, 30$^{\underline{o}}$ and 54.46$^{\underline{o}}$ respectively have been investigated.

Details for these sites are here presented in fig (4.6). Fig (4.6 (i)) shows the distribution of amplitudes and phases of M_2 for the latitude $\theta = 54.46^{\underline{o}}$. One can see that two amphidromes take place for the parameters chosen in the central axis of the channel and the first amphidromic point occurs near the head of the channel, which indicates that there is no loss of energy and results in perfect reflection. The Kelvin wave

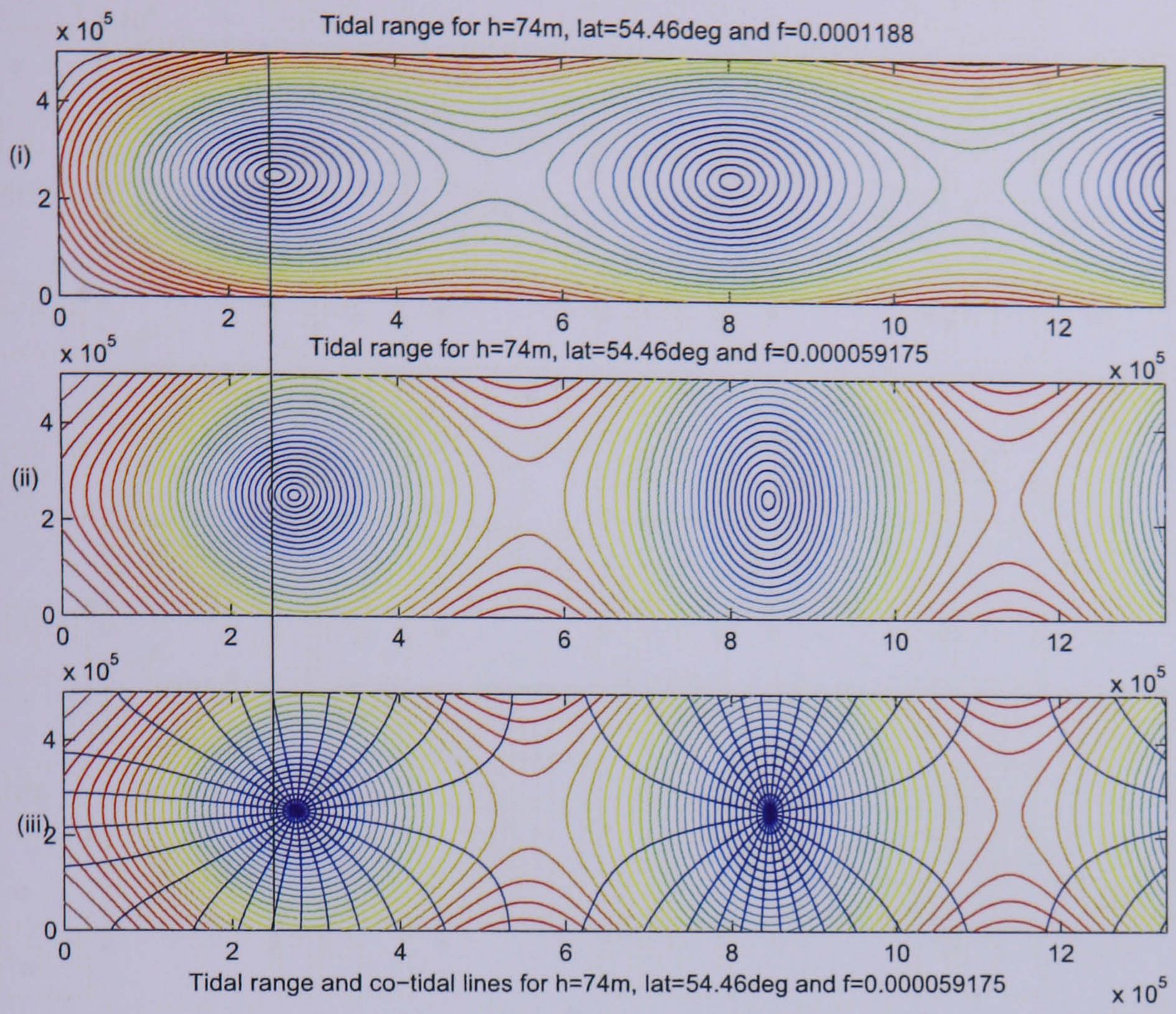

Figure 4.5: Tidal range and phase lines for the case where $h = 74m$, lat=54.46º and $f = 5.9175 \times 10^{-5}$

motion dominates in the system. In fig (4.6 (ii)) one can still see two amphidromic points along the central axis of the channel but the one near the head of the channel to moved down to the north and also perfect reflection remains. If we compare the results exhibited in fig (4.6 (iii)) we can see the two amphidromic points still lies along the central axis and perfect reflection still occurs but the amphidromes tend to degenerate to loose the identity of tidal phenomenon. We also note the amplitude lines become sets of almost parallel lines. Moreover, S.Rizal ([32]) in her experiments found that the varying frictional effect would move the amphidromic points toward the side of the channel along which the reflected Kelvin wave travels. This has been observed also by M.C.Hendershott and A.Speranza ([34]) and Tim Brown ([4]). As the frictional effect increases beyond a critical value all amphidromic points become virtual. In low latitudes the frequency of the waves relatively increases and *Poincaré*

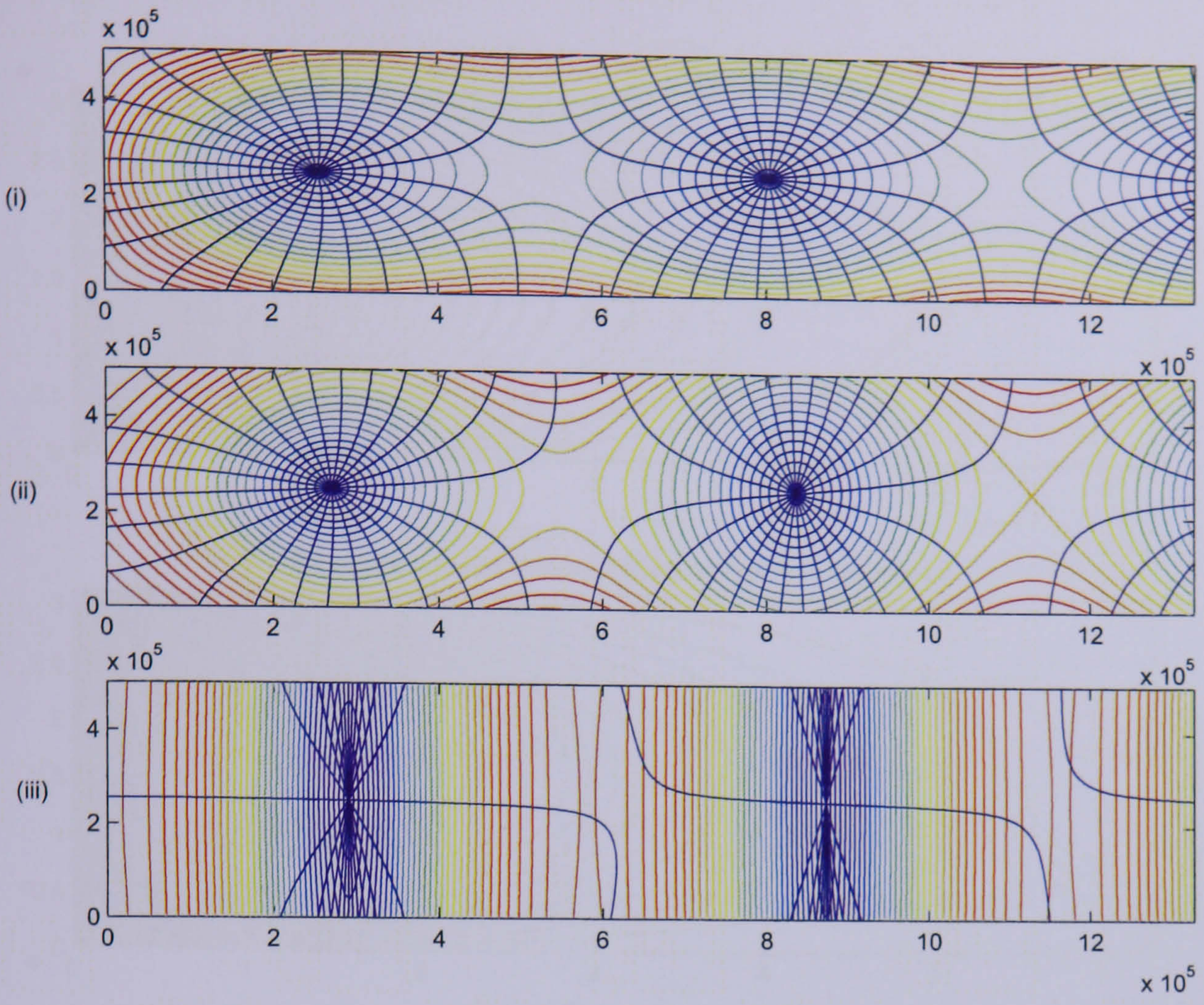

Figure 4.6: Amplitudes and phases for the cases of (i) lat=$54.46^{\underline{0}}$ (ii) lat=$30^{\underline{0}}$ (iii) lat=$3^{\underline{0}}$, respectively.

modes become a more dominant feature of the phenomenon.

In fig (4.7) is given the profiles for the transverse velocity of the *Poincaré* modes for the case h=74 cm and latitude, $\theta = 54.46^{\underline{o}}$. In this diagram one can see the crowding of the waves occur on the side of the channel along which the incident wave travels.

4.5 Fourier Series treatment of the Taylor problem:

As an alternative to the collocation treatment we consider instead solving this problem by using Fourier series development. In this method, we express the Kelvin wave system using a Fourier synthesis across the channel.

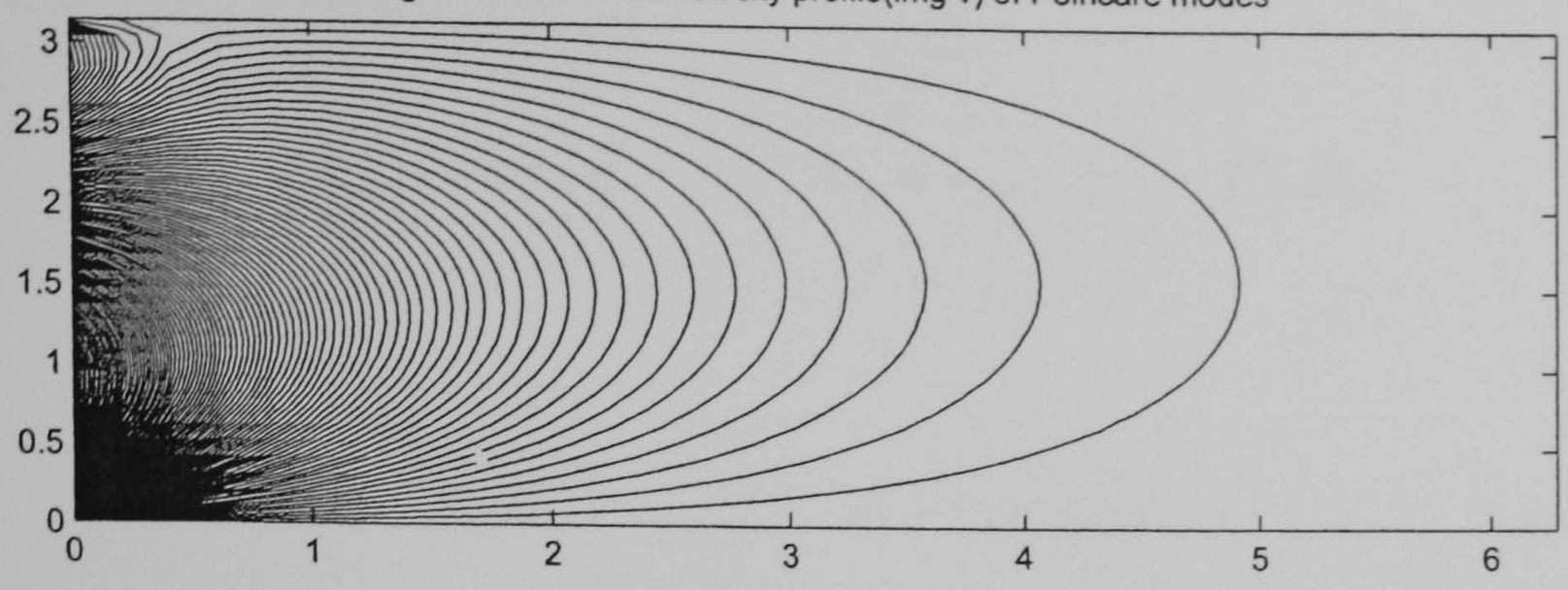

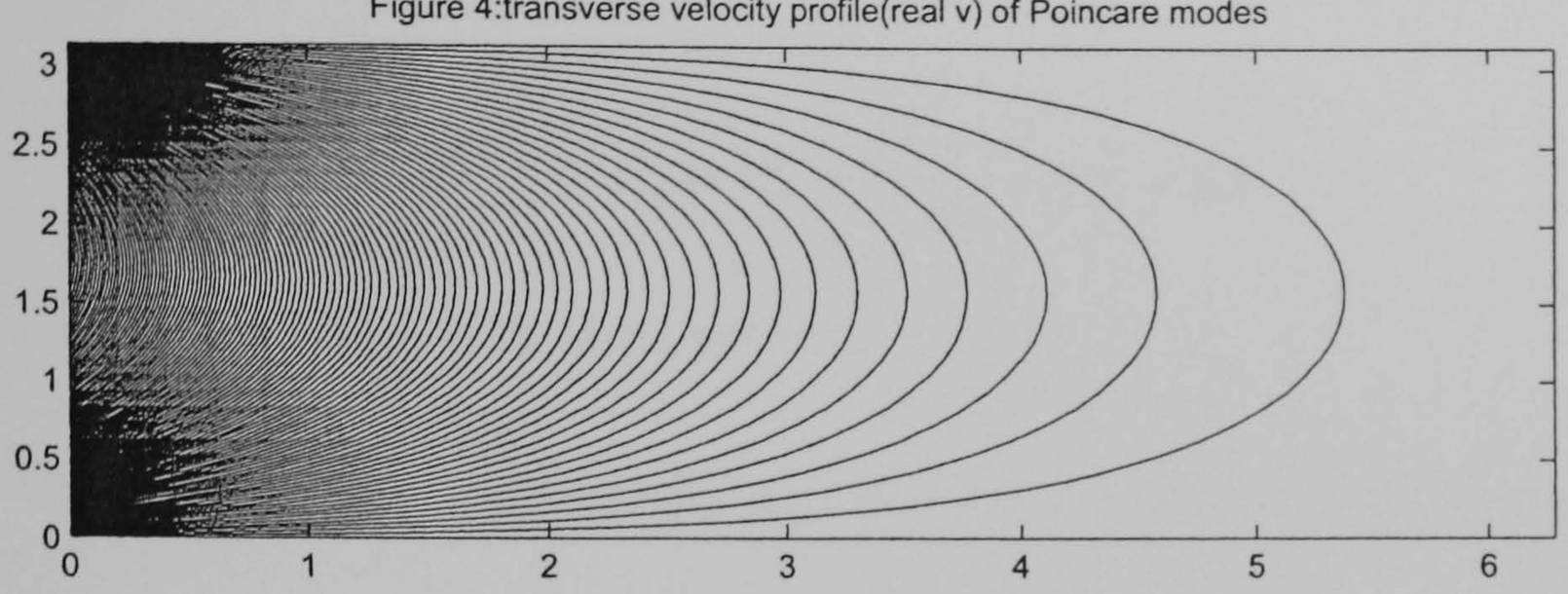

Figure 4.7: Velocity profile of *Poincaré* modes for the case h=74m and lat=54.46^{o}

4.5.1 The consistency relations:

We might enquire about the precise nature of these relations in the wake of the notation we adopted. They arise from the elimination of ζ in the two momentum equations (see section-1) and are therefore tantamount to the requirement

$$\sum_{m=1}^{\infty} \left(\rho_m \cos \nu_m y + i\delta_m \sin \nu_m y\right) e^{-s_m x} = 0$$

where $\rho_m = f A_m s_m - \nu_m \sigma B_m - f \nu_m D_m$ and $\delta_m = f s_m B_m - \sigma \nu_m A_m + \sigma s_m D_m$.

Normally, we have 'blindly' equated each of ρ_m and δ_m to zero for a fixed value of x. Here, because we have a half-range series, we have instead to observe the relation has to be satisfied at every point of our solution domain. It should be possible to argue that this can only happen (even for half-range series) if each of the coefficients ρ_m and δ_m vanish independently.

This then yields

$$\sigma f\left(s_m^2-\nu_m^2\right)A_m=\nu_m s_m\left(\sigma^2-f^2\right)B_m.$$

or

$$\sigma f A_m=-\nu_m c^2 s_m B_m \tag{4.9}$$

since

$$s_m^2=\nu_m^2+\frac{f^2-\sigma^2}{gh},\ c^2=gh.$$

4.5.2 Dealing with the system:

We wish to place the boundary at $x=0$. The condition of no flow across this is

$$u_k+\sum_{m=1}^{\infty}\left(A_m\cos\nu_m y+iB_m\sin\nu_m y\right)=0$$

where, $u_k=(A+R)\cosh(\frac{fy}{c})+(A-R)\sinh(\frac{fy}{c})$.

Whilst it is possible to expand u_k in both sine and cosine half-range series, the problem with, for example, $\cosh(Y)$ expanded as a sine series, is that the coefficients will be only $O(\frac{1}{n})$. Whereas if $\cosh(Y)$ is expanded as a cosine series, the coefficients will be $O(\frac{1}{n^2})$. This effects both convergence and (as a consequence) also differentiability. So we formally write u_k as

$$u_K=(A+R)\sum_{m=0}\epsilon_m\lambda_m\cos(\nu_m y)+(A-R)\sum_{m=1}\mu_m\sin(\nu_m y).$$

where

$$\lambda_m=(-1)^m\frac{2\alpha\sinh(\alpha b)}{(\nu_m^2+\alpha^2)b},\ \ \lambda_0=\frac{2\sinh(\alpha b)}{b\alpha},$$

$$\mu_m=(-1)^{m+1}\frac{2\nu_m\sinh(\alpha b)}{(\nu_m^2+\alpha^2)b}=-\frac{\nu_m}{\alpha}\lambda_m,\ \alpha=\frac{f}{c}\ \text{ and }\ \epsilon_0=\frac{1}{2},\ \epsilon_m=1\ \text{ if }\ m\geq 1.$$

Now, for convenience, we write also

$$\alpha_m = A_m + (A+R)\epsilon_m\lambda_m \quad \text{and} \quad \beta_m = iB_m + (A-R)\mu_m$$

taking $A_0 = 0$. Thus $\alpha_0 = (A+R)\,\frac{\lambda_0}{2}$. The boundary condition is then simply

$$\alpha_0 + \sum_{m=1}^{\infty}(\alpha_m \cos\nu_m y + \beta_m \sin\nu_m y) = 0.$$

but this is only a half-range series, we cannot equate terms to zero in the usual way. Instead, we multiply the equation successively by $\sin\nu_m y$ integrate and then by $\cos\nu_m y$ integrate. But first integrate from 0 to b. Note the orthogonality relations

$$\int_0^b \sin(\nu_n y)\cos(\nu_m y)dy = \frac{bn(1-(-1)^{n+m})}{\pi(n^2-m^2)},$$

$$\int_0^b \sin(\nu_n y)\sin(\nu_m y)dy = \int_0^b \cos(\nu_n y)\cos(\nu_m y)dy = (\frac{b}{2})\delta_{m,n}\ ,$$

where m, n are integers. This gives

$$\pi\alpha_0 + \sum_{m=1}^{\infty}\frac{\beta_m}{m}(1-(-1)^m) = 0. \tag{4.10}$$

whilst the other two integrated relations are

$$\beta_n + \frac{2\alpha_0}{n\pi}(1-(-1)^n) + \frac{2}{\pi}\sum_{m\neq n}^{\infty}\frac{n\alpha_m}{n^2-m^2}(1-(-1)^{m+n}) = 0, \quad n = 1,2,3..... \tag{4.11}$$

$$\alpha_n + \frac{2}{\pi}\sum_{m\neq n}^{\infty}\frac{m\beta_m}{m^2-n^2}(1-(-1)^{m+n}) = 0, \quad n = 1,2,3..... \tag{4.12}$$

In deciding how to deal with the system we remember that α_m and β_m are related through the consistency relation (4.9) which can now be rewritten in the form

$$ir_m\alpha_m - \beta_m = (A+R)ir_m\lambda_m + (A-R)(\frac{\nu_m}{\alpha})\lambda_m, \tag{4.13}$$

where $\frac{A_m}{B_m} = \frac{1}{r_m}$ and $r_m = -\frac{f\sigma}{\nu_m s_m c^2}$.

Moreover, we find that the above two systems (4.11) and (4.12) are not entirely independent. To better understand this, we can take the alternative approach to the above boundary condition. That is, expand the cosines as a series of (even) sines. We will then, following Taylor's arguments, get one of the two systems above. If we repeat this but instead expand the sines in a series of (odd) cosines we will get the other system. Clearly we would not expect these two to be independent since they arise from what is essentially the same process applied to the same equation!

The numerical approach here, will therefore be to take only m equations from either system and supplement these with an equation containing R. This gives a system which, when solved for the vector $\mathbf{x}= (\beta_1, \beta_2, \beta_3, ...\beta_m, R)$ should converge to the correct reflection coefficient amplitude which would be $A\exp(fb/c)$.

4.5.3 A definitive system:

We choose to use the system given by equation (4.10) and (4.12, n=1,2,3,....m) with the equation (4.10) placed last. Thus writing this system as $C\mathbf{x} = \mathbf{b}$, the kth equation $(1 \leq k \leq m)$ is

$$\beta_k + R(ir_k\lambda_k + \mu_k) + ir_k \sum_{n=1}^{m} d_{kn}\beta_n = A(\mu_k - ir_k\lambda_k), \tag{4.14}$$

where,

$$d_{mn} = \frac{2}{\pi}\frac{n(1-(-1)^{n+m})}{n^2 - m^2},$$

whilst the (m+1)th equation is

$$\sum_{n=1}^{m} \frac{\beta_n}{n}(1-(-1)^{n+m}) + \pi\lambda_0 R/2 = -\pi\lambda_0 A/2.$$

On constructing the matrices C, $\mathbf{x}$ and $\mathbf{b}$ using the equation (4.14) we have,

$$C_{i,j} = \begin{pmatrix} 1 & \frac{4ir_1*2}{\pi(2^2-1^2)} & 0 & .... & \frac{4ir_1*m}{\pi(m^2-1^2)} & (ir_1\lambda_1+\mu_1) \\ \frac{4ir_2*1}{\pi(1^2-2^2)} & 1 & \frac{4ir_2*3}{\pi(3^2-2^2)} & 0 & ..... & (ir_2\lambda_2+\mu_2) \\ 0 & \frac{4ir_3*2}{\pi(2^2-3^2)} & 1 & ..... & \frac{4ir_3*m}{\pi(m^2-3^2)} & (ir_3\lambda_3+\mu_3) \\ \frac{4ir_4*1}{\pi(1^2-4^2)} & 0 & \frac{4ir_4*3}{\pi(3^2-4^2)} & 1 & ..... & (ir_4\lambda_4+\mu_4) \\ ..... & ..... & ..... & .... & ... & ..... \\ ..... & ..... & ..... & ..... & ..... & ..... \\ ..... & \frac{4ir_m*2}{\pi(2^2-m^2)} & ..... & .... & ..... & (ir_m\lambda_m+\mu_m) \\ \frac{1}{1} & 0 & \frac{1}{3} & ..... & \frac{1}{m} & \pi\frac{\lambda_0}{2} \end{pmatrix}$$

$$\underline{x} = \begin{pmatrix} \beta_1 \\ \beta_2 \\ \beta_3 \\ . \\ . \\ . \\ \beta_m \\ R \end{pmatrix} \quad \text{and} \quad \underline{b} = \begin{pmatrix} A(\mu_1 - ir_1\lambda_1) \\ A(\mu_2 - ir_2\lambda_2) \\ A(\mu_3 - ir_3\lambda_3) \\ . \\ . \\ . \\ A(\mu_m - ir_m\lambda_m) \\ -\frac{\pi}{2}A\lambda_0 \end{pmatrix}$$

By solving the matrix equation, $C\mathbf{x} = \mathbf{b}$, we obtain the reflection coefficient R.

We solve this system using MATLAB.

The values of the reflection coefficient R are computed for various values of N.

We compared the convergence of the solution for the above two treatments in the fig(4.8) below.

We can see that the convergence of the solution is somewhat more rapid for the collocation method.

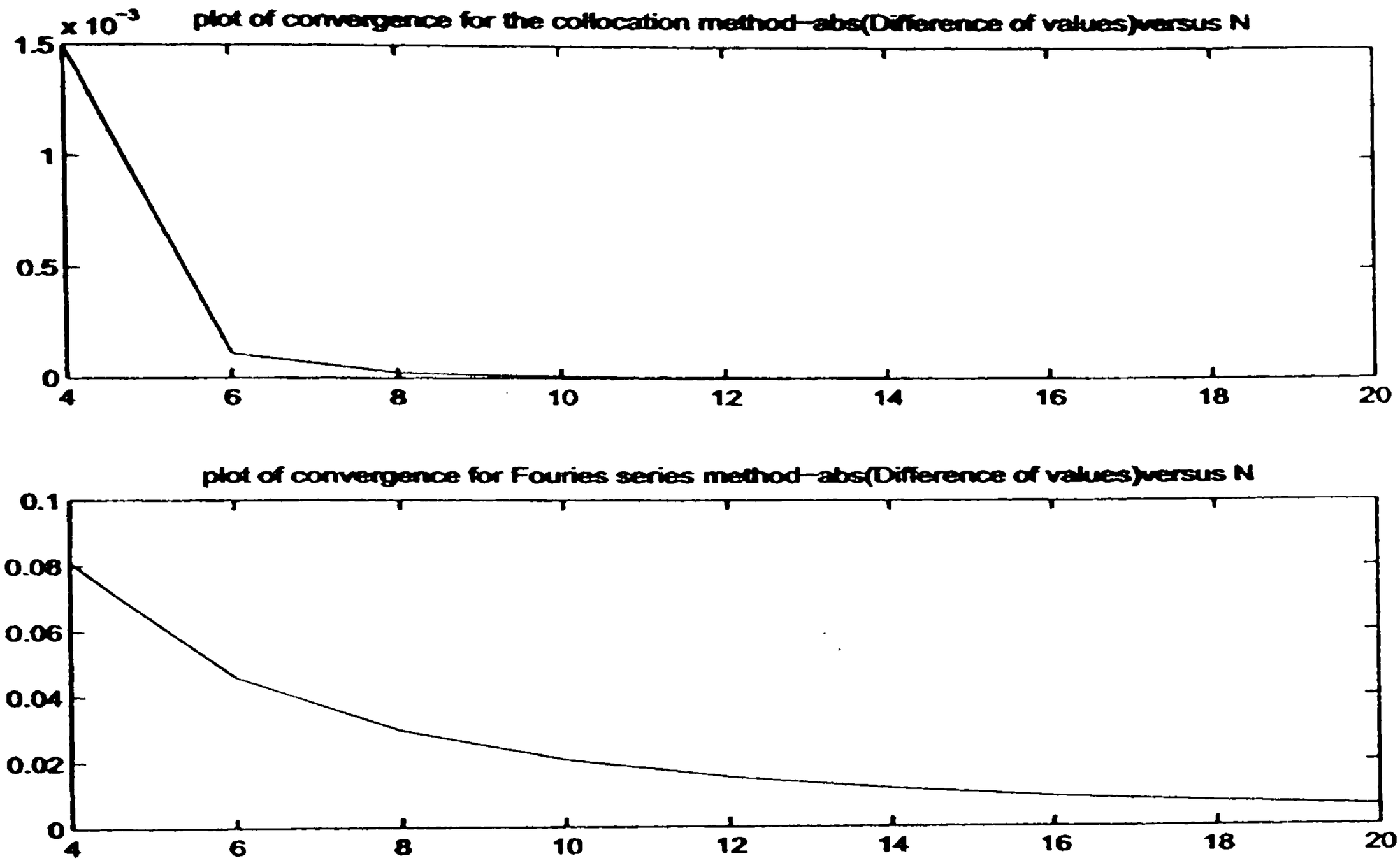

Figure 4.8: We compare the convergence of the solution for the above two treatments, top figure for collocation method and the bottom one for Fourier series method.

Having obtained the reflection coefficient R we are able to determine the Fourier coefficients A_m, B_m and D_m.

Now, we write these coefficients as

$$B_m = -i[\beta_m - (A - R)\mu_m)], \qquad A_m = \frac{B_m}{r_m} \qquad \text{and}$$

$$D_m = \frac{s_m}{\nu_m} A_m - \frac{\sigma}{f} B_m. \tag{4.15}$$

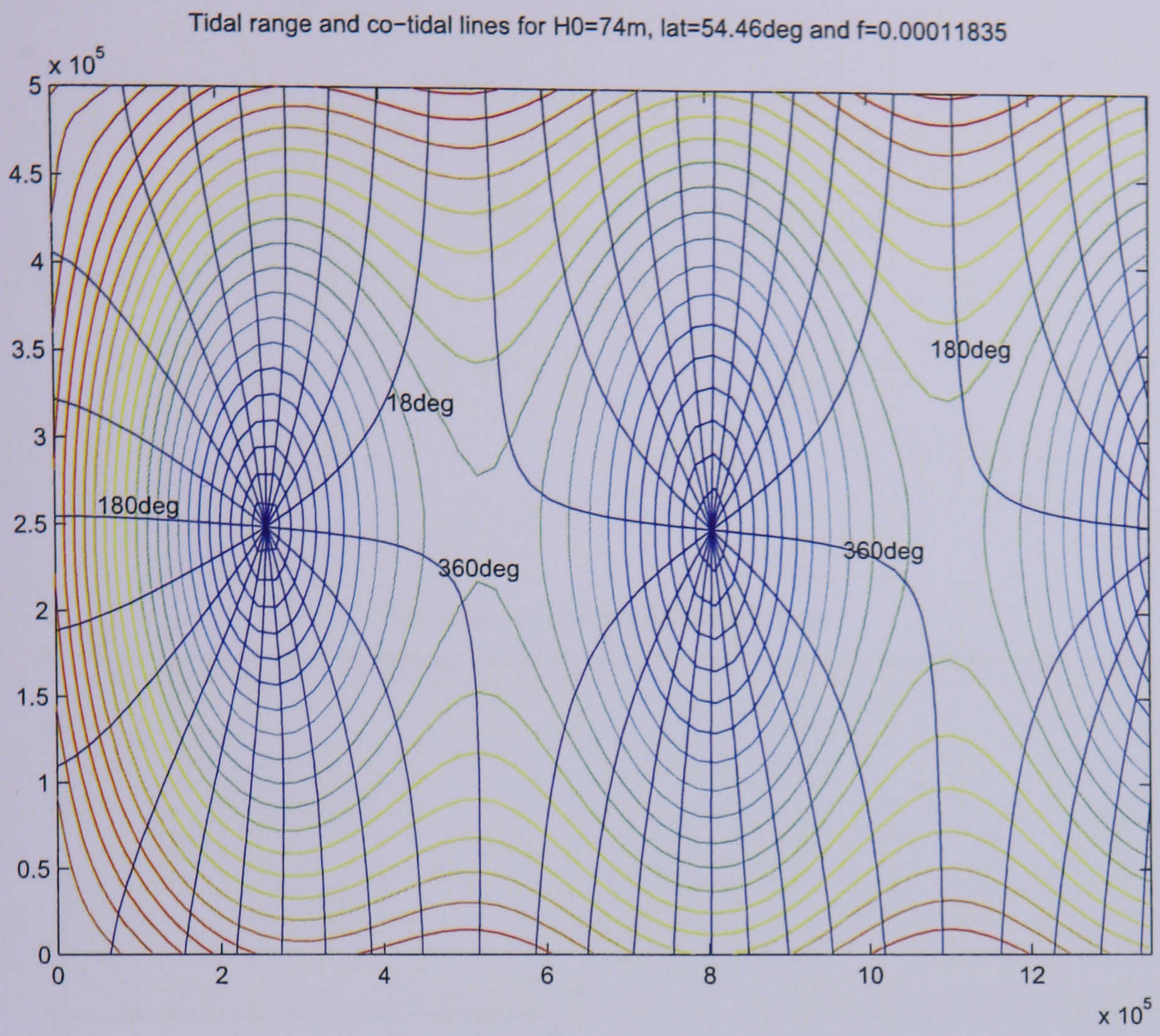

Figure 4.9: Tidal range and phase lines for the case where $h = 74\ m$, lat= 54.46 degree and $f = 1.1835 * 10^{-4} sec^{-1}$

In fig (4.9), the diagram illustrates the behavior of the tidal range and co-tidal lines for the case where $h = 74\ m$, latitude, $\theta = 54.46^{o}$ and $f = 1.1835 \times 10^{-4}$ whilst in fig (4.10(a, b)) the case $h = 74\ m$ and latitude, $\theta = 54.75^{o}$ and $f = 1.1878 \times 10^{-4}$ being considered. In fig (4.10a) depicted the tidal range and in fig (4.10b) plotted the tidal range and phase lines.

The co-tidal lines are drawn for every 36 *mins* in fig (4.9). It can be further seen that higher amplitude tides are experienced in the co-ordinates points near the right hand corner and left hand corner of the basin. The rest of the basin experiences lower amplitude waves. The highest tide in the basin is about 2 m high for the parameters chosen.

fig(10a)

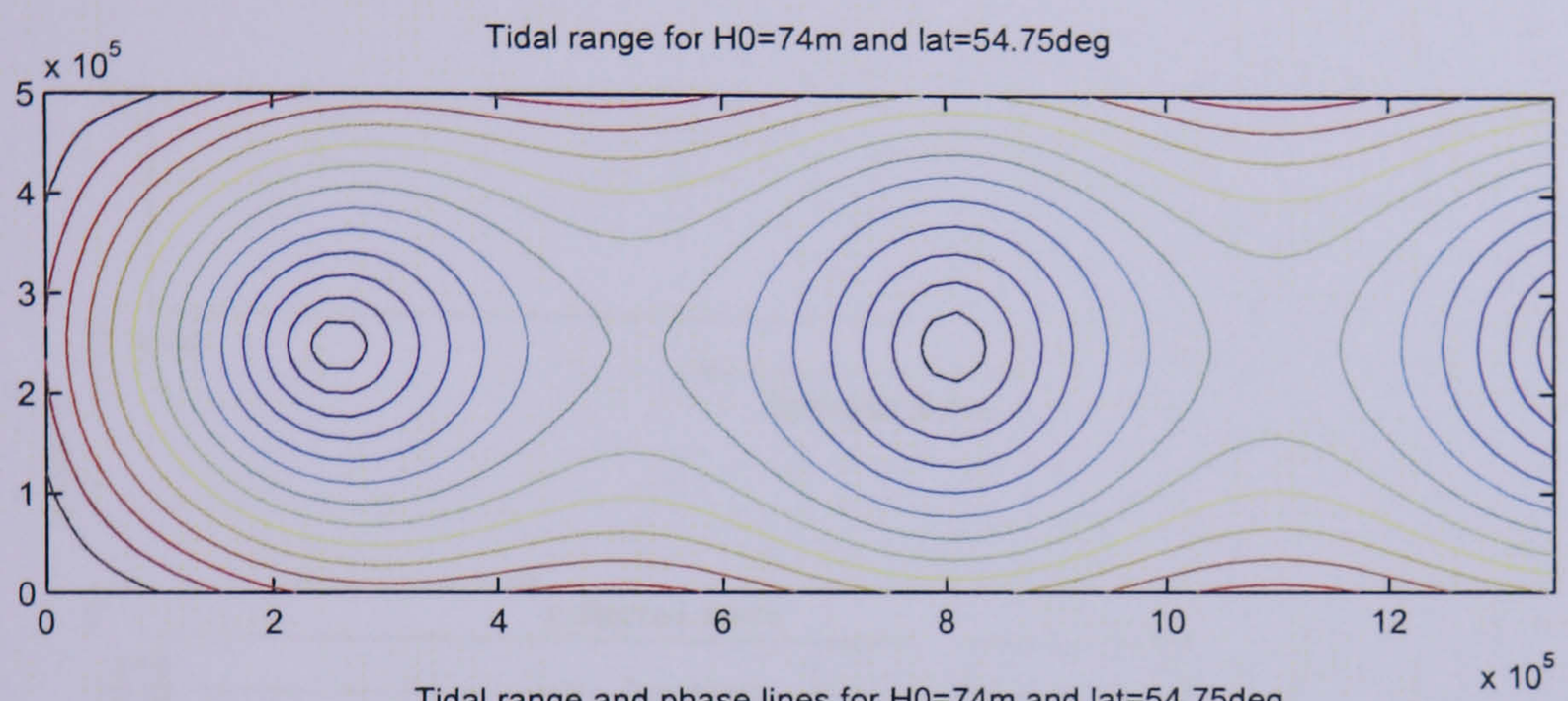

fig(10b)

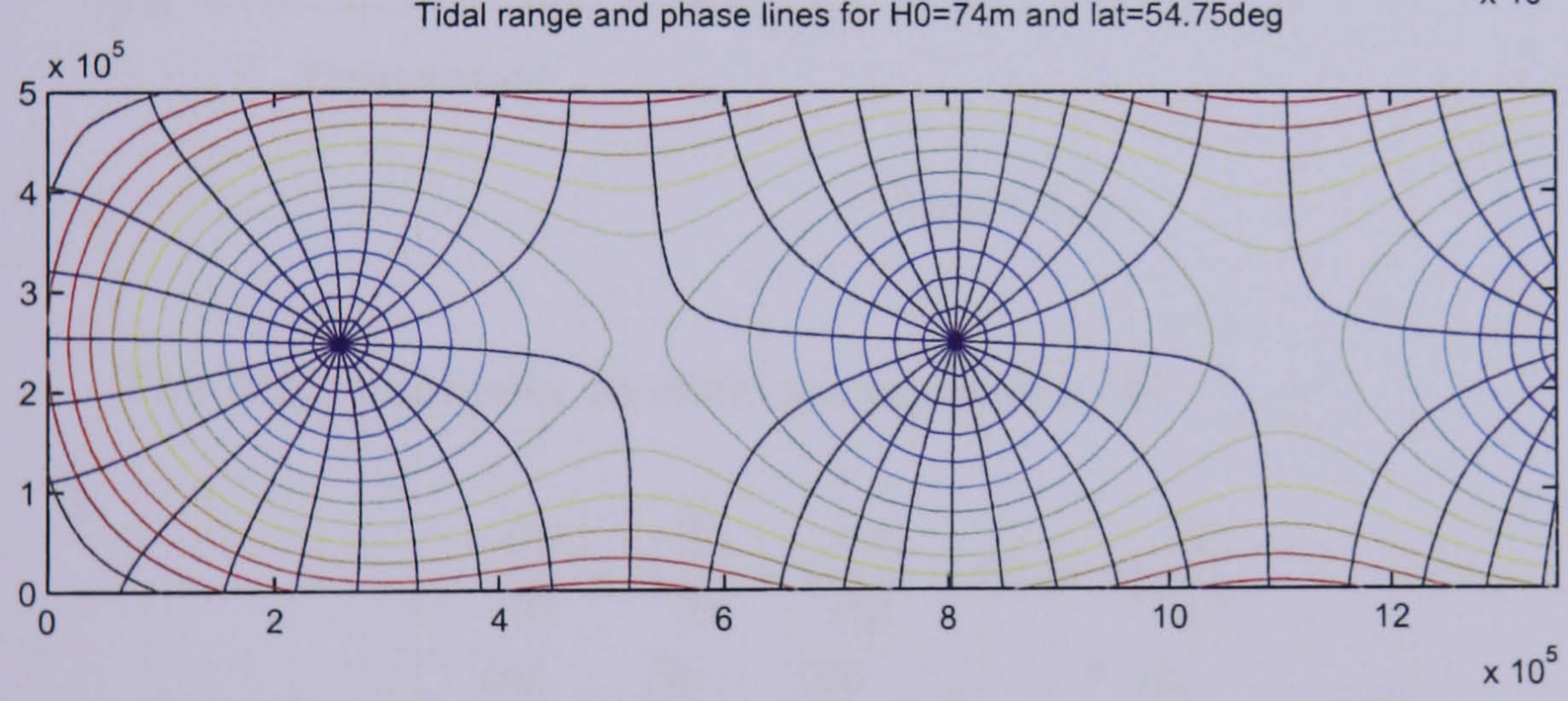

Figure 4.10 (a,b):

Chapter 5

Computation of Kelvin wave propagation into a semi-infinite rectangular basin with uniform depth

Here, we consider a time dependent solution of the Taylor problem from a numerical method with a view to comparison with the analytical solution.

5.1 Defining Equation:

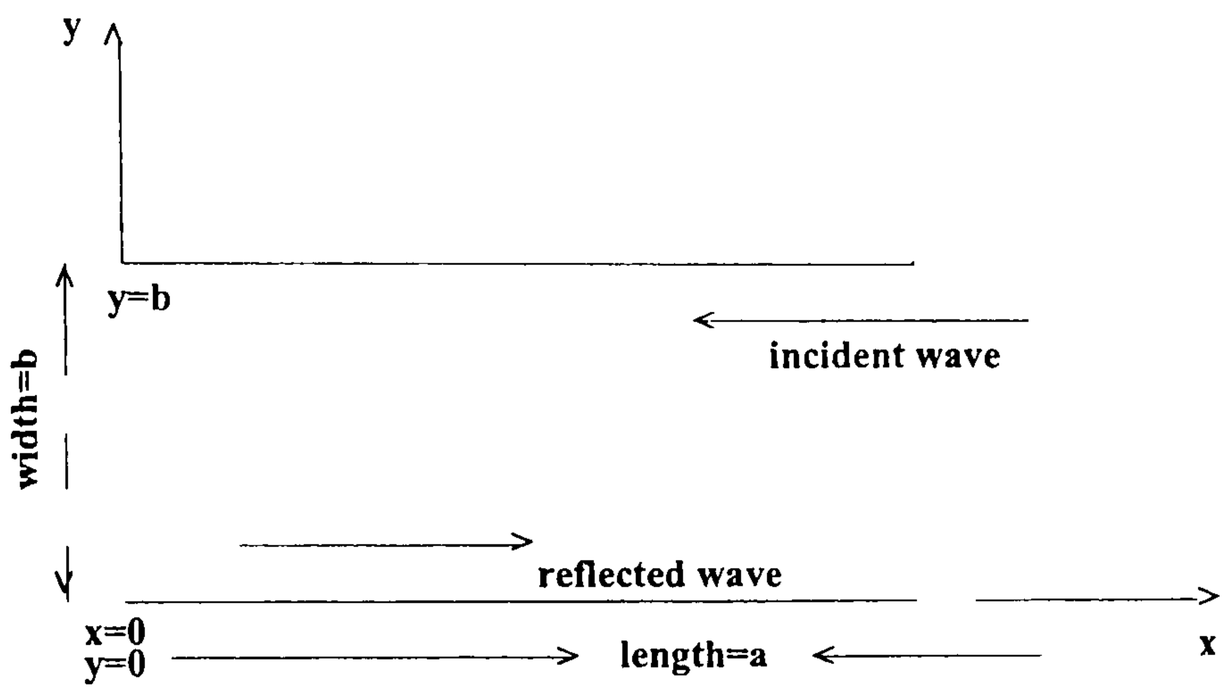

Figure 5.1:

The basic nonlinear momentum equations are:

$$\frac{\partial u}{\partial t} + u\frac{\partial u}{\partial x} + v\frac{\partial u}{\partial y} - fv = -g\frac{\partial \zeta}{\partial x} \qquad \text{(i)}$$

$$\frac{\partial v}{\partial t} + u\frac{\partial v}{\partial x} + v\frac{\partial v}{\partial y} + fu = -g\frac{\partial \zeta}{\partial y}. \qquad \text{(ii)} \qquad (5.1)$$

The nonlinear continuity equation is written as

$$\frac{\partial \zeta}{\partial t} + \frac{\partial[(\zeta + h)u]}{\partial x} + \frac{\partial[(\zeta + h)v]}{\partial y} = 0, \qquad (5.2)$$

where the field quantities (u, v, ζ) take the usual meaning as longitudinal velocity, transverse velocity and surface elevation from the undisturbed level.

Further, h = depth, f = Coriolis parameter and g = gravitational attraction.

5.2 Derivation of the system:

For Kelvin wave system the latitudinal velocity component $v \equiv 0$. For such system the momentum equations (5.1) yield,

$$\frac{\partial u}{\partial t} + u\frac{\partial u}{\partial x} = -g\frac{\partial \zeta}{\partial x} \qquad \text{(i)}$$

$$fu = -g\frac{\partial \zeta}{\partial y}. \qquad \text{(ii)} \tag{5.3}$$

Similarly, the continuity equation (5.2) reduce to

$$\frac{\partial \zeta}{\partial t} + \frac{\partial[(\zeta + h)u]}{\partial x} = 0. \tag{5.4}$$

We let $c^2 = g(h + \zeta)$, then $c = \pm\sqrt{g(h+\zeta)}$, and we take, $c = +\sqrt{g(h+\zeta)}$, $h = constant$.

This implies that $2c\frac{\partial c}{\partial x} = g\frac{\partial \zeta}{\partial x}$ and $2c\frac{\partial c}{\partial t} = g\frac{\partial \zeta}{\partial t}$ and so the equation (i) of (5.3) written as

$$\frac{\partial u}{\partial t} + u\frac{\partial u}{\partial x} = -2c\frac{\partial c}{\partial x}. \tag{5.5}$$

And from equation (5.4) we obtain,

$$2\frac{\partial c}{\partial t} + c\frac{\partial u}{\partial x} + 2u\frac{\partial c}{\partial x} = 0. \tag{5.6}$$

By adding (5.5) and (5.6) we obtain,

$$\frac{\partial(u + 2c)}{\partial t} + (u + c)\frac{\partial(u + 2c)}{\partial x} = 0. \tag{5.7}$$

By subtracting (5.6) from (5.5) we obtain,

$$\frac{\partial(u - 2c)}{\partial t} + (u - c)\frac{\partial(u - 2c)}{\partial x} = 0. \tag{5.8}$$

Both equations (5.7) and (5.8) are true only when $h = const$, (ie. at $x = 0$ and at $x = a$).

So if $u + c > 0$, $u + 2c$ must be specified at $x = 0$.

We always have $|u| < c$.

So if $u - c < 0$, $u - 2c$ must be specified at $x = a$.

Now,

$$u + 2c = u + 2\,[g(h + \zeta)]^{\frac{1}{2}}$$

$$= u + 2(gh)^{\frac{1}{2}}[1 + \frac{1}{2}(\frac{\zeta}{h}) + o(\frac{\zeta}{h})^2].$$

So, for an incoming wave at $x = 0$,

$$u + (gh)^{\frac{1}{2}}(\frac{\zeta}{h}) \quad \text{must be specified at } x = 0. \tag{5.9}$$

Similarly,

$$u - 2c = u - 2(gh)^{\frac{1}{2}}[1 + \frac{1}{2}(\frac{\zeta}{h}) + o(\frac{\zeta}{h})^2].$$

So, for an incoming wave at $x = a$,

$$u - (gh)^{\frac{1}{2}}(\frac{\zeta}{h}) \quad \text{must be specified at } x = a. \tag{5.10}$$

We now consider the basic linearized field equations

$$\frac{\partial u}{\partial t} - fv = -g\frac{\partial \zeta}{\partial x},$$

$$\frac{\partial v}{\partial t} + fv = -g\frac{\partial \zeta}{\partial y},$$

momentum equations

$$\frac{\partial \zeta}{\partial t} + \frac{\partial (hu)}{\partial x} + \frac{\partial (hv)}{\partial y} = 0,$$

continuity equation

where $u = u(x, y, t), \quad v = v(x, y, t), \quad \zeta = \zeta(x, y, t) \quad \text{and} \quad h = h(x, y).$

We write $U = hu, \ V = hv \ \text{and} \ c^2 = gh$, then

$$\begin{aligned} \frac{\partial U}{\partial t} - fV &= -c^2 \frac{\partial \zeta}{\partial x}, \\ \frac{\partial V}{\partial t} + fU &= -c^2 \frac{\partial \zeta}{\partial y}, \end{aligned} \qquad \text{momentum equations} \qquad (5.11)$$

$$\frac{\partial \zeta}{\partial t} + \frac{\partial U}{\partial x} + \frac{\partial V}{\partial y} = 0. \qquad \text{continuity equation} \qquad (5.12)$$

5.3 Determination of Boundary Conditions:

We linearize (i) of (5.3) and (5.4), taking h=const.

So,

$$\begin{aligned} \frac{\partial u}{\partial t} &= -g \frac{\partial \zeta}{\partial x} \qquad \text{(i)} \\ \frac{\partial \zeta}{\partial t} + h \frac{\partial u}{\partial x} &= 0. \qquad \text{(ii)} \end{aligned} \qquad (5.13)$$

whilst (ii) of (5.3) remains unchanged. That is,

$$fu = -g \frac{\partial \zeta}{\partial y} \qquad (5.14)$$

Seeking a solution of the form

$$\zeta = \zeta_0(y) \ \ e^{i(kx - \sigma t)},$$

$$u = u_0(y) \ \ e^{i(kx - \sigma t)}.$$

Then,

$$-i\sigma u_0(y) = -g(ik)\zeta_0(y), \quad \text{so} \quad u_0(y) = \frac{gk}{\sigma}\zeta_0(y),$$

$$-i\sigma \zeta_0(y) = -h(ik)u_0(y), \quad \text{so} \quad \zeta_0(y) = \frac{hk}{\sigma}u_0(y).$$

Also from above it can be seen,

$$\frac{\sigma}{k} = (gh)^{\frac{1}{2}} = c \quad \text{to the lowest order.}$$

The equation (5.14) implies,

$$\frac{du_0}{dy} + \frac{f}{c}u_0 = 0. \tag{5.15}$$

The solution of (5.15) is given as

$$u_0(y) = Ce^{-\frac{f}{c}y}, \quad \text{where } C = \text{constant;} \tag{5.16}$$

which implies

$$\zeta_0(y) = C(\frac{h}{c})e^{-\frac{f}{c}y} = ae^{\frac{-f}{c}y}, \quad \text{where } a = C(\tfrac{h}{c}).$$

Thus,

$$\zeta = ae^{-\frac{f}{c}y}e^{i(kx-\sigma t)}, \qquad \text{(i)}$$

$$u = \frac{a}{h}c\, e^{-\frac{f}{c}y}\ \ e^{i(kx-\sigma t)}. \quad \text{(ii)} \tag{5.17}$$

Now by specifying (5.17) as the incoming Kelvin wave solution we have

$$u + (\frac{g}{h})^{\frac{1}{2}}\zeta = \left[\frac{c}{h} + (\frac{g}{h})^{\frac{1}{2}}\right] ae^{-\frac{f}{c}y}e^{i(kx-\sigma t)}$$

which in turn can be written as

$$\zeta + (\frac{h}{g})^{\frac{1}{2}}u = 2\ a\ e^{-\frac{f}{c}y}e^{i(kx-\sigma t)}. \tag{5.18}$$

Thus, for a channel with constant depth and open at both ends with an incoming Kelvin wave at $x = 0$, there must be no incoming wave at $x = a$. Hence,

$$u - (gh)^{\frac{1}{2}}(\frac{\zeta}{h}) = 0 \qquad \text{at } x = a.$$

So, on taking the imaginary part of (5.18) we write down the boundary conditions

for a channel open at both ends with an incoming Kelvin wave at $x = 0$, where h =constant, as

$$\begin{aligned} \zeta + (\frac{h}{g})^{\frac{1}{2}} u &= -2\ a\ e^{-\frac{f}{c}y} \sin(\sigma t) \quad \text{(i), at } x = 0 \\ \zeta + (\frac{h}{g})^{\frac{1}{2}} u &= 0. \qquad\qquad\qquad \text{(ii), at } x = a \end{aligned} \tag{5.19}$$

In order to obtain a suitable boundary condition for this problem where propagation of Kelvin wave in a semi-infinite channel closed at one end with an incoming Kelvin wave at $x = 0$, we consider first the linear form of the first momentum equation of (i) of (5.1).

$$\frac{\partial u}{\partial t} - fv = -g\frac{\partial \zeta}{\partial x}. \tag{5.20}$$

For this incoming Kelvin wave at $x = 0$, we let $v \equiv 0$ and thus the local acceleration in the vicinity of $x = 0$ is given by the gradient force.

$$\frac{\partial u}{\partial t} = -g\frac{\partial \zeta}{\partial x}. \tag{5.21}$$

5.3.1 Expressing the function $Z(t)$ in Fourier Series:

Any suitable periodic function in t, $Z(t)$ with period t_p can be expressed as

$$\begin{aligned} Z(t) &= \frac{1}{2}a_0 + \sum_{n=1}^{\infty}[a_n \cos(\frac{2\pi nt}{t_p}) + b_n \sin(\frac{2\pi nt}{t_p})] \\ &= \frac{1}{2}a_0 + Re(\sum_{n=1}^{\infty}[(a_n + ib_n)e^{\frac{-2i\pi nt}{t_p}}]) \end{aligned}$$

where,

$$\begin{aligned} c_n &= a_n + ib_n, \\ a_n &= \frac{2}{t_p}\int_0^{t_p} Z(t)\cos(\frac{2\pi nt}{t_p})dt, \\ b_n &= \frac{2}{t_p}\int_0^{t_p} Z(t)\sin(\frac{2\pi nt}{t_p})dt, \\ c_n &= \frac{2}{t_p}\int_0^{t_p} Z(t)e^{(\frac{2i\pi nt}{t_p})}dt. \end{aligned} \tag{5.22}$$

5.4 Method of Solution:

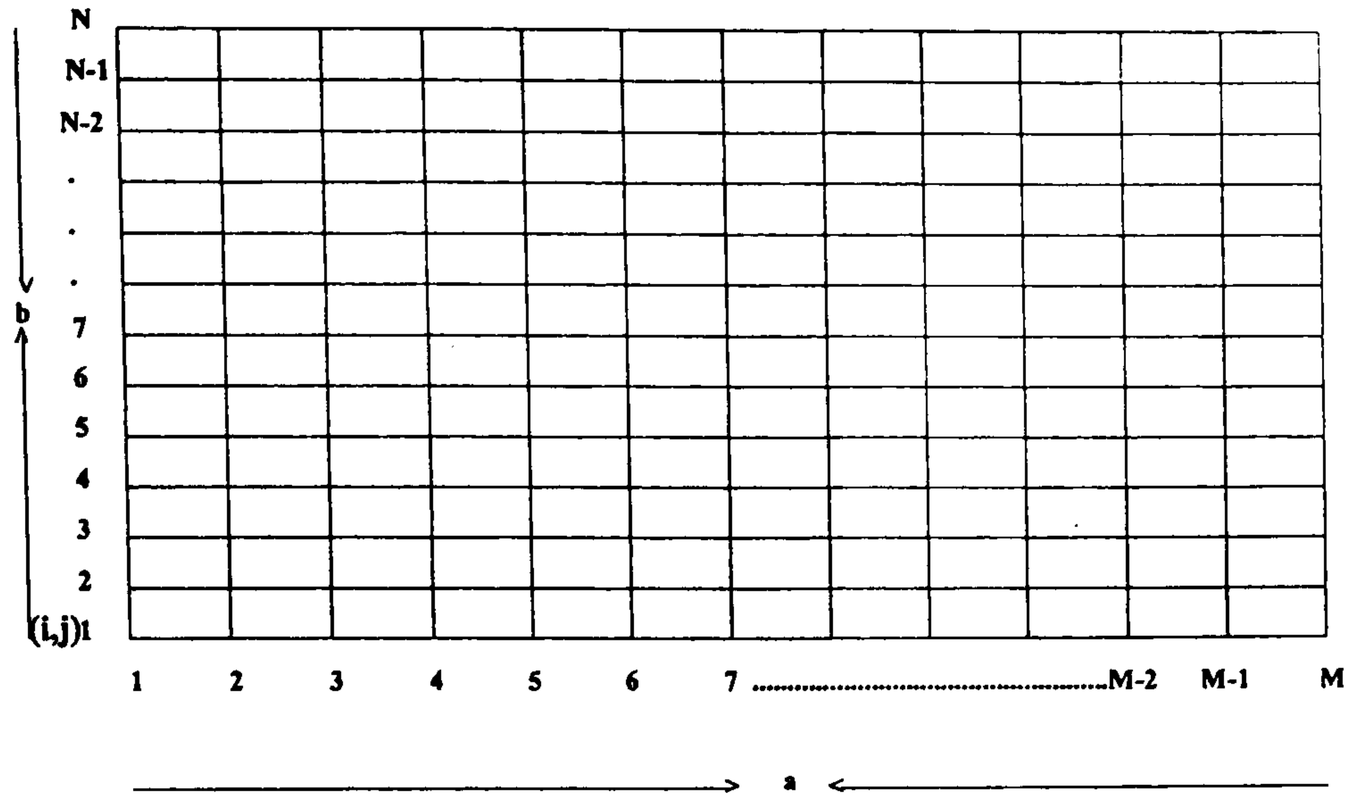

Figure 5.2:

The method used here is a numerical procedure based on discretizing the length and the width of the channel. The width, b, and the length, a, of the channel are discretized by N grid points y direction and M grid points x direction, where M and N take odd values or even values according to the problem considered (see fig (5.2)).

In this present case the value of $M = even$ and $N = odd$.

5.4.1 Finite Difference Equations:

<u>Notation:</u>

$$U(x_i, y_j, t_p) = U_{ij}^p, \quad V(x_i, y_j, t_p) = V_{ij}^p, \quad \zeta(x_i, y_j, t_p) = Z_{ij}^p.$$

$$x_i = (i-1)\triangle x, \quad y_j = (j-1)\triangle y, \quad t_p = p\triangle t,$$

where $\quad i = 1, 2, 3, ...m, \quad j = 1, 2, 3, ...n, \quad p = 0, 1, 2, 3, ...$

Using the above notations the equation (5.21) in turn is written in discrete form

in space and time as

$$\left(\frac{\partial u}{\partial t}\right)_{2,j}^{p} = -g\left(\frac{\partial \zeta}{\partial x}\right)_{2,j}^{p+1}. \tag{5.23}$$

By using the Taylor series we expand the velocity vector $u_{2,j}^{p+1}$ to the second order in time as

$$u_{2,j}^{p+1} = u_{2,j}^{p} + \triangle t\left(\frac{\partial u}{\partial t}\right)_{2,j}^{p} + 0\left(\triangle t^{2}\right).$$

On introducing (5.23) into this expansion and write down it in finite difference form we obtain,

$$u_{2,j}^{p+1} = u_{2,j}^{p} - g\triangle t\left(\frac{\zeta_{3,j}^{p+1} - \zeta_{1,j}^{p+1}}{2\triangle x}\right)_{2,j}^{p} + 0\left(\triangle t^{2}\right). \tag{5.24}$$

By substituting for $u_{2,j}^{p+1}$ from (5.24) into the equation (i) of the boundary condition (5.19) we obtain a FD equation for elevation along $x = 0$.

$$(1-\beta)\zeta_{1,j}^{p+1} = -(1-\beta)\zeta_{3,j}^{p+1} - 2(\frac{h_{2,j}}{g})^{\frac{1}{2}}u_{2,j}^{p} - 4ae^{\frac{-f}{c}\nu}\sin(\sigma t). \tag{5.25}$$

where, $\beta = \frac{c\triangle t}{\triangle x}$

Now write the momentum equations (5.11) and continuity equation (5.12) in finite difference form.

$$U_{ij}^{p+1} - \frac{1}{2}f\triangle tV_{ij}^{p+1} = U_{ij}^{p} + \frac{1}{2}f\triangle tV_{ij}^{p} - \frac{c_{ij}^{2}\triangle t}{2\triangle x}\left(Z_{i+1j}^{p+1} - Z_{i-1j}^{p+1}\right). \tag{5.26}$$

Similarly, the second equation of (5.11) is written in finite difference method.

That is,

$$\frac{1}{2}f\triangle tU_{ij}^{p+1} + V_{ij}^{p+1} = V_{ij}^{p} - \frac{1}{2}f\triangle tU_{ij}^{p} - \frac{c_{ij}^{2}\triangle t}{2\triangle y}\left(Z_{ij+1}^{p+1} - Z_{ij-1}^{p+1}\right). \tag{5.27}$$

Solving (5.26) and (5.27) for V_{ij}^{p+1} and U_{ij}^{p+1} we obtain,

$$A_1(t)V_{ij}^{p+1} = A_2(t)V_{ij}^{p} - A_3(t)U_{ij}^{p} + c_{ij}^2\Delta t\left[\frac{1}{2}f\Delta t\left(\frac{Z_{i+1,j}^{p+1} - Z_{i-1,j}^{p+1}}{2\Delta x}\right) - \left(\frac{Z_{ij+1}^{p+1} - Z_{ij-1}^{p+1}}{2\Delta y}\right)\right] \quad (5.28$$

where $A_1(t) = \left[1 + \frac{1}{4}(f\Delta t)^2\right]$, $A_2(t) = \left[1 - \frac{1}{4}(f\Delta t)^2\right]$ and $A_3(t) = f\Delta t$.

We also have

$$U_{ij}^{p+1} = U_{ij}^{p} + \frac{1}{2}f\Delta t\left(V_{ij}^{p+1} + V_{ij}^{p}\right) - c_{ij}^2\ \Delta t\ \frac{Z_{i+1j}^{p+1} - Z_{i-1j}^{p+1}}{2\Delta x}, \quad (5.29)$$

and

$$\frac{Z_{ij}^{p+1} - Z_{ij}^{p}}{\Delta t} + \frac{U_{i+1j}^{p} - U_{i-1j}^{p}}{2\Delta x} + \frac{V_{ij+1}^{p} - V_{ij-1}^{p}}{2\Delta y} = 0. \quad (5.30)$$

The following equations are used to interpolate the respective field variables v, u, and ζ.

$$V_{i,j}^{p+1} = \frac{1}{4}\left[V_{i-1,j+1}^{p+1} + V_{i+1,j+1}^{p+1} + V_{i-1,j-1}^{p+1} + V_{i+1,j-1}^{p+1}\right] \quad (5.31)$$

$$U_{i,j}^{p+1} = \frac{1}{4}\left[U_{i-1,j+1}^{p+1} + U_{i+1,j+1}^{p+1} + U_{i-1,j-1}^{p+1} + U_{i+1,j-1}^{p+1}\right] \quad (5.32)$$

$$Z_{i,j}^{p+1} = \frac{1}{4}\left[Z_{i-1,j+1}^{p+1} + Z_{i+1,j+1}^{p+1} + Z_{i-1,j-1}^{p+1} + Z_{i+1,j-1}^{p+1}\right] \quad (5.33)$$

5.5 Solution to Taylor's Problem by applying FD technique:

Here, we consider an incoming Kelvin wave defined by

$$\zeta = ae^{-\frac{f}{c}y}e^{i(kx-\sigma t)}, \quad \text{(i)}$$

$$u = \frac{a}{h}c\ e^{-\frac{f}{c}y}\ \ e^{i(kx-\sigma t)}. \quad \text{(ii)}$$

propagating from north to south in a channel of length, a, and the width, b, in an area where the geographical latitude is 50 ^{0} north so that the coriolis parameter is

$f = 0.0001169$. The basin is of uniform depth of h_0=74 $meters$ closed at one end. By taking the period of the semi-diurnal tidal wave as $T = 12$ $hour$, we take the length, a ,analysis domain in kilometres as $a = 1.1415504 * (\sqrt{gh_0} * T * 3600)/1000$=1.1415504 reference wavelengths = 1328.71 km. In discretization of the length and the width of the channel, $M = 224$, $N = 85$, see the fig (5.2) so that the width of the analysis domain can be chosen proportionally as $b = \frac{84}{223} * a = 500.499$ km. Thus the length and the width of the basin are discretized by 224 grid points x-direction and 85 grid points y-direction. It means $\triangle y$=$\triangle x$ has the value of 5.95834 km.

By considering 300 time steps per tidal period, which corresponds to $\triangle t$=144 seconds, we integrate the system in space and time for 50 tidal cycles.

The integration is performed as follows.

Firstly , by using the FD equation (5.30) we update the elevation at interior points of the mesh. These points are, here, termed as 'elevation points' and denoted by symbol ◯ in fig (5.3).

Then using the boundary value (5.25), elevation is updated along the open boundary $x = 0$.

Now, by using the equations (5.28) and (5.29) both y -velocity and x-velocity are updated at interior V-points and U-points respectively. These points are respectively denoted by symbols $\overline{\square}$ and $\triangle$ respectively in fig (5.3). Using (5.31) the updated y-velocity should have been interpolated at interior U-points before x-velocity being updated. Finally, using (5.32) the x-velocity is interpolated at interior V-points. This process continues for all 49 tidal periods. Then for the final tidal period the updated elevations plug into (5.22) and the product is obtain for some specific mesh points (ie $i = 1, M-1, 2$; $j = 2, N-1, 2$) and the integration process is repeated for whole

tidal period. The final sum at each specific mesh points is multiplied by $\frac{2}{t_p}$.

Finally the integrated elevations are interpolated at U-points, V-points, null points, coastal end, along sides and end points on open boundary of the channel to obtain complete solutions in the whole domain.

5.5.1 Solution:

In figs (5.4) and (5.5) are shown for co-range and co-tidal lines of Kelvin wave propagation through a semi-infinite channel of constant depth closed at one end. The parameters used in this numerical technique correspond exactly to those in the Taylor problem. The diagram in fig (5.4) exhibits the wave height at different parts of the region and it can be seen that the solution obtained by this numerical method is consistent with the solution obtained by the analytical method described in chapter-4. The complex reflection coefficient derived directly from numerical model is $(0.7411, -0.6714)$ whereas the complex reflection coefficient obtained by the analytical method is $(0.7395, -0.6732)$.

5.6 Comparison:

The comparison between the numerical solution and analytical solution is performed by comparing the mid-channel wave height for numerical solution and analytical solution. This is done in fig (5.6) where the red curve indicates the numerical part and the blue color indicates the analytical curve. On inspection one could see that it is a very good comparison.

It is also noted in fig (5.4) that the wave height in the lower left and right corners of the basin are higher than that in the rest of the basin.

In fig (5.5) the co-tidal lines are drawn for every $\frac{1}{20}$ part of a period (ie for every 36 *mins*).

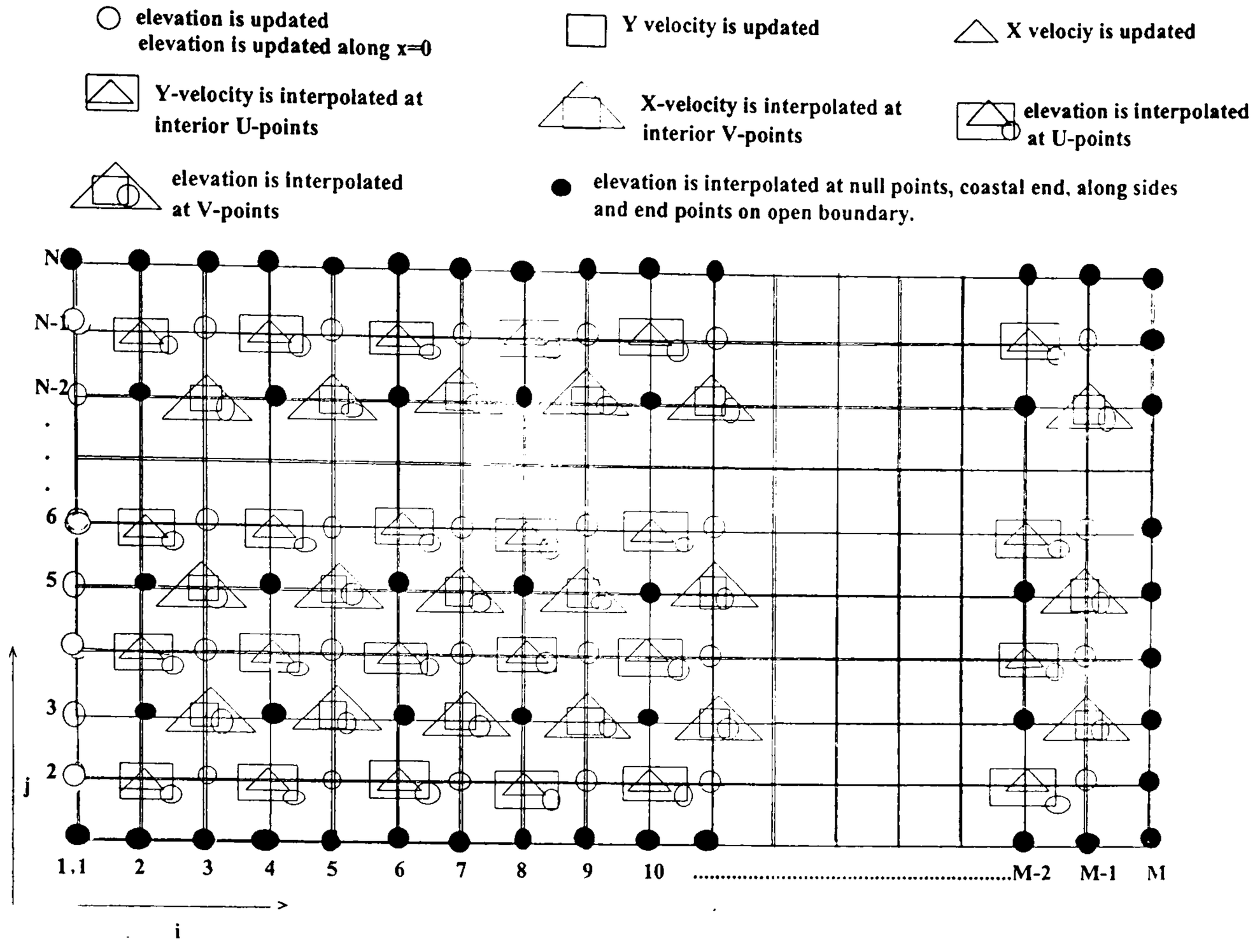

Figure 5.3:

Both in analytical and numerical solutions we can see two real and one semi-real amphidromic points lie along the central axis of the channel. In the above test we see that the comparison is good along the mid-section of the channel. We wish to have a global measure of the difference between the analytical and numerical solutions. This is done by finding the root mean square error between two sets of data.

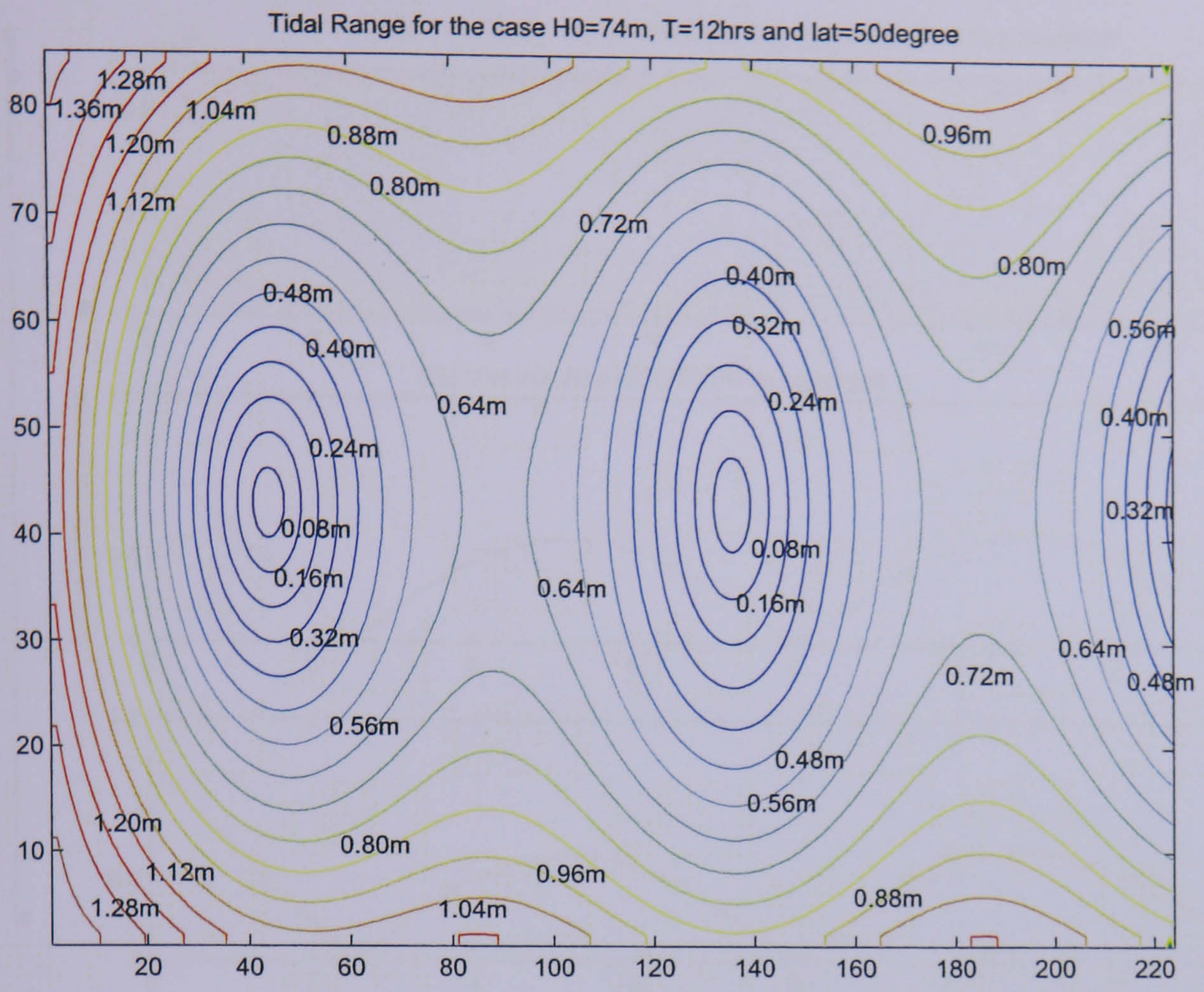

Figure 5.4: Parameters: $H_0 = 74m$, $\sigma = 0.0001454sec^{-1}$, $f = 0.00011867sec^{-1}$ and $T = 12hrs$

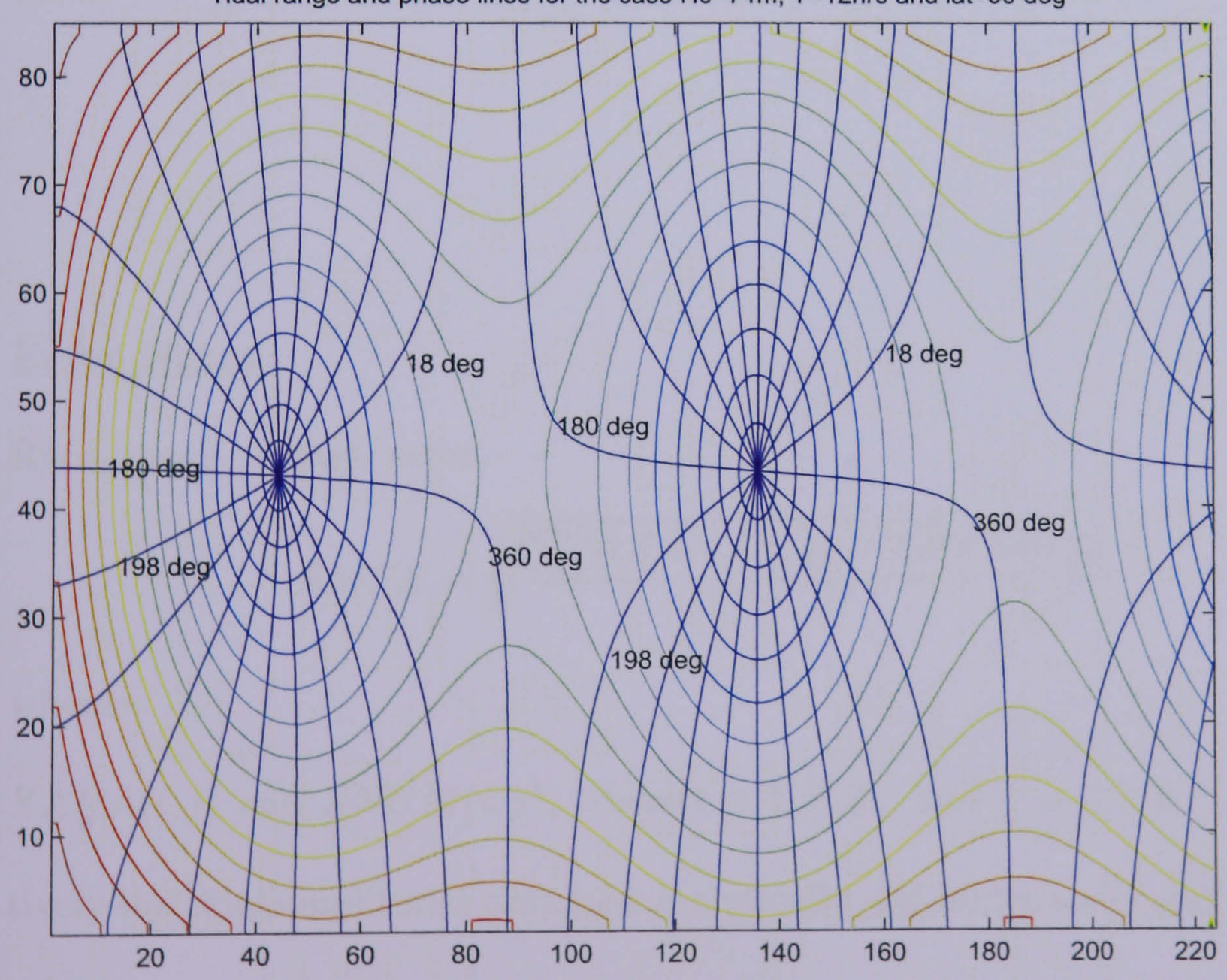

Figure 5.5: Parameters: $H_0 = 74m$, $\sigma = 0.0001454sec^{-1}$, $f = 0.00011867sec^{-1}$ and $T = 12hrs$

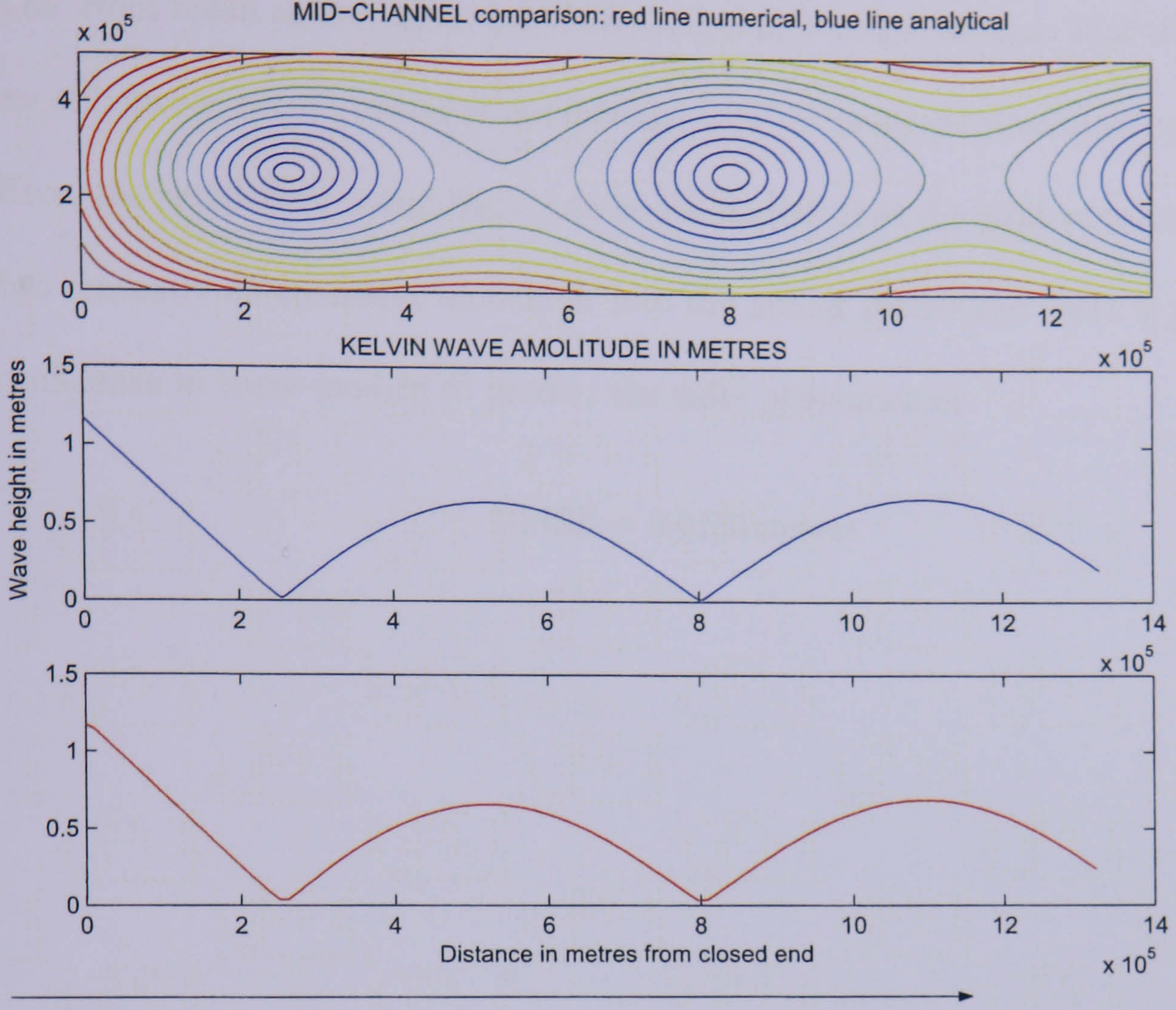

Figure 5.6:

Error Norm

Root mean square error

$$RMSE = \sqrt{\frac{\sum_1^n ((ZANA(i,j) - ZNUM(i,j))^2}{N}}.$$

where,

$ZANA(i,j)$ and $ZNUM(i,j)$, where($i = 1,2,3...$ and $j = 1,2,3....$) denote respectively the tidal amplitudes obtained analytically and numerically and N is the number of computational points.

The 'Root mean square error' ($RMSE$) is merely a single number that defines differences between actual values (observations) and the response predicted by a model. Here, the small error value thus obtained indicates that the data extracted by these two mutually independent models fit into the actual values and there is about 95 % confidence in these models to predict the tidal phenomenon.

$$\text{RMSE} = 0.0134\text{metres}.$$

Chapter 6

Propagation of a Kelvin wave over a step-bottom in a Semi-infinite Canal closed at one end

6.1 Introduction:

The incident Kelvin wave approaches the shallow water region from the deep sea in the north of the channel. The origin of coordinates chosen naturally at one corner of the canal such that the Kelvin waves traveling in opposite directions in the two regions are in phase at the boundaries $x = 0$ and $x = L$ respectively. The end-effect terms are added at the boundaries $x = 0$ and $x = L$ so as to exclude any incoming *Poincaré* modes. A collocation method is used to determine the relevant coefficients. The results are checked to see whether they are in agreement with those obtained by a numerical method developed by Johns (personal communication).

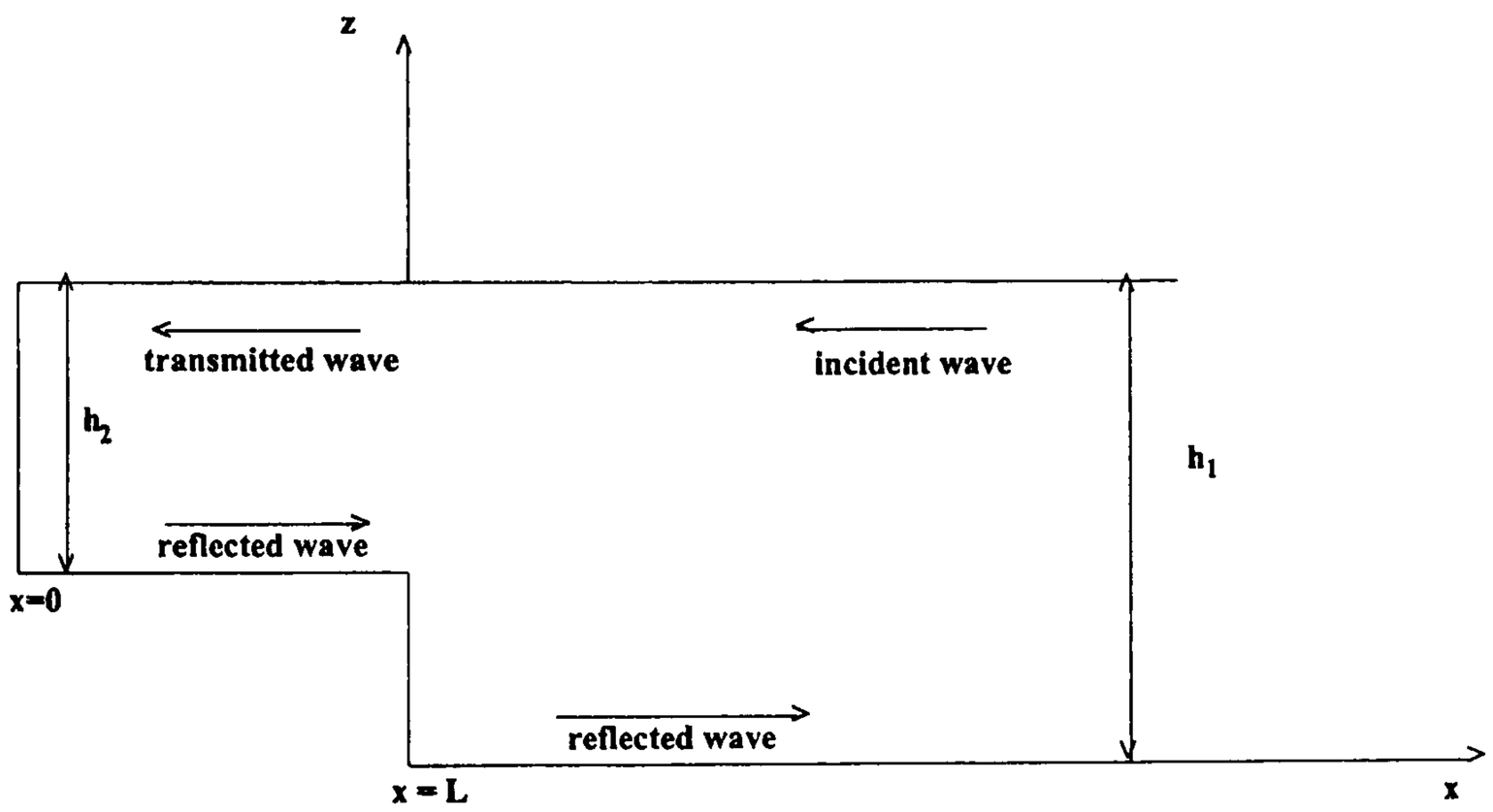

Figure 6.1:

6.2 Formulation of the Model:

As mentioned above, we consider a semi-infinite canal rotating about the vertical axis with an angular velocity $\underline{\omega} = \omega\, \underline{k}$. The horizontal coordinates are (x, y), defined such that the canal occupies the region $x \geq L,\ 0 \leq y \leq b$ and region $0 \leq x \leq L, 0 \leq y \leq b$.

The depth averaged velocity components in the two regions are respectively, (u_1, v_1) and (u_2, v_2). The respective canal depth are h_1 and h_2 assumed constant (see fig (6.1)).

The Kelvin waves system in the region $x \geq L,\ 0 \leq y \leq b$ is defined by

$$\left.\begin{aligned} \zeta_I &= e^{\alpha_1(y-b)+i(\sigma t+\frac{\sigma}{c_1}(x-L))} && \text{incident wave} \\ \zeta_{R_1} &= R_1 e^{-\alpha_1 y+i\left(\sigma t-\frac{\sigma}{c_1}(x-L)\right)} && \text{reflected wave} \end{aligned}\right\}. \tag{6.1}$$

where ζ, t, and g are surface elevation, time and gravity respectively.

Also σ, α_1, and c_1 are positive and

$$c_1^2 = gh_1 \quad \text{and} \quad \alpha_1 = \frac{f}{c_1}\ (for\ brevity).$$

Here c_1 is the velocity of the long wave in the absence of earth's rotation in the region $x > L$.

The associated velocities are

$$u_I = -(\frac{g}{c_1})\zeta_I, \quad u_{R_1} = (\frac{g}{c_1})\zeta_{R_1}, \quad \text{and} \quad v_I = v_{R_1} = 0. \tag{6.2}$$

The end effect is written as a set of *Poincaré* modes, u_E, v_E and ζ_E defined as

$$\left.\begin{aligned} v_E &= (\tfrac{g}{c_1}) \textstyle\sum_1^\infty \gamma_n \sin(l_n y) e^{-s_n(x-L)+i\sigma t}, \\ u_E &= (\tfrac{g}{c_1}) \textstyle\sum_1^\infty \gamma_n \left\{A_n \cos(l_n y) + B_n \sin(l_n y)\right\} e^{-s_n(x-L)+i\sigma t}, \\ \zeta_E &= \textstyle\sum_1^\infty \gamma_n \left\{C_n \cos(l_n y) + D_n \sin(l_n y)\right\} e^{-s_n(x-L)+i\sigma t}, \qquad \text{for } x \geq L, \end{aligned}\right\} \tag{6.3}$$

where $l_n = \frac{n\pi}{b}$, $s_n^2 = l_n^2 - k_1^2$ and $k_1^2 = \frac{\sigma^2 - f^2}{c_1^2}$

We rewrite the linearized momentum equations for field variables (ζ, u, v), and uniform ocean depth h :

$$\left.\begin{aligned} h\ k^2 u &= i\sigma\zeta_x + f\zeta_y \\ h\ k^2 v &= i\sigma\zeta_y - f\zeta_x \end{aligned}\right\} \tag{6.4}$$

where

$k^2 = \dfrac{\sigma^2 - f^2}{c^2}$, and f, σ respectvely Coriolis parameter and wave frequency.

Clearly the set (u_E, v_E, ζ_E) in (6.3) satisfies the momentum equation (6.4) and as such by introducing (6.3) into (6.4) we obtain

$$C_n = \frac{i\sigma l_n c_1}{\triangle_n}, \qquad D_n = \frac{-f s_n c_1}{\triangle_n},$$
$$A_n = \frac{s_n l_n c_1^2}{\triangle_n}, \qquad B_n = \frac{-i\sigma f}{\triangle_n}, \tag{6.5}$$

where

$$\triangle_n = \sigma^2 + s_n^2 c_1^2 = f^2 + l_n^2 c_1^2.$$

The Kelvin wave system in the region $0 \leq x \leq L$, constitutes:

(i) The transmitted wave moving towards the south. This has associated velocities (u_T, v_T) and the wave height ζ_T is given by

$$\zeta_T = Te^{\alpha_2(y-b)+i(\sigma t - \frac{\sigma}{c_2}(L-x))}; \tag{6.6}$$

where, σ, α_2, and c_2 are positive and

$$c_2^2 = gh_2, \quad \text{and} \quad \alpha_2 = \frac{f}{c_2}.$$

Here c_2 is the velocity of the long wave in the absence of earth's rotation in the region $x < L$.

The associated velocities are

$$u_T = (-\frac{g}{c_2})\zeta_T, \qquad v_T = 0.$$

(ii) The reflected wave ζ_{R_2} propagating towards the north with associated velocities (u_{R_2}, v_{R_2}) is defined as

$$\zeta_{R_2} = R_2 e^{-\alpha_2 y + i(\sigma t - \frac{\sigma}{c_2}x)}; \tag{6.7}$$

Its associated velocities are

$$u_{R_2} = (\frac{g}{c_2})\zeta_{R_2}, \quad v_{R_2} = 0.$$

The *Poincaré* modes in the vicinity of the region $x \leq L$ are given by

$$\left.\begin{aligned} v'_E &= (\tfrac{g}{c_2}) \textstyle\sum_1^\infty \gamma'_n \sin(l_n y) e^{-t_n(L-x)+i\sigma t}, \\ u'_E &= (\tfrac{g}{c_2}) \textstyle\sum_1^\infty \gamma'_n \left\{A'_n \cos(l_n y) + B'_n \sin(l_n y)\right\} e^{-t_n(L-x)+i\sigma t}, \\ \zeta'_E &= \textstyle\sum_1^\infty \gamma'_n \left\{C'_n \cos(l_n y) + D'_n \sin(l_n y)\right\} e^{-t_n(L-x)+i\sigma t}, \qquad \text{for } x \leq L. \end{aligned}\right\} \tag{6.8}$$

where $t_n^2 = l_n^2 - k_2^2$ and $k_2^2 = \frac{\sigma^2 - f^2}{c_2^2}$

The set of *Poincaré* modes (6.8) satisfy the momentum equations (6.4) and as such by introducing (6.7) into (6.4) we obtain the required coefficients.

$$\begin{aligned} A'_n &= \frac{-t_n l_n c_2^2}{\Delta'_n}, \qquad B'_n = \frac{-i\sigma f}{\Delta'_n}, \\ C'_n &= \frac{i\sigma l_n c_2}{\Delta'_n}, \qquad D'_n = \frac{f t_n c_2}{\Delta'_n}, \end{aligned} \tag{6.9}$$

where

$$\Delta'_n = \sigma^2 + t_n^2 c_2^2 = f^2 + l_n^2 c_2^2.$$

The *Poincaré* modes that emanate from the condition at the boundary $x = 0$ are

$$\left.\begin{aligned} v''_E &= (\tfrac{g}{c_2}) \textstyle\sum_1^\infty \gamma''_n \sin(l_n y) e^{-t_n x+i\sigma t}, \\ u''_E &= (\tfrac{g}{c_2}) \textstyle\sum_1^\infty \gamma''_n \left\{A''_n \cos(l_n y) + B''_n \sin(l_n y)\right\} e^{-t_n x+i\sigma t}, \\ \zeta''_E &= \textstyle\sum_1^\infty \gamma''_n \left\{C''_n \cos(l_n y) + D''_n \sin(l_n y)\right\} e^{-t_n x+i\sigma t}, \qquad \text{for } x \geq 0. \end{aligned}\right\} \tag{6.10}$$

These modes are also substituted into momentum equations (6.4) and yield

$$\begin{aligned} A''_n &= \frac{t_n l_n c_2^2}{\Delta'_n}, \qquad B''_n = \frac{-i\sigma f}{\Delta'_n}, \\ C''_n &= \frac{i\sigma l_n c_2}{\Delta'_n}, \qquad D''_n = \frac{-f t_n c_2}{\Delta'_n}. \end{aligned} \tag{6.11}$$

6.3 Boundary conditions at $x = L$ and $x = 0$:

(i) The continuity of total mass flow across the boundary $x = L$ implies

$$R_1 e^{-\frac{f}{c_1}y} - e^{\frac{f}{c_1}(y-b)} + \sum_1^\infty \gamma_n [A_n \cos(l_n y) + B_n \sin(l_n y)] + \beta_0 T e^{\frac{f}{c_2}(y-b)} - \beta_0 R_2 e^{-\frac{f}{c_2}y} e^{-i\frac{\sigma L}{c_2}}$$

$$-\beta_0 \left(\sum_1^\infty \gamma_n' [A_n' \cos(l_n y) + B_n' \sin(l_n y)] + \sum_1^\infty \gamma_n'' [A_n'' \cos(l_n y) + B_n'' \sin(l_n y)] \, e^{-t_n L} \right) = 0. \quad (6.1$$

where $\beta_0 = \sqrt{\frac{h_2}{h_1}}$

(ii) The continuity of surface elevation at the boundary $x = L$ provides

$$R_1 e^{-(\frac{f}{c_1})y} + e^{(\frac{f}{c_1})(y-b)} - T e^{(\frac{f}{c_2})(y-b)} + \sum_1^\infty \gamma_n \{C_n \cos(l_n y) + D_n \sin(l_n y)\} - R_2 e^{-(\frac{f}{c_2})y} e^{\frac{-i\sigma L}{c_2}}$$

$$- \sum_1^\infty \gamma_n' \left\{ C_n' \cos(l_n y) + D_n' \sin(l_n y) \right\} - \sum_1^\infty \gamma_n'' \left\{ C_n'' \cos(l_n y) + D_n'' \sin(l_n y) \right\} e^{-t_n L} = 0,$$

$$\forall y \, \epsilon [0, b]. \quad (6.13)$$

(iii) The longitudinal velocities at $x = 0$ must vanish, hence

$$R_2 e^{-(\frac{f}{c_2})y} - T e^{(\frac{f}{c_2})(y-b)} e^{-i\frac{\sigma}{c_2}L} + \sum_1^\infty \gamma_n'' \left\{ A_n'' \cos(l_n y) + B_n'' \sin(l_n y) \right\}$$

$$+ \sum_1^\infty \gamma_n' \left\{ A_n' \cos(l_n y) + B_n' \sin(l_n y) \right\} e^{-t_n L} = 0,$$

$$\forall y \, \epsilon [0, b]. \quad (6.14)$$

6.4 Solution:

6.4.1 Collocation Method:

As a first treatment to solve the system of three non homogeneous equations (6.12), (6.13) and (6.14) we introduce the collocation method. The equations (6.12), (6.13) and (6.14) imply a requirement to invert an infinite matrix. However, we take that the equations (6.12), (6.13) and (6.14) hold at a finite set of points on $[0, b]$ with the series truncated to an appropriate finite number of terms.

Now we set up a matrix $C\underline{\mathbf{x}} = \underline{\mathbf{b}}$ system based on

the unknown vector, $(\gamma_1, \gamma_2, ..., \gamma_N, \gamma_1^{'}, \gamma_2^{'}, ...\gamma_N^{'}, \gamma_1^{''}, \gamma_2^{''}, ...\gamma_N^{''}, R_1, R_2, T)^T$. This means we form one equation from each of the $N+1$ collocation points,

$y_k = \frac{(k-1)b}{N}$, $k = 1, 2, ...N+1$,

yielding $3N+3$ equations. This process is continued for the other two system of equations. This would finally produce a square matrix C of order $(3N+3 \times 3N+3)$. Now we write this system as $C\mathbf{x} = \mathbf{b}$.

Then on solving the system of equations (6.12), (6.13) and (6.14) as a whole through $C\underline{\mathbf{x}} = \underline{\mathbf{b}}$ as defined above, we obtain contours for 'cotidal range' and 'phase lines' respectively in fig (6.2) and fig (6.3). It can be seen in fig (6.2) that the tidal elevation in the shallow water region is much higher than that in the offshore region. The highest elevation is experienced in the two corners at the closed end. In fig (6.3) the phase-lines are drawn for every $\frac{1}{24}$ of the tidal period i.e. for every 30 *mins*.

Furthermore we can notice the crowing of co-range and co-tidal lines in the vicinity of the closed end indicating that the water in the shelf-region is more perturbed than that in the rest of the sea.

Here, it is remarkable to add the following points.

In solving this problem one of the boundary conditions used at the boundary $x = L$ above is 'Surface elevation is continuous across the boundary'. It can then be expected that if the elevation is continuous then the gradient of the elevation may be discontinuous.

Fig (6.4) is drawn examine this conjecture. In the middle and the last parts of this figure, plots of both imaginary and real parts of the elevations in the mid-channel

and the coastal-ends respectively are given. On the top part of the figure is given the contours for the tides, so that the comparison can be made easily. It is clearly seen in

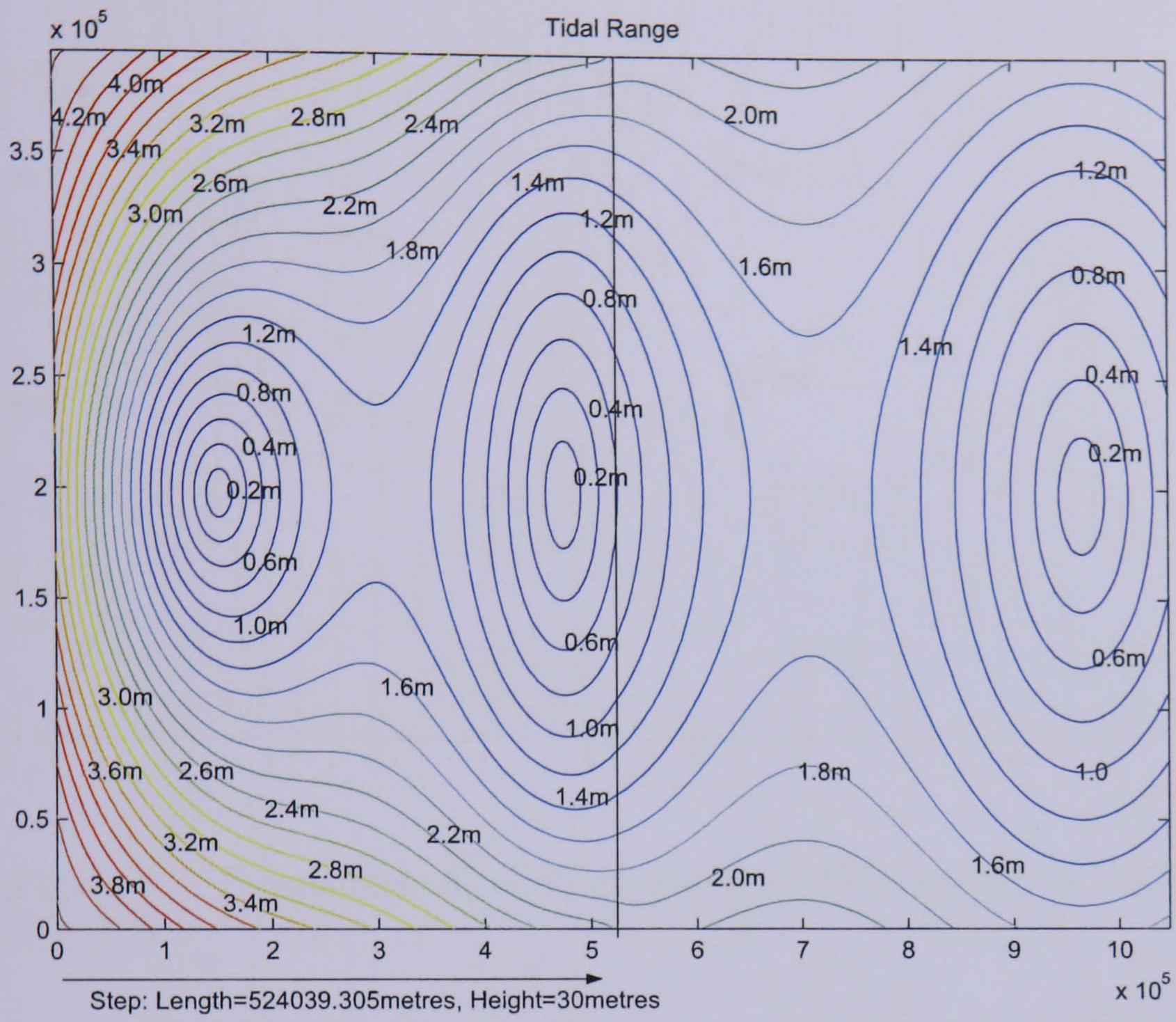

Figure 6.2: Parameters: h_1=60 m, σ = 0.0001454 sec^{-1}, f=0.0001188 sec^{-1} and T = 12 hrs

fig (6.4c) that the elevation gradient is discontinuous at the boundary. Interestingly, this is less pronounced in the mid-channel but more so near the lateral boundaries.

6.4.2 The Numerical Model:

The intention here of having this numerical counterpart is to serve as a numerical check on the analytical solution obtained above.

As before we consider an incoming Kelvin wave defined by

$$\zeta = ae^{-\frac{f}{c}y}e^{i(kx-\sigma t)}, \qquad \text{(i)}$$

$$u = \frac{a}{h}c\ e^{-\frac{f}{c}y}\ \ e^{i(kx-\sigma t)}. \qquad \text{(ii)}$$

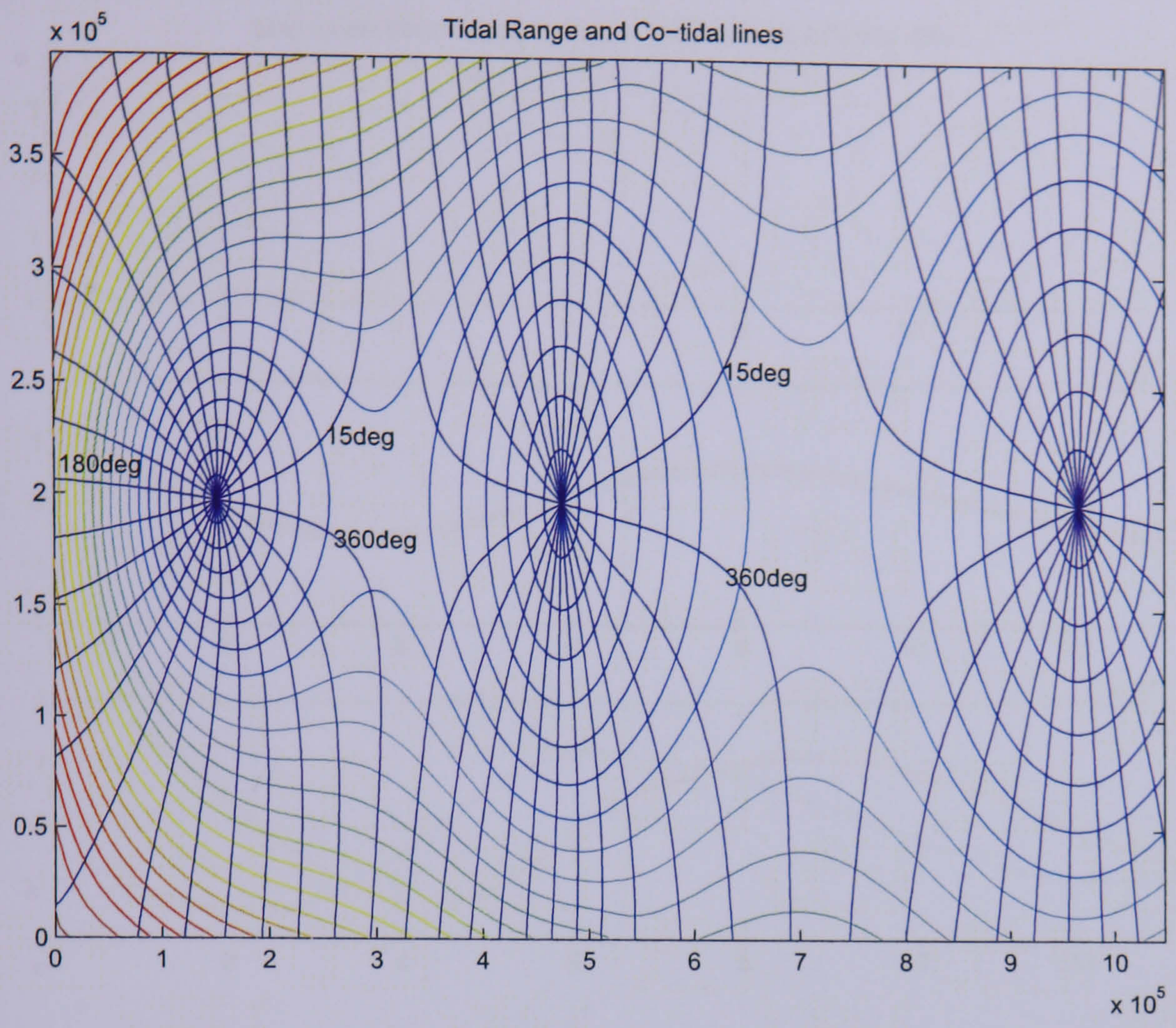

Figure 6.3: Parameters: $h_1 = 60\ m$, $\sigma = 0.0001454\ sec^{-1}$, $f = 0.0001188\ sec^{-1}$ and $T = 12hrs$

propagating from north to south in a semi-infinite channel of length, A, and the width, b, in an area where the geographical latitude is $50\ \underline{0}$ north so that the coriolis parameter is $f = 0.0001169\ sec^{-1}$. The sea bottom is of abrupt change in depth where the constant total depth is $h_0 = 60$ meters and the bathymetric relief is defined by a step of height $30\ m$ and length $524.0393\ km$ extended right across the width of the channel. By taking the period of the semi-diurnal tidal wave as $T = 12\ hours$, we take the length, A, analysis domain in kilometers as $A = (\sqrt{gh_0} * T * 3600)/1000 = 1048.08 = 1$ reference wavelength.

In discretization of the length and the width of the channel, $M = 224$, $N = 85$, see the fig (6.5) so that the width of the analysis domain can be chosen proportionally as $b = \frac{84}{223} * A = 394.792\ km$. Thus the length and the width of the basin are discretized by 224 grid points x-direction and 85 grid points y-direction. It means $\triangle y = \triangle x$

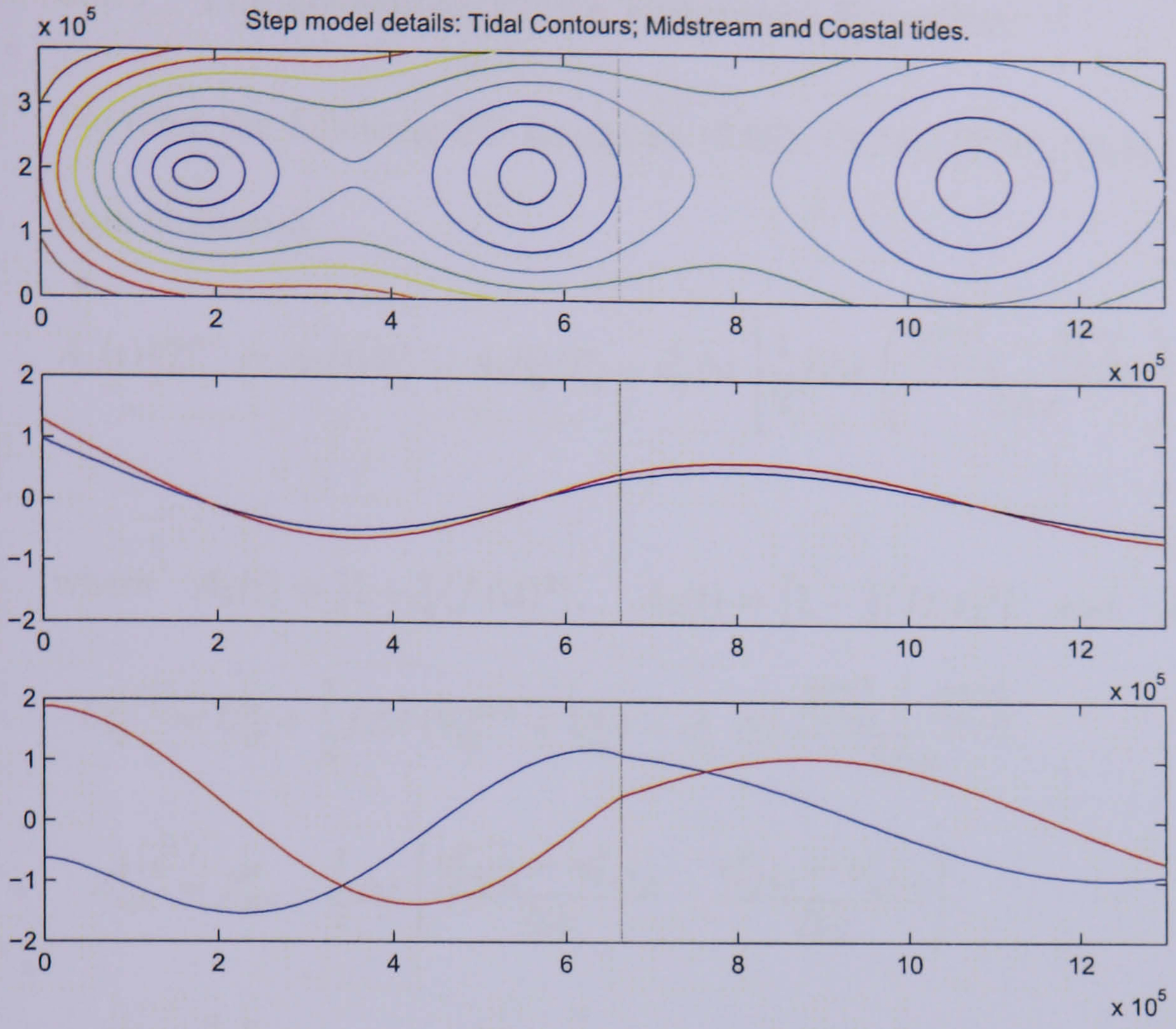

Figure 6.4: Parameters: $H_0 = 60\ m$, $\sigma = 0.0001454\ sec^{-1}$, $f = 0.0001188\ sec^{-1}$ and $T = 12\ hrs$

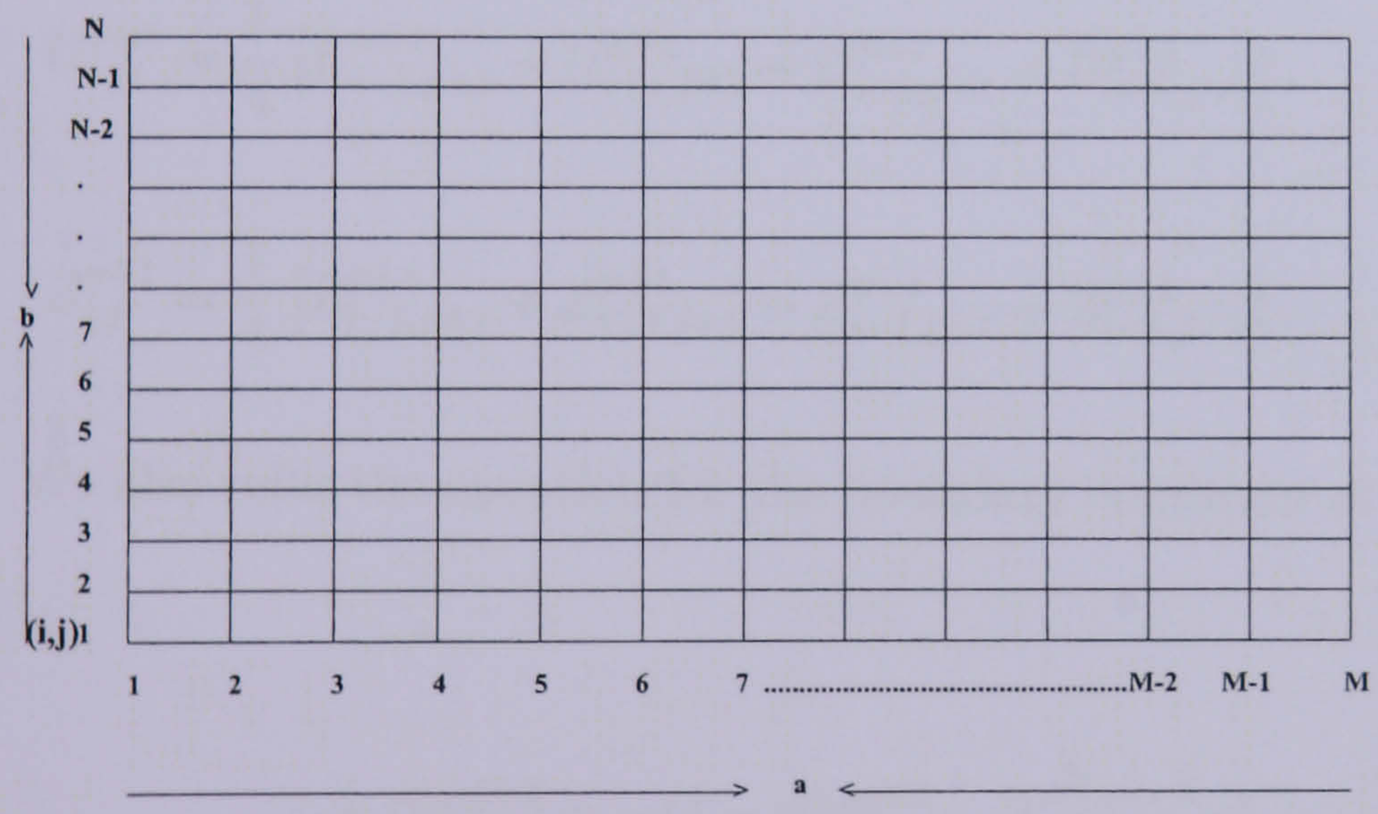

Figure 6.5:

has the value of 4.69991 km. By considering 300 time steps per tidal period, which corresponds to $\triangle t = 144\ seconds$, we integrate the system in space and time for 50 tidal cycles.

The integration is performed using the FD equations as follows.

6.4.3 The governing Finite Difference Equation:

We refer the following FD equations (5.28), (5.29), (5.30), (5.31), (5.32) and (5.33) from chapter-5

$$A_1(t)V_{ij}^{p+1} = A_2(t)V_{ij}^{p} - A_3(t)U_{ij}^{p} + c_{ij}^2\Delta t\left[\frac{1}{2}f\Delta t\left(\frac{Z_{i+1,j}^{p+1} - Z_{i-1,j}^{p+1}}{2\Delta x}\right) - \left(\frac{Z_{ij+1}^{p+1} - Z_{ij-1}^{p+1}}{2\Delta y}\right)\right] \quad (6.15)$$

where $A_1(t) = \left[1 + \frac{1}{4}(f\Delta t)^2\right]$, $A_2(t) = \left[1 - \frac{1}{4}(f\Delta t)^2\right]$ and $A_3(t) = f\Delta t$.

$$U_{ij}^{p+1} = U_{ij}^{p} + \frac{1}{2}f\Delta t\left(V_{ij}^{p+1} + V_{ij}^{p}\right) - c_{ij}^2\ \Delta t\ \frac{Z_{i+1j}^{p+1} - Z_{i-1j}^{p+1}}{2\Delta x}. \quad (6.16)$$

$$Z_{i,j}^{p+1} = Z_{i,j}^{p} - \frac{1}{2}\Delta t\left[\frac{u_{i+1,j}^{p} - u_{i-1,j}^{p}}{\Delta x} - \frac{v_{i,j+i}^{p} - v_{i,j-i}^{p}}{\Delta y}\right]. \quad (6.17)$$

$$V_{i,j}^{p+1} = \frac{1}{4}\left[V_{i-1,j+1}^{p+1} + V_{i+1,j+1}^{p+1} + V_{i-1,j-1}^{p+1} + V_{i+1,j-1}^{p+1}\right]. \quad (6.18)$$

$$U_{i,j}^{p+1} = \frac{1}{4}\left[U_{i-1,j+1}^{p+1} + U_{i+1,j+1}^{p+1} + U_{i-1,j-1}^{p+1} + U_{i+1,j-1}^{p+1}\right]. \quad (6.19)$$

$$Z_{i,j}^{p+1} = \frac{1}{4}\left[Z_{i-1,j+1}^{p+1} + Z_{i+1,j+1}^{p+1} + Z_{i-1,j-1}^{p+1} + Z_{i+1,j-1}^{p+1}\right]. \quad (6.20)$$

We also refer the equation for the boundary condition at $x = 0$ from chapter-5. That is,

$$(1-\beta)\zeta_{1,j}^{p+1} = -(1-\beta)\zeta_{3,j}^{p+1} - 2(\frac{h_{2,j}}{g})^{\frac{1}{2}}u_{2,j}^{p} - 4ae^{\frac{-f}{c}y}\sin(\sigma t). \quad (6.21)$$

where, $\beta = \frac{c\Delta t}{\Delta x}$

6.4.4 The propagation of a Kelvin wave into a basin closed at one end:

Firstly, by using the FD equation (6.17) we update the elevation at interior points of the mesh. These points are, here, termed as 'elevation points' and denoted by symbol

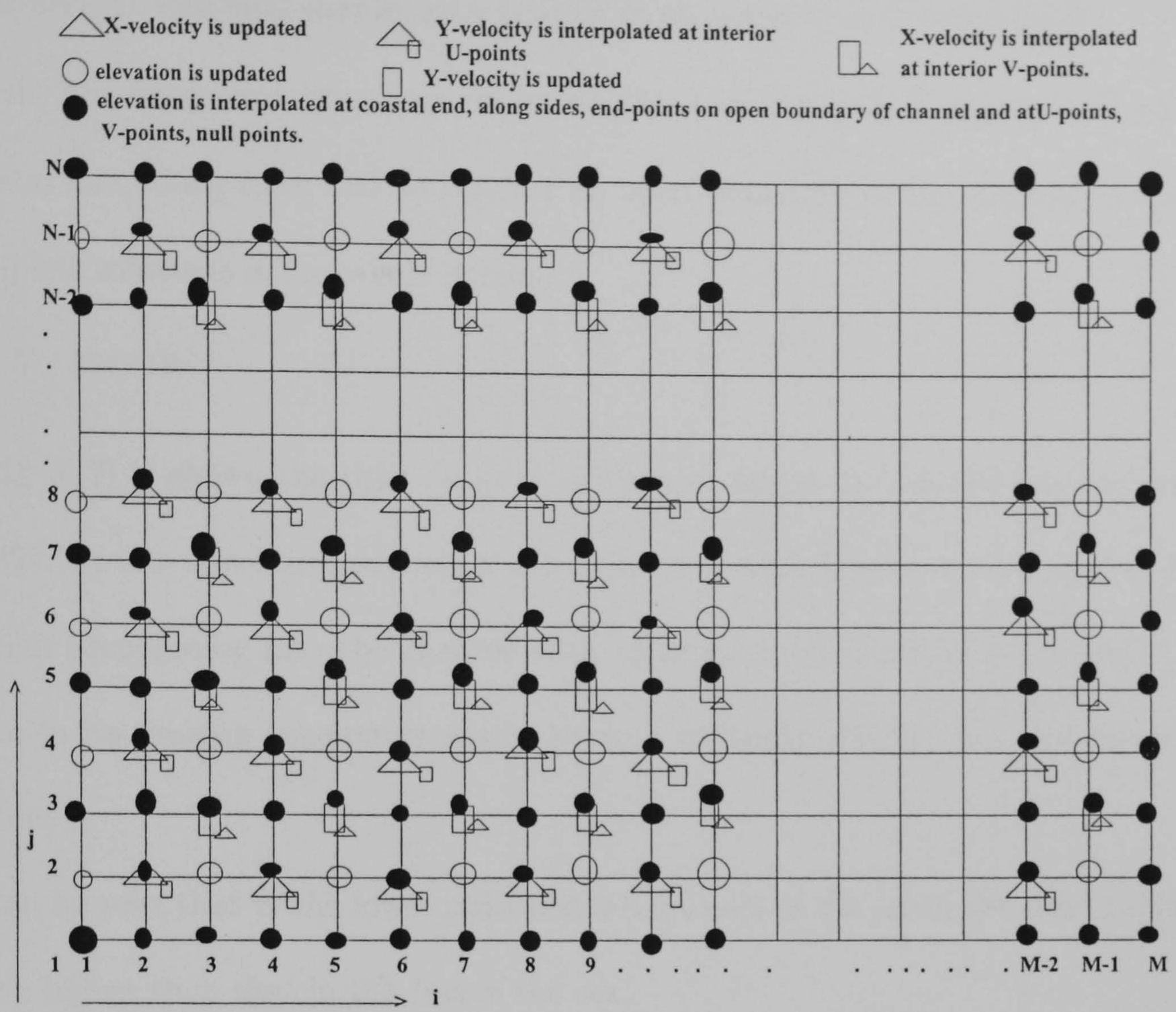

Figure 6.6:

◯ in fig (6.6). Then using the boundary value (6.21), elevation is updated along the open boundary $x = 0$.

Now, by using the equations (6.15) Y-velocity is updated at interior V-points. These points are denoted by symbol $\overline{\square}$. Having updated these Y-velocity at interior V-points, Y-velocity is interpolated at interior U-points by using the FD equation (6.18). Similarly, by using the FD equation (6.16) we update the X-velocity at interior U-points. These points are denoted by $\triangle$.

Finally, using (6.19) the X-velocity is interpolated at interior V-points. This process continues for all 49 tidal periods. Then for the final tidal period the updated elevations plug into (5.22) of chapter 5 and the product is obtain for some specific mesh points

(ie $i = 1, M-1, 2$; $j = 2, N-1, 2$) and the integration process is repeated for whole tidal period. The final sum at each specific mesh points is multiplied by $\frac{2}{t_p}$.

Finally the integrated elevations are interpolated at U-points, V-points, null points, coastal end, along sides and end points on open boundary of the channel to obtain complete solutions in the whole domain.

6.4.5 Result:

In fig (6.7) is shown the tidal range in a basin of length 1048.07861 km and width of 394.791 km approximately when a Kelvin wave with forcing wave height of 0.75 meters propagating into the channel with constant total depth of 60 meters. The wave in its passage encounters a step bottom of length 524.039 km and height 30 meters.

It can be seen that in the lower right and left corners of the basin the tidal height is much higher than that in the rest of the sea.

In fig (6.8) given co-tidal lines which are drawn for every $\frac{1}{24}$ of the period or for every 30 mins.

6.5 Comparison:

The accuracy of the solutions is tested by performing a mid-channel comparison where the plots of elevations in the mid-channel for both analytical and numerical treatments are given in fig (6.9). Here, the red-color curve represents the numerical solution whereas the blue-color curve represents the analytical solution. In comparison it can be seen a good matching of the two solutions of the problem.

In the above comparison we have considered elevations only in specific area of the channel (i.e. along the mid-channel). Though this set of values acts as a representa-

tive of whole region of analysis it is desirable to consider the overall estimate of the error between analytical and numerical values. For this reason we define a way of evaluating the error between the analytical solution and numerical solution.

Error Norm

Root mean square error

$$RMSE = \sqrt{\frac{\sum_1^n((ZANA(i,j) - ZNUM(i,j))^2}{N}}.$$

where,

$ZANA(i,j)$ and $ZNUM(i,j)$, where($i = 1,2,3...$ and $j = 1,2,3....$) denote respectively the tidal amplitudes obtained analytically and numerically and N is the number of computational points.

The 'Root mean square error' ($RMSE$) is merely a single number that defines differences between actual values (observations) and the response predicted by a model. This simple small error value (RMSE) implies that the results predicted by these two mutually independent methods are significantly the same. It also evident that the results produced by them represent over 95 % of the true value of the tidal wave.

RMSE = 0.0160 metres.

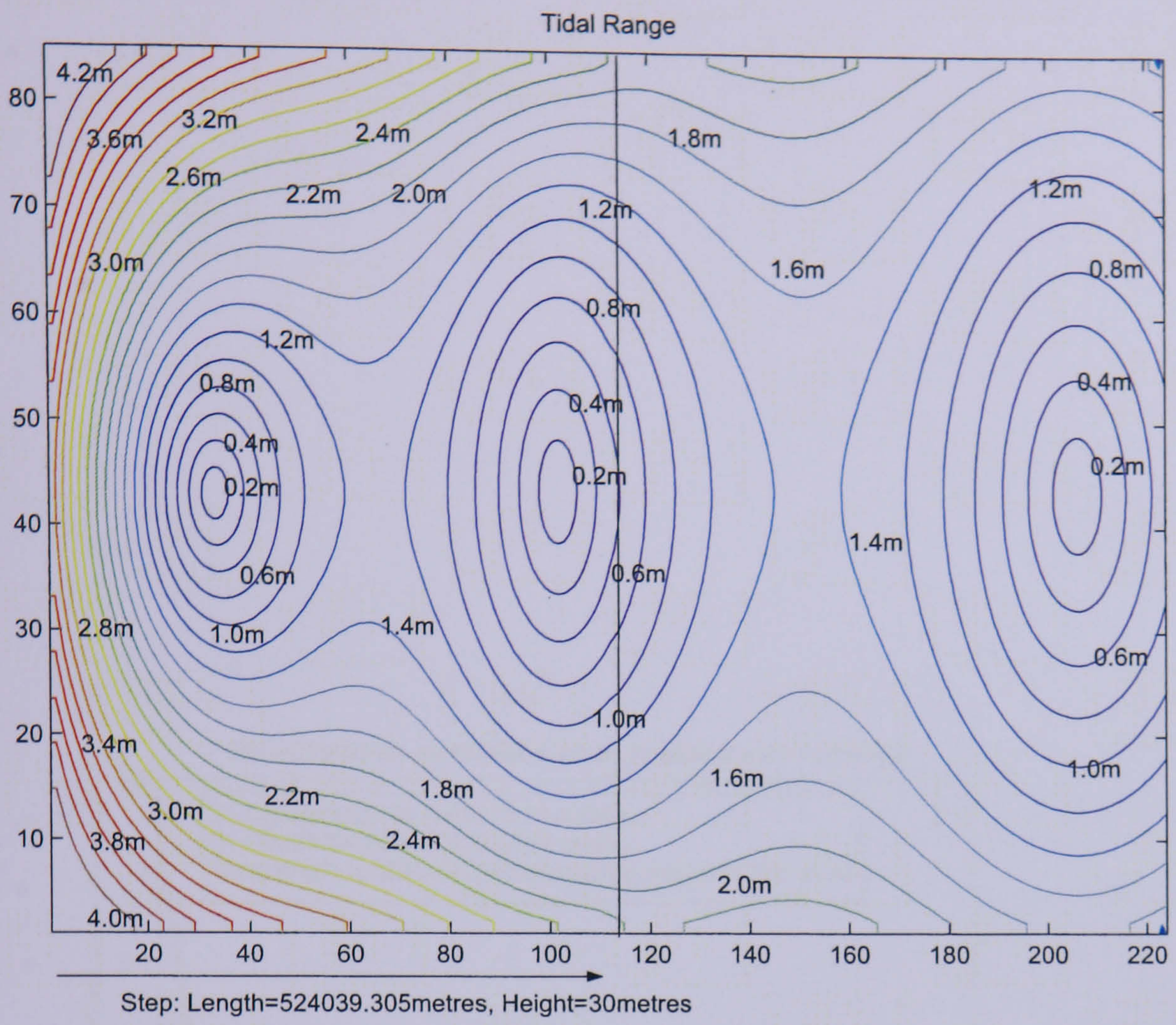

Figure 6.7: Parameters: $h_1 = 60m$, $\sigma = 0.0001454sec^{-1}$, $f = 0.000126sec^{-1}$ and $T = 12hrs$

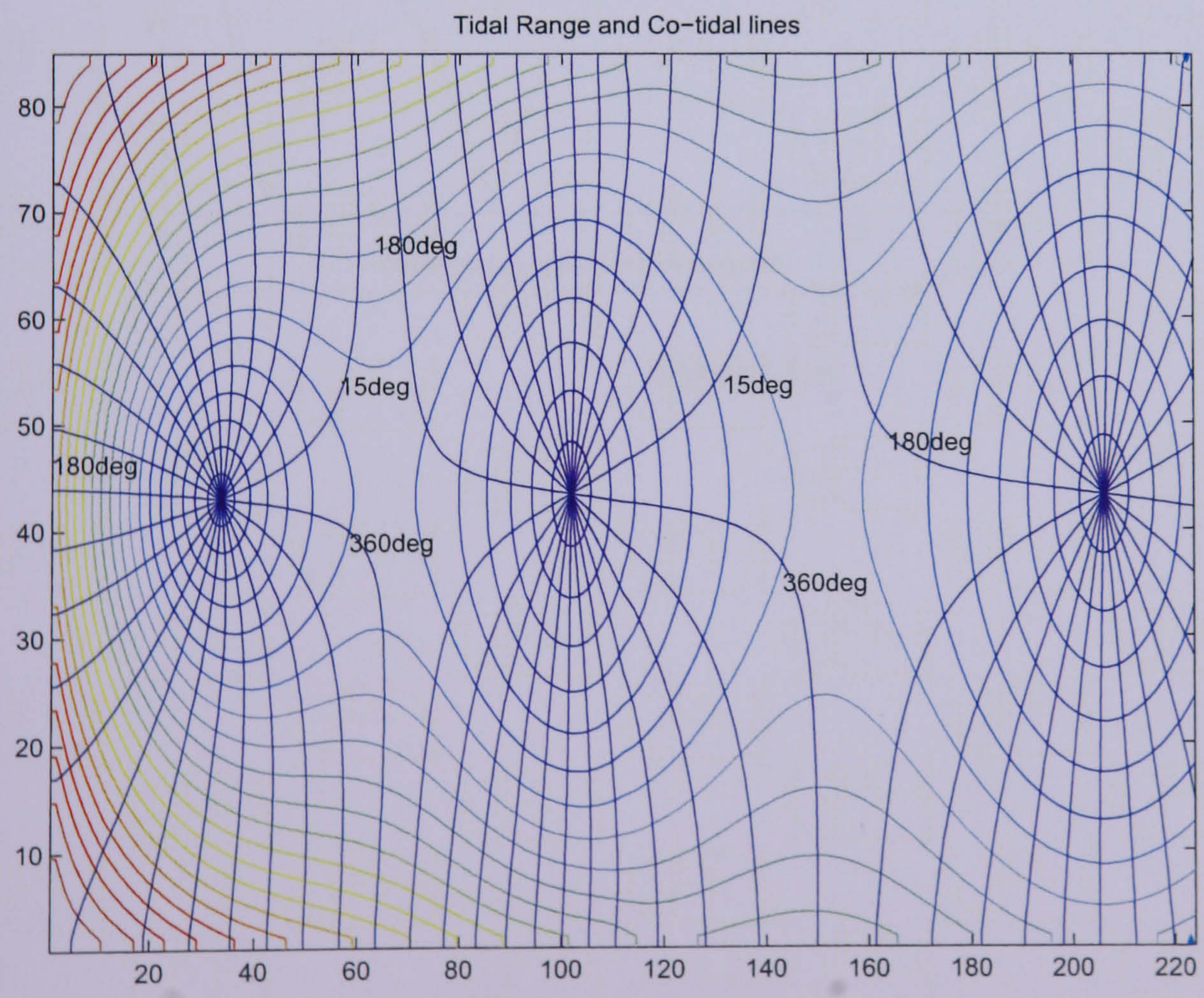

Figure 6.8: Parameters: $h_1 = 60m$, $\sigma = 0.0001454sec^{-1}$, $f = 0.000126sec^{-1}$ and $T = 12hrs$

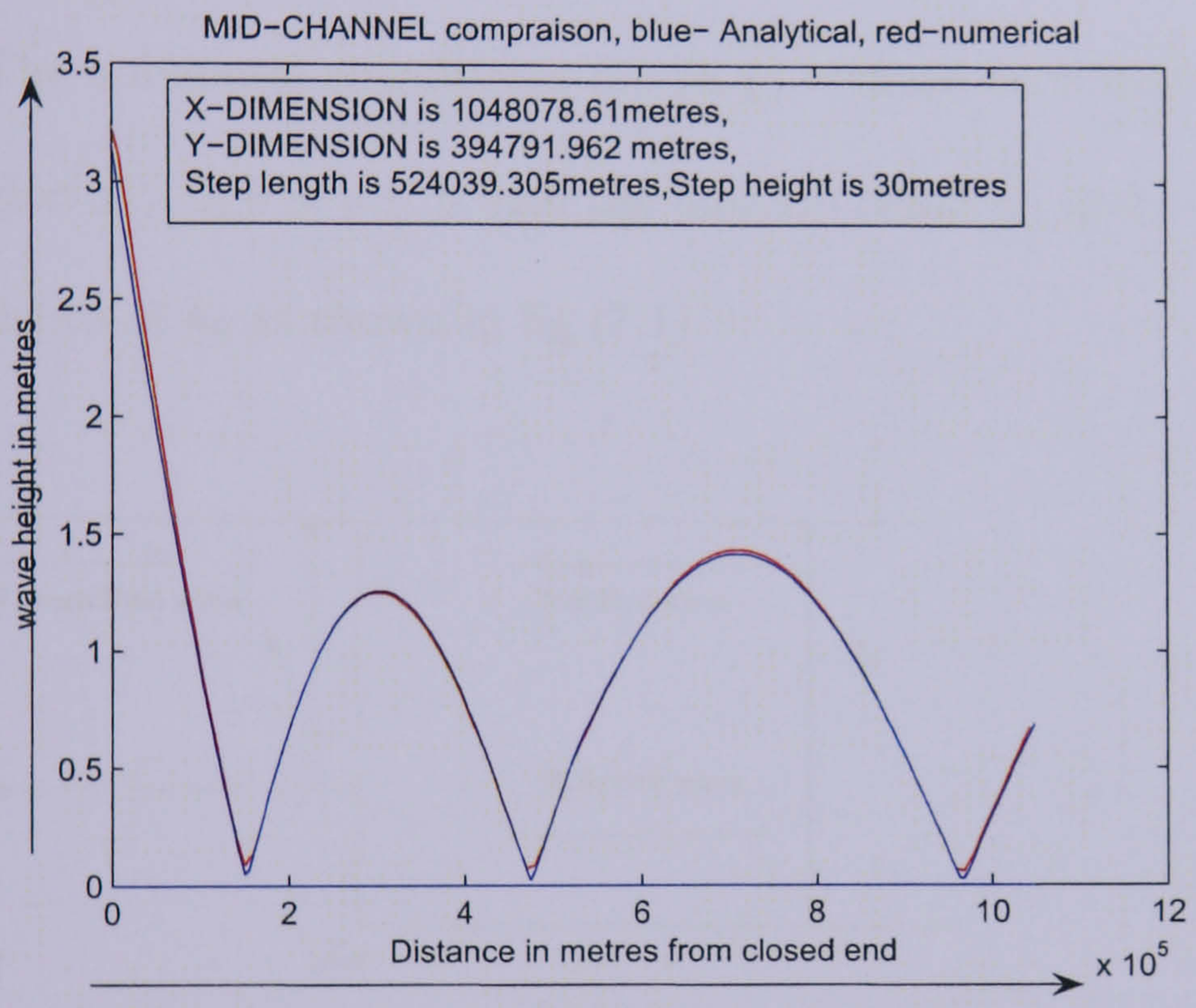
MID−CHANNEL compraison, blue− Analytical, red−numerical
X−DIMENSION is 1048078.61metres,
Y−DIMENSION is 394791.962 metres,
Step length is 524039.305metres,Step height is 30metres
wave height in metres
Distance in metres from closed end
x 10^5
0
0.5
1
1.5
2
2.5
3
3.5
0
2
4
6
8
10
12

Figure 6.9:

Chapter 7
Propagation of a Kelvin wave over a step in a rotating channel

We consider here the effects of abrupt change in depth on an incident Kelvin wave in a rotating channel.

We now consider a further generalization to Taylor's problem. In this model two intercommunicating semi-infinite channels of different uniform depths meet at $x = 0$. The horizontal coordinates are (x, y), defined such that the channel occupies the region $x > 0$, $0 \leq y \leq b$ with the uniform depth h_1 and $x < 0$, $0 \leq y \leq b$ with uniform depth of h_2 as shown in fig (7.1).

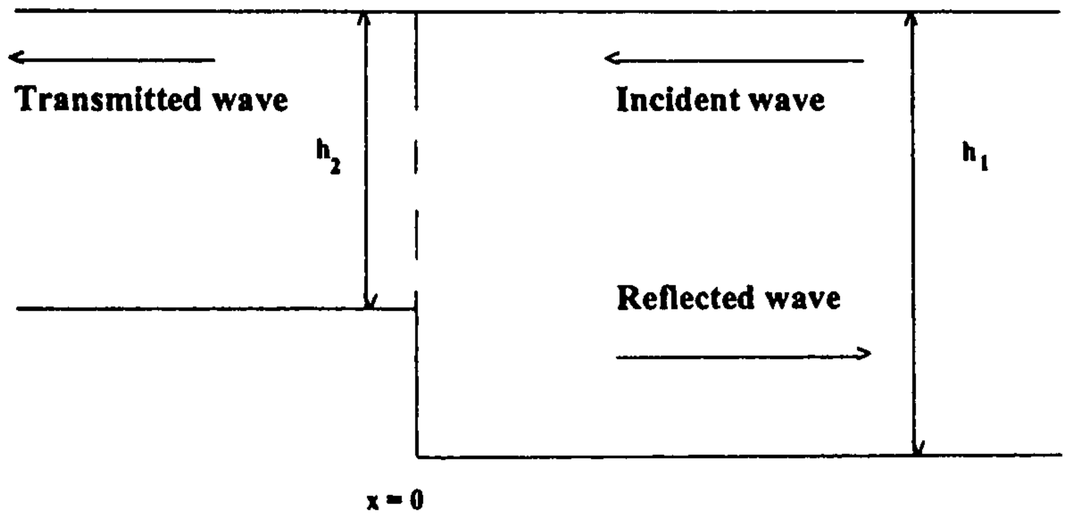

Figure 7.1: Schematic representation of the cross-section of the sea

7.1 Defining equation:

The incident and reflected wave in the region $x > 0$ are defined by

$$\left.\begin{aligned} \zeta_I &= e^{-(\frac{f}{c_1})(b-y)+i(\sigma t+\frac{\sigma}{c_1}x)} \\ \zeta_R &= Re^{-(\frac{f}{c_1})y+i(\sigma t-\frac{\sigma}{c_1}x)} \end{aligned}\right\}. \tag{7.1}$$

where R is a complex constant to be determined.

Similarly, in the region $x < 0$, we have the transmitted Kelvin wave defined by

$$\zeta_T = Te^{-(\frac{f}{c_2})(b-y)+i(\sigma t+\frac{\sigma}{c_2}x)}, \tag{7.2}$$

where T is a complex constant to be determined.

In order for suitable conditions on $x = 0$, $y = 0$ and $y = b$ to be satisfied it is necessary to have an end-effect. The end-effect may be written as sets of *Poincaré* modes in a manner similar to the classical closed end problem as described in a previous chapter(4).

Thus, we write

$$v_1 = (\frac{g}{c_1})\sum_1^\infty \gamma_n \sin(l_n y)e^{-s_n x+i\sigma t},$$

$$u_1 = (\frac{g}{c_1})\sum_1^\infty \gamma_n \left\{A_n \cos(l_n y) + B_n \sin(l_n y)\right\} e^{-s_n x+i\sigma t},$$

$$\zeta_1 = \sum_1^\infty \gamma_n \left\{C_n \cos(l_n y) + D_n \sin(l_n y)\right\} e^{-s_n x+i\sigma t} \quad \text{for } x > 0, \text{ and}$$

$$v_2 = (\frac{g}{c_2})\sum_1^\infty \delta_n \sin(l_n y)e^{t_n x+i\sigma t},$$

$$u_2 = (\frac{g}{c_2})\sum_1^\infty \delta_n \left\{H_n \cos(l_n y) + L_n \sin(l_n y)\right\} e^{t_n x+i\sigma t},$$

$$\zeta_2 = \sum_1^\infty \delta_n \left\{M_n \cos(l_n y) + N_n \sin(l_n y)\right\} e^{t_n x+i\sigma t} \qquad \text{for } x < 0. \tag{7.3}$$

Here

$$l_n = \frac{n\pi}{b}, \quad s_n^2 = l_n^2 - k_1^2, \quad t_n^2 = l_n^2 - k_2^2, \quad k_1^2 = \frac{\sigma^2 - f^2}{c_1^2}, \quad k_2^2 = \frac{\sigma^2 - f^2}{c_2^2}.$$

The above sets of *Poincaré* modes satisfy the linearized momentum equations in the respective regions ($x > 0$ and $x < 0$).

Thus by introducing these *Poincaré* modes into the corresponding momentum equations we obtain the following set of equations:

$$h_1k_1^2(\frac{g}{c_1}) = fs_nD_n - i\sigma l_nC_n, \qquad h_2k_2^2(\frac{g}{c_2}) = -ft_nN_n - i\sigma l_nM_n,$$

$$0 = fs_nC_n + i\sigma l_nD_n, \qquad 0 = -ft_nM_n + i\sigma l_nN_n,$$

$$h_1k_1^2(\frac{g}{c_1})A_n = fl_nD_n - i\sigma s_nC_n, \qquad h_2k_2^2(\frac{g}{c_2})H_n = fl_nN_n + i\sigma t_nM_n,$$

$$h_1k_1^2(\frac{g}{c_1})B_n = -fl_nC_n - i\sigma s_nD_n, \qquad h_2k_2^2(\frac{g}{c_2})L_n = -fl_nM_n + i\sigma t_nN_n.$$

From these there follows

$$C_n = \frac{i\sigma l_nc_1}{\triangle_1}, \qquad D_n = \frac{-fs_nc_1}{\triangle_1}, \qquad M_n = \frac{i\sigma l_nc_2}{\triangle_2}, \qquad N_n = \frac{-ft_nc_2}{\triangle_2},$$

$$A_n = \frac{s_nl_nc_1^2}{\triangle_1}, \qquad B_n = \frac{-i\sigma f}{\triangle_1}, \qquad H_n = \frac{t_nl_nc_2^2}{\triangle_2}, \qquad L_n = \frac{-i\sigma f}{\triangle_2}. \tag{7.4}$$

where

$$\triangle_1 = \sigma^2 + s_n^2c_1^2 = f^2 + l_n^2c_1^2 \qquad \text{and} \qquad \triangle_2 = \sigma^2 + t_n^2c_2^2 = f^2 + l_n^2c_2^2 .$$

7.1.1 Boundary conditions at the step:

At the step it will be necessary to match flows on either side. The shallow water problem for a step was treated originally by Lamb (1932§176). He applied continuity of total mass flow perpendicular to the step. Also he invokes a second condition, the continuity of the sea surface elevation at the position $x = 0$ of the discontinuity in the depth.

These boundary conditions are therefore $x = 0$.

(i) The continuity of mass flux across the boundary:

$$h_1(\frac{g}{c_1})Re^{-\frac{f}{c_1}y} - h_1(\frac{g}{c_1})e^{\frac{f}{c_1}(y-b)} + h_2(\frac{g}{c_2})Te^{\frac{f}{c_2}(y-b)} + h_1(\frac{g}{c_1})\sum_{1}^{\infty}\gamma_n[A_n\cos(l_ny) + B_n\sin(l_ny)]$$

$$-h_2(\frac{g}{c_2})\sum_{1}^{\infty}\delta_n[H_n\cos(l_ny) + L_n\sin(l_ny)] = 0 \quad \forall\, y\,\epsilon\,[0,b], \qquad (7.5)$$

(ii) The continuity of surface elevation at the boundary:

$$Re^{-(\frac{f}{c_1})y} + e^{(\frac{f}{c_1})(y-b)} - Te^{(\frac{f}{c_2})(y-b)} + \sum_{1}^{\infty}\gamma_n\{C_n\cos(l_ny) + D_n\sin(l_ny)\}$$

$$-\sum_{1}^{\infty}\delta_n\{M_n\cos(l_ny) + N_n\sin(l_ny)\} = 0,$$

$$\forall\, y\,\epsilon\,[0,b]. \qquad (7.6)$$

7.2 Methods of Solution:

Two essentially different methods of solution are investigated.

7.2.1 Collocation Method:

On rewriting the system (7.5) in a suitable form, we obtain

$$Re^{-(\frac{f}{c_1})y} - e^{(\frac{f}{c_1})(y-b)} + \beta Te^{(\frac{f}{c_2})(y-b)} + \sum_{1}^{\infty}\gamma_n\left[A_n\cos(l_ny) + B_n\sin(l_ny)\right]$$

$$-\beta\sum_{1}^{\infty}\delta_n\left[H_n\cos(l_ny) + L_n\sin(l_ny)\right] = 0. \qquad (7.7)$$

where $\beta^2 = (\frac{h_2}{h_1})$.

The equations (7.7) and (7.6) imply a requirement to invert an infinite matrix.

We take that (7.7) and the equation (7.6) hold at finite sets of points on $[0, b]$ with the series' truncated to an appropriate finite number of terms.

We set up a matrix $M\mathbf{x}=\mathbf{b}$ associated with the vector,

$\mathbf{x}$= $(\gamma_1, \gamma_2, \gamma_3, ..., \gamma_N, \delta_1, \delta_2, \delta_3, ..., \delta_N, R, T)$. This means we form one equation from each of the $N+1$ collocation points.

$$y_k = \frac{(k-1)b}{N}, \quad k = 1, 2, 3, ...N+1,$$

yielding $2N+1$ equations from the two systems of equations.

7.2.2 Numerical Evaluation of Solution:

In solving the above system we obtain the reflection coefficient, R and the transmitted coefficient, T.

In fig (7.2) is given the variation of the reflected coefficient with respect to the depth ratio $\frac{h_2}{h_1}$. As the depth ratio increases the $|R|$ decreases allowing more incident energy to be transmitted through the system to the other side.

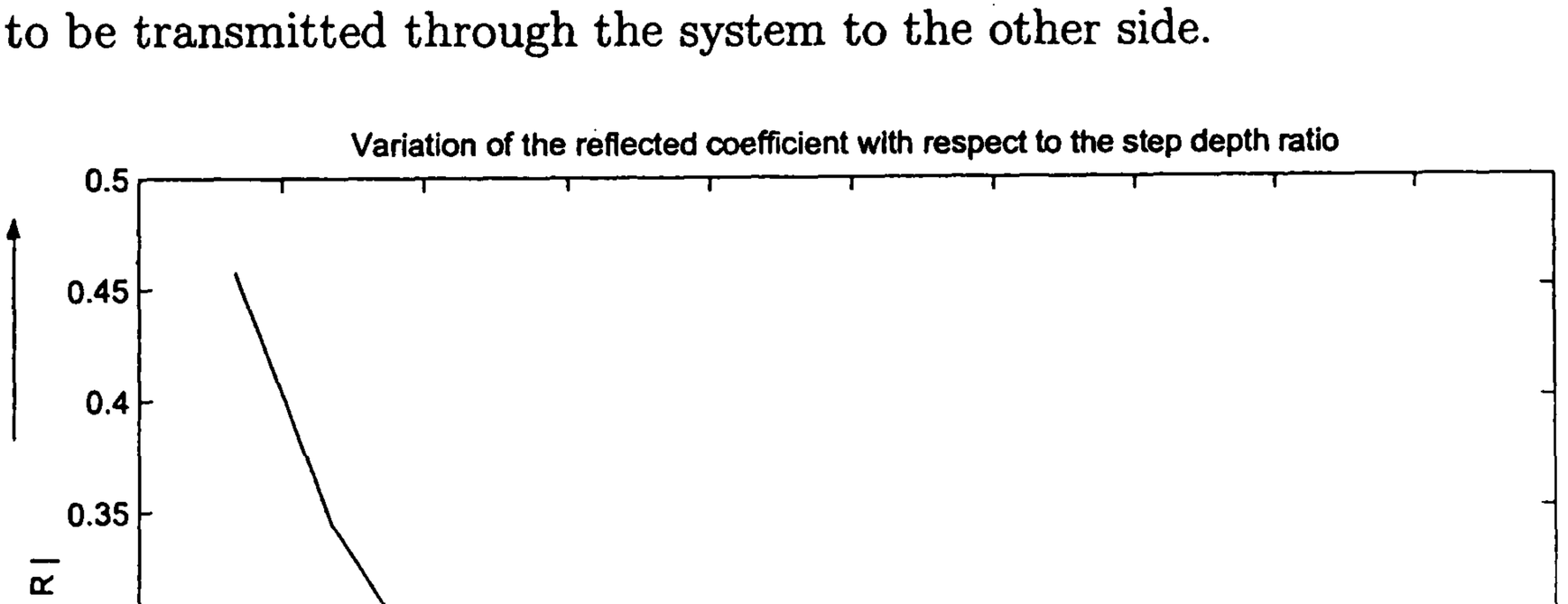

Figure 7.2:

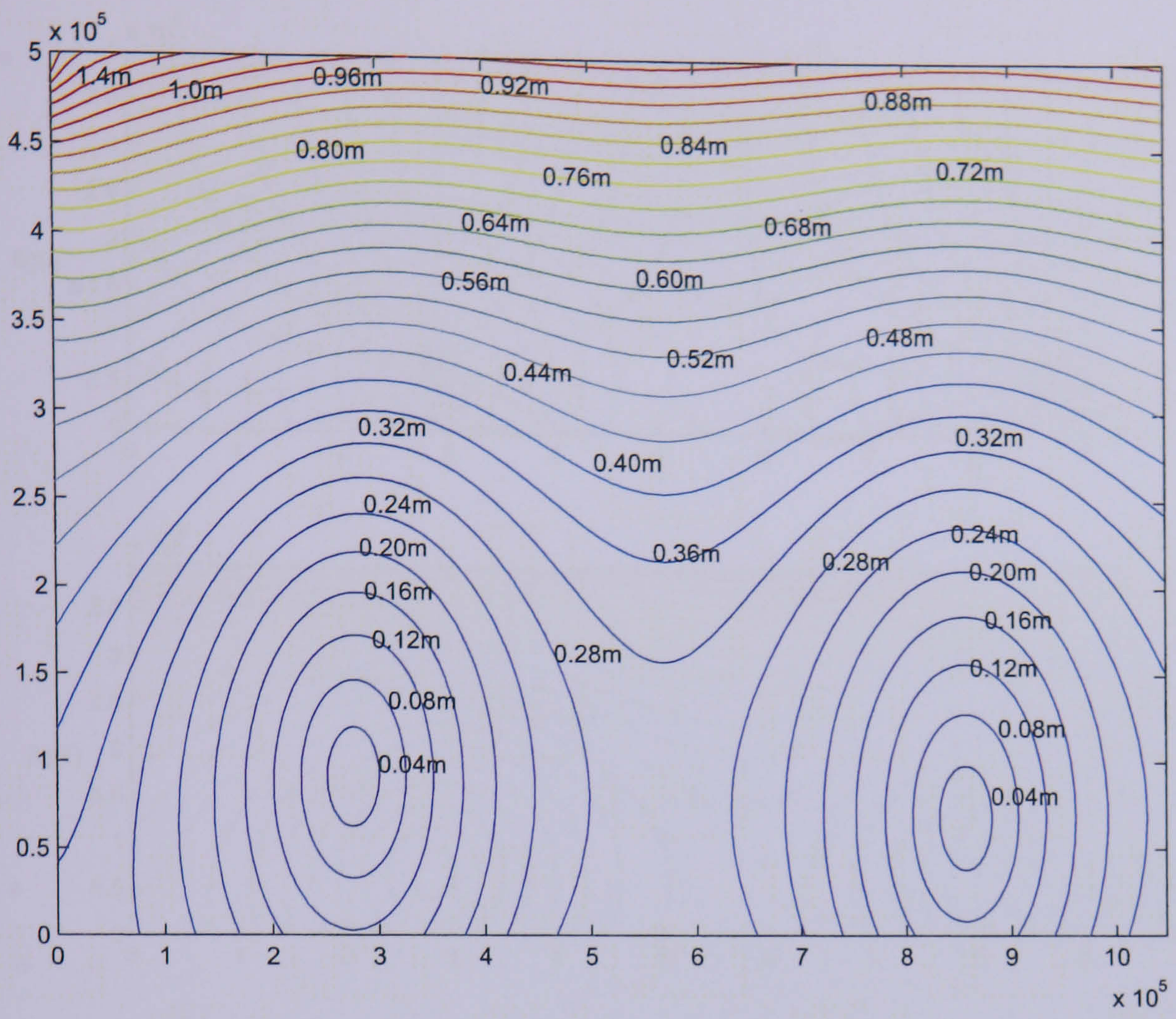

Figure 7.3: Tidal range for the case $h_1 = 74\ m$, latitude=$54.46^{\underline{0}}$ and $\beta^2 = 0.1351$

The surface-elevation contours and phase lines contours, drawn for the case where $h = 74\ m$, $lat = 54.46^{\underline{o}}$ and $\beta^2 = 0.1351$, are shown in fig (7.3) and fig (7.4). These are shown for the region $x > 0$ only.

A maximum value of amplitude of about $1.46\ m$ high (see fig (7.3)) can be seen in the co-ordinate point near the right hand corner of the basin.

Fig (7.4) shows

(i) Co-tidal lines which are drawn through the points where it is high water at any specified time and represents the height of the tidal wave.

(ii) the lines of equal tidal range to show the amount of rise and fall of tide in different parts of the basin.

The co-tidal lines are drawn for every 30 min (or rather for every $\frac{1}{24}$ part of a period).

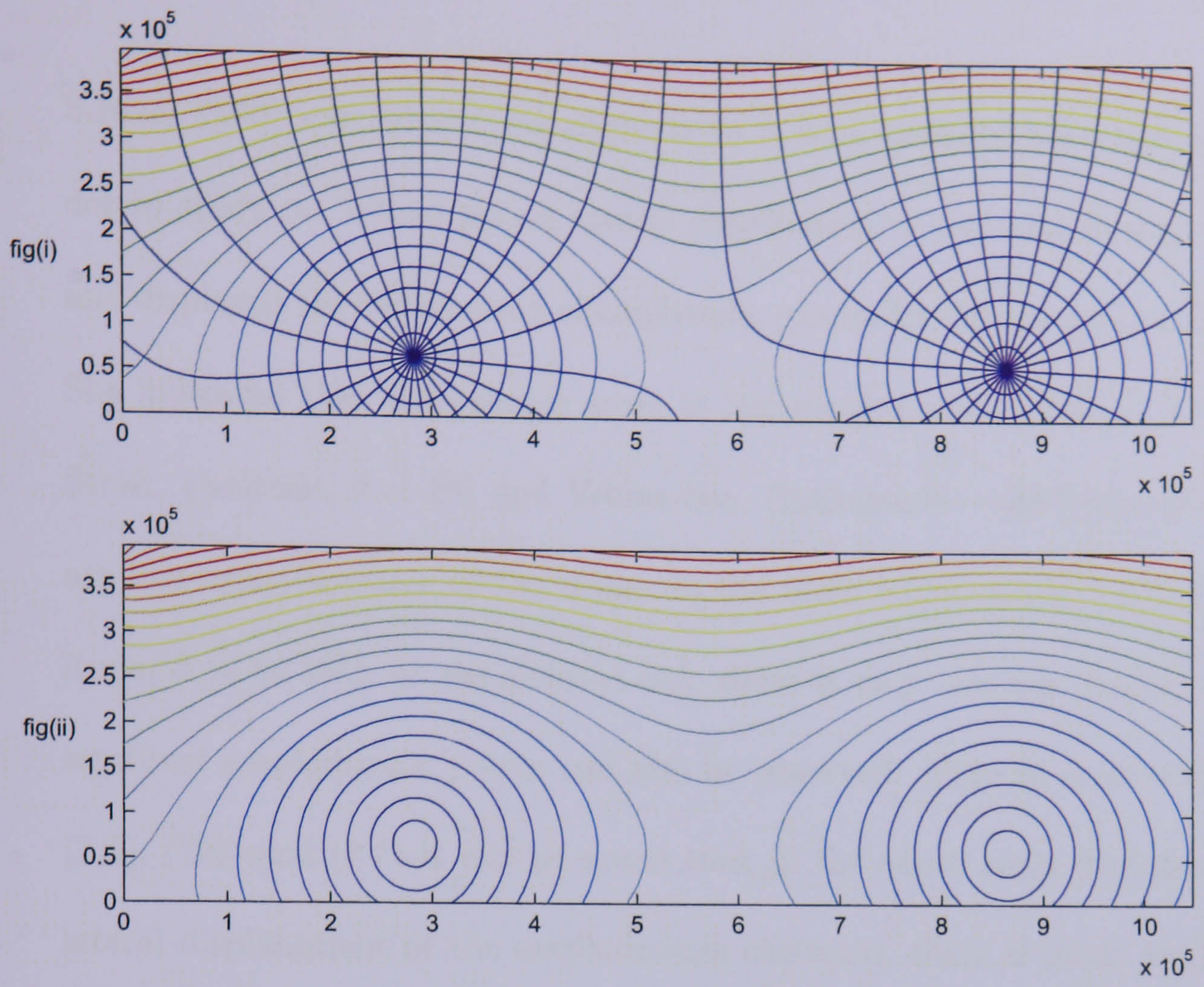

Figure 7.4: In fig (i) is given tidal range and co-tidal lines and in fig (ii) is given tidal range for the case $h_1 = 74\ m$, lat= $54.46^{\underline{0}}$ and f=0.0001188 sec^{-1}

In this figure we are able to identify the amphidromic displacement which is toward the side of the reflected Kelvin wave. This displacement is caused by the topographical change. The figure shows also that the first amphidromic point is closer to the reflector (step in the channel) in x-direction whilst the second amphidromic point lies further from this region of the channel.

As T.Brown [4] put it in his thesis; an important feature of the North sea tide which Taylor fails to explain is the easterly displacement of the Northern amphidromic point. It can be further seen in chapter 2 of this thesis that a lateral displacement of an amphidromic point is associated with an imbalance of the amplitudes of component Kelvin waves. Thus in this case the easterly displaced amphidromic points indicate that the reflected Kelvin wave is of reduced amplitude. This also can be noted in fig(7.3) and fig(7.4).

S.Rizal ([32]) carried out experiments in a semi-enclosed rectangular basin in order to study on 'influences on spatial distribution of real and virtual amphidromes' and displayed the distribution of amplitude, phases for various geographical latitudes. She indicated that the oceanic areas in low geographical latitudes such as Malacca Strait, (latitude, $\theta \sim 3^{o}$) and Yellow Sea, (latitude, $\theta \sim 30^{o}$) virtual amphidromes are important features of the tides. In the main basin of the North Sea also, (latitude, $\theta \sim 54.46^{o}$), as she pointed out, there is only one real amphidrome but one semi-real amphidromic points can also be observed. Thus in examining the figures, (7.5), (7.6) and (7.7) it can be noted that as the depth ratio increases, besides the lateral displacement of the amphidromes eastward, there is great tendency to have virtual amphidromes and this is well away from the central axis. This means that the topography of the basin plays an important role in wave dynamics. In other words, the topographical effect can have significant effects on tides in the North sea.

In the work of Hendershott and Speranza ([34]) they described the displacement of amphidromic points from the central axis of semi-enclosed basin as a measure of tidal dissipation. Further they state that this dissipation is strongly localized at the head of channel. So, in examining the distribution of co-amplitude and co-phase lines, in figures, (7.5), (7.6) and (7.7) particularly in the nearshore there is a reduction in tidal amplitude due to the sudden discontinuity in depth distribution.

In fig (7.8) are illustrated trapped *Poincaré* modes. In the first figure the outgoing *Poincaré* wave is on the reflected wave side whereas in second figure it is on the transmitted wave side. Further in the first figure it is noted that the *Poincaré* modes

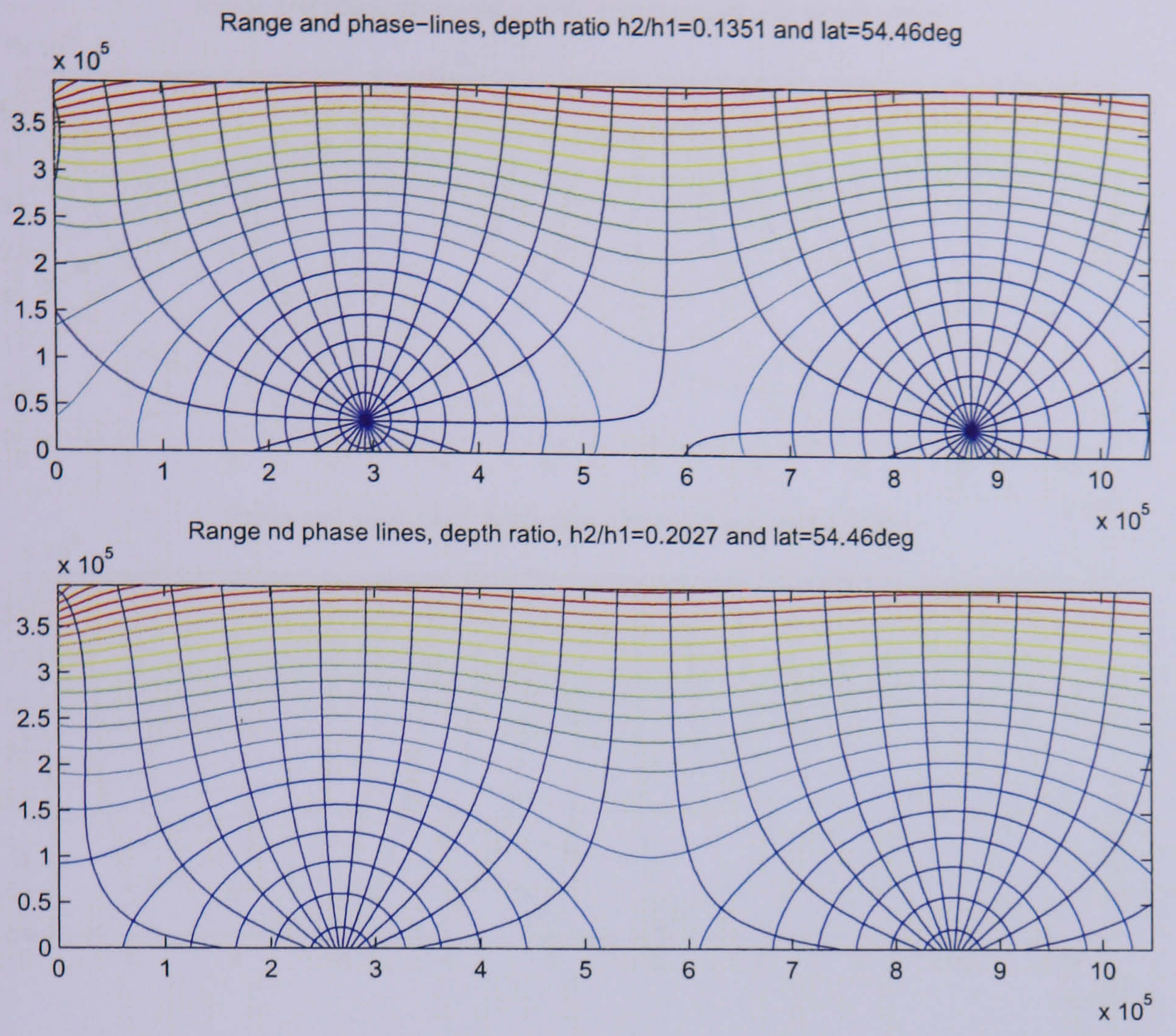

Figure 7.5:

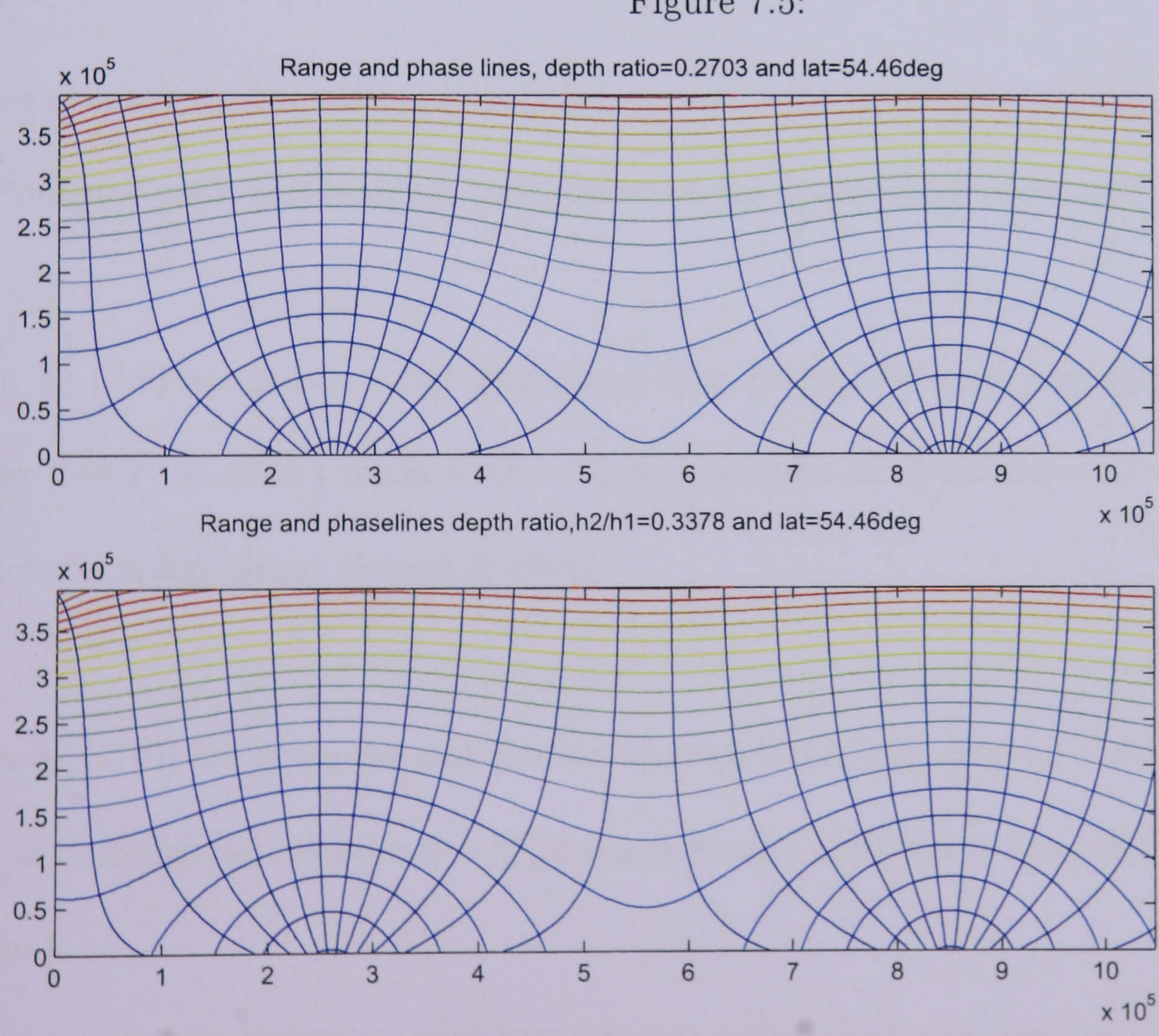

Figure 7.6:

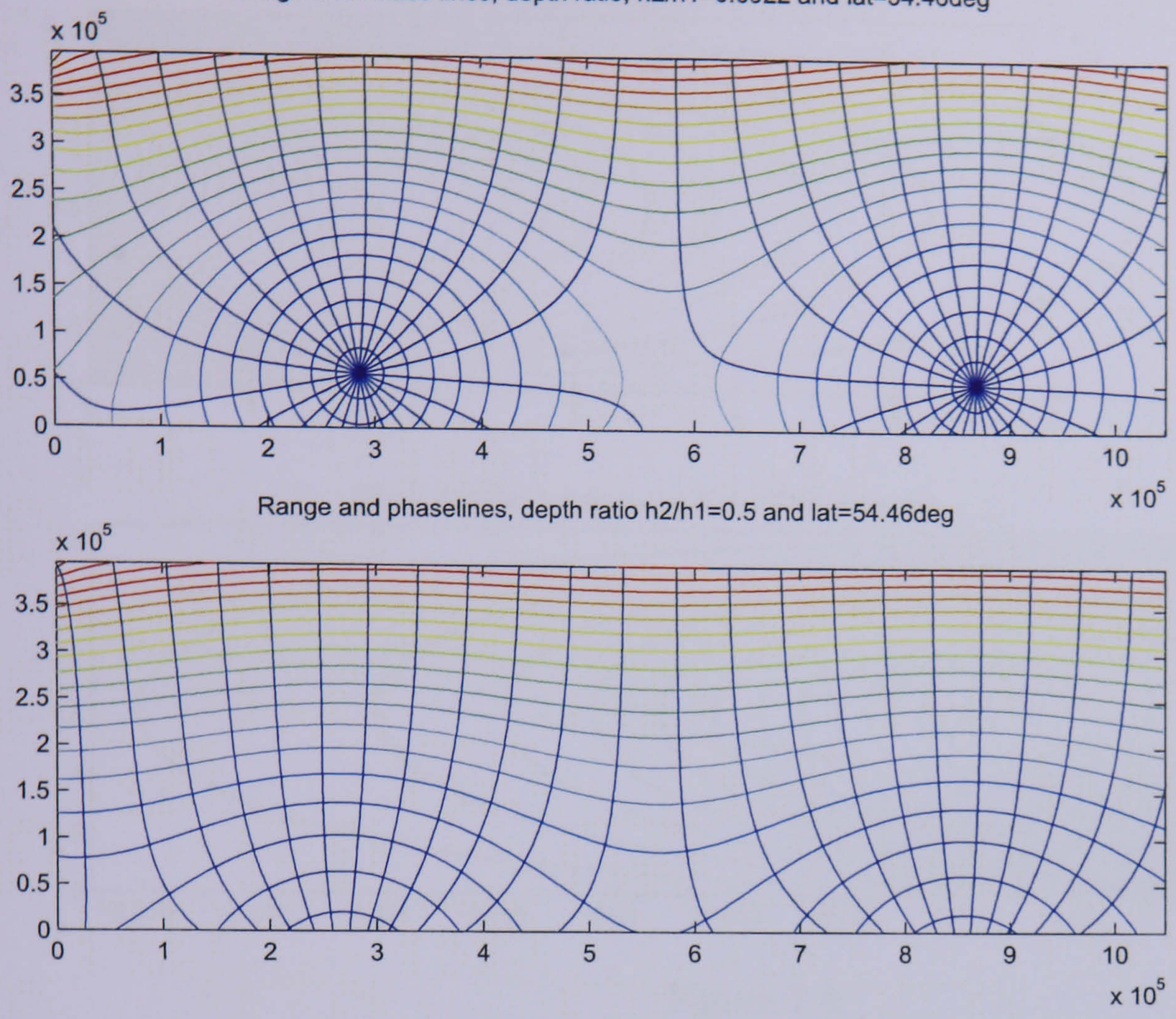

Figure 7.7:

are concentrated toward the same side as the incoming Kelvin wave and the effective *Poincaré* wave movement is centralized on the transmitted wave side.

In fig (7.9) are shown range and phase lines at two different geographical locations (ie. $50^{o}N$, $54.46^{o}N$) respectively. On examination of these contours we see there is not much significant change in effect.

In fig (7.10) are given the distribution of amplitudes and phases for various geographical latitudes (ie latitudes,$\theta = 3^{o}$(Malacca Strait), 30^{o}(Yellow Sea) and 54.46^{o} (North Sea).

Here it is interesting to note how models with associated bottom topography can predict tidal behavior in different geographical locations. On comparisons, one can

Fig−i: Poincare waves on the Reflected wave side

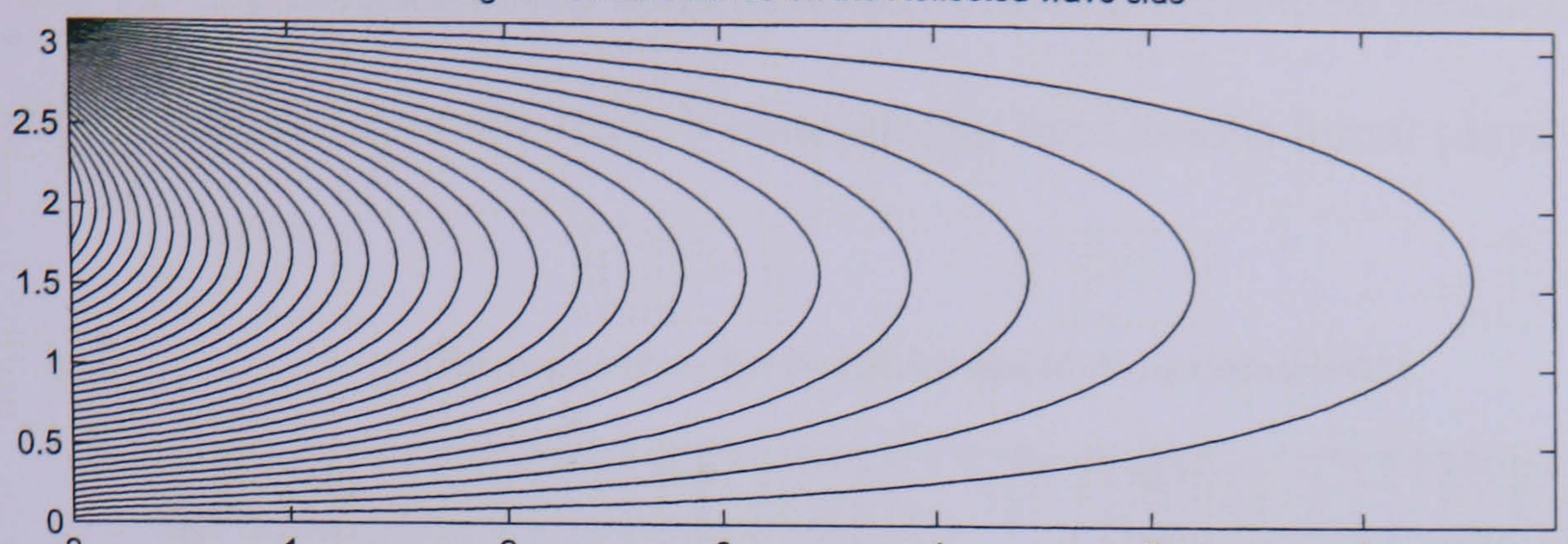

Fig−ii: Poincare waves on the Transmitted wave side

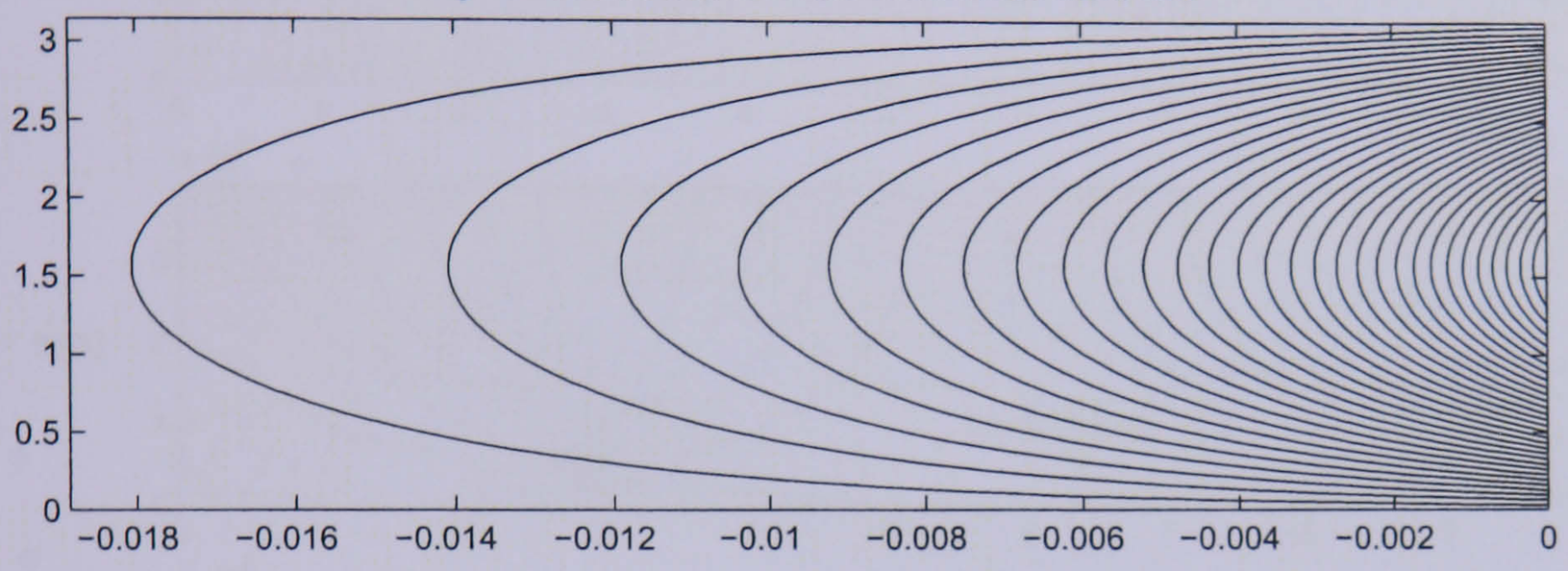

Figure 7.8:

Tidal range and co−tidal lines for the case of h1=74m, lat=50deg, h2/h1=0.1351

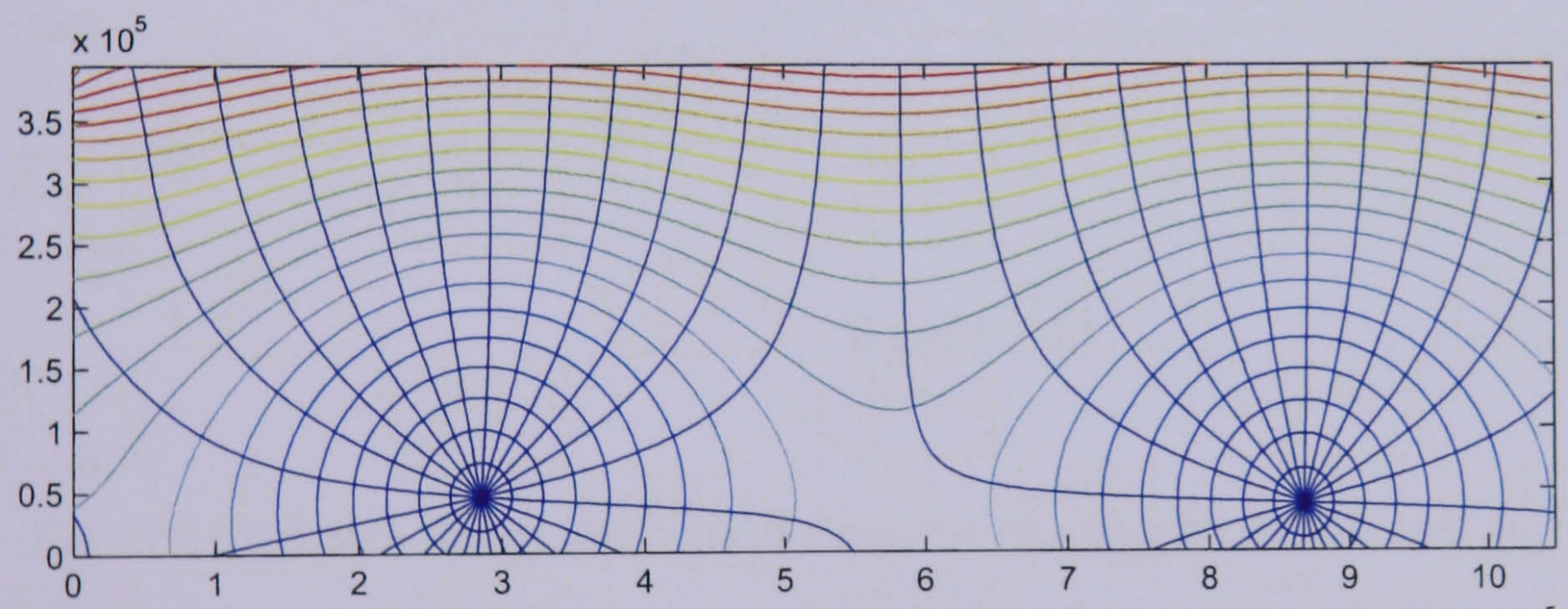

Tidal range and co−tidal lines for the case of h1=74m, lat54.46deg, h2/h1=0.1351 x 10^5

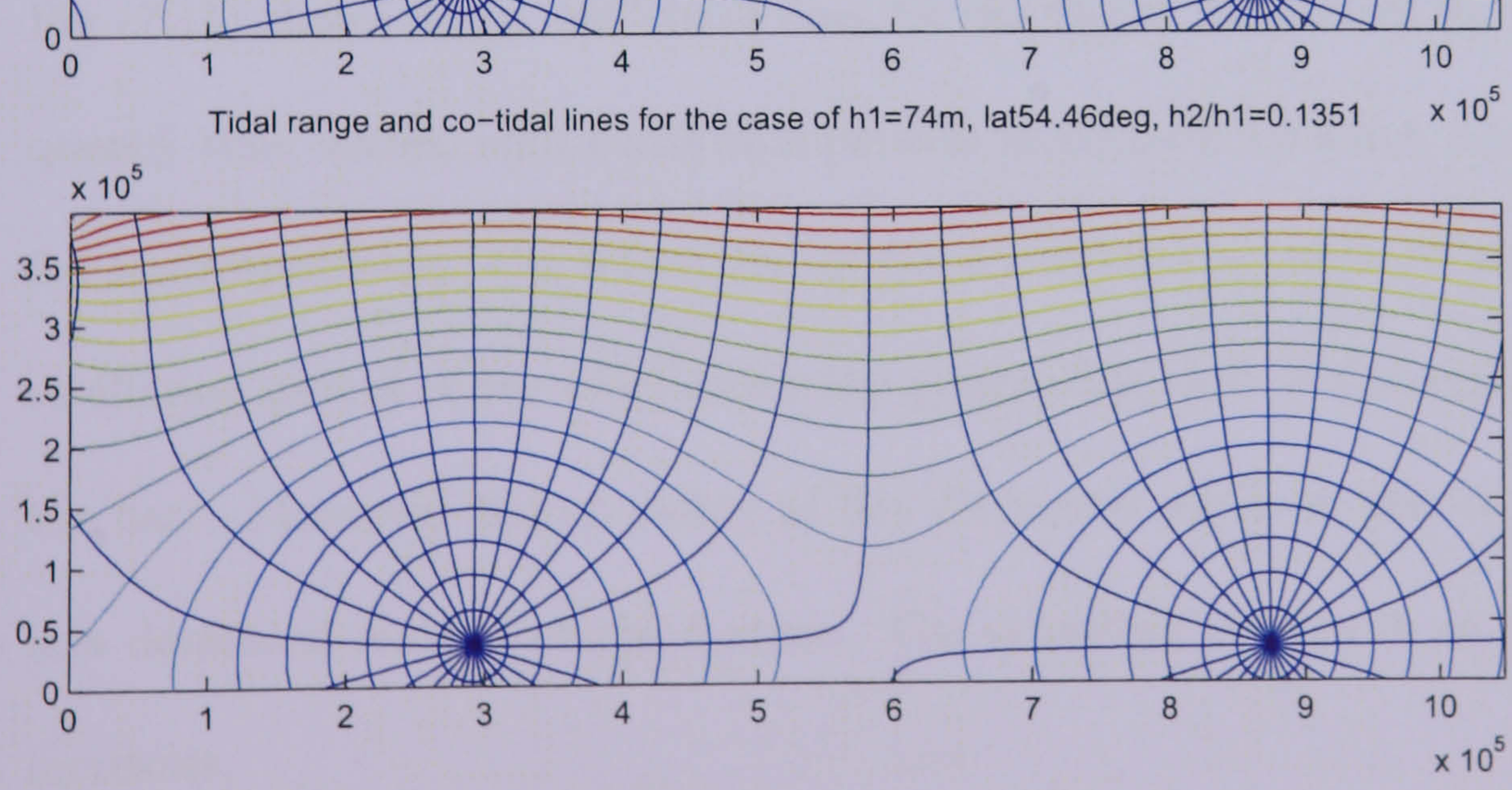

Figure 7.9:

see the dependence of the tidal phenomenon on geographical locations. This confirms the significant role the earth's rotation (i.e the Coriolis force) plays on tidal waves.

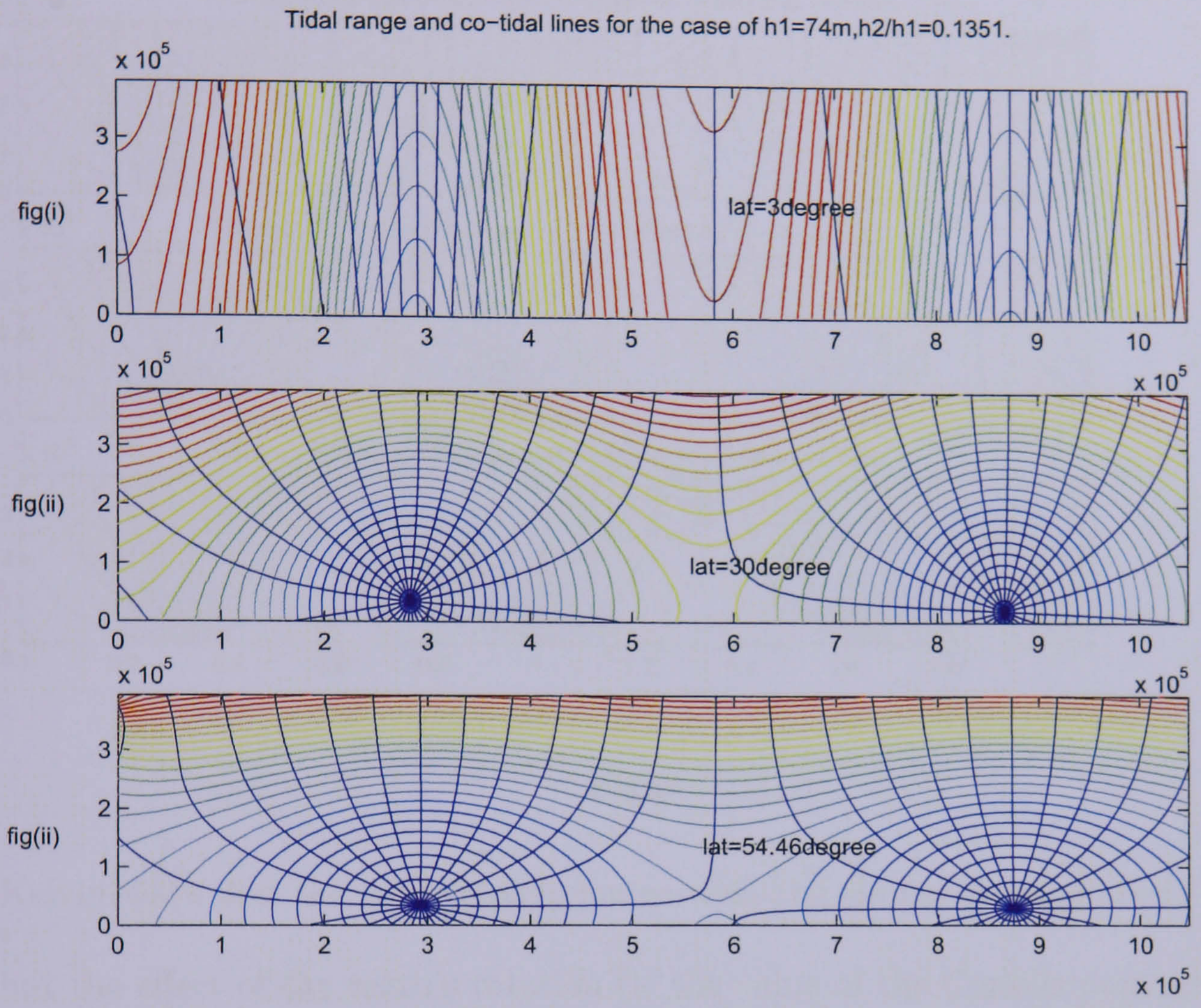

Figure 7.10:

Fig (7.11) shows range and phase lines for the North Sea drawn for varying high frequency tidal waves, with oscillation periods as follows; T=6 hrs, 6.2 hrs, 6.4 hrs and 6.6 hrs respectively. On inspection of these contours we notice that the greater the oscillation period of the tidal waves the greater the shift of the amphidrome towards the east. Moreover the crowding of the *Poincaré* mode on the incoming wave side is a dominant feature of the system. The crowding intensifies as the wave periods increases.

In fig (7.12) we contour range and phase lines for the interaction of the incoming

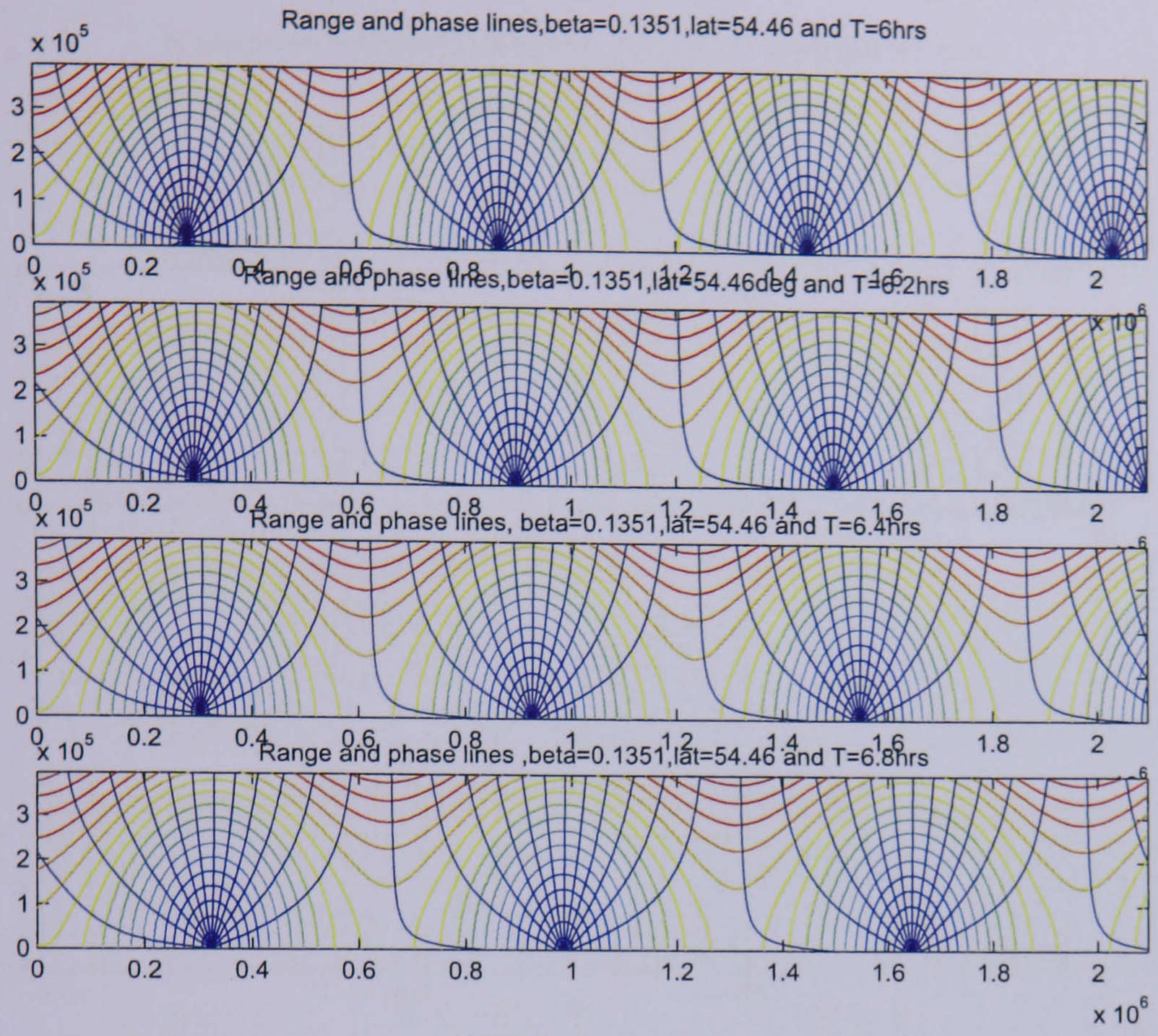

Figure 7.11:

Kelvin wave and the topography change with the similar parameters of the system but the effect of the earth's rotation (ie the value of the Coriolis parameter) is doubled this time. Here again the system of amphidromic points moves eastward as the ratio of depths ($\beta = \sqrt{h_2/h_1}$) increases. The effect of the topography change is very remarkable in this case.

The fig (7.13) displays the distribution of tidal range in a basin of length about 1048 km and width about 395 km incorporated with a step bottom of length about 524 km and height 15 m situated in a locality where the latitude is $54.75^{\underline{0}}$. The constant depth of the channel is 74 m. It can be seen in the figure that on the west coast of the shallow water region experiences high tides and the *Poincaré* mode manifest predominantly. We observe two amphidromic points, one occurs in the shallow water

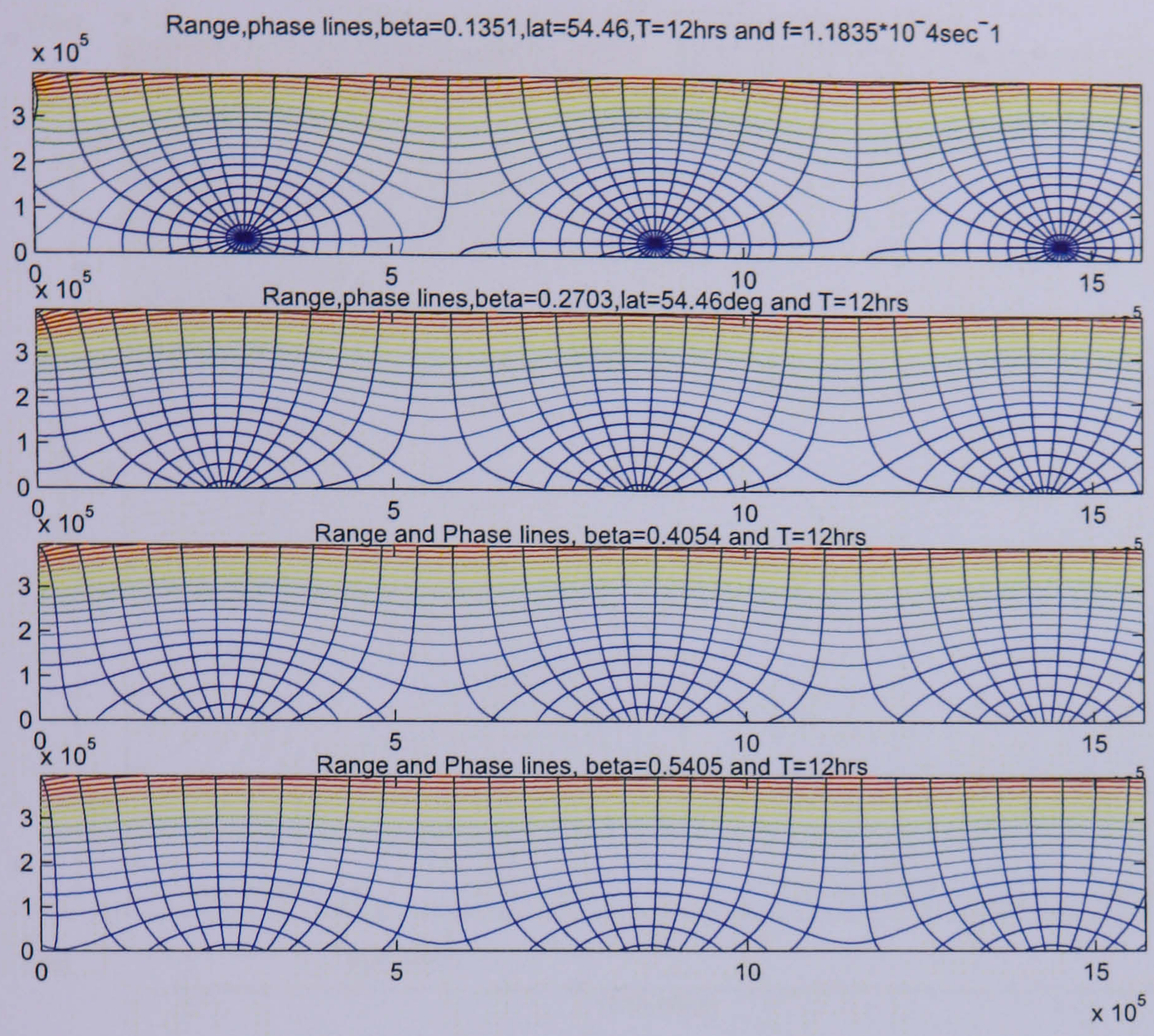

Figure 7.12:

region and other one occurs in the region where the depth of the channel is 74 m. These two amphidromic points are found on the eastern side of the region.

7.2.3 Fourier Series treatment of the step problem:

The second method of solution examined uses a Fourier Series treatment across the channel.

We refer to the equations for the incident, reflected and transmitted waves respectively from the section-1 of this chapter.

In the region $x > 0$ we take the same ansatz as in the chapter-4 for the Poincaré waves.

We also refer to the consistency requirements arising from the momentum equations for the u, v Poincaré contributions from chapter-4.

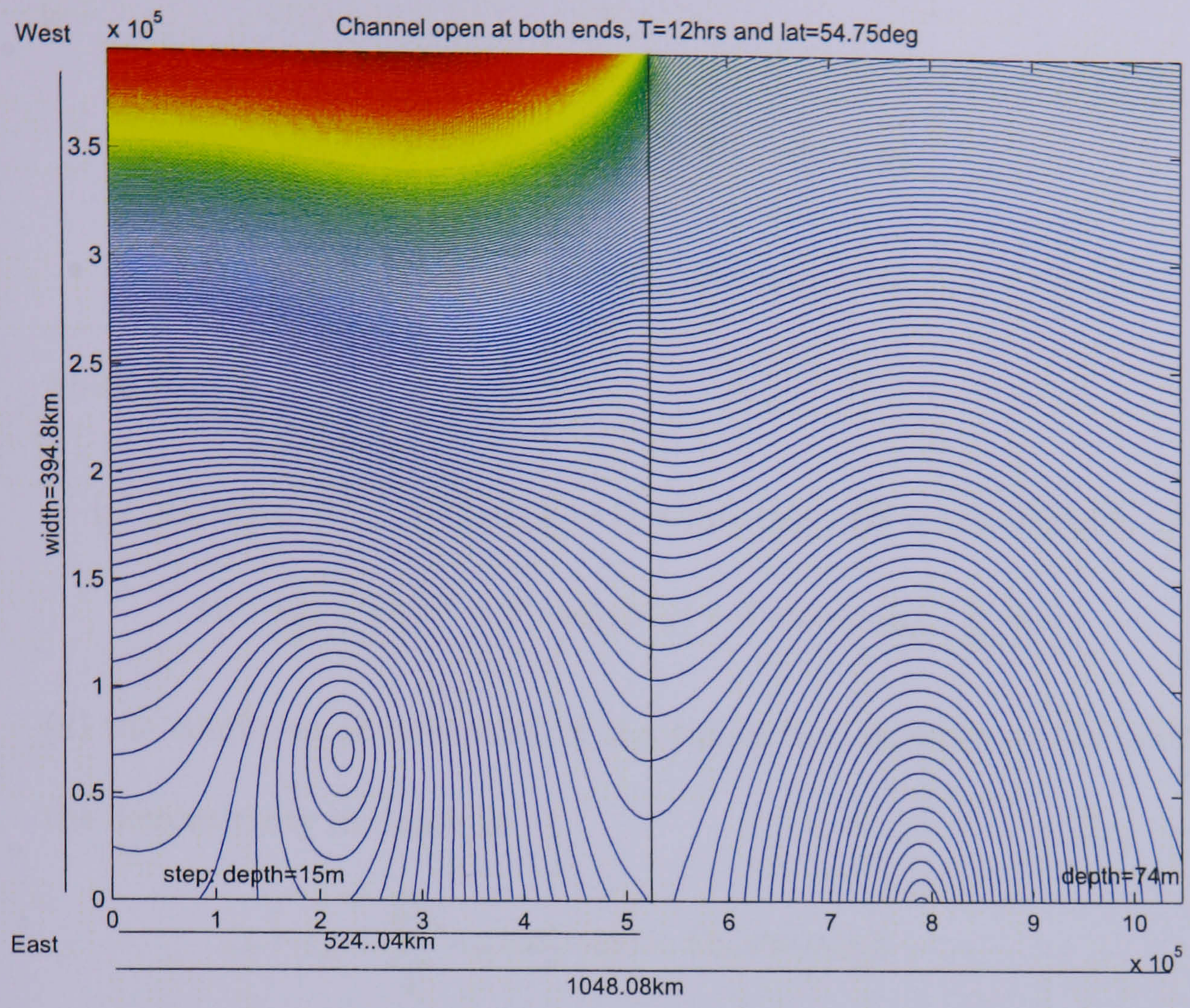

Figure 7.13: Distribution of tidal range in a basin of length 1048 km and width about 395 km incorporated with a step bottom of length 524 km and situated in a locality where the latitude is $54.75^{\underline{0}}$. The constant depth of the channel is 74 m.

In the region when $x < 0$ the Poincaré waves can similarly be written as

$$v_p^{(2)} = \sum_{m=1}^{\infty} D_m^{'} \sin(\nu_m y) e^{t_m x + i\sigma t},$$

$$u_p^{(2)} = \sum_{m=1}^{\infty} (A_m^{'} \cos \nu_m y + i B_m^{'} \sin \nu_m y) e^{t_m x + i\sigma t}. \tag{7.8}$$

Where now we have $t_m^2 = \nu_m^2 - k_2^2$ and $k_2^2\, c_2^2 = \sigma^2 - f^2$.

Now for the case $x < 0$, we have the consistency requirements for the $u^{'}$, $v^{'}$ Poincaré contribution as

$$\nu_m A_m^{'} - t_m D_m^{'} = \frac{f}{\sigma} t_m B_m^{'},$$

$$\nu_m B_m^{'} + \frac{f}{\sigma} \nu_m D_m^{'} = \frac{f}{\sigma} t_m A_m^{'}.$$

We wish to place the step at $x = 0$. Then

(1) the condition of continuity of total mass flow perpendicular to the step at $x = 0$

is

$$u_k + \beta u_k^{'} + \sum_{1}^{\infty}[A_m \cos(\nu_m y) + iB_m \sin(\nu_m y)]$$

$$-\beta \sum_{1}^{\infty}[A_m^{'} \cos(\nu_m y) + iB_m^{'} \sin(\nu_m y)] = 0. \qquad \forall y \, \epsilon [0, \pi]. \tag{7.9}$$

where

$$(i)\ \ u_k = Re^{-\frac{f}{c_1}y} - e^{\frac{f}{c_1}y} = (R-1)\cosh(\alpha_1 y) - (R+1)\sinh(\alpha_1 y), \quad \frac{f}{c_1} = \alpha_1.$$

$$(ii)\ \ u_k^{'} = Te^{\frac{f}{c_2}y} = T\cosh(\alpha_2 y) + T\sinh(\alpha_2 y), \quad \frac{f}{c_2} = \alpha_2.$$

(2) the condition of continuity of the sea surface elevation at the position $x = 0$ of the discontinuity in depth is

$$\zeta_k - \zeta_k^{'} + \sum_{1}^{\infty}[a_m \cos(\nu_m y) + ib_m \sin(\nu_m y)]$$

$$-\sum_{1}^{\infty}[a_m^{'} \cos(\nu_m y) + ib_m^{'} \sin(\nu_m y)] = 0. \qquad \forall y \epsilon [0, \pi]. \tag{7.10}$$

where

$$(i)\ \ \zeta_k = Re^{-\frac{f}{c_1}y} + e^{\frac{f}{c_1}y} = (1+R)\cosh(\alpha_1 y) + (1-R)\sinh(\alpha_1 y), \quad \frac{f}{c_1} = \alpha_1$$

$$(ii)\ \ \zeta_k^{'} = Te^{\frac{f}{c_2}y} = T\cosh(\alpha_2 y) + T\sinh(\alpha_2 y), \quad \frac{f}{c_2} = \alpha_2$$

where $\beta^2 = (\frac{h_2}{h_1})$

and $\exists$ relationships between coefficients $(A_m, a_m), (B_m, b_m), (A_m^{'}, a_m^{'}), (B_m^{'}, b_m^{'})$.

To find relationships between (a_m, A_m),(b_m, B_m),$(a_m^{'}, A_m^{'})$,$(b_m^{'}, B_m^{'})$

We invoke the velocity field and the consistency requirements for the Poincaré modes on the reflected wave side as given in (7.4) in section-2 of this chapter. The surface elevation of the Poincaré modes as considered above is

$$\zeta_E = \sum_{1}^{\infty} \{a_m \cos(\nu_m y) + ib_m \sin(\nu_m y)\} e^{-s_m x + i\sigma t}.$$

We recall the continuity of mass equation,

$$h\left[\frac{\partial u}{\partial x}+\frac{\partial v}{\partial y}\right]=-\frac{\partial \zeta}{\partial t}.$$

By substitution into this equation we obtain

$$(\frac{gh_1}{c_1})\sum_{1}^{\infty}\left[(\nu_m D_m - s_m A_m)\cos(\nu_m y)+i(-s_m B_m)\sin(\nu_m y)\right]e^{-s_m x+i\sigma t}=i\sigma\zeta.$$

Thus we obtain from these equations,

$$a_m=-\frac{igh_1}{\sigma c_1}\left[(\nu_m D_m - s_m A_m)\right],\qquad b_m=\frac{igh_1}{\sigma c_1}s_m B_m. \tag{7.11}$$

Similarly, we invoke the velocity field and consistency requirements for the Poincaré modes on the transmitted wave side as given in (7.4). The surface elevation of the Poincaré modes as considered above is

$$\zeta_E^{'}=\sum_{1}^{\infty}\left\{a_m^{'}\cos(\nu_m y)+ib_m^{'}\sin(\nu_m y)\right\}e^{t_m x-i\sigma t}.$$

As before, from the continuity equation we obtain

$$(\frac{gh_2}{c_2})\sum_{1}^{\infty}\left[(\nu_m D_m^{'}+t_m A_m^{'})\cos(\nu_m y)+i(t_m B_m^{'})\sin(\nu_m y)\right]e^{t_m x-i\sigma t}=i\sigma\zeta_E^{'}.$$

We obtain from these equations

$$a_m^{'}=-\frac{igh_2}{\sigma c_2}\left[(\nu_m D_m^{'}+t_m A_m^{'})\right],\qquad b_m^{'}=-\frac{igh_2}{\sigma c_2}t_m B_m^{'}. \tag{7.12}$$

Now, we express the Kelvin wave system in (7.9) in Fourier series. We formally write u_k and $u_k^{'}$as

$$\begin{aligned} u_k &= (R-1)\sum_{m=0}\lambda_m\cos(\nu_m y)-(R+1)\sum_{m=1}\mu_m\sin(\nu_m y).\\ u_k^{'} &= T\sum_{m=0}\lambda_m^{'}\cos(\nu_m y)+T\sum_{m=1}\mu_m^{'}\sin(\nu_m y) \end{aligned} \tag{7.13}$$

where

$$\lambda_m = (-1)^m \frac{2\alpha_1 \sinh(\alpha_1 b)}{(\nu_m^2 + \alpha_1^2)b}, \quad \mu_m = (-1)^{m+1} \frac{2\nu_m \sinh(\alpha_1 b)}{(\nu_m^2 + \alpha_1^2)b} = -\frac{\nu_m}{\alpha_1}\lambda_m \quad \text{and} \quad \alpha_1 = \frac{f}{c_1},$$

$$\lambda_m^{'} = (-1)^m \frac{2\alpha_2 \sinh(\alpha_2 b)}{(\nu_m^2 + \alpha_2^2)b}, \quad \mu_m^{'} = (-1)^{m+1} \frac{2\nu_m \sinh(\alpha_2 b)}{(\nu_m^2 + \alpha_2^2)b} = -\frac{\nu_m}{\alpha_2}\lambda_m^{'} \quad \text{and} \quad \alpha_2 = \frac{f}{c_2}.$$

Incorporating the above form for μ and $\mu^{'}$ the expressions (7.13) can be re-written as

$$u_k = (R-1)\sum_{m=0} \lambda_m \cos(\nu_m y) + (R+1)\sum_{m=1} \frac{\nu_m}{\alpha_1}\lambda_m \sin(\nu_m y).$$
$$u_k^{'} = T\sum_{m=0} \lambda_m^{'} \cos(\nu_m y) - T\sum_{m=1} \frac{\nu_m}{\alpha_2}\lambda_m^{'} \sin(\nu_m y) \tag{7.14}$$

Now, for convenience, we write

$$\alpha_m = A_m + (R-1)\lambda_m, \qquad \alpha_m^{'} = -A_m^{'} + T\lambda_m^{'} \quad \text{and}$$
$$\beta_m = iB_m - (1+R)\mu_m, \qquad \beta_m^{'} = -iB_m^{'} + T\mu_m^{'}). \tag{7.15}$$

By taking $A_0 = 0$ and $A_0^{'} = 0$ the boundary condition can then simply written as

$$\left[\alpha_0 + \sum_{m=1}^{\infty} (\alpha_m \cos \nu_m y + \beta_m \sin \nu_m y)\right] + \beta\left[\alpha_0^{'} + \sum_{m=1}^{\infty} \left(\alpha_m^{'} \cos \nu_m y + \beta_m^{'} \sin \nu_m y\right)\right] = 0. \tag{7.16}$$

but this is only a half-range series, we cannot equate terms to zero in the usual way.

Thus first, we simply integrate (7.16) from 0 to b. This gives

$$\left[\pi\alpha_0 + \sum_{m=1}^{\infty} \left(\frac{\beta_m}{m}(1-(-1)^m)\right)\right] + \beta\left[\pi\alpha_0^{'} + \sum_{m=1}^{\infty} \left(\frac{\beta_m^{'}}{m}(1-(-1)^m)\right)\right] = 0. \tag{7.17}$$

where

$$\alpha_0 = (R-1)\lambda_0/2, \qquad \alpha_0^{'} = T\lambda_0^{'}/2.$$

Now, we multiply the equation(7.16) by $\cos(\nu_m y)$ and then integrate from 0 to b gives

$$\alpha_n + \frac{2}{\pi}\sum_{m\neq n}^{\infty} \frac{m\beta_m}{m^2-n^2}(1-(-1)^{m+n}) + \beta\left[\alpha_n^{'} + \frac{2}{\pi}\sum_{m\neq n}^{\infty} \frac{m\beta_m^{'}}{m^2-n^2}(1-(-1)^{m+n})\right] = 0,$$
$$n = 1, 2, 3.....(7.18$$

In deciding how to deal with the system we remember that α_m and β_m; $\alpha_m^{'}$ and $\beta_m^{'}$ are related through the consistency relations

$$\alpha_m = \frac{\beta_m}{ir_m} + \frac{(ir_m - \frac{\nu_m}{\alpha_1})R\lambda_m}{ir_m} - \frac{(ir_m + \frac{\nu_m}{\alpha_1})\lambda_m}{ir_m}, \quad \alpha_m^{'} = \frac{\beta_m^{'}}{ir_m^{'}} + \frac{(ir_m^{'} + \frac{\nu_m}{\alpha_2})T\lambda_m^{'}}{ir_m^{'}}, \quad (7.19)$$

where $\frac{A_m}{B_m} = \frac{1}{r_m}$, $r_m = \frac{f\sigma}{\nu_m s_m c_1^2}$, $\frac{A_m^{'}}{B_m^{'}} = \frac{1}{r_m^{'}}$ and $r_m^{'} = \frac{f\sigma}{\nu_m t_m c_2^2}$.

Now, the system of equations (7.17) and (7.18) can be written as

$$\left[\pi(R-1)\lambda_0 + \sum_{m=1}^{\infty}\left(\frac{\beta_m}{m}(1-(-1)^m)\right)\right] + \beta\left[\pi T\lambda_0^{'} + \sum_{m=1}^{\infty}\left(\frac{\beta_m^{'}}{m}(1-(-1)^m)\right)\right] = 0.$$

$$\frac{\beta_n}{ir_n} + \frac{(ir_n - \frac{\nu_n}{\alpha_1})R\lambda_n}{ir_n} - \frac{(ir_n + \frac{\nu_n}{\alpha_1})\lambda_n}{ir_n} + \frac{2}{\pi}\sum_{m\neq n}^{N}\frac{m\beta_m}{m^2-n^2}(1-(-1)^{m+n}) + \beta\frac{\beta_n^{'}}{ir_n^{'}} +$$

$$\beta\frac{(ir_n^{'} + \frac{\nu_m}{\alpha_2})T\lambda_n^{'}}{ir_n^{'}} + \frac{2\beta}{\pi}\sum_{m\neq n}^{N}\frac{m\beta_m^{'}}{m^2-n^2}(1-(-1)^{m+n}) = 0, \quad n = 1,2,3..... \quad (7.20)$$

In a similar manner, we express the Kelvin wave system in (7.10) in Fourier series. We formally write ζ_k and $\zeta_k^{'}$ as

$$\zeta_k = (R+1)\sum_{m=0}\lambda_m\cos(\nu_m y) - (R-1)\sum_{m=1}\mu_m\sin(\nu_m y),$$
$$\zeta_k^{'} = T\sum_{m=0}\lambda_m^{'}\cos(\nu_m y) + T\sum_{m=1}\mu_m^{'}\sin(\nu_m y), \quad (7.21)$$

where (λ, μ) and $(\lambda_m^{'}, \mu_m^{'})$ have the usual meaning as defined in (7.13).

For convenience, we write

$$\gamma_m = a_m + (R+1)\lambda_m, \qquad \gamma_m^{'} = a_m^{'} + T\lambda_m^{'} \quad \text{and}$$
$$\delta_m = ib_m + (1-R)\mu_m, \qquad \delta_m^{'} = ib_m^{'} + T\mu_m^{'}. \quad (7.22)$$

By taking $a_0 = 0$ and $a_0^{'} = 0$ the boundary condition (7.10) can then simply written as

$$\left[\gamma_0 + \sum_{m=1}^{\infty}(\gamma_m\cos\nu_m y + \delta_m\sin\nu_m y)\right] - \left[\gamma_0^{'} + \sum_{m=1}^{\infty}\left(\gamma_m^{'}\cos\nu_m y + \delta_m^{'}\sin\nu_m y\right)\right] = 0. \quad (7.23)$$

We perform similar integrations as before.

We obtain the relationships between γ_m and δ_m; $\gamma_m^{'}$ and $\delta_m^{'}$ using consistency relations

$$\gamma_m = \frac{\delta_m}{iR_m} + \frac{(iR_m - \frac{\nu_m}{\alpha_1})R\lambda_m}{iR_m} + \frac{(iR_m + \frac{\nu_m}{\alpha_1})\lambda_m}{iR_m}, \quad \gamma_m^{'} = \frac{\delta_m^{'}}{iR_m^{'}} + \frac{(iR_m^{'} + \frac{\nu_m}{\alpha_2})T\lambda_m^{'}}{iR_m^{'}}, \tag{7.24}$$

where $\frac{a_m}{b_m} = \frac{1}{R_m}$, $\frac{1}{R_m} = -\frac{1}{r_m}\left[\frac{\nu_m^2 - s_m^2}{s_m^2}\right] + \frac{\nu_m f}{s_m \sigma}$, $\frac{a_m^{'}}{b_m^{'}} = \frac{1}{R_m^{'}}$ and $\frac{1}{R_m^{'}} = \frac{2}{r_m^{'}} - \frac{\nu_m \sigma}{t_m f}$.

Now the system of equations to be solved can be written as

$$\frac{\beta_n}{ir_n} + \frac{(ir_n - \frac{\nu_n}{\alpha_1})R\lambda_n}{ir_n} - \frac{(ir_n + \frac{\nu_n}{\alpha_1})\lambda_n}{ir_n} + \frac{2}{\pi}\sum_{m\neq n}^{N}\frac{m\beta_m}{m^2 - n^2}(1 - (-1)^{m+n}) + \beta\frac{\beta_n^{'}}{ir_n^{'}} +$$

$$\beta\frac{(ir_n^{'} + \frac{\nu_n}{\alpha_2})T\lambda_n^{'}}{ir_n^{'}} + \frac{2\beta}{\pi}\sum_{m\neq n}^{N}\frac{m\beta_m^{'}}{m^2 - n^2}(1 - (-1)^{m+n}) = 0, \quad n = 1, 2, 3.....$$

$$\frac{\delta_n}{iR_n} + \frac{(iR_n - \frac{\nu_n}{\alpha_1})R\lambda_n}{iR_n} + \frac{(iR_n + \frac{\nu_n}{\alpha_1})\lambda_n}{iR_n} + \frac{2}{\pi}\sum_{m\neq n}^{N}\frac{m\delta_m}{m^2 - n^2}(1 - (-1)^{m+n}) - \frac{\delta_n^{'}}{iR_n^{'}} -$$

$$\frac{(iR_n^{'} + \frac{\nu_n}{\alpha_2})T\lambda_n^{'}}{iR_n^{'}} - \frac{2}{\pi}\sum_{m\neq n}^{N}\frac{m\delta_m^{'}}{m^2 - n^2}(1 - (-1)^{m+n}) = 0, \quad n = 1, 2, 3..... \tag{7.25}$$

$$\left[\pi(R-1)\lambda_0 + \sum_{m=1}^{N}\left(\frac{\beta_m}{m}(1 - (-1)^m)\right)\right] + \beta\left[\pi T\lambda_0^{'} + \sum_{m=1}^{N}\left(\frac{\beta_m^{'}}{m}(1 - (-1)^m)\right)\right] = 0,$$

$$\left[\pi(R-1)\lambda_0 + \sum_{m=1}^{N}\left(\frac{\delta_m}{m}(1 - (-1)^m)\right)\right] - \left[\pi T\lambda_0^{'} + \sum_{m=1}^{N}\left(\frac{\delta_m^{'}}{m}(1 - (-1)^m)\right)\right] = 0. \tag{7.26}$$

7.2.4 Numerical Evaluation:

We consider the first N finite terms of the first series of (7.25) associated with vector $(\beta_1, \beta_2, \beta_3, ...\beta_N)$ and another N terms associated with the vector $(\beta_1^{'}, \beta_2^{'}, \beta_3^{'}, ...\beta_N^{'})$.

Similarly, N terms of the second series of (7.25) associated with vector $(\delta_1, \delta_2, \delta_3, ...\delta_N)$ and another N terms associated with the vector $(\delta_1^{'}, \delta_2^{'}, \delta_3^{'}, ...\delta_N^{'})$ are considered. Then we define a matrix system based on the unknown vector,

$(\beta_1, \beta_2, ..\beta_N, \beta_1^{'}, \beta_2^{'}, ...\beta_N^{'}, \delta_1, \delta_2, ..\delta_N, \delta_1^{'}, \delta_2^{'}, ...\delta_N^{'}, R, T)$,

there exists $4N + 2$ constants to be determined in (7.25). Thus we construct matrix system of matrices, A, $\mathbf{b}$ and $\mathbf{x}$ of orders, $((4N+2) \times (4N+2))$, $((4N+2) \times 1)$ and $((4N+2) \times 1)$ respectively by truncating each series in the system (7.25) to N terms. By solving the matrix system, $A\ \mathbf{x} = \mathbf{b}$, the reflected coefficient R and the transmitted coefficient T can be obtained.

The system is solved for the parameters' values $h_1 = 74m$, $lat = 54.46^{o}$ and $\beta = \sqrt{\frac{h_2}{h_1}} = 0.3076$ and plotted in fig (7.14) and fig (7.15).

7.2.5 Results and Discussion:

Having obtained the solution, the vector $(\beta_1, \beta_2, ...\beta_N, ...\beta_{N+1}^{'}, \beta_{N+2}^{'}, ...\beta_{2N}^{'})$ can be used to evaluate the coefficients B_m.

$$B_m = \frac{-i\sigma}{\sigma + i\beta c s_m}\left[\beta_m + (1+R)\mu_m\right], \quad A_m = \frac{B_m}{r_m}, \quad \text{and}$$

$$D_m = \frac{\nu_m A_m}{s_m} - \frac{f B_m}{\sigma} \tag{7.27}$$

Similarly, on the transmitted wave side we obtain

$$B_m^{'} = \frac{i\sigma}{\sigma\beta + ic^{'}t_m}\left[\beta_m^{'} - (1+\beta)T\mu_m^{'}\right], \quad A_m^{'} = \frac{B_m^{'}}{r_m^{'}}, \quad \text{and}$$

$$D_m^{'} = \frac{t_m A_m^{'}}{\nu_m} - \frac{\sigma B_m^{'}}{f} \tag{7.28}$$

We contour the tidal range ζ using the formula

$$\frac{\sigma\zeta}{h} = -i\left(\frac{\partial u}{\partial x} + \frac{\partial v}{\partial y}\right)$$

The contours are obtained in fig (7.16) and fig (7.17) for transverse velocity profile for *Poincaré* modes.

In fig (7.18) we see transverse velocity profiles for *Poincaré* modes both in reflected and transmitted wave sides.

Two sets of contours are given in fig (7.19) and fig (7.20). In both figures the cotidal lines at 30 mins intervals are plotted. In the second figure, the stronger influence of the earth's rotation is considered more than the first figure. By examining the figures (7.12), (7.19) and (7.20) one can observe a common physical phenomenon. The easterly displacement of the amphidromic points is striking evidence one can find from these figures. This displacement increases as the depth ratio, β increases.

Another important phenomenon demonstrated in these figures is the displacement of amphidromic points from the step in the south towards the north as β increases.

In fig (7.21)given the variation of amplitude of the reflected wave and transmitted wave for sequence of values of the ratio $\beta^2 = \frac{h_2}{h_1}$. The amplitude of reflected wave decreases and transmitted increases as the ratio (h_2/h_1) increases.

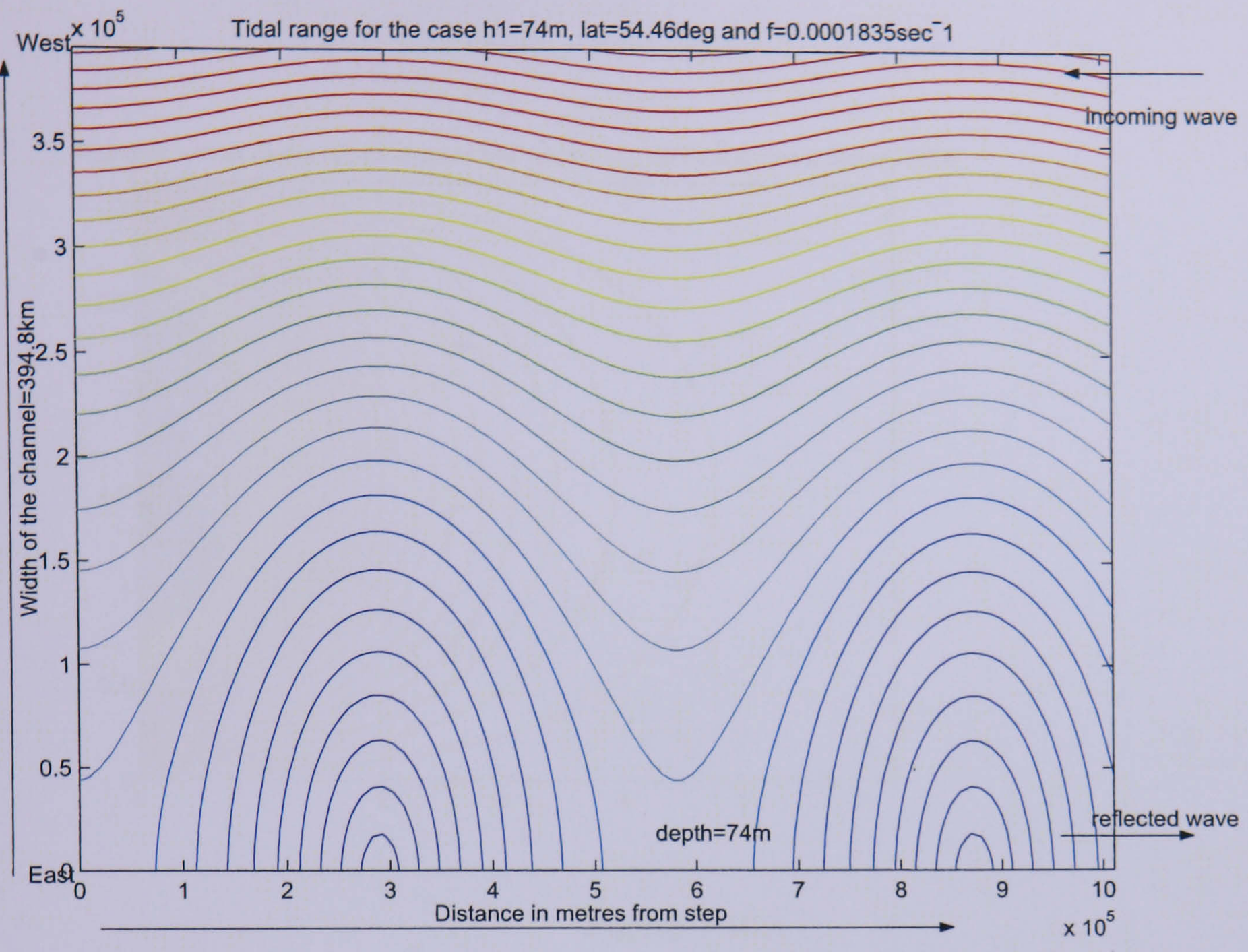

Figure 7.14:

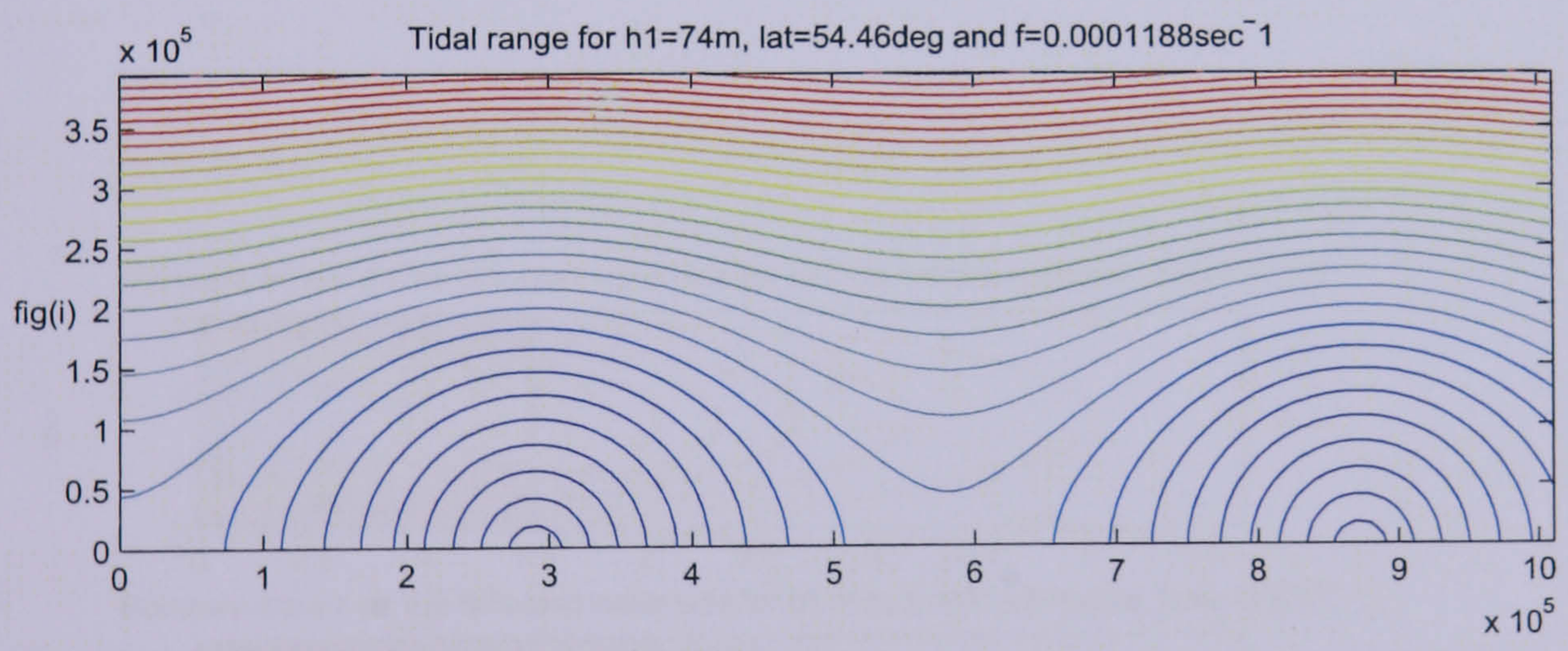

Figure 7.15:

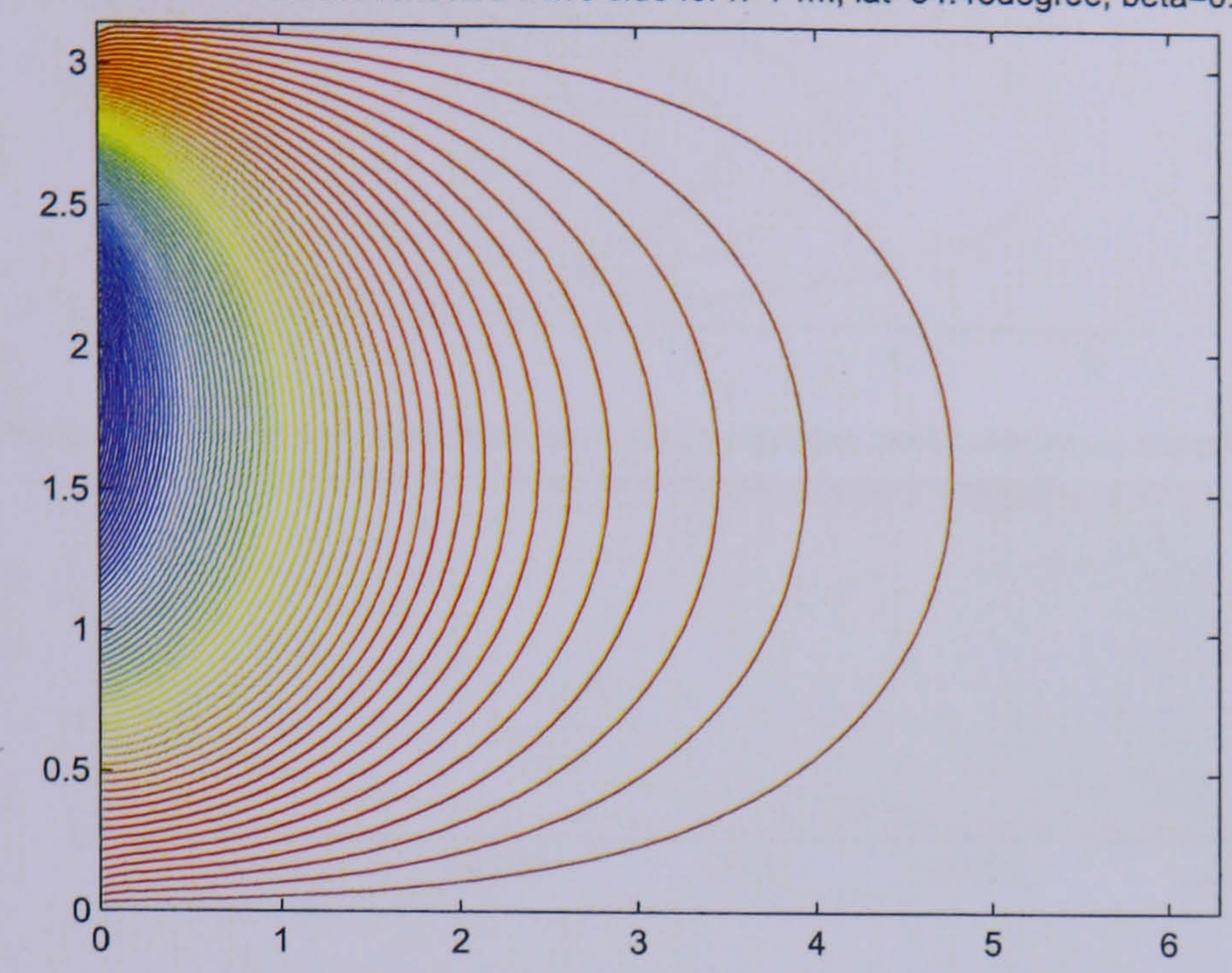

Figure 7.16:

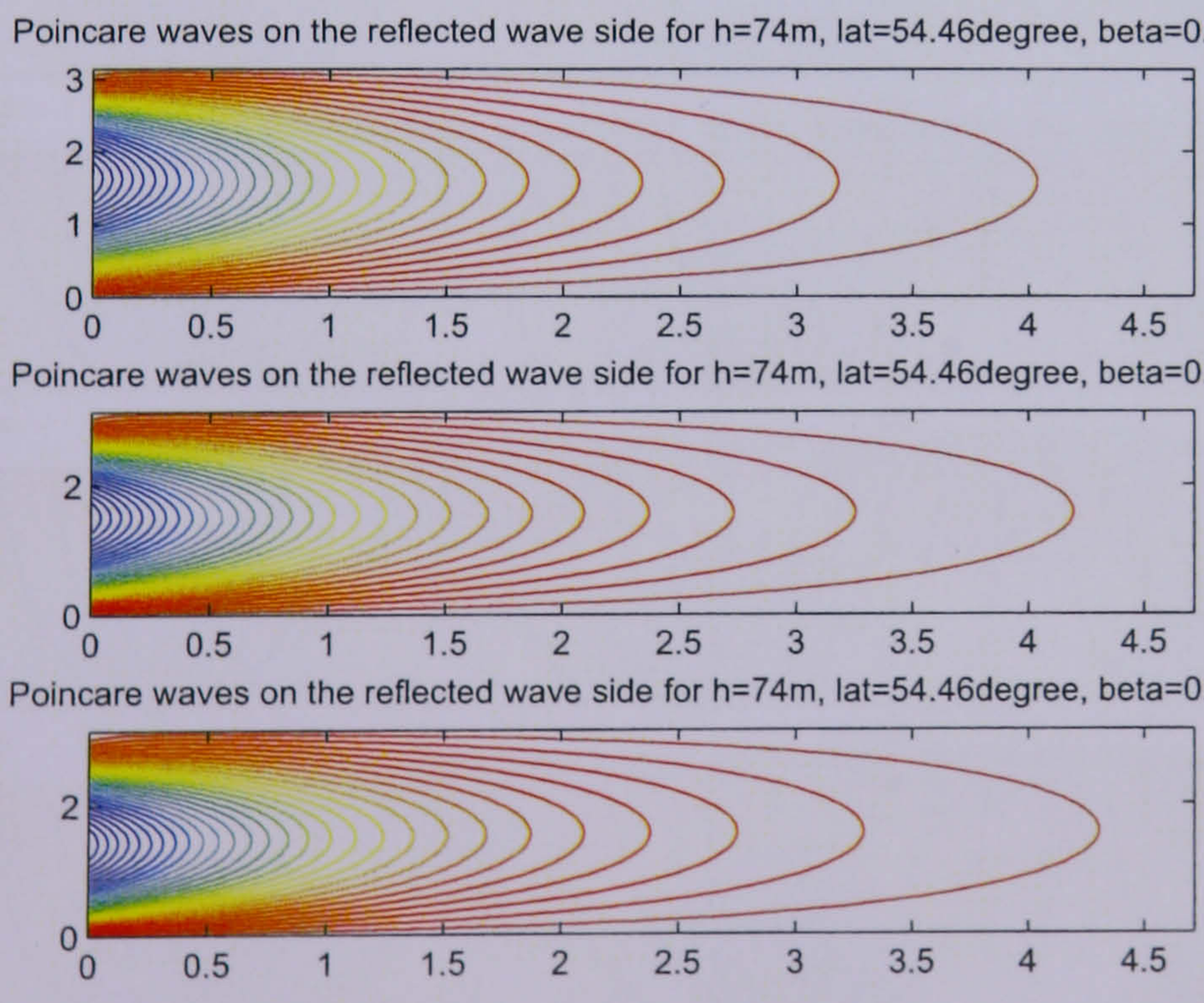

Figure 7.17:

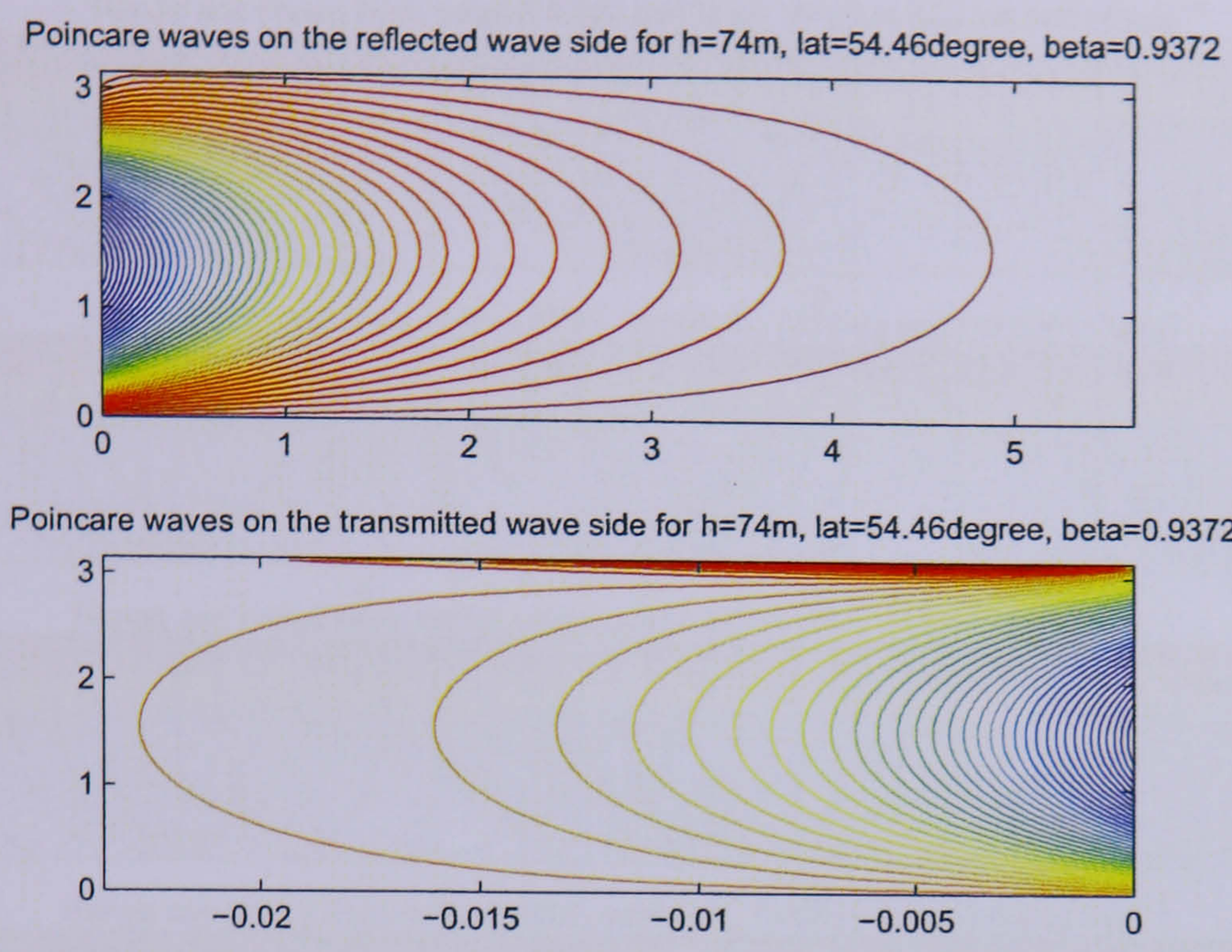

Figure 7.18:

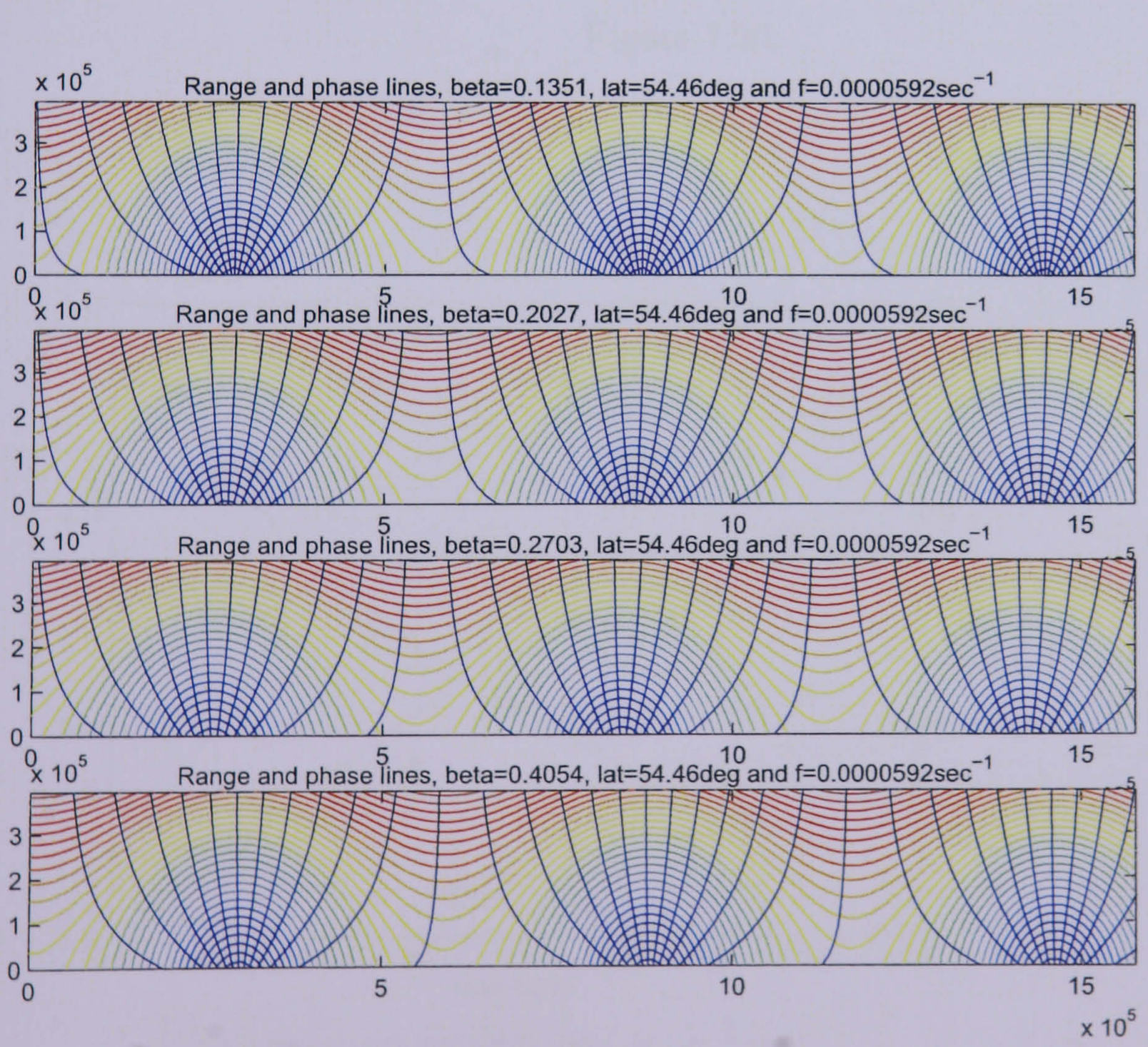

Figure 7.19:

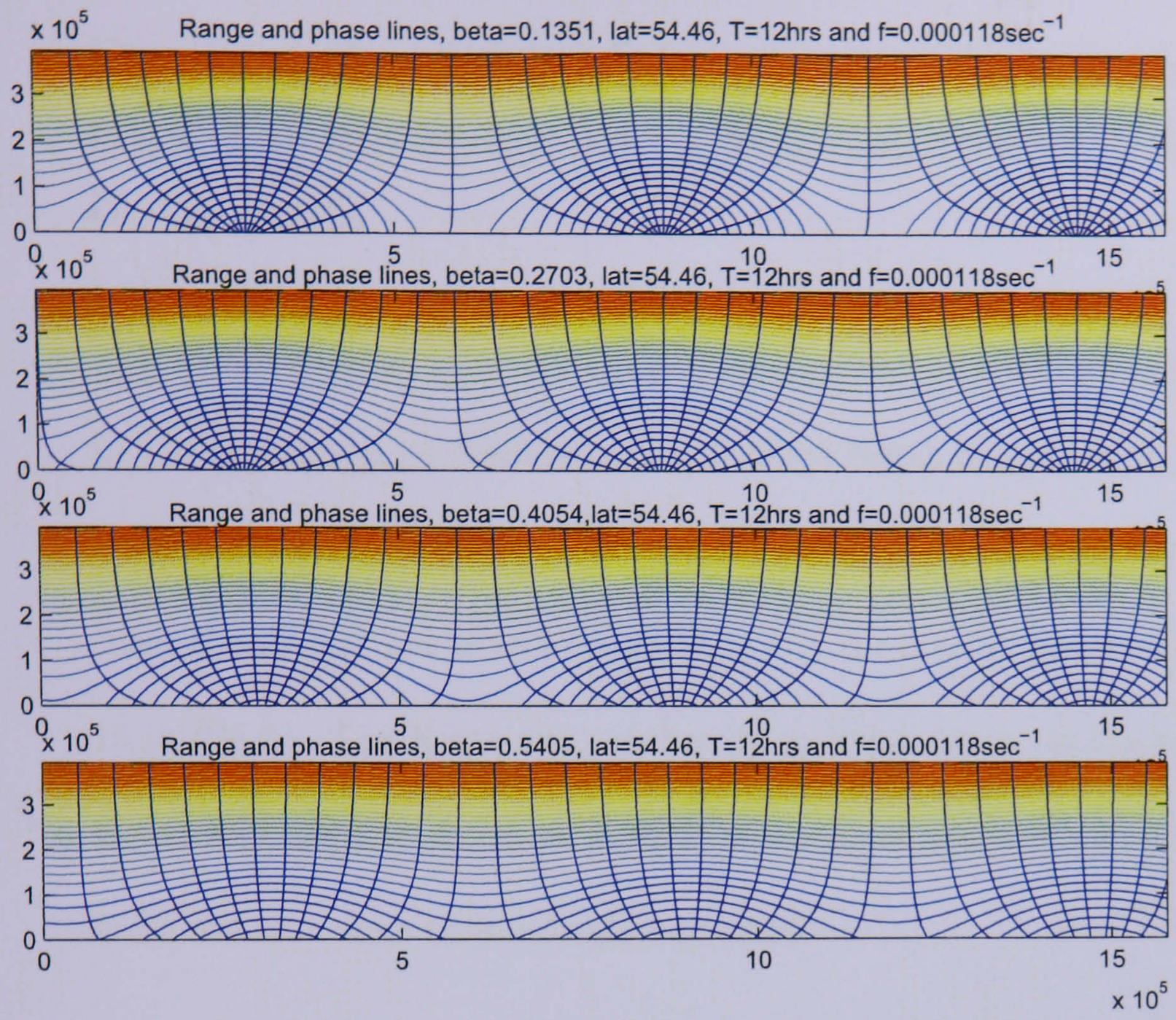

Figure 7.20:

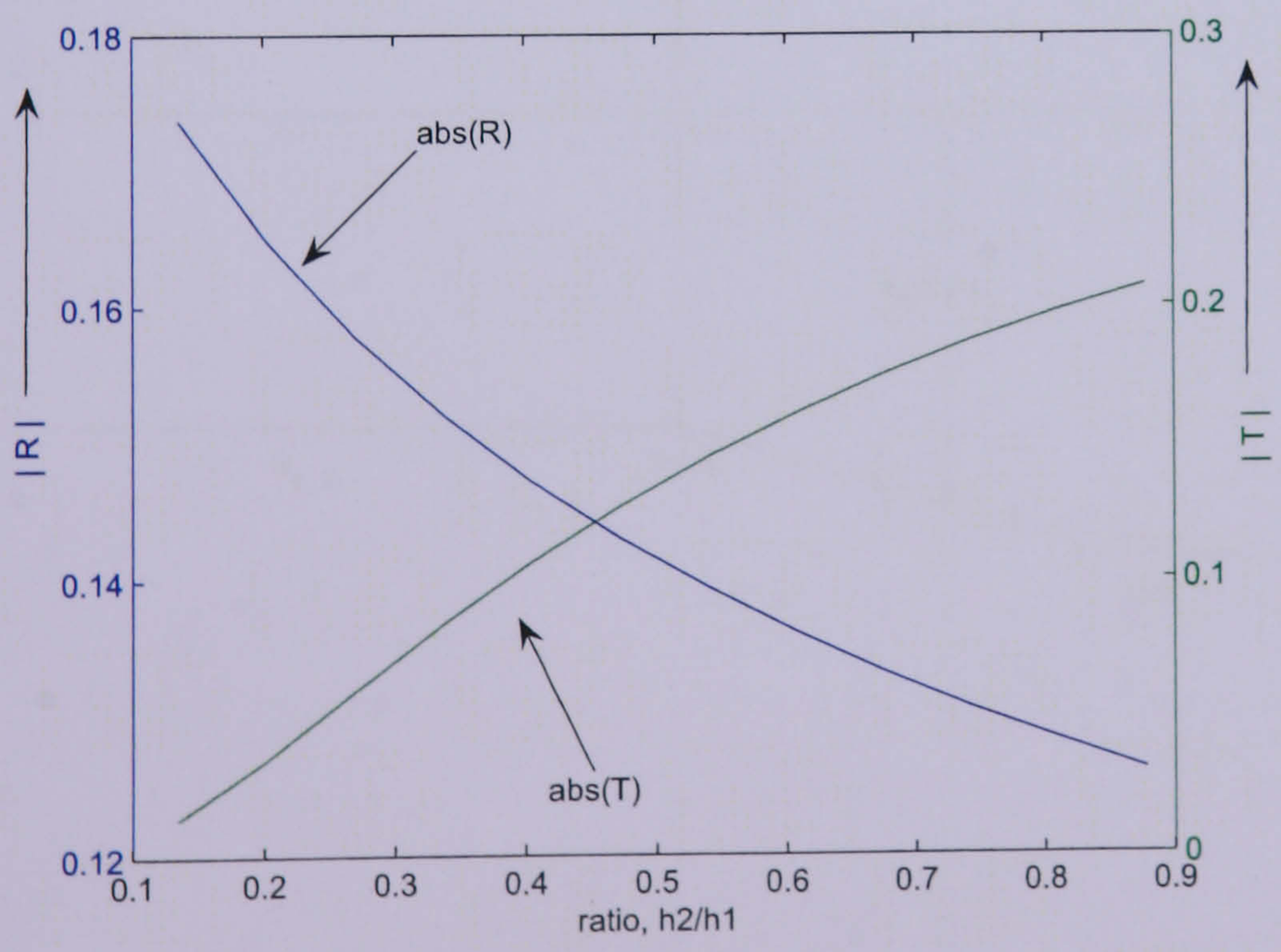

Figure 7.21:

Chapter 8

Propagation of a Kelvin wave over a slope-like bottom topography in a Semi-infinite Canal open at both ends

This is a semi-analytical study of Kelvin waves in a depth-changing canal.

In Taylor's model he considered an idealized North Sea in which the depth and width are both taken as uniform. However, it is documented that the depth near the Danish coast is only just less than 37 m (120 ft) and the depth near the English coast is about 15 m (50 ft). The North Sea reaches its greatest depth off the coast of Norway.

By considering the above variations in depth, we assume a model which is somewhat more realistic than that considered earlier.

8.1 Kelvin wave in 2 semi-infinite canals connected by a short sloping sea-bed:

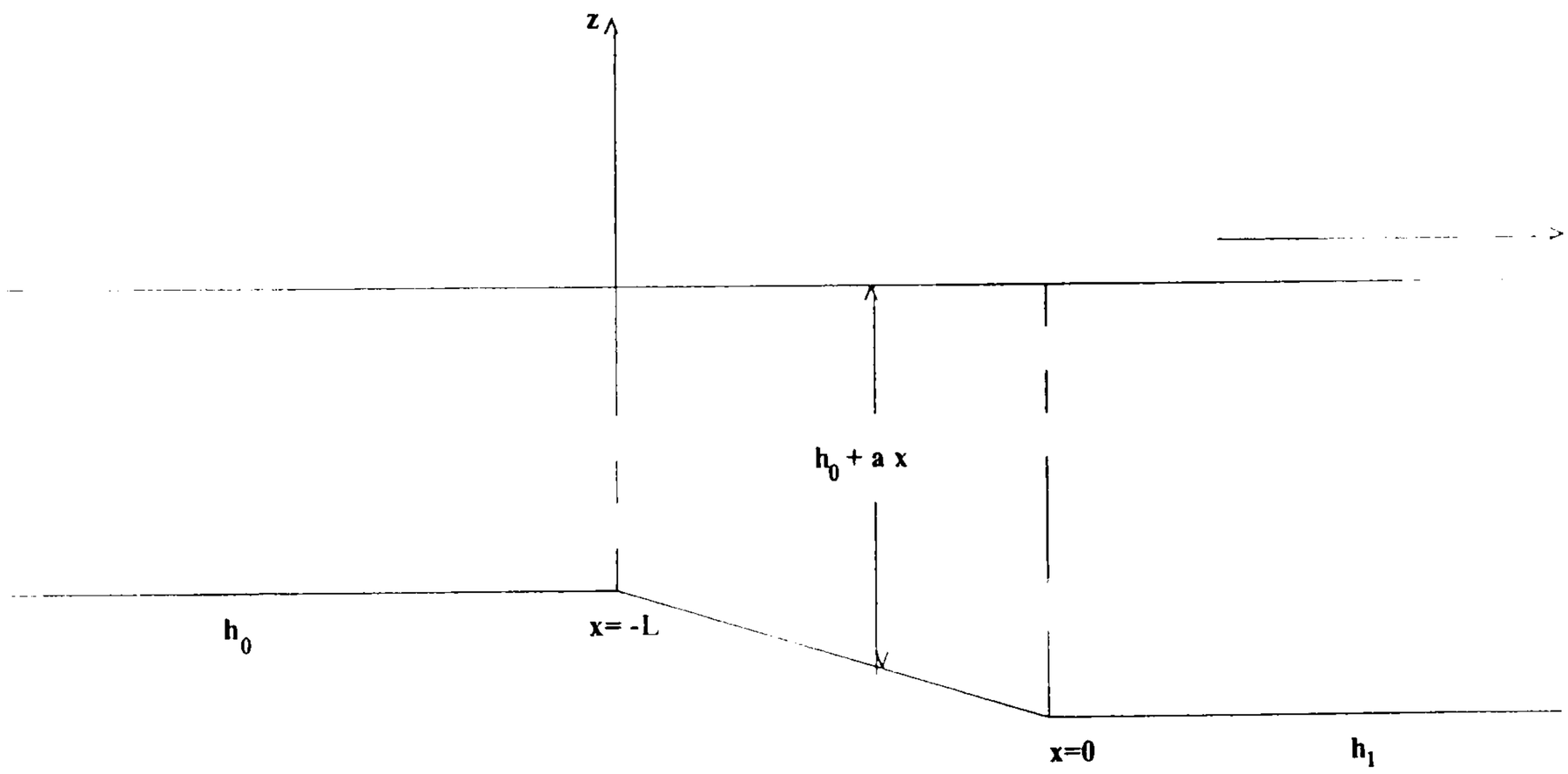

Figure 8.1: Cross-sectional view of the sea

8.2 Formulation of the Model:

We first rewrite the system in the constant depth regions.

The incident and reflected wave in the region $x > 0$ are defined by

$$\left.\begin{aligned} \zeta_I &= e^{\alpha(y-b)+i(\sigma t+\frac{\sigma}{c_1}x)} \\ \zeta_R &= Re^{-\alpha y+i(\sigma t-\frac{\sigma}{c_1}x)} \end{aligned}\right\}. \tag{8.1}$$

where ζ, t, g and b are surface elevation, time, gravity and the width of the channel respectively.

Also σ, α, and c_1 are positive and

$$c_1^2 = gh_1 = \frac{\sigma^2}{\alpha^2} \quad \text{and} \quad \alpha = \frac{f}{c_1}.$$

Here c_1 is the velocity of the long wave in the absence of earth's rotation in the region $x > 0$.

If u_I, v_I, u_R, v_R are the corresponding depth averaged velocities then

$$u_I = (-\frac{g}{c_1})\zeta_I, \qquad u_R = (\frac{g}{c_1})\zeta_R, \qquad v_I = 0, \qquad v_R = 0.$$

Similarly, in the region $x < -L$, we have the transmitted Kelvin wave defined by

$$\zeta_T = Te^{\alpha'(y-b)+i(\sigma t-\frac{\sigma}{c_2}(x+L))}. \tag{8.2}$$

where, σ, α', and c_2 are positive constants such that

$$c_2^2 = gh_0 = \frac{\sigma^2}{(\alpha')^2}, \quad \text{and} \quad \alpha' = \frac{f}{c_2}.$$

Here c_2 is the velocity of the long wave in the absence of earth's rotation in the region $x < -L$.

The associated depth averaged velocities are

$$u_T = (-\frac{g}{c_2})\zeta_T, \qquad v_T = 0.$$

The sets of *Poincaré* modes that emanate from the boundaries $x = 0$ and $x = -L$ are respectively written as,

$$v_1 = (\frac{g}{c_1}) \sum_1^\infty \gamma_n \sin(l_n y) e^{-s_n x + i\sigma t},$$

$$u_1 = (\frac{g}{c_1}) \sum_1^\infty \gamma_n \left\{ A_n \cos(l_n y) + B_n \sin(l_n y) \right\} e^{-s_n x + i\sigma t},$$

$$\zeta_1 = \sum_1^\infty \gamma_n \left\{ C_n \cos(l_n y) + D_n \sin(l_n y) \right\} e^{-s_n x + i\sigma t} \qquad \text{for } x > 0 \text{ and}$$

$$v_2 = (\frac{g}{c_2}) \sum_1^\infty \gamma_n' \sin(l_n y) e^{t_n (x+L) + i\sigma t},$$

$$u_2 = (\frac{g}{c_2}) \sum_1^\infty \gamma_n' \left\{ A_n' \cos(l_n y) + B_n' \sin(l_n y) \right\} e^{t_n (x+L) + i\sigma t},$$

$$\zeta_2 = \sum_1^\infty \gamma_n' \left\{ C_n' \cos(l_n y) + D_n' \sin(l_n y) \right\} e^{t_n (x+L) + i\sigma t} \qquad \text{for } x < -L. \qquad (8.3)$$

where, as before,

$$s_n^2 = l_n^2 - k_1^2, \quad t_n^2 = l_n^2 - k_2^2, \quad k_1^2 = \frac{\sigma^2 - f^2}{c_1^2}, \quad k_2^2 = \frac{\sigma^2 - f^2}{c_2^2} \text{ and } l_n = \frac{n\pi}{b}.$$

8.3 The Sloping region formulation:

The shoaling region is divided into just three sections as illustrated in the diagram. It will be assumed that the flow is 'known' at both extremities of the slope and the finite difference form of the equations of motion can then be used to continue the solution into the interior. This is done from both ends and finally the middle section has dependent variables computed from two sides. Their equality is then tantamount to the application of a boundary condition as in earlier work.

Clearly the technique is extendable, in principle, to any odd number of sections. In the interest of brevity we here take the simplest configuration.

Thus the basic procedure is adopted here with only two sub-intervals on the slope in

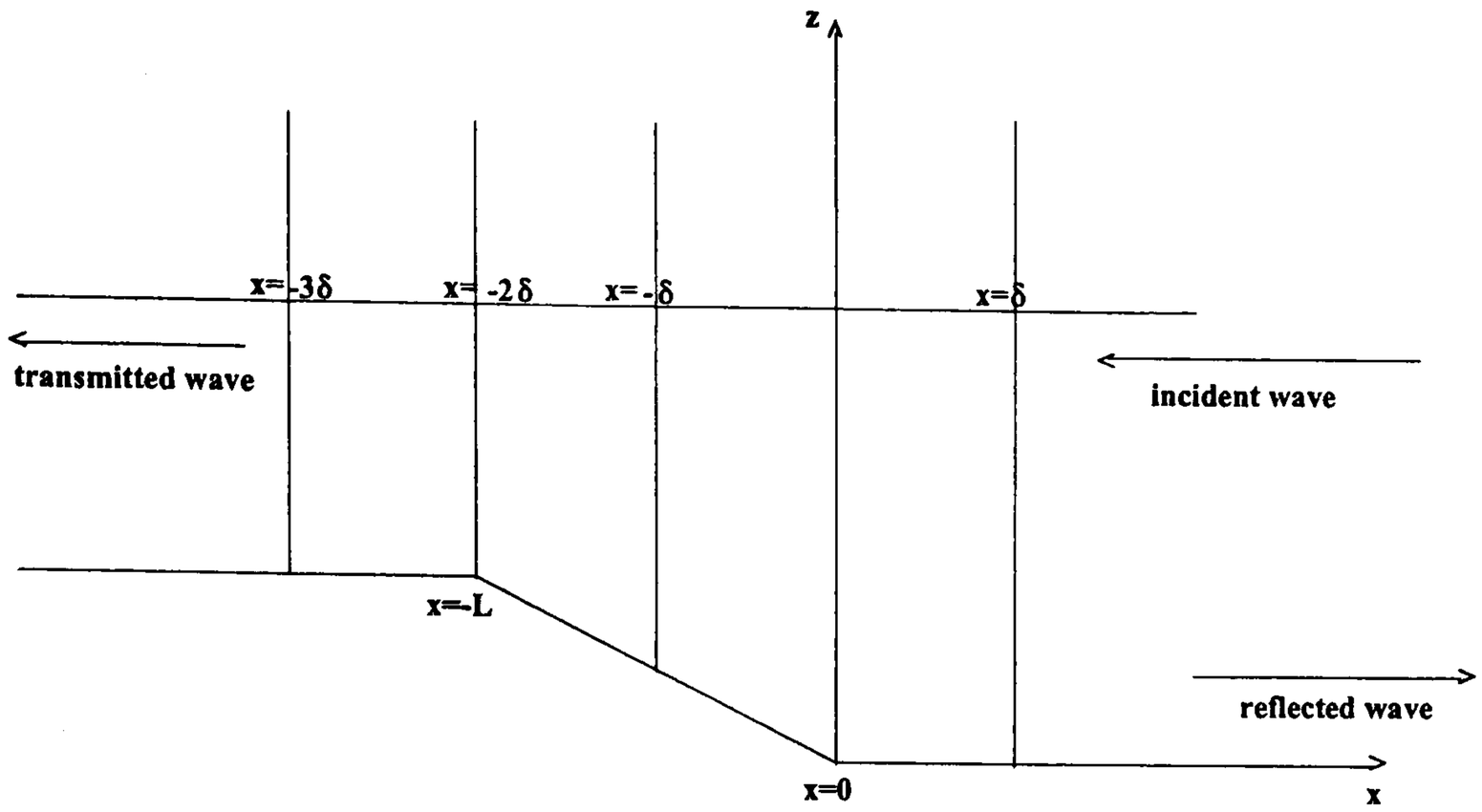

Figure 8.2:

order to facilitate description of a possible technique.

By integrating the continuity equation at across the section $x = 0$, (see fig (8.2)), obtain,

$$\frac{(hu)_{x=\delta} - (hu)_{x=-\delta}}{2\delta} + ((hv)_y)_{x=0} + i\sigma(\zeta)_{x=0} = \mathrm{O}(\delta). \qquad \text{for small step-size } 2\delta, \quad (8.4)$$

where the first term in equation (8.4) is obtained using Taylor's theorem,

$$f(a+h) = f(a) + hf'(a) + \mathrm{O}(h^2).$$

Similarly, on integrating the continuity equation at across the section $x = -2\delta$ which is the other boundary of the bathymetric region obtain,

$$\frac{(hu)_{x=-\delta} - (hu)_{x=-3\delta}}{2\delta} + ((hv)_y)_{x=-2\delta} + i\sigma(\zeta)_{x=-2\delta} = \mathrm{O}(\delta). \qquad (8.5)$$

In a similar manner by integrating the first momentum equation at across the section $x = 0$ obtain,

$$-g\left(\frac{\zeta_{x=\delta} - \zeta_{x=-\delta}}{2\delta}\right) = i\sigma u_{x=0} - f v_{x=0} + \mathrm{O}(\delta). \qquad (8.6)$$

Similarly, the momentum equation at across the section $x = -2\delta$ is written as

$$-g\left(\frac{\zeta_{x=-\delta} - \zeta_{x=-3\delta}}{2\delta}\right) = i\sigma u_{x=-2\delta} - f v_{x=-2\delta} + \mathrm{O}(\delta). \qquad (8.7)$$

8.3.1 Boundary Conditions and their application:

We apply the following two conditions.

(i) The continuity of total flux across the section $x = -\delta$.

(ii) The continuity of surface elevation at any vertical cross-section.

Using the relation (8.4) we obtain the total mass flow across a vertical cross-sectional area at, $x = -\delta$, in terms of field variables, (u, v, ζ) in the region $x \geq 0$ where

$u = u_I + u_R + u_1$, $v = v_I + v_R + v_1$ and $\zeta = \zeta_I + \zeta_R + \zeta_1$,

$$(hu)_{x=-\delta} = (\frac{gh_1}{c_1}) \left\{ Re^{-\alpha y} e^{-i\rho\delta} - e^{\alpha(y-b)} e^{i\rho\delta} + \sum_1^\infty \gamma_n \left[A_n \cos(l_n y) + B_n \sin(l_n y) \right] e^{-s_m \delta} \right\} +$$

$$2\delta \left\{ (\frac{gh_1}{c_1}) \sum_1^\infty (l_n \gamma_n) \cos(l_n y) + i\sigma R e^{-\alpha y} + i\sigma e^{\alpha(y-b)} + i\sigma \sum_1^\infty \gamma_n \left[C_n \cos(l_n y) + D_n \sin(l_n y) \right] \right\}.$$

where $\alpha = \frac{f}{c_1}$ and $\rho = \frac{\sigma}{c_1}$.

In a similar manner using the relation (8.5) we obtain the total mass flow across a vertical cross-sectional area at, $x = -\delta$, in terms of field variables, (u, v, ζ) in the region $x \leq -L$ where $u = u_T + u_2$, $v = v_T + v_2$ and $\zeta = \zeta_T + \zeta_2$,

$$(hu)_{x=-\delta} = (\frac{gh_0}{c_2}) \left\{ \sum_1^\infty \gamma_n' \left[A_n' \cos(l_n y) + B_n' \sin(l_n y) \right] e^{t_m(L-3\delta)} - T e^{\alpha'(y-b)} e^{i\rho'(L-3\delta)} \right\} -$$

$$2\delta \left\{ i\sigma T e^{\alpha'(y-b)} e^{i\rho'(L-2\delta)} + (\frac{gh_0}{c_2}) \sum_1^\infty (l_n \gamma_n') \cos(l_n y) e^{t_m(L-2\delta)} \right\}$$

$$+2\delta i\sigma \sum_1^\infty \gamma_n' \left[C_n' \cos(l_n y) + D_n' \sin(l_n y) \right] e^{t_m(L-2\delta)}$$

where $\alpha' = \frac{f}{c_2}$ and $\rho' = \frac{\sigma}{c_2}$.

By applying the condition of continuity of total mass flux across a vertical cross

section at $x = -\delta$ we obtain,

$$Re^{-\alpha y}(e^{-i\rho\delta} + 2i\delta\rho) - e^{\alpha(y-b)}(e^{i\rho\delta} - 2i\delta\rho) + Te^{\alpha'(y-b)}(\beta e^{-i\rho'(L-3\delta)} + 2i\delta\rho e^{-i\rho'(L-2\delta)}) +$$
$$\sum_{1}^{\infty} \gamma_n(e^{-s_m\delta}A_n + 2i\delta\rho C_n + 2l_n\delta)\cos(l_n y) + (e^{-s_m\delta}B_n + 2i\delta\rho D_n)\sin(l_n y)] -$$
$$\sum_{1}^{\infty} \gamma_n'[(\beta e^{-t_m(L-3\delta)}A_n' - 2i\delta\rho e^{-t_m(L-2\delta)}C_n' - 2\beta l_n\delta e^{-t_m(L-2\delta)})\cos(l_n y) +$$
$$(\beta e^{-t_m(L-3\delta)}B_n' - 2i\delta\rho e^{-t_m(L-2\delta)}D_n')\sin(l_n y)] = 0. \qquad (8.8)$$

We now repeat this idea for the surface elevation.

Using the relation (8.6) we obtain the surface elevation at, $x = -\delta$, in terms of field variables, (u, v, ζ) in the region $x \geq 0$ where $u = u_I + u_R + u_1$, $v = v_1$ and $\zeta = \zeta_I + \zeta_R + \zeta_1$,

$$\zeta_{-\delta} = Re^{-\alpha y}\left(e^{-i\rho\delta} + 2i\rho\delta\right) + e^{\alpha(y-b)}\left(e^{i\rho\delta} - 2i\rho\delta\right) +$$
$$\sum_{1}^{\infty} \gamma_n\left[(2i\rho\delta A_n + e^{-s_m\delta}C_n)\cos(l_n y) + (2i\rho\delta B_n + e^{-s_m\delta}D_n - 2\alpha\delta)\sin(l_n y)\right].$$

In a similar manner using the relation(8.7) we obtain the surface elevation on the cross sectional area at $x = -\delta$ in terms of field variables, (u, v, ζ) in the region $x \leq -L$ where $u = u_T + u_2$, $v = v_2$ and $\zeta = \zeta_T + \zeta_2$,

$$\zeta_{-\delta} = Te^{\alpha'(y-b)}\left(e^{-i\rho'(L-3\delta)} + 2i\rho'\delta e^{-i\rho'(L-2\delta)}\right) +$$
$$\sum_{1}^{\infty} \gamma_n'[(-2i\rho'\delta e^{-t_m(L-2\delta)}A_n' + e^{-t_m(L-3\delta)}C_n')\cos(l_n y) +$$
$$(-2i\rho'\delta e^{-t_m(L-2\delta)}B_n' + e^{-t_m(L-3\delta)}D_n' + 2\delta\alpha' e^{-t_m(L-2\delta)})\sin(l_n y)].$$

By applying the condition of continuity of free surface elevation across a vertical cross section at $x = -\delta$ we obtain,

$$Re^{-\alpha y}(e^{-i\rho\delta} + 2i\rho\delta) + e^{\alpha(y-b)}(e^{i\rho\delta} - 2i\rho\delta) - Te^{\alpha'(y-b)}(e^{-i\rho'(L-3\delta)} + 2i\rho'\delta e^{-i\rho'(L-2\delta)}) +$$

$$\sum_{1}^{\infty} \gamma_n[(2i\rho\delta A_n + e^{-s_m\delta}C_n)\cos(l_n y) + (2i\rho\delta B_n + e^{-s_m\delta}D_n - 2\alpha\delta)\sin(l_n y)] -$$

$$\sum_{1}^{\infty} \gamma_n'[(-2i\rho'\delta e^{-t_m(L-2\delta)}A_n' + e^{-t_m(L-3\delta)}C_n')\cos(l_n y) +$$

$$(-2i\rho'\delta e^{-t_m(L-2\delta)}B_n' + e^{-t_m(L-3\delta)}D_n' + 2\delta\alpha' e^{-t_m(L-2\delta)})\sin(l_n y)] = 0.$$

8.4 Method of Solution:

Now we define a matrix equation $\mathbf{Cx} = \mathbf{b}$, where

$$\mathbf{b} = \begin{pmatrix} e^{\alpha(y_1-b)}(e^{i\rho\delta} - 2i\delta\rho) \\ e^{\alpha(y_2-b)}(e^{i\rho\delta} - 2i\delta\rho) \\ .. \\ .. \\ .. \\ e^{\alpha(y_n-b)}(e^{i\rho\delta} - 2i\delta\rho) \\ e^{\alpha(y_{n+1}-b)}(e^{i\rho\delta} - 2i\delta\rho) \\ -e^{\alpha(y_{n+2}-b)}(e^{i\rho\delta} - 2i\delta\rho) \\ -e^{\alpha(y_{n+3}-b)}(e^{i\rho\delta} - 2i\delta\rho) \\ .. \\ .. \\ .. \\ -e^{\alpha(y_{2n}-b)}(e^{i\rho\delta} - 2i\delta\rho) \\ -e^{\alpha(y_{2n+1}-b)}(e^{i\rho\delta} - 2i\delta\rho) \\ -e^{\alpha(y_{2n+2}-b)}(e^{i\rho\delta} - 2i\delta\rho) \end{pmatrix} \qquad \mathbf{x} = \begin{pmatrix} \gamma_1 \\ \gamma_2 \\ .. \\ .. \\ .. \\ \gamma_{n+1} \\ \gamma_{n+2}' \\ \gamma_{n+3}' \\ .. \\ .. \\ .. \\ \gamma_{2n+1}' \\ \gamma_{2n+2}' \\ R \\ T \end{pmatrix}$$

$$
\mathrm{C} = \begin{pmatrix}
a_1^1 & a_1^2 & \ldots & a_1^{m-1} & a_1^m & b_1^{m+1} & b_1^{m+2} & .. & b_1^{2m} & p_1 & q_1 \\
a_2^1 & a_2^2 & \ldots & a_2^{m-1} & a_2^m & b_2^{m+1} & b_2^{m+2} & .. & b_2^{2m} & p_2 & q_2 \\
.. & .. & .. & \ldots & .. & .. & .. & .. & .. & .. & .. \\
.. & .. & .. & \ldots & .. & .. & .. & .. & .. & .. & .. \\
a_n^1 & a_n^2 & \ldots & a_n^{m-1} & a_n^m & b_n^{m+1} & b_n^{m+2} & .. & b_n^{2m} & p_n & q_n \\
a_{n+1}^1 & a_{n+1}^2 & \ldots & a_{n+1}^{m-1} & a_{n+1}^m & b_{n+1}^{m+1} & b_{n+1}^{m+2} & .. & b_{n+1}^{2m} & p_{n+1} & q_{n+1} \\
d_{n+2}^1 & d_{n+2}^2 & .. & d_{n+2}^{m-1} & d_{n+2}^m & e_{n+2}^{m+1} & e_{n+2}^{m+2} & .. & e_{n+2}^{2m} & p_{n+2} & q_{n+2} \\
d_{n+3}^1 & d_{n+3}^2 & .. & d_{n+3}^{m-1} & d_{n+3}^m & e_{n+3}^{m+1} & e_{n+3}^{m+2} & .. & e_{n+3}^{2m} & p_{n+3} & q_{n+3} \\
.. & .. & .. & .. & .. & .. & .. & .. & .. & .. & .. \\
.. & .. & .. & .. & .. & .. & .. & .. & .. & .. & .. \\
d_{2n+1}^1 & d_{2n+1}^2 & .. & d_{2n+1}^{m-1} & d_{2n+1}^m & e_{2n+1}^{m+1} & e_{2n+1}^{m+2} & .. & e_{2n+1}^{2m} & p_{2n+1} & q_{2n+1} \\
d_{2n+2}^1 & d_{2n+2}^2 & .. & d_{2n+2}^{m-1} & d_{2n+2}^m & e_{2n+2}^{m+1} & e_{2n+2}^{m+2} & .. & e_{2n+2}^{2m} & p_{2n+2} & q_{2n+2}
\end{pmatrix}
$$

where,

$$a_r^\kappa = (e^{-s_\kappa \delta} A_\kappa + 2i\delta\rho C_\kappa + 2l_\kappa\delta)\cos(l_\kappa y_r) + (e^{-s_\kappa\delta} B_\kappa + 2i\delta\rho D_\kappa)\sin(l_\kappa y_r)],$$

κ=1, 2, ...m, r= 1, 2, ...$n+1$;

$$b_r^\kappa = [(\beta e^{-t_\kappa(L-3\delta)} A'_\kappa - 2i\delta\rho e^{-t_\kappa(L-2\delta)} C'_\kappa - 2\beta l_\kappa \delta e^{-t_\kappa(L-2\delta)})\cos(l_\kappa y_r) +$$

$$(\beta e^{-t_\kappa(L-3\delta)} B'_\kappa - 2i\delta\rho e^{-t_\kappa(L-2\delta)} D'_\kappa)\sin(l_\kappa y_r)],$$

$\kappa = m+1, m+2, \ldots 2m$, $r = 1, 2, \ldots n+1$;

$$d_r^\kappa = [(2i\rho\delta A_\kappa + e^{-s_\kappa\delta} C_\kappa)\cos(l_\kappa y_r) + (2i\rho\delta B_\kappa + e^{-s_\kappa\delta} D_\kappa - 2\alpha\delta)\sin(l_\kappa y_r)],$$

$\kappa = 1, 2, \ldots m$, $r = n+2, n+3, \ldots 2n+2$;

$$e_r^\kappa = [(-2i\rho'\delta e^{-t_\kappa(L-2\delta)} A'_\kappa + e^{-t_\kappa(L-3\delta)} C'_\kappa)\cos(l_\kappa y_r) +$$

$$(-2i\rho'\delta e^{-t_\kappa(L-2\delta)} B'_\kappa + e^{-t_\kappa(L-3\delta)} D'_\kappa + 2\delta\alpha' e^{-t_\kappa(L-2\delta)})\sin(l_\kappa y_r)],$$

$\kappa = m+1, m+2, ...2m, \;\; r = n+2, n+3, ...2n+2;$

$p_r = e^{-\alpha y_r}(e^{-i\rho\delta} + 2i\delta\rho), \quad r = 1, 2, ...2n+2, \quad q_r = e^{\alpha'(y_r - b)}(\beta e^{-i\rho'(L-3\delta)} +$

$2i\delta\rho e^{-i\rho'(L-2\delta)}),$

$r = 1, 2, ...n+1$

and $q_r = -e^{\alpha'(y_r-b)}(e^{-i\rho'(L-3\delta)} + 2i\delta\rho' e^{-i\rho'(L-2\delta)})$

$r = n+2, n+3.....2n+2.$

8.5 Solution:

In fig (8.3) is given a contour for tidal range. This is obtained for the deep water depth, h_1=74 m, the shallow water depth, h_0=10 m and the Coriolis parameter f=0.0001188 sec^{-1}. Tidal wave height is given at various parts of the region and it can be seen that high amplitude tides occur along the right coastal side of the channel.

In fig (8.4) tidal range and phase lines are given. It can be seen that except the first amphidromic point the other two amphidromic points lie along a straight line parallel to the central axis and on the eastern coastal side of the channel. The phase lines are drawn for every 30 *mins*. The fig (8.5) is given to show the movement of the amphidromic points towards the eastern side of the channel as the parameter β varies. As the shallow water depth increases the amphidromic points move towards the east and become virtual amphidromic points.

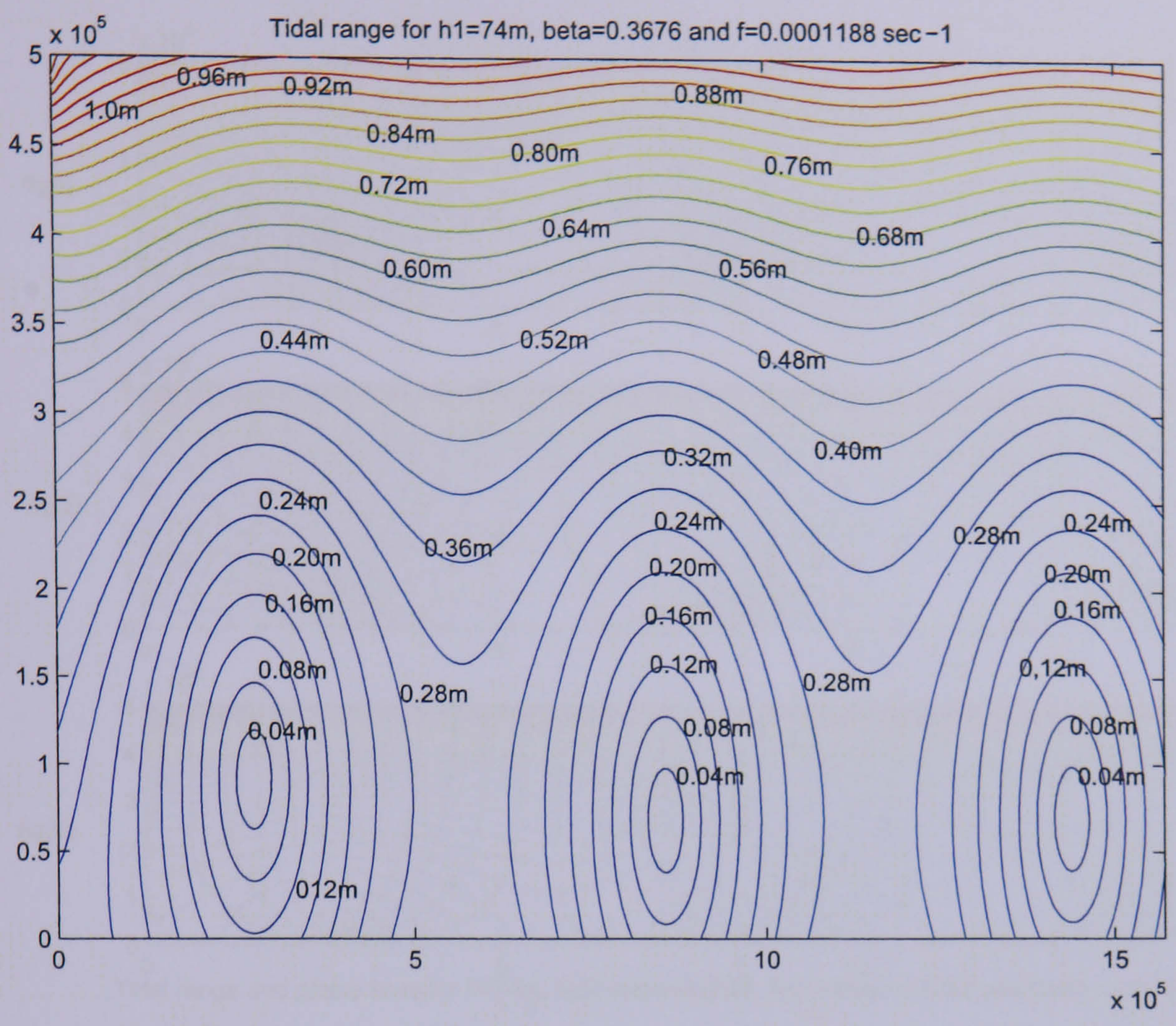

Figure 8.3:

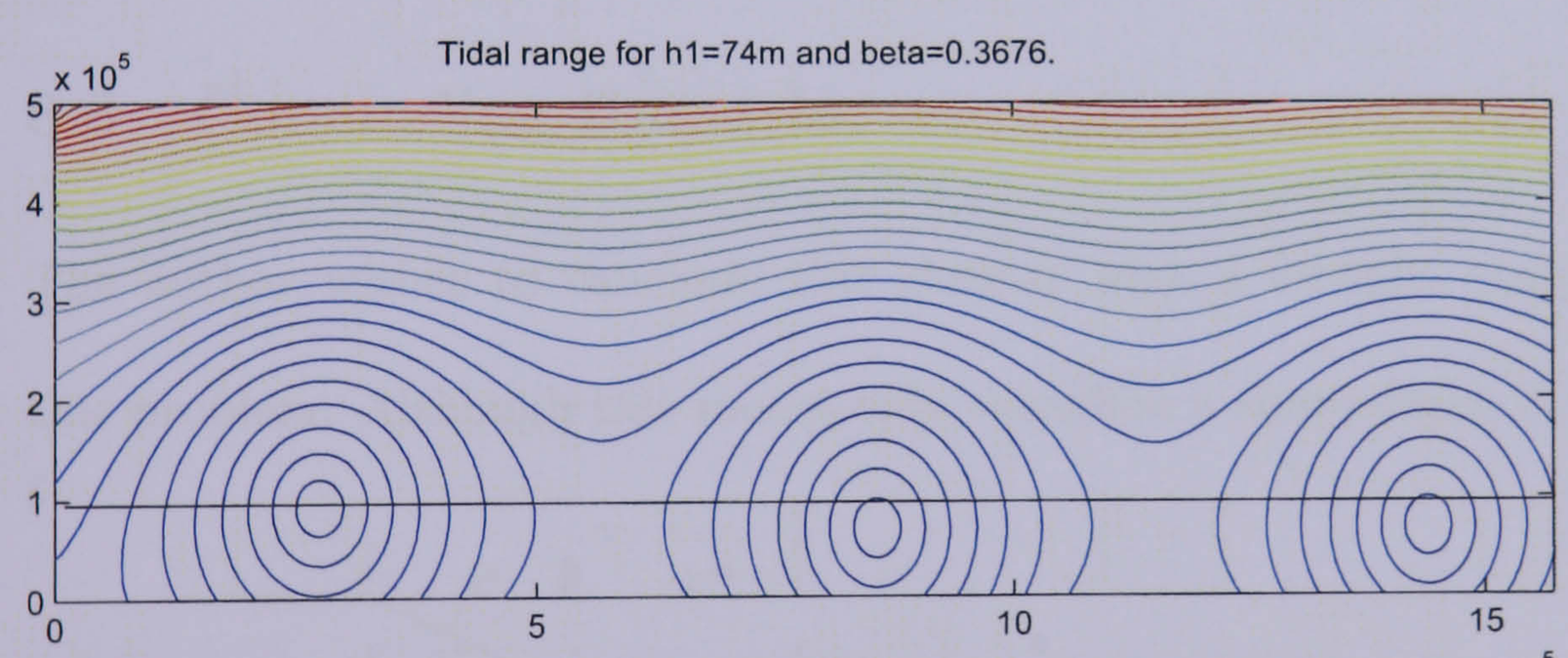

Figure 8.4:

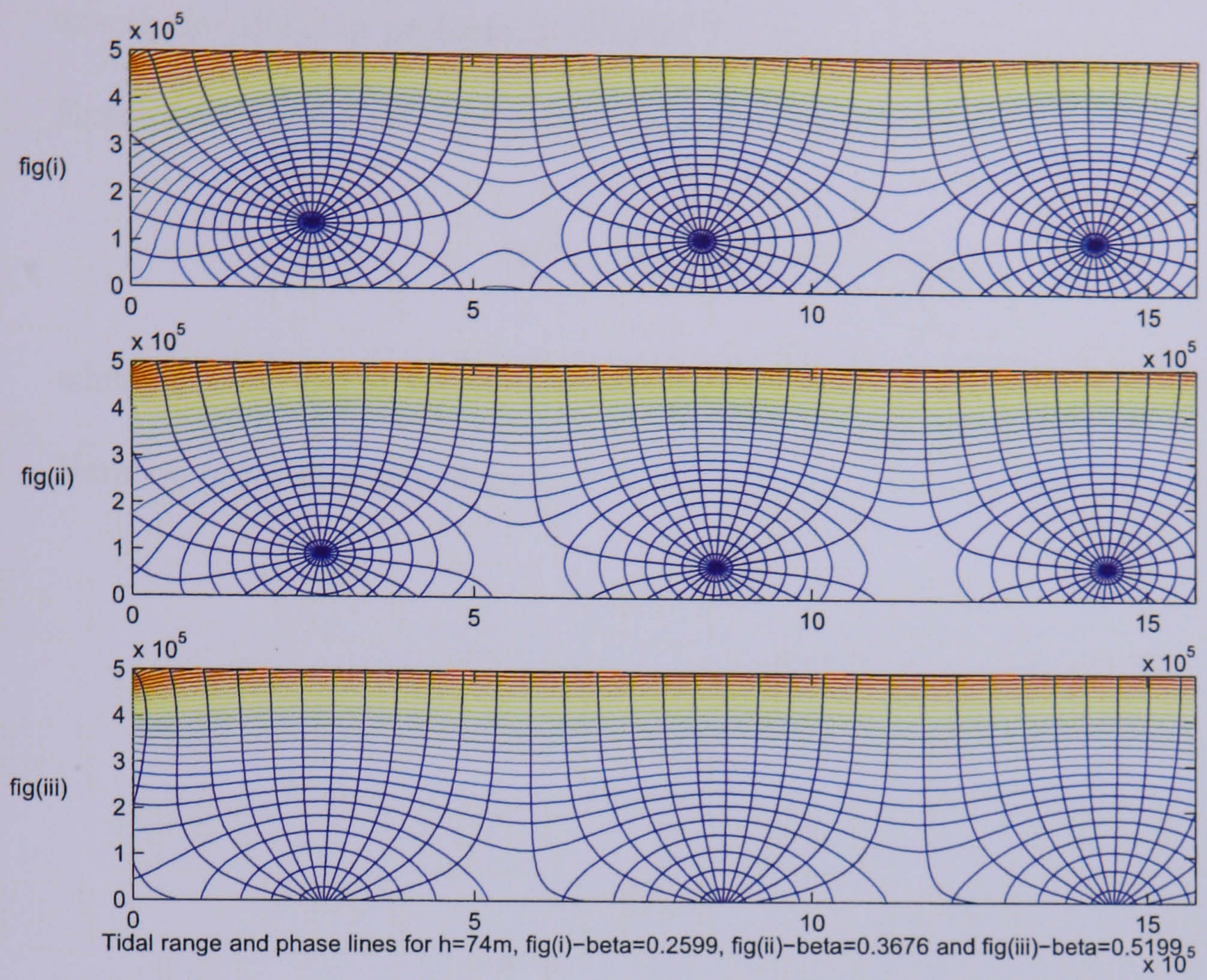

Figure 8.5:

8.6 Concluding Remarks:

The author wishes to conclude this chapter with a forsight about future work in this problem. Although this model only considers a short slope, it might possible to

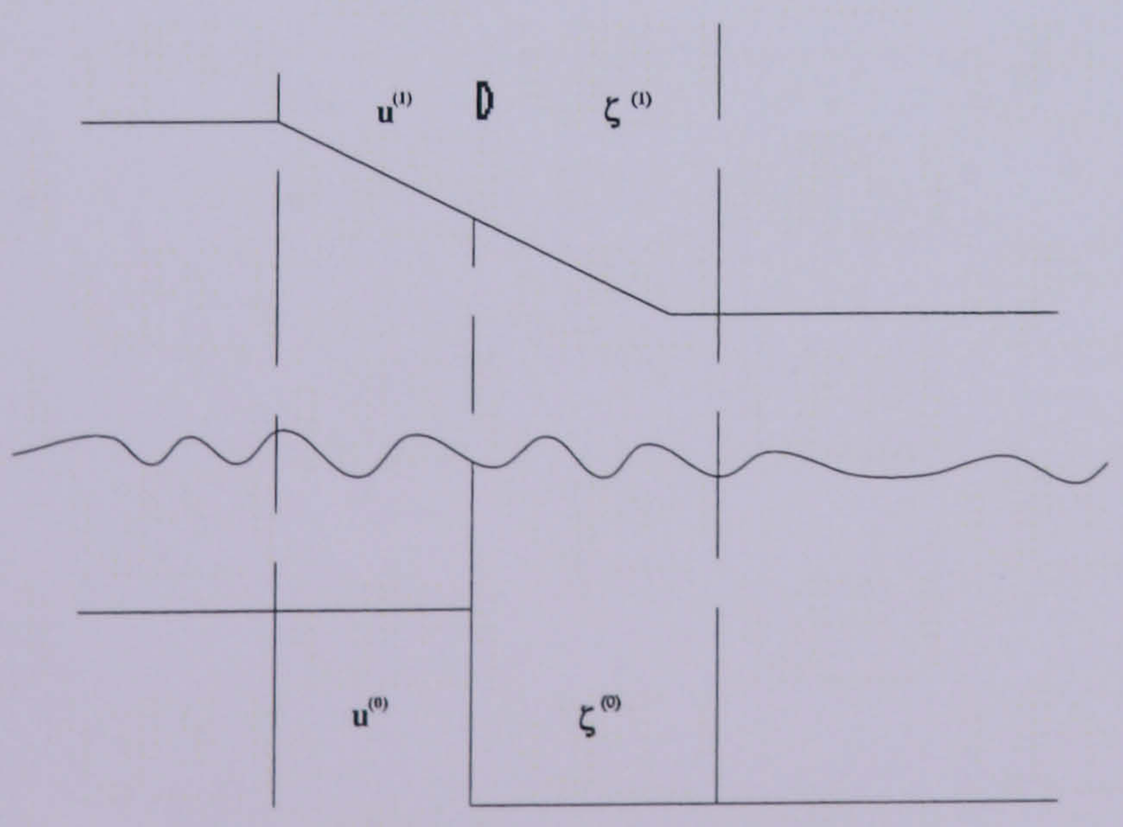

Figure 8.6:

extend it by considering the flow as a perturbation of the flow that we can calculate

exactly for the step problem in chapter 7.

Example: Suppose $u^{(0)}$, $\zeta^{(0)}$ is the exact flow then

$$(u^{(1)}, \zeta^{(1)}) = (u^{(0)}, \zeta^{(0)}) + 0(\epsilon),$$

where the $0(\epsilon)$ might be calculated through a method of multiple scales.

Here ϵ= order of depth change.

Chapter 9

Conclusion

In this work our main objective has been to extend Taylor's solution for perfect Kelvin wave reflection in a semi-infinite channel with uniform depth so as to incorporate the bottom topography, which is one of the most important factors to consider in a wave propagation model.

The accurate prediction of wave propagation from offshore to near shore locations is an important requirement in coastal engineering.

We have seen in chapter 3 the limitation of the use of Fourier series in solving boundary value problems when first derivatives are appended to the Laplace operator.

Taylor's procedure of replacing sines or cosines in one expansion, by further series of even or odd multiples appears to be a very useful approach. We have found that Taylor's gives a better approximated solution of our boundary value problem than a finite difference method.

The Green's function technique, which consists in writing a Green's function integral for the even A_n in terms of an integral of odd ones and vice versa allows us to approximate the solution with an n-term expansion. The greater the expansion we take, the better the approximation is.

We have looked into these problems with a view that the more difficult generalization of Taylor's problem may be reduced to a sequence of problems each of which may be approached by these methods.

On taking into account depth variation we first considered a simple model with the problem of a Kelvin wave reflection over a step in a semi-infinite channel. We solved this problem and made comparisons with numerical results. The formula (0.11) I

discussed within my introduction is used here to analytically validate my own results. The problem considered within Chapter 4 (Taylor's problem) and Chapter 6 were tested and verified with their numerical counterparts. Comparison of the results found to match perfectly with no errors. I therefore use this formula to theoretically explain the difference between the behavior of tides within the continental shelf compared to tides in the deep sea.

On the scale chosen to the problem in chapter 4 Fig (4.4) the range of tide at the two corners are given by 1.28 m whereas the range in the other parts of the channel is less than this value (i.e., 1.28).

In the problem in Chapter 6 Fig (6.2) the greatest value obtained to the tidal range at the corners of the channel is about 4.2 m.

The formula we are interested implies that when a Kelvin wave moves through a region in which depth (H) or f (Coriolis parameter) varies, the energy flux remains constant and therefore the amplitude varies in proportion with $(f/H)^{\frac{1}{2}}$.

Thus on comparison we can see in particular large amplitudes are produced when a Kelvin wave moves in shallow water. We can therefore compare and verify these findings with the observed phenomenon of Kelvin wave components of tide entering the North Sea and then moving south into shallow water.

Moreover the width of the channel chosen in the analysis domain of our model is about 394 km which is very much less than $2a$ ($a = 230\ km$ = Rossby radius). Our modeling therefore satisfies the condition that the width of the channel must be less than 1160 km.

Miles (1972) [26] investigation on Kelvin wave diffraction by an abrupt change in

depth varying alongshore in an semi-infinite sea with boundary on one side (parallel to the direction of propagation of waves) found a Fourier integral formulation which leads to a singular integral equation that may be solved exactly.

When we compare this model with our model in chapter 6, Miles' model has got an un-bounded sea in our y- direction whereas our model is a channel bounded on either sides by two coasts.

Moreover, because there is no energy can be radiated from the coastline and from the result in section 4 in Miles' work it is found that,

$$|T| = \left(\frac{(1+\epsilon)}{(1-\epsilon)}\right)^{\frac{1}{2}} \quad \text{provided that -1} < \epsilon < 1 \tag{9.1}$$

where,

$\epsilon = \dfrac{(h_+ - h_-)}{(h_+ + h_-)}$ (total change in depth, h is the depth outside the continental shelf)

provides an excellent approximation throughout the tidal regime. In fig (9.1) shown the variation of $|T|$ with respect to parameter $\sqrt{\epsilon}$ in the tidal regime considered.

Also along the boundary, in addition to incident and diffracted Kelvin waves, disturbances are excited by the discontinuity and are necessary to satisfy the boundary conditions. However, these disturbances radiate energy away from the coastline for certain ranges of values of parameters ϵ and f.

Having defined the above parameters ϵ and f, it was possible to set up parametric regimes implied by the results of the interaction.

(i) If $0 < \mathrm{f} < 1$, Kelvin and Pincaré waves

(ii) if $-1 < \epsilon < 1/\mathrm{f} < 1$, Kelvin waves

(iii) if $1/\mathrm{f} < \epsilon < 1$, Kelvin and double Kelvin waves. This area can be investigated further.

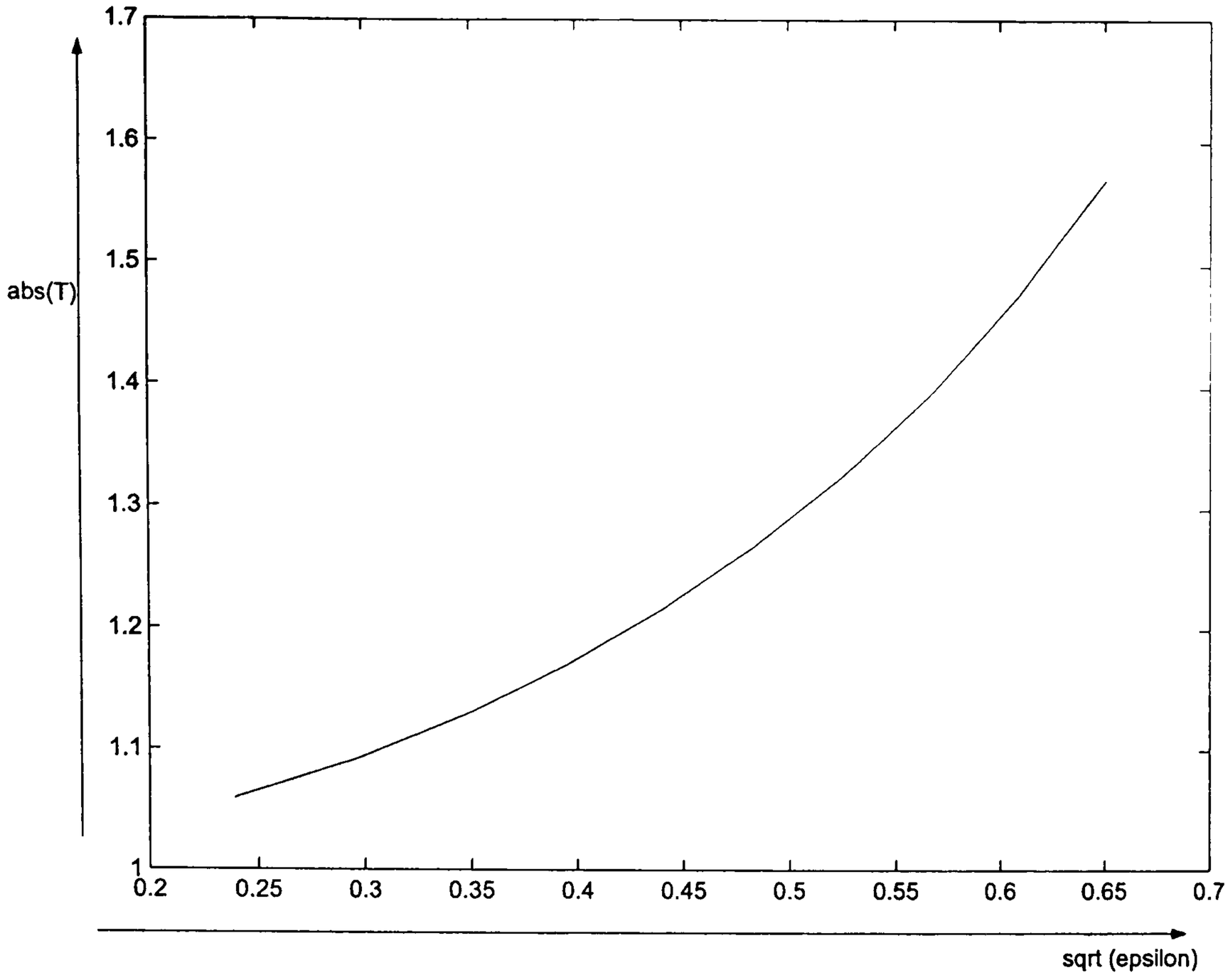

Figure 9.1: Variation of $|T|$ with respect to $\sqrt{(}\epsilon)$ in the tidal regime chosen

where

$\mathbf{f} = f/\sigma$.

We also solved the problem of Kelvin wave reflection over a step in an infinite channel opened at both ends. We found the displacement of the amphidromic points from the central axis towards the east was due to reduced amplitude of the reflected wave resulting in energy dissipation as we anticipated (see Brown, 1978 [4]).

We would therefore hope to examine for our future investigation tidal motion in a finite channel incorporated with change in depth. We will also consider an oscillating boundary at one end of the channel.

APPENDIX A_1 Kelvin wave over a step bottom in a semi-infinite channel closed at one end:

This is one of the main problems we investigated in chapter-6. Initially we intended to treat the problem non-dimensionally but in order to effect a comparison with the numerical counterpart we treated the problem dimensionally. However, the non-dimensional form of the governing equation is given here should we continue to treat the problem non-dimensionally.

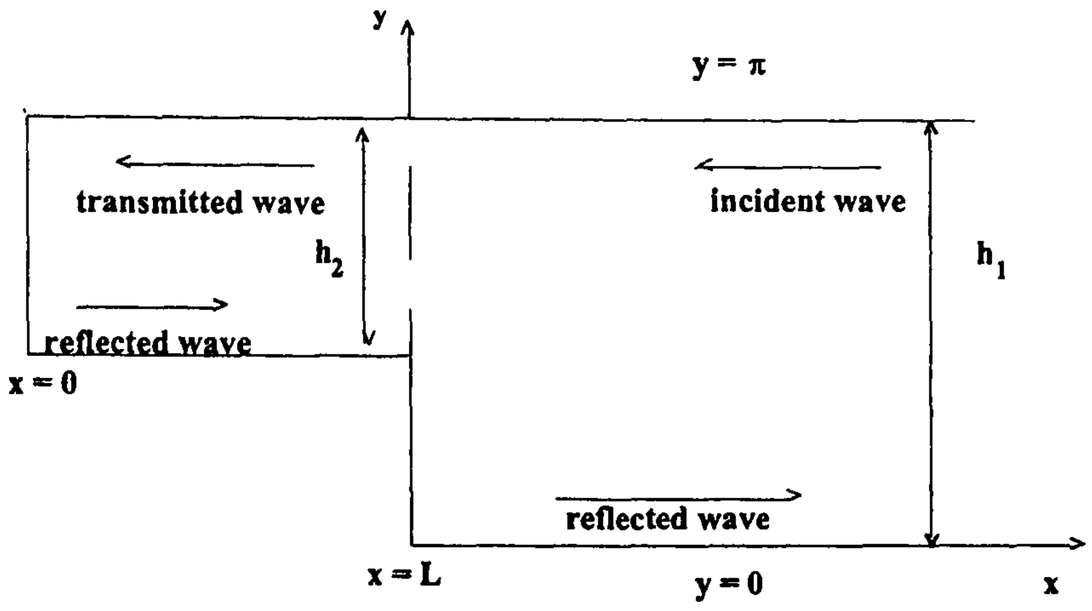

Figure 9.2:

The basic dimensional equations of motion are

$$\left.\begin{aligned} \frac{\partial u}{\partial t} - fv &= -g\frac{\partial \zeta}{\partial x}; \\ \frac{\partial v}{\partial t} + fu &= -g\frac{\partial \zeta}{\partial y}. \end{aligned}\right\} \tag{9.2}$$

The corresponding continuity equation is

$$\frac{\partial (hu)}{\partial x} + \frac{\partial (hv)}{\partial y} + \frac{\partial \zeta}{\partial t} = 0. \tag{9.3}$$

It is convenient to convert the problem to non-dimensional form by introducing characteristic lengths a and b to describe the horizontal scale of motion. We characterize the horizontal velocity by u_0 and use τ as a characteristic value of time t. Also we use h_0 to characterize the depth $h = h(x)$.

Each variable divided by its characteristic magnitude becomes a non-dimensional

variable such that

$$x' = \frac{x}{a}, \qquad y' = \frac{y}{b}, \qquad u' = \frac{u}{u_0}, \qquad v' = \frac{v}{u_0}, \qquad \zeta' = \frac{\zeta}{h_0}, \qquad h' = \frac{h}{h_0}, \qquad t' = \frac{t}{\tau}.$$

where, the non-dimensional variables are denoted by primes.

In new variables (9.2) and (9.3) take the form as

$$\left.\begin{aligned} \frac{\partial u'}{\partial t'} - \alpha v' &= -\beta \frac{\partial \zeta'}{\partial x'} \ , \\ \frac{\partial v'}{\partial t'} + \alpha u' &= -\gamma \frac{\partial \zeta'}{\partial y'}, \\ \frac{\partial \zeta'}{\partial t'} + p\frac{\partial (h'u')}{\partial x'} + q\frac{\partial (h'v')}{\partial y'} &= 0. \end{aligned}\right\}$$

where the basic non-dimensional parameters are

$$\alpha = f\tau, \qquad \beta = \frac{gh_0\tau}{au_0}, \qquad \gamma = \frac{gh_0\tau}{bu_0}, \qquad p = \frac{u_0\tau}{a}, \qquad q = \frac{u_0\tau}{b}.$$

It is plausible to take $\beta = \gamma$ so $b = a$ and then $p = q$.

On ignoring the primes for simplicity we can now write the above non-dimensional form as

$$\left.\begin{aligned} \frac{\partial u}{\partial t} - \alpha v &= -\beta \frac{\partial \zeta}{\partial x} \ , \quad \text{(i)} \\ \frac{\partial v}{\partial t} + \alpha u &= -\beta \frac{\partial \zeta}{\partial y}, \quad \text{(ii)} \\ \frac{\partial \zeta}{\partial t} + p\left(\frac{\partial (hu)}{\partial x} + \frac{\partial (hv)}{\partial y}\right) &= 0. \quad \text{(iii)} \end{aligned}\right\} \tag{9.4}$$

where,

$$\alpha = f\tau, \qquad \beta = \frac{gh_0\tau}{au_0}, \qquad p = \frac{u_0\tau}{a}.$$

If we assume a time factor $e^{i\sigma t}$, then (i) and (ii) of (9.4) gives

$$\left.\begin{aligned} i\sigma u - \alpha v &= -\beta \frac{\partial \zeta}{\partial x}, \\ i\sigma v + \alpha u &= -\beta \frac{\partial \zeta}{\partial y} \end{aligned}\right\} \quad \text{such that}$$

$$u = \frac{\beta}{\sigma^2 - \alpha^2}\left(i\sigma \frac{\partial \zeta}{\partial x} + \alpha \frac{\partial \zeta}{\partial y}\right),$$

$$v = -\frac{\beta}{\sigma^2 - \alpha^2}\left(\alpha \frac{\partial \zeta}{\partial x} - i\sigma \frac{\partial \zeta}{\partial y}\right). \tag{9.5}$$

Thus (iii) of (9.4) becomes using (9.5)

$$i\sigma\zeta + p\left(\frac{\partial (hu)}{\partial x} + \frac{\partial (hv)}{\partial y}\right) = 0,$$

$$\nabla_H^2 \zeta + \frac{\sigma^2 - \alpha^2}{\beta p h}\zeta = 0. \tag{9.6}$$

where $\nabla_H^2 = \frac{\partial^2}{\partial x^2} + \frac{\partial^2}{\partial y^2}$.

In the wave equation (9.6) it has been assumed that the depth is constant. In this problem we consider an interconnecting channels with an abrupt change in depth. Thus the wave equation (9.6) is independently true in the two regions of the channel as shown in fig (9.2). Furthermore, since (9.6) is linear, u and v also satisfy the same wave equation.

The wave equation (9.6) is re-written as

$$\nabla_H^2 \zeta + \frac{\sigma^2 - \alpha^2}{g' h}\zeta = 0.$$

where $g^{'} = \frac{g}{g_0}$, g_0 is a characteristic value of the gravitational acceleration, given as, $g_0 = \frac{b^2}{\tau^2 h_0}$.

On dropping the prime the above equation can be written as

$$\nabla_H^2 \zeta + \frac{\sigma^2 - \alpha^2}{gh} \zeta = 0. \tag{9.7}$$

Assuming a solution of the form $\zeta = e^{imx+iny+i\sigma t}$ in (9.7) in terms of constants m, n.

Then we must have a condition, $m^2 + n^2 = \frac{\sigma^2 - \alpha^2}{gh}$.

But, since $k^2 = \frac{\sigma^2 - \alpha^2}{gh}$, we note that if $m = \frac{\sigma}{c}$, $n^2 = k^2 - m^2 = -\frac{\alpha^2}{c^2}$.

Thus, on taking $in = -\frac{\alpha}{c}$ (9.7) yields the Kelvin wave $\zeta = e^{i(\frac{\sigma}{c}x+\sigma t)} e^{-\frac{\alpha}{c}y}$ which travels with a speed$= \sqrt{gh}$.

In solving this problem we can use the following non-dimensional parameters and the characteristic values.

$\alpha = f\sqrt{\frac{h_0}{g}}$, $\sigma = \frac{2\pi}{T}\sqrt{\frac{h_0}{g}}$, where T is the period of the input Kelvin wave and h_0 is the scale depth.

time-scale, $\tau = \sqrt{\frac{h_0}{g}}$, scale fluid velocity, $u_0 = A\sqrt{\frac{g}{h_0}}$, A is the prescribed amplitude of the input Kelvin wave. The horizontal length scale is chosen as $\frac{b}{\pi}$ where b is the width of the channel and is equal to $394.79km$.

APPENDIX A_2

The final problem we attempt to solve assumes a model illustrated in fig (9.3) below which is deemed more realistic than step problem. To generate solutions of this much difficult problem we were looking at a series of model problems in order to build up gradually to the complicated structure of the generalized Taylors problem.

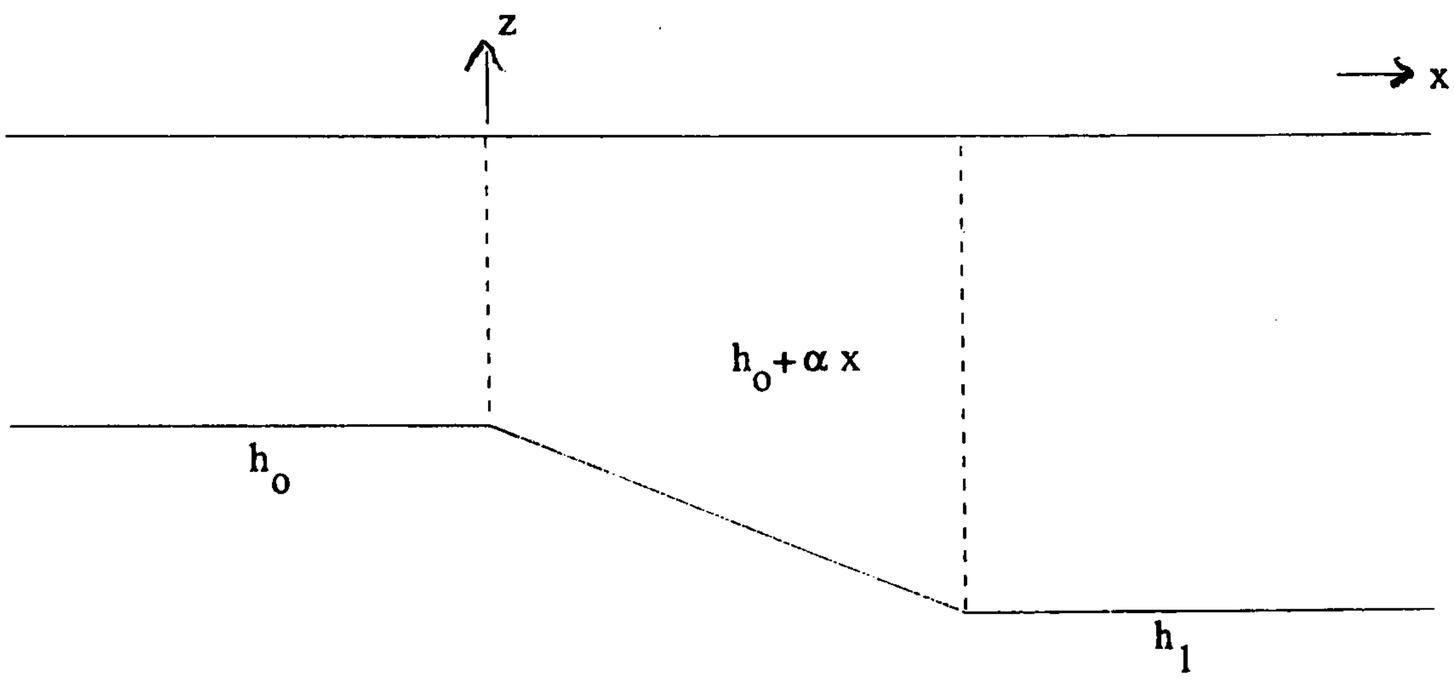

Figure 9.3: Schematic representation of the cross-section of the idealized sea

The linearized frictionless rotational equations under the hydrostatic pressure approximation.

$$\frac{\partial u}{\partial t} - fv = -g\frac{\partial \zeta}{\partial x}$$

$$\frac{\partial v}{\partial t} + fu = -g\frac{\partial \zeta}{\partial y}$$

$$\frac{\partial \zeta}{\partial t} + \frac{\partial}{\partial x}(hu) + \frac{\partial}{\partial y}(hv) = 0 \tag{9.8}$$

where

x, y, u and v are the same symbol we used in our work.

g is the acceleration due to gravity.

h is the depth of water.

f is Coriolis parameter.

ζ is the height of the tide above the mean level.

By assuming the field quantities u, v and ζ are $e^{i\sigma t}$ dependence the equation (9.8)

can be written as

$$v(f^2-\sigma^2) = g(f\frac{\partial\zeta}{\partial x} - i\sigma\frac{\partial\zeta}{\partial y})$$

$$u(f^2-\sigma^2) = -g(i\sigma\frac{\partial\zeta}{\partial x} + f\frac{\partial\zeta}{\partial y})$$

$$i\sigma\zeta + \alpha u + h\frac{\partial u}{\partial x} + h\frac{\partial v}{\partial y} = 0 \tag{9.9}$$

We can express u and v in terms of ζ and obtain, from the last equation of the system (9.9) a single equation for ζ

We thus get

$$h\left(\frac{\partial^2\zeta}{\partial x^2} + \frac{\partial^2\zeta}{\partial y^2}\right) + \left(\frac{f^2-\sigma^2}{g}\right)\zeta + \alpha\left(\frac{\partial\zeta}{\partial x} - \frac{if}{\sigma}\frac{\partial\zeta}{\partial y}\right) = 0. \tag{9.10}$$

Here v does not satisfy this equation.

We set, for convenience $\lambda = \frac{f^2-\sigma^2}{g}$ and $L \equiv f\frac{\partial}{\partial x} - i\sigma\frac{\partial}{\partial y}$.

We thus have from the equation

$$v(f^2-\sigma^2) = g(f\frac{\partial\zeta}{\partial x} - i\sigma\frac{\partial\zeta}{\partial y})$$

$$\lambda v = L\zeta.$$

On multiplying the equation (9.10) by L, we get

$$\lambda^{-1}\alpha f\nabla^2\zeta + \left(h\nabla^2 - \lambda + \alpha\frac{\partial}{\partial x} - \alpha\frac{if}{\sigma}\frac{\partial}{\partial y}\right)v = 0. \tag{9.11}$$

And by multiplying the equation (9.11) by L, we get

$$2\alpha f\nabla^2 v + h\nabla^2 Lv - \lambda Lv + \left(\alpha\frac{\partial}{\partial x} - \alpha\frac{if}{\sigma}\frac{\partial}{\partial y}\right)Lv = 0. \tag{9.12}$$

This variable slope generalization to Taylor's method model leads to a major problem for v;

We considered here below two approaches how to tackle the above model equations (9.10) and (9.12) respectively.

Defining equation

We have

$$h(x)\nabla^2\zeta - \lambda\zeta + \alpha(\frac{\partial\zeta}{\partial x} - \frac{if}{\sigma}\frac{\partial\zeta}{\partial y}) = 0$$

and the lateral boundary condition

$$L|\zeta| = 0, y = \pm\frac{\pi}{2}$$

where $L = f\frac{\partial}{\partial x} - i\sigma\frac{\partial}{\partial y}$ and $\lambda = \frac{(f^2-\sigma^2)}{g}$.

A Fourier Ansatz

We expand the wave height in a Fourier Series across the channel.

We propose, purely formally, a solution in the form

$$\zeta = \sum_{n=0}^{\infty}(a_n(x)\cos ny + b_n(x)\sin ny).$$

Substituting in equation and equating cosine and sine terms separately to zero, we get (with $\mu = \frac{f}{\sigma}$) the pair

$$h(a_n^{''} - n^2a_n) - \lambda a_n + \alpha(a_n^{'} - i\mu nb_n) = 0 \tag{9.13}$$

$$h(b_n^{''} - n^2b_n) - \lambda b_n + \alpha(b_n^{'} + i\mu na_n) = 0 \tag{9.14}$$

The significant problem will be that only the Fourier series for v can be expected to take its limiting values at the boundaries of the channel. This is because $v = 0$. So applied to ζ we would need to consider limiting values from within the fluid. This

may be difficult.

Let us nevertheless examine what can be done with the system above. Setting $\omega_n = a_n + ib_n$ we obtain easily a single equation for the complex valued function $\omega_n(x)$. It is

$$h\omega_n^{''} + \alpha\omega_n^{'} - (n^2h + \lambda + \alpha\mu n)\omega_n = 0.$$

or changing to h as the independent variable (so that dash denotes d/dh) the equivalent equation

$$h\omega_n^{''} + \omega_n^{'} - \alpha^{-2}(n^2h + \lambda + \alpha\mu n)\omega_n = 0. \tag{9.15}$$

and the further substitution (when $n > 0$) $h = (\frac{\alpha}{4n}{}^2t^2$ transforms this to the Weber equation

$$\omega_n^{''} - \left(\frac{1}{4}t^2 + \frac{\lambda + \alpha\mu n}{\alpha^2}\right)\omega_n = 0$$

whose solutions are well known in terms of parabolic cylinder functions. (see Whittaker & Watson page 205)[13]

The fundamental question remains, of course, of how to satisfy the lateral boundary conditions. If we work out v from the development for ζ, we get

$$\lambda v = L|\zeta| = \sum_{n=0}^{\infty}\Big((fa_n^{'}(x) - i\sigma nb_n(x))\cos(ny) + (fb_n^{'}(x) + i\sigma na_n(x))\sin(ny)\Big)$$

It is hard to see how we might satisfy the lateral boundary conditions with this, given that both a_n and b_n are essentially already known in terms of Weber functions.

One possible line of enquiry might be to try a 'collocation' approach with say M points on the 2 lateral boundaries and N points on the 2 longitudinal boundaries taking a total of $2(M+N)$ Fourier terms.

Using the v-equation approach

Although the equation for v would be third order, it might be worthwhile looking at the implications of starting there. To do this, let us try with the lateral boundaries at $y = 0$, $y = \pi$ and the slope confined to the region $-L \leq x \leq 0$.

This means that we need to retain a variable (complex) reflection coefficient in the region $x \geq 0$.

Thus we write the Kelvin/Poincaré wave system on the right in the form

$$u_I = e^{\frac{fy}{c_2}} e^{i\sigma(\frac{x}{c_2}+t)}$$

$$u_R = Re^{-\frac{fy}{c_2}} e^{-i\sigma(\frac{x}{c_2}-t)}$$

$$u_{p_2} = \sum_{m=1}^{\infty} (A_m \cos my + iB_m \sin my) e^{-s_m^{(2)}x+i\sigma t}$$

$$v_{p_2} = \sum_{m=1}^{\infty} D_m \sin my) e^{-s_m^{(2)}x+i\sigma t}$$

whilst that on the left ($x < -L$) can be written

$$u_T = Te^{\frac{fy}{c_1}} e^{i\sigma(\frac{(x+L)}{c_1}+t)}$$

$$u_{p_1} = \sum_{m=0}^{\infty} (a_m \cos my + ib_m \sin my) e^{s_m^{(1)}(x+L)+i\sigma t}$$

$$v_{p_1} = \sum_{m=1}^{\infty} d_m \sin my \; e^{s_m^{(1)}(x+L)+i\sigma t}$$

where, as usual, the equations demand that

$$(s_m^{(j)})^2 = m^2 - \frac{\sigma^2 - f^2}{gh_j}, \quad j = 1, 2.$$

There are also the 'consistency' relations arising from substituting back into the momentum equations. These evidently give

$$B_m = -\left(\frac{\sigma f}{gh}\right) \frac{1}{ms_m^{(2)}} A_m, \quad b_m = \left(\frac{\sigma f}{gh}\right) \frac{1}{ms_m^{(1)}} a_m, \quad m \geq 1,$$

so that as pointed out in Taylor's model, the A_m and B_m cannot be chosen independently.

Also, we can now write down expressions for the wave heights in the constant depth regions.

The variable depth region

Here we have third order equation developed previously in the form

$$2\alpha f\nabla^2 v + h(x)\nabla^2 Lv - \lambda Lv + \left(\alpha\frac{\partial}{\partial x} - \alpha\frac{if}{\sigma}\frac{\partial}{\partial y}\right) Lv = 0. \tag{9.16}$$

and to this we propose to look for a solution in the form

$$v = \sum_{n=1}^{\infty} c_n(x)\sin ny$$

in order to try to satisfy automatically the boundary condition on the banks.

This of course assumes that the series turns out to be uniformly convergent.

Formal substitution into the equation (9.16) gives

$$\sum_{n=1}^{\infty} \Omega_n \sin ny + in\varpi_n \cos ny = 0. \tag{9.17}$$

where

$$\Omega_n = \left\{3\alpha c_n'' + h(c_n''' - n^2 c_n') - \lambda c_n' - n^2\alpha c_n\right\}$$

and

$$\varpi_n = \left\{-\mu h(c_n'' - n^2 c_n) + \mu(\lambda c_n - \alpha c_n') - \mu^{-1}\alpha c_n'\right\}.$$

We cannot expect the individual sine and cosine series here to converge (thus we cannot equate each of Ω_n, ϖ_n to zero) but we could now try to use the ideas explored in the model M_2 where we would expand each $\cos ny$ as a half range sine series.

Writing

$$\cos ny = \sum_{m=1}^{\infty} a_m^{(n)} \sin my$$

we find readily that

$$a_m^{(n)} = \begin{cases} \frac{4}{\pi}\left(\frac{m}{m^2-n^2}\right) & \text{if } m-n \text{ is odd} \\ 0 & \text{if } m-n \text{ is even} \end{cases}$$

To help us better understand how we might now proceed, let us take the very simple approximation afforded by just two terms of both the v-expansion and the representation of $\cos ny$ above. This appears to give the simultaneous system

$$\Omega_1 + 2i\varpi_2 a_1^{(2)} = 0$$

$$\Omega_2 + 2i\varpi_1 a_2^{(1)} = 0. \tag{9.18}$$

We find that the operator may be expressed in the slightly simpler form

$$\Omega_n = D^3(hc_n) - n^2 D(hc_n) - \lambda D c_n,$$

$$\varpi_n = D^2(hc_n) - n^2(hc_n) - \lambda\left(c_n - \frac{\alpha g^2}{\sigma}\, c_n^{'}\right),$$

so that, in particular, $D\varpi_n - \Omega_n = \beta D^2 c_n$.

It may now be possible to set up a Green's function solution in an iterative manner, taking appropriate terms to the r.h.s. of each equation. Doing one integration, we could, for example, write the equation pair in the form

$$(D^2 - 1)hc_1 = f_2(x), \tag{9.19}$$

$$(D^2 - 4)hc_2 = f_1(x), \tag{9.20}$$

where

$$f_j(x) = (-1)^j \frac{8i}{3\pi} \int_{x_j}^{x} \varpi_j(t) Dt + \lambda c_j(x).$$

If we solve this iteratively with c_1, c_2 'known' on $x = 0$, $-L$, we will still retain two arbitrary constants x_1, x_2 for later use. This method should be investigated.

References

[1] W.S. Von Arx, *Introduction to physical oceanography*, Addison-Wesley, 2007.

[2] Bondok, *Some effects of varying depth on trapped waves and ocean currents in one and two layer oceans*, Ph.D thesis, University of London, 1980.

[3] P. J. Brown, *Kelvin-wave reflection in a semi-infinite canal*, Journal of Marine Research. **31** (1973), 1–10.

[4] Tim Brown, *Tidal model with application to the north sea*, Ph.D Thesis,City of London Polytechnic, 1978.

[5] ———, *Kelvin wave reflection at an oscillating boundary with applications to the north sea*, Continenta Shelf Research. **7** (1987), no. 4, 351–365.

[6] ———, *On the general problem of kelvin wave reflection at an oscillating boundary*, Continenta Shelf Research. **9** (1989), no. 10, 931–937.

[7] V.T Buchwald, *The diffraction of kelvin waves at a corner*, Journal of Fluid Mechanics Digital Archive **31** (1968).

[8] Alan Davies and Herman Gerritsen, *An intercomparison of three-dimensional tidal hydrodynamic models of the irish sea*, Tellus **46A** (1994), 200–221.

[9] Albert Defant, *Physical oceanography*, Pergamon Press, 1961.

[10] Phil Dyke, *Modeling coastal and offshore processes*, Imperial College Press, 2007.

[11] Adrian E Gill, *Atmosphere-ocean dynamics*, Academic Press, 1982.

[12] G.I.Taylor, *Tidal oscillations in gulfs and rectangular basins*, Proc. Camb.Phil. Soc. **74** (1973), 539–547.

[13] E.T.Whittaker & G.N.Watson, *A course of modern analysis*, 4 ed., C.U.P., 1952.

[14] G. Godin, *The m2 tide in the labrador, davis strait and baffin bay*, Deep Sea Research **12** (1965), 469–477.

[15] G. Godin and A. Martinez, *On the possibility of kelvin-type motion in actual seas*, Continental Shelf Research **14** (1993), no. 7/8, 707–721.

[16] P. Hall and A. M. Davies, *Modelling tidally induced sediment-transport paths over the northwest european shelf: the influence of sea-level reduction.*, Ocean Dynamics. **54** (2004), 126–141.

[17] W. Hansen, *Theorie zur errechnung des wasserstandes und der strÖmungen in randmeeren nebst anwendungen.*, J. Fluid Mech. **8** (1956), 287–300.

[18] H.Lamb, *Hydrodynamics*, 6 ed., Cambridge Mathematical Society, 1932.

[19] H.Poincare, *Theorie des marees*, Lecons de Macanique Celeste **3** (1910).

[20] J.E.Banks, *A mathematical model of a river-shallow sea system used to investigate tide, surge and their interaction in the thames-southern north sea region*, Phil.Trans.Roy.Soc.London.ser.A **275** (1974), 567–609.

[21] Hunt& Johns, *Currents induced by tides and gravity waves*, Tellus **XV** (1963), no. 4, 341–351.

[22] W. Thomson (Lord Kelvin, *On gravitational oscillations of rotating water*, Proc. Roy. Soc. Edinburgh. **10** (1879), 92–100.

[23] P. D. Killworth, *How much of a baroclinic coastal kelvin wave gets over a ridge?.*, Journal of Physical Oceanography **19** (1989), 321–341.

[24] ———, *Transmission of a two layer coastal kelvin wave over a ridge.*, Journal of Physical Oceanography **19** (1989), 1131–1148.

[25] Wolfgang Krauss, *Dynamics of the homogeneous and the quasihomogeneous ocean*, 1 ed., Fotosatz tuttle, 1973.

[26] John W Miles, *Kelvin waves on oceanic boundaries.*, Journal of Fluid Mechanics **55** (1972), 113–127.

[27] ———, *Kelvin waves diffraction by changes in depth.*, Journal of Fluid Mechanics **57** (1973), no. 2, 401–413.

[28] S. Piney N. Carbajal and J. G. Rivera, *A numerical study on the influence of geometry on the formation of sandbanks*, Ocean Dynamics **55** (2005), 559–568.

[29] Theodore Off, *Rhythmic linear sand bodies caused by tidal currents.*, Bulletin of the American association of Petroleum Geoologists **47** (1963), no. 2, 324–341.

[30] B.A Packham and W.E. Williams, *Diffraction of kelvin waves at a sharp bend*, Journal of Fluid Mechanics Digital Archive **34** (1968).

[31] George W Platzman, *'ocean tides and related waves' in mathematical problems in the geophysical sciences*, American Mathematical Society **2** (1971), 239–291.

[32] Syamsul Rizal, *Taylor's problem-influences on the spatial distribution of real and virtual amphidromes.*, Continental Shelf Research **22** (2002), 2147–2158.

[33] Ouafaa Sadiki, *The use of Fourier series and their limitations in solving a class of linear boundary value problems.*, London Guildhall University Project Document (1999), 24 pages.

[34] M.C.Hendershott & A. Speranza, *Co-oscillating tides in long, narrow bays; the taylor problem revisited*, Deep-Sea Research **18** (1971), 959–980.

[35] A. J. Webb and S. Pond, *The propagation of a kelvin wave around a bend in a channel.*, J. Fluid Mech. **169** (1986), 257–274.

[36] W.Krauss, *Methods and results of theoretical oceanography*, Gebrüder Borntraeger, 1973.

[37] A.M. Muir Wood, *Coastal hydraulics*, Macmillan, 1969.